ELECTROCHEMICAL TREATMENT OF DYE BEARING WASTEWATER

Ph.D. THESIS

by

SEEMA SINGH

DEPARTMENT OF CHEMICAL ENGINEERING
INDIAN INSTITUTE OF TECHNOLOGY ROORKEE
ROORKEE - 247 667 (INDIA)
MAY, 2014

ELECTROCHEMICAL TREATMENT OF DYE BEARING WASTEWATER

A THESIS

Submitted in partial fulfilment of the requirements for the award of the degree

of

DOCTOR OF PHILOSOPHY

in

CHEMICAL ENGINEERING

by

SEEMA SINGH

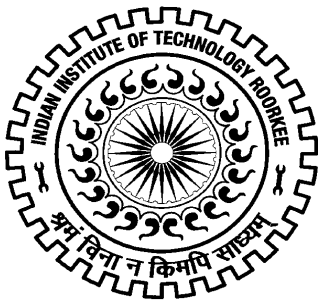

DEPARTMENT OF CHEMICAL ENGINEERING
INDIAN INSTITUTE OF TECHNOLOGY ROORKEE
ROORKEE - 247 667 (INDIA)
MAY, 2014

INDIAN INSTITUTE OF TECHNOLOGY ROORKEE ROORKEE

CANDIDATE'S DECLARATION

I do hereby certify that the work which is being presented in this thesis entitled **"ELECTROCHEMICAL TREATMENT OF DYE BEARING WASTEWATER**" in partial fulfilment of the requirement for the award of the Degree of Doctor of Philosophy and submitted in the **Department of Chemical Engineering of the Indian Institute of Technology Roorkee** is an authentic record of my own work carried out during a period from December, 2010 to May, 2014 under the supervision of Dr. I. D. Mall, Professor, and Dr. V. C. Srivastava, Associate Professor, Department of Chemical Engineering, Indian Institute of Technology Roorkee, Roorkee.

The matter presented in this thesis has not been submitted by me for the award of any other degree of this or any other Institute.

(SEEMA SINGH)

This is to certify that the above statement made by the candidate is correct to the best of our knowledge.

Date: May , 2014

(V. C. Srivastava)
Supervisor

(I. D. Mall)
Supervisor

The Ph.D. Viva-Voice Examination of **Mrs. SEEMA SINGH**, Research Scholar, has been held on……..

Signature of Supervisors **Chairman, SRC** **External Examiner**

Head of the Department/Chairman, O.D.C.

ABSTRACT

Textile industries, although provide clothes which are one of the basic needs of human beings, however, they are one of the largest exploiters of water and other complex chemicals during various stages of processing such as preparation, dyeing, finishing, sizing and other operations during manufacturing of textile materials. In India, a large number of cotton, composite and spinning mills are located in Ludhiana, Kanpur, Coimbatore, Mumbai, Surat, and Ahmadabad. Textile industries widely use organic dyes in finishing and coloring processes. About 20% of these dyes enter into the aquatic environment through discharge of effluents from treatment plants. Many synthetic dyes, also called as triarylmethane dyes are derived from triphenylmethane by substitution, and are well known for higher color intensity, brilliant shades and low light fastness. These cationic dyes have positive charge and are used for dying fabrics which have negative charge such as wool, silk, nylon, cotton, etc. Triphenylmethane dyes such as basic green 4 (malachite green) on photo–oxidation via nascent oxygen break into various N–de–alkylated primary and secondary amine derivatives which are similar to carcinogenic aromatic amines. Discharge of colored effluents containing dyes reduces the photosynthetic activity in aquatic environment, thus reducing the quantity of oxygen available in the water for use by the aquatic life.

Different treatment technologies have been examined for dye removal. These include biological, physical and chemical methods and their various combinations. Biological treatment of dying wastewater is cheaper than other methods, but it cannot be applied to most textile wastewaters due to the toxicity of most commercial dyes to the organisms used in the biological treatment methods. Physico-chemical methods such as coagulation, adsorption, chemical oxidation, advanced chemical oxidation, photocatalytic degradation, Fenton's processes, etc. are most widely researched methods for textile wastewater treatment. Advantages and disadvantages of each method have been extensively reviewed in literature.

In the last one decade, electrochemical (EC) treatment methods have received great attention for treatment of various types of wastewaters including dye bearing wastewater. EC method is comparatively inexpensive and is characterized by its easy operation, reduction in sludge volume and equipment costs. EC method utilizes metal electrodes as anode and cathode. Anode produces the coagulant via dissolution of electrodes by electrolytic reaction. Finally the coagulant turns into precipitates in the form of metal hydroxides in the appropriate pH range. Electrode potential, surface properties of electrode, type of electrolyte, and type of

transient intermediates formed affect the EC degradation of dyes. A lot of literature is available in EC treatment of dye bearing wastewater in the open literature. However, a number of research gaps were identified from the exhaustive literature review in the present study.

Variation in zeta potential during the interactions between Al ions generated from anode dissolution and cationic dye helps to understand the mechanism of removal. Only scarce studies are reported in the literature explaining the removal mechanism of EC process in relation to change in zeta potential during variation of current density (j), initial dye concentration (C_o) and initial pH (pH_o).

Very few studies are available in open literatures which try to elucidate mechanism of degradation of chemical structure of organic dye into smaller one during degradation processes. Most of these studies are, however, based on catalytic degradation, biological degradation and advance oxidation processes. No study is reported in the literature on mineralization of any dye during EC treatment.

Local dyers in small towns produce huge amount textile printing dye-bath effluent (DBE) during dying of textiles, woollens, etc. in small dye bath, and discharge them without any treatment to open channels. Our research group previously carried out parametric optimization of parameters for EC treatment of DBE using SS and Al electrodes separately. However, there was a further need to study the treatment of DBE with SS and Al in different anode-cathode combinations (Al–Al, Al–SS, SS–SS and SS–Al). It is also important to study the change in zeta potential and colloid particle size distribution (PSD) of colloids in the solution during the treatment.

Despite small amount of sludge generation in the EC method as compared to conventional coagulation and biological methods, still the sludge containing the electrode material needs to be disposed off. Only scarce studies are reported on preparation of useful material from different solid wastes but not with EC sludge. Nano-composite materials (NCMs) possessing meso- and micro-pores have received much attention in wastewater treatment in recent years. A study of literature on preparation of NCMs shows that there is a probability of conversion of EC residues to NCMs which can further be used as catalysts for dye degradation.

Based on the research gaps identified, following aims and objectives were set for the present work:

- To perform multi-step optimization of operating parameters using Plackett-Burman (PB) design, steepest accent/descent method and Box-Behnken (BB) design for EC

treatment of synthetic textile wastewater (STW) containing basic dyes with aluminum electrode.

- To study the effect of zeta potential during EC treatment with aluminum electrode of basic green 4 dye with variation in current density, pH, and initial dye concentration and to study the performance in terms of color, COD and total organic carbon (TOC) removal efficiencies; and energy consumption (ENC) and electrode consumption (ELC).
- To identify intermediates formed at various treatment time by mass spectroscopic and chromatographic techniques and to explain degradation mechanism by different possible schemes.
- To perform EC treatment of actual (real) DBE using aluminum (Al) and stainless steel (SS) electrodes in various anode-cathode combinations in a batch EC reactor and to study the effect of operating parameters on the removal efficiency in terms of color, COD, TOC and turbidity; and other performance parameters such as ENC and ELC
- To convert EC sludge generated by aluminium and stainless steel electrodes into NCMs and NMs by thermally heating method and to characterize the NCMs and use them as catalyst for degradation of dyes.

Circular shape batch reactor having working volume of 1.0 litre was used to conduct the EC treatment experiments. Magnetic stirrer was used to agitate the dye wastewater. One pairs of Al, SS and metal oxides coated electrodes having thickness of 1.5, 2.5 and 4.0 mm, respectively, each having dimensions of 10 cm × 9 cm with inter-electrode spacing of 1 cm were used.

STW was synthetically prepared using basic orange 30, basic violet 16 and basic green 4 dyes as per the method reported in the literature using chemicals such as carboxymethyl cellulose, starch, acetic acid, NaOH, H_2SO_4, Na_2CO_3, $NaHCO_3$ and glucose which are commonly found in textile mill wastewater. Multi-step optimization of EC treatment of STW by aluminum electrode was then carried out. A multi-step procedure was applied to screen and optimize the factors. First, PB design was employed to screen most significant three factors among a largest number of parameters. Afterwards, method of steepest ascent and BB design were used to determine the optimum levels of the factors that significantly influence the COD and color removal efficiencies. At the optimum operating conditions of current density=185.30 A/m^2, time=190 min and pH~5, more than 70.5% COD and 98.2% color

removal efficiencies was observed. Electro-coagulation and electro-flotation were found to be the main reasons for COD and color removal in STW.

In this part of the study, the degradation mechanism of basic green 4 dye during EC treatment with aluminum electrode was investigated. Zeta potential was measured with changes in operating variables such as j, pH_o, and C_o. At the optimum condition, 82.4% COD, 63.5% TOC and 99.4% color removal efficiencies were observed for C_o=100 mg/L within 45 min with j=117.64 A/m^2 and pH_o=6.2. The ELC and ENC values at the optimum conditions were 0.16 kg Al/kg COD and 2.48 kWh/kg COD removed.

It was found that the zeta potential of the dye solution was always negative during the treatment. The decolorization rate increased with an increase the pH from acidic to alkaline pH due to conversion of dye to leuco form. Zeta potential study helped to identify the conditions of maximum interaction between the hard acid (Al ions and hydroxides) and basic dye. More ever, since basic green 4 dye itself is positively charged, maximum removal of dye was found to occur at the lowest value of negative zeta potential (-15.2 mV at pH≈6.2), that is, when the concentration of positively charged colloids in the solution were least. It seems that overall the removal was due to adsorption on neutral aluminum hydroxide.

UV–visible and Fourier transform infrared (FTIR) spectroscopy, high performance liquid chromatography (HPLC), gas chromatography–mass spectroscopy (GCMS) and high resolution mass spectroscopy (HRMS) analysis showed that the degradation occurred via the cleavage of conjugated structure and N–de–methylation. The intermediates products identified included hydroxymethylated intermediates during the N–de–methylation of the dye; and N, N, N', N'–tetramethyl–4, 4'–diaminobenzophenone; 4, 4'–bis–aminobenzophenone and N–methyl–para–aminophenol after cleavage of conjugated triphenylmethane ring (Fig. 4). Generation of active species such as hydrogen peroxide, ozone and chlorinated oxidizing compounds was observed during the EC treatment process; and that the basic green 4 dye degradation occurred via $^{\bullet}OH$ radical attack.

Present study also investigates the EC treatment of actual DBE with different combination of Al and SS electrodes as anode and cathode. Effects of j and pH with different anode-cathode combinations (Al–Al, Al–SS, SS–SS and SS–Al) were studied. The change in zeta potential with current density at different time intervals, and the change in colloid particle diameters at different pH gave information regarding potential stability of colloidal suspension. Color, COD, TOC and turbidity removal efficiencies, residual zeta potential,

average colloid particle diameter, ELC and ENC values after treatment were in the following order: SS–SS > SS–Al > Al–Al > Al–SS.

It was found that higher value of j produced higher amount of metallic cationic species which in turn increase the color and COD removal efficiencies because of which zeta potential of the treated DBE moves toward positive value. Charge neutralization and sweep coagulation by respective hydroxides allowed the different particles at come together by van der Waals interaction and adsorption mechanism, respectively. These mechanisms increased the particle size at optimum pH which later on settles to the bottom and cause highest color and COD removal efficiencies. At high pH (>9), ClO^- formed via secondary reactions of chlorine direct oxidizes the colloidal matter present in DBE. Maximum color, COD, TOC and turbidity removal efficiencies were found to be 99.90%, 82.50%, 68.8% and 98.8%, respectively, at j=117.64 A/m^2 and pH=8.5 with SS–SS electrode combination.

FTIR, powder X-ray diffraction (PXD), Field emission scanning electron microscopy (FESEM), energy dispersive spectroscopy of X-rays (EDX) and thermogravimetric analysis (TGA) techniques were used to characterize the solid residues (sludge) obtained during EC treatment. FESEM and EDX also used for determine the morphology of various types of electrodes. The Barrett–Joyner–Halenda (BJH) method was used to determine the pore size distribution. Brunauer–Emmett–Teller (BET) surface area of sludge was found to be in the following order: Al–Al > Al–SS > SS–SS >SS–Al. However, the trend was opposite for BJH pore volume and pore diameter. All the anode-cathode combinations sludge was meso-porous in nature. Thermo-gravimetric analysis showed that the heating value of sludges was about one-tenth of the Indian coal.

Solid waste (sludge) generated during EC treatment of dye wastewater with SS and Al-electrodes was recycled by heating the solid waste at different temperatures under controlled condition to produce nano composite and nanomaterials materials (NCMs and NMs), respectively. Characterization by PXD, FE-SEM and EDX, TEM, BET and X-ray photoelectron spectroscopy (XPS) confirmed that NCMs synthesized from SS-EC sludge contains iron, chromium, nickel and oxygen in the form of α-Fe_2O_3 (metal: oxygen= 40:60), $(Fe,Cr,Ni)_2O_3$ and trevorite $NiFe_2O_4$, (Ni,Fe,Cr) $(Fe,Cr,Ni)_2O_4$ (metal: oxygen = 43:57). Similarly, active aluminum oxide nanoparticles (NPs) in different nano-crystalline forms γ-, α- and β-alumina's (Al_2O_3) were obtained from Al-EC sludge when incinerated at different temperatures. Degradation studies using the recycled NCMs and NMs on dye wastewater showed high removal efficiency and good adaptability.

ACKNOWLEDGEMENTS

First and foremost, my greatest regards to the almighty GOD for bestowing upon me the courage to face the complexities of life and complete this thesis successfully.

I would like to express my heartfelt gratitude and thanks to my supervisor Dr. I. D. Mall, Professor, and Dr. V. C. Srivastava, Associate Professor, Department of Chemical Engineering, Indian Institute of Technology, Roorkee for their proficient guidance, advice, and supervision throughout this investigation. I unfaltering acknowledge their infinite patience, ever-lasting support and the belief in me. They provided me unflinching encouragement and support. Their guidance helped me in all the time of research and writing of this thesis.

I wish to express my sincere thanks to Dr. Tapas Kumar Mandal, Assistant Professor Department of Chemistry, Indian Institute of Technology, Roorkee, for his expert advice and guidance during some part of my research work. I wish to express my warm and sincere thanks Prof. I. M. Mishra, Department of Chemical Engineering and Prof. S. C. Sharma, Department of Mechanical Engineering, IIT Roorkee, Roorkee for their invaluable and unconditional support. His inspiration provided me the strength to carry out this research. I wish to express my sincere gratitude to the members of advisory committee namely Prof. Pradeep Kumar, Prof. Shri Chand and Prof. Bakash Mohanty for their encouragement and critical input to work hard during the course of my Ph.D. degree.

I would like to take this opportunity to put on record my gratitude to Head, Prof. V. K. Agarwal, Department of Chemical Engineering, IIT Roorkee for providing the various basic facilities for carrying out the present research work. My sincere thanks are also for Prof. Basheshwar Prasad, Prof C. B. Majumder, Prof. Shishir Sinha, Dr. Vimal Kumar and all faculty members of the Department of Chemical Engineering, IIT, Roorkee for their kind assistance and encouragement.

I am thankful to the Council of scientific Industrial Research (CSIR), Government of India for providing Senior Research Fellowship (SRF) during the period of research.

I am thankful to the technical staff of the laboratory Shri Rajendra Bhatnagar and Shri Sisodiya for their continuous help. I expressed my thanks to Shri Satpal Singh, Shri Arvind Kumar and Shri Vipin Ekka for their helped me during the course of my experimental work. Finally my warm thanks to Shri Arun Kumar, Shri Shadab Ali, Shri Sudesh and other non-teaching staff of the Department of Chemical Engineering for their help and support.

I wish to thank my seniors Dr. J. P. Kushwaha, Dr. C. K. Thakur, Dr. V. Subbaramaiah, and Mr. Hiwarkar Ajay, my friends/colleagues Mr. Praveen Singh, Jay Singh Meena, Abhishek Baheti, Abhishek Pathak, Ajendra Singh, Ashish Upadhya, Nishant Gautam, G. Naresh, Nitin Singh, Dr. Shilpi Verma, Bhumika Agarwal, Mrs. Payal Chaudhari, Joyati Kaushik, and Geeta Saini and my brother for their help and support.

I am also very thankful to Ms. Indira Mall and Ms. Kanchan Lata Srivastava and their family members for their cooperation and warm-hearted nature, whenever I went to their residence.

I am hearty thankful to my younger sister Shivani and Monika Pundir who always care my twin baby during all time in my research work. I wish to thank everybody with whom I have shared experiences in life and specially those who played a significant role in my life.

I would like to express my sincere love and affection to my parents Late Shri Mahipal Singh father, Smt Surendari Devi mother and parents in lows Shri Sadhu Singh father in low, Smt Omwati Devi mother in low for their persistent love, support and encouragement in my life. I never forget my father desire for me. A feeling of my father always lives in my heart and encourages me from my childhood days. I have no any suitable word for my mother, for her everlasting love to me. She is simply perfect.

I am extremely conscious of the crucial role played by my husband Mr. Shriom Singh during my research work. Without his support it is simply impossible for me to complete my doctoral research work. I thank his copiously. I am also thankful for my beloved twin girl baby Nanhi and Vashu Singh for her patience always wait for me and search always her mother from outside the door and window.

Finally I would like to thank everybody who contributed to the successful realization of this thesis, and wish express my apology for not mention by them all by name.

May, 2014 **SEEMA SINGH**

Roorkee

CONTENTS

LIST OF FIGURES

LIST OF TABLES

ABBREVIATIONS AND NOTATIONS

Abbreviations

ADMI	Association of diagnostics manufacturers of India
AFM	Atomic fluroscence microscopy
TFC	Thin-film composite
AFM	Atomic force microscope
Al	Aluminum
ANOVA	Analysis of variance
An-SBR	Anaerobic sequencing batch reactor
AOMBR	Anaerobic sequencing batch reactor plus oxicmembrane bioreactor
AOP	Advanced oxidation processes
BFA	Bagasse fly ash
BBD	Box-behnken design
BET	Brunauer-Emmett-Teller
BG-4	Basic green 4
BJH	Barrett-Joyner-Halenda
BOD	Biological oxygen demand
BS	Bench scale
C.U.	Color unit
CCD	Central composite design
CE	Current efficiency
CMC	Carboxyl methyl cellulose
COD	Chemical oxygen demand
CPCB	Central pollution control board
DBE	Dye-bath effluent
DC	Direct current
DF	Degree of freedom
DE	Decolorisation efficiency
DLS	Dynamic light scattering
DO	Dissolve oxygen

DOC	Dissolve oxygen chemical
DTA	Derivative thermal analysis
DTG	Differential thermogravimetric analysis
DY	Disperse yellow
EAOPs	Electrochemical advance oxidation process
EBT	Eriochrome black T
EC	Electrochemical
EDAX	Energy-dispersive x-ray analysis
ELC_e	Experimental electrode consumption
ELC_t	Theoretical electrode consumption
ENC	Energy consumption
EPA	Environmental protection agency
ESCA	Electron spectroscopy with chemical analysis
FA	Fly ash
Fe	Iron
FESEM	Field emission scanning electron microscope
FTEC	Flow-through electro-coagulation
FTIR	Fourier transform infrared spectroscopy
GAC	Granular activated carbon
GCMS	Gas chromatography-mass spectroscopy
GDP	Gross domestic product
HPLC	Higher performance liquid chromatography
HPLC-MS	Higher performance liquid chromatography-mass spectroscopy
HPTLC	High performance thin layer chromatography
HRAP	High rate algae ponds
HRMS	Higher resolution mass spectroscopy
HU	Hazen units
IC	Inorganic carbon
ICDD	International centre for diffraction data
ISPCH	Industrial safety and pollution control handbook
IUPAC	International union of pure applied chemistry
JCPDS	Joint committee on powder diffraction standards

LA	Organic polymer flocculant
LC–MS	Liquid chromatography-mass spectroscopy
LMG	Leucomalachite green
MBR	Membrane biological reactor
MF	Microfiltration
MINAS	Minimal national standards
MLSS	Mixed liquid suspended solids
MP	Monopolar
MR	Methyl red
MV	Methyl Violet
MWCO	Molecular weight cut-off
NCMs	Nano-composite materials
NDIR	Non dispersive infra-red
NF	Nano-filtration
NMs	Nanomaterials
OG	Orange-G
ORP	Oxidation reduction potential
PAC	Polyaluminium chloride
PB	Plackett–Burman
PFC	Polyferric chloride
PS	Polysulfone
PS	Pilot scale
PSD	Particle size distribution
PTFE	Poly ethyl tetra ethyl
PVA	Polyvinyl alcohol
PXRD	Powder x-ray diffraction techniques
RB	Reactive blue
RE	Removal efficiency
RO	Reverse osmosis
RO-XLE	Extra-low energy reverse osmosis
RSM	Response surface methodology
SAED	Selected area electron diffraction

SBR	Sequencing batch reactor
SEM	Scanning electron microscopy
SNF	Submerged nano-filtration
SS	Stainless steel
STW	Synthetic textile wastewater
TC	Total carbon
TDS	Total dissolve electrode
TEM	Transmission electron microscope
TGA	Thermogravimetric analysis
TMP	Trans-membrane pressures
TOC	Total organic carbon
TSS	Total suspending solid
TW	Textile wastewater
UASB	Un-aerobic sludge blanket
UF	Ultrafiltration
UHV	Ultrahigh vacuum
UNICEF	United nations children's fund
UV	Ultraviolet
VCF	Volume concentrating factor
XPS	X-Ray photoelectron spectroscopy
XRD	X-ray diffraction

Notations

A	Area of electrode
A	Current density
Å	Average pore width
B	Time
C	Gap
C_f	Final concentration
C_o	Initial concentration
D	Temperature
E	pH

F	Faraday's constant
F	Salt
g	Electrode gap
I	Current
j	Current density
k	Pseudo-first order rate constant
k_h	Heterogeneous rate constant
m	Salt concentration
M_w	Molecular weight of anode
n	Number of involved variables
pH	pH_o
pH_{PZC}	Zero charge
p_o	Saturated vapor pressure
Q_1	Liquefaction
R^2	Correlation coefficient
r_k	Kelvin's radius
S_{BET}	Surface area
t	Time
T	Temperature
t_{EC}	Electrochemical treatment
T_{max}	Maximum weight loss temperature
U	Cell voltage
V	Volume
v	Volume of gas adsorbed
Vapp	Applied voltage
v_m	Equilibrium pressure
V_p	Pore volume
X_1	Current density
X_2	Time
X_3	pH_o
X_i	Level of the independent variable
Y_1	Percentage of COD removal

Y_2	Percentage of Color removal
Z	Chemical equivalence
β_i	Linear coefficient
β_o	Model intercepts
κ	Conductivity
λ_{max}	Wave length

Greek letters

α	Alpha
β	Beta
γ	Gamma
θ	Wetting angle
σ	Surface tension

Chapter-I

INTRODUCTION

1.1. GENERAL

Social and economic demands of increasing population have led to rapid industrialization in India. Fast industrialization, increasing population and unplanned urbanization cause large scale water pollution. This puts enormous challenge to provide clean water for drinking, agricultural and industrial use. Most of the industries produce wastewater containing large number of chemicals in quantities much beyond the toxic limits. Textile industries are one of the largest exploiters of complex chemicals and water during various stage of processing such as preparation, dyeing, finishing, sizing, etc. [UNICEF, 2008]. In developing countries particularly south Asian countries, approximately 35% of the industrial wastewater is accounted by the textile industry wastewater [World Bank, 2005]. Most of the textile industries in India are located in Ludhiana, Kanpur, Coimbatore, Mumbai, Surat and Ahmadabad. In addition to this, large number small dying and printing industries are located in different parts of countries and are located in particular region. Textile industries generate huge volume of high strength wastewater. The use of different chemicals and refractory dyes makes textile industry wastewater highly polluting in nature [Kim et al., 2004]. High chemical oxygen demand (COD), burly color, dissolved solid, highly fluctuating pH and poor biological degradation make the textile industry wastewater carcinogenic, toxic, mutagenic and teratogenic to various fish and microbiologic species [Mall et al., 2006; Singh et al., 2013a]. Various compounds present in textile wastewater resist light penetration in the receiving bodies of water and disturb the ecosystem [Szpyrkowicz et al., 2001; Wu et al., 2012]. Therefore, it is necessary to treat textile industry effluents before their discharge into aquatic bodies [Rangel et al., 2013].

1.2. TEXTILE INDUSTRY AND PROCESS

1.2.1. Indian Textile and Dying Industry

Textile industry contributes about 14% of industrial production in India, which is 4% of the gross domestic product (GDP) of India [MoT-GoI, 2013]. Textile production in India is estimated to be around 7% of the world production. India is the second largest producer of dyes and dye intermediaries in Asia

[www.fibre2fashion.com., 2010]. Indian textile industry comprises of organized sector (around 50 units) and unorganized sector comprising of a large number of small manufacturers (around 1,000 units) [www.ipomonitor.net]. Cotton industry, man-made fiber and filament yarn industry, wool and woolen textiles industry, sericulture and silk textiles industry, handlooms, handicrafts, jute and jute textiles industry, and textiles exports are the major sub-sectors of Indian textile industry. India's planning commission envisages that the exports of textiles and clothing will be 64.11 billion $ by the end of March, 2017 [MoT-GoI, 2013].

Various other industries such as leather, cosmetic, food and pharmaceutical industries use various types of dyes. There are more than 100,000 commercially available dyes with annual production of over 7×10^5 tons [Khandegar and Saroha, 2013]. On the basis of chemical structure and their application, dyes can be classified into various classes. Table 1.2.1 shows the classification of dyes on the basis of their usage and application [Robinson et al., 2001; Christie, 2001].

1.2.2. Processing steps in textile industry

Textile dyeing industries are classified on the basis of raw materials being used and solid waste and/or wastewater generation. These are cotton, woolen and synthetic fiber industries and dry and/or wet processing industries, respectively [ISPCH 1995; USPEA, 1997]. Dry processing mills generate solid wastes while wet processing textile industries produce wastewater in various stages of operations [USPEA, 1997; Dos Santos et al., 2007]. Most of the textiles dyeing industry have common operation steps broadly classified as pretreatment, dyeing and finishing techniques. Pretreatment process includes sizing, desizing, scouring, washing, and other processes. During sizing, carboxyl methyl cellulose (CMC), polyvinyl alcohol (PVA) and starch are used for minimizing the breakage and providing the strength to the fibers. During desizing, sizing materials are removed whereas during the scouring process, impurities such as waxes, surfactants, fats, etc. are removed from the fiber by using the alkali solution. Unwanted color from the fiber is removed by using the sodium hypochlorite and hydrogen peroxide during the bleaching step. Mercerizing uses concentrated alkaline and acid solution to increase luster, fiber appearance and dye-ability before the dyeing process. Dyeing process mainly aims at producing colored fabric under certain conditions. Dyeing process contains residual dyes, auxiliary chemicals, by-products cleaning solvents like as oxalic acid. Large amount of water is required during dyeing and rinsing steps. Finishing processes use a number of finishing agents for softening,

cross-inking and waterproofing the finished fabric [Gregory 2000; Gupta and Suhas, 2009]. A typical textile dyeing process along with chemical constituents used during the process and the characteristic of wastewater generated is shown in Figure 1.2.1. The composition of wastewater depends upon the water and chemicals used in various processes. A large numbers of chemicals such as acids, alkali, solvents, starch, dyes, bleaching chemicals, enzymes, resins, oils, waxes, etc. are used in textile mills which also get discharged in the effluent also [Dos Santos et al., 2007; Verma et al., 2007; Verma et al., 2011].

1.3. DISCHARGE QUALITY AND HARMFUL EFFECTS OF DYE BEARING WASTEWATER

Textile industries widely use organic dyes in finishing and coloring processes. About 20% of these dyes enter into the aquatic environment through discharge of effluents from treatment plants [Arslan et al., 2000; Mane et al., 2007a, b]. Wastewater generated from dyeing and finishing processes in the textile industries contains suspended solids, high amount of dissolved solids, un-reacted dyestuffs (color) and other auxiliary chemicals used in the various stages of dyeing and other processing [RajKumar et al., 2006]. Dyes are stable compounds with low biodegradability and are carcinogenic in nature [Yang and McGarrahan, 2005]. Textile wastewater contains a composite mixture of chemicals due to the complexity of different stages of different processes. Main characteristic of textile industries wastewater as reported in the literature is compared in Table 1.3.1. Discharge of colored effluents containing dyes reduces the photosynthetic activity in aquatic environment, thus reducing the quantity of oxygen available in the water for use by the aquatic life. Also, toxic nature of the dyes has detrimental effect on liver, gill and kidney of aquatic animals [Namasivayam et al., 2001; Mall et al., 2005; Kariminiaae-Hamedaani et al., 2007; Singh et al., 2013b].

Triphenylmethane is a colorless crystalline hydrocarbon having the formula $(C_6H_5)_3CH$. Many synthetic dyes contain triphenylmethane group and are called as triarylmethane dyes. Basic green 4 (BG), bromocresol green, methyl violet, crystal violet, victoria blue, brilliant green, ethyl violet, pararosaniline, cresol red, bromopheno1blue, methyl green, basic fuchsin, etc. are some of the most commonly used triphenylmethane or triarylmethane dyes.

Table 1.2.1. Characteristic of dyes and application

Class	Chemical types	Principal substrates	Method of Application
Direct	Phthalocyanines, Poly azo, Stilbene and Oxazine	Cotton, Rayon, nylon, paper leather	Applied for neutral and slightly alkaline bath
Disperse	Azo, Anthraquinone, Benzodifuranone and Nitro	Polyester, acrylic and plastics, polyamide acetate	Fine dispersion at high temperature and pressure
Basic (Cationic)	Diphenylmethane, Azo, Cyanine, Xanthenes, Anthraquinone and	Modified nylon, poly-acrylonitrile, polyester	Applied on acidic dye-baths
Acid	Azo, Anthraquinone, Azine, xanthenes, Nitro	Nylon, wool, silk, paper. and leather	Applied on neutral for acidic dyestuff
Azoic	Azo	Cotton, rayon,-cellulose, polyester	Fiber impregnated with coupling component
Mordant	Anthraquinone and Azo	Wool, leather	Conjunction with crystals
Solvent	Tri-phenyl-methane, Anthraquinone, Azo, and Phthalocyanine	Plastics, gasoline, waxes, stains, oils inks, varnish	Dissolution on the substrate
Vat	Anthraquinone, Indigoids	Cotton, rayon, and wool	Water-insoluble react by reduction and oxidation
Reactive	Azo, Anthraquinone, Oxazine	Cotton, wool, silk, and nylon	Bind covalently on heat and pH (alkaline)

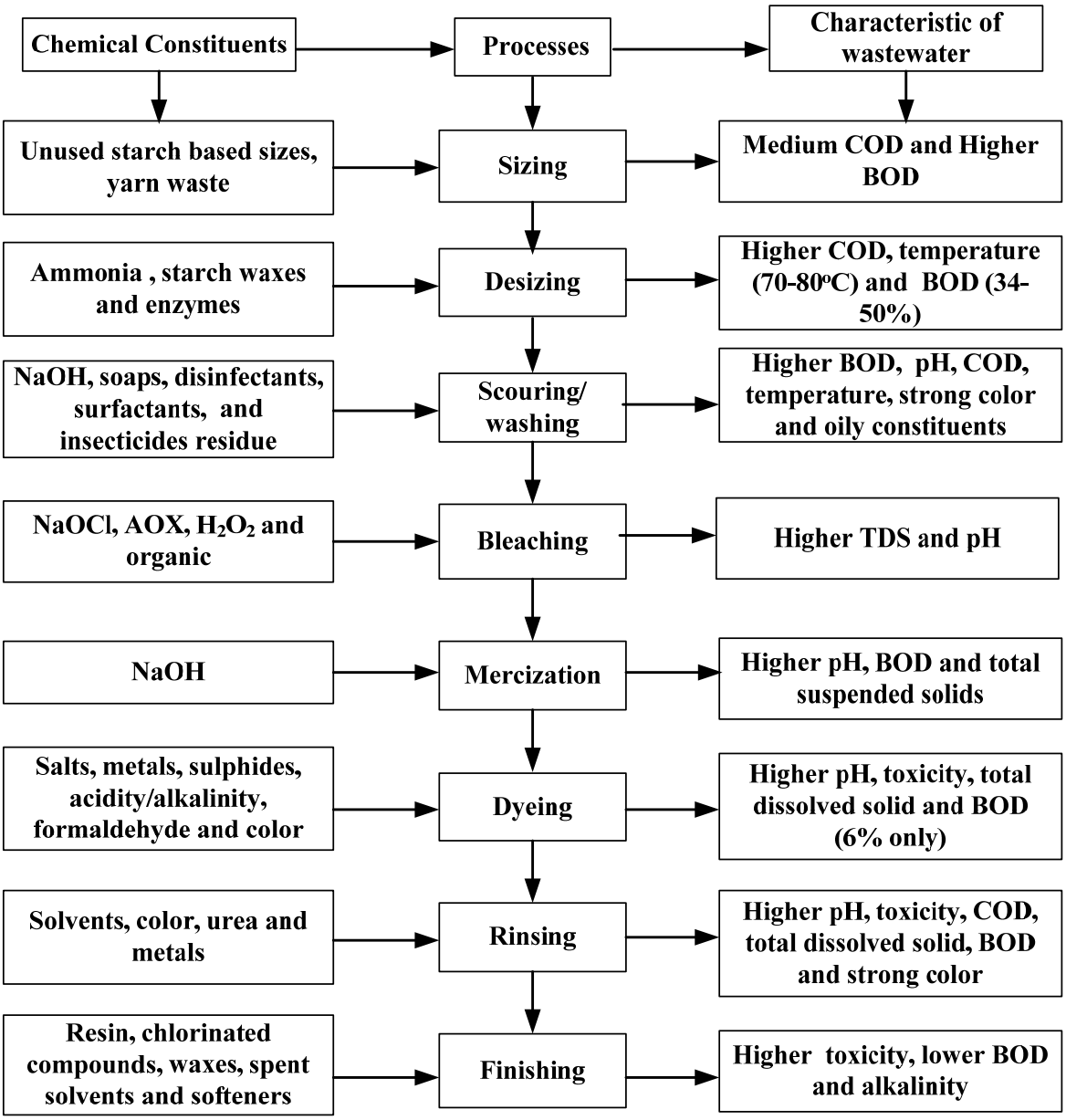

Figure 1.2.1. Chemical compositions and major pollutants generating various steps in textile manufacturing industry [USEPA, 1997; Dos Santos et al., 2007; Charoenlarp and Choyphan, 2009].

Table 1.3.1. Characteristic of textile dye bearing wastewater as reported in the literature.

Types of wastewater	Color	COD (mg/L)	TSS (mg/L)	Turbidity (NTU)	TDS (mg/L)	pH	References.
Textile wastewater	-	3422	1112	5700	-	6.9	Bayramoglu et al., 2004
Textile wastewater	-	2276		-	47.9	11.2	Golob et al., 2005
Synthetic textile wastewater	-	485	70	1.45 NTU	-	10.6	Zaroual et al., 2006
Textile wastewater	-	2031	102	671 NTU		8.8	Bayramoglu and Arica 2007
Textile wastewater	1460 (ADMI)	1100-4500	-	-	50	5.0-10	Dos Santos et al., 2007
Textile wastewater	-	17980	23980	-	1250	8.7	Rodriduez et al., 2008
Textile wastewater	-	3900	-	240	-	9.3	Pachcoal et al., 2009
Textile wastewater	>300 (C.U.)	50-5000	50-500	-		2.0-10	Lau and Ismali 2009
Dye wastewater	-	278-736	83-354	-	1750-6100	8.3-9.3	Phalakomkule et al., 2010
Dye wastewater	>200 (pt-co)	340	300	130	-	7.8	Merzouk 2010
textile dyes	>350(pt-co)	380	-	-	-	8.5	Kusmierekvar et al., 2011
Textile wastewater	-	5800	-	-	-	10.9	Basha et al., 2012
Dye bath effluent	46600	5660	2.47	-	14.42	6.5	Mondel et al., 2013
Synthetic wastewater	14,40	2900	120	-	12.30	9.75	Singh et al., 2013a

Dyes having triphenylmethane are well known for higher color intensity, brilliant shades and low light fastness [Soloman et al., 2010]. These cationic dyes have positive charge and are used for dying fabrics which have negative charge such as wool, silk, nylon, cotton, etc. [Zhang et al., 2009]. BG [(N,N,N',N'–tetramethyl–4,4'diaminotriphenylcarbenium a tri–phenyl methane] dye is most widely used as a direct dye for coloring jute, wool and silk in textile industry [Janos et al., 2003; Mall et al., 2005; Gregory 2006; Zheng et al., 2012]. Other industries such as leather and paper also use this dye [Crini et al., 2007].

Triphenylmethane dyes such as BG on photo–oxidation via nascent oxygen break into various N–de–alkylated primary and secondary amine derivatives which are similar to carcinogenic aromatic amines [Cho et al., 2003]. BG is sometimes used as antiseptic and fungicide in aquatic and fisheries industry where it easily gets reduced to lipophilic leucomalachite green (LMG) which can induce renal and hepatic tumors in mice and reproductive abnormalities in fishes [Srivastav and Shina, 2004; Sudoval et al., 2007]. Hence, treatment of BG dye is essential before its discharge into water bodies [Singh et al., 2013a].

Dyes are considered as toxic, mutagenic, carcinogenic and teratogenic in nature. Dyes are known to affect kidneys, liver, immune systems and reproductive functions of living beings [Srivastav and Shina, 2004]. Chronic effect of dye wastewater can cause loss of hair, decrease in appetite and increase anemia problem. Dyes also affect the central nervous system, bone marrow, liver and heart. Some of the azoic and acidic dyes have been linked to bladder cancer in humans. Most of the known dyes produce toxic substances inside living organisms by the reduction process [Dos Santos et al., 2007]. Similarly, decomposition derivatives of dyes are toxic to the aquatic life [Mall et al., 2006b; Khandegar and Saroha 2013]. Azo and nitro dye increase the concentration of carcinogenic amines in the aquatic bodies [Mall et al., 2005; Singh et al., 2013b].

Dye bearing wastewater is very harmful and toxic for both human being and aquatic environment if released without proper treatment. Figure 1.3.1 summarizes the direct and indirect toxic effects of textile dyes industries wastewater. Untreated textile effluents disturb the ecosystem of receiving water bodies like lakes and rivers by changing the color and decreasing the light penetration [Khaled et al., 2009; Merzouk et al., 2010]. Moreover, color substances generate the eutrophication problem by

biological and chemical assimilations; accelerating microtoxicity and genotoxicity by consuming dissolved oxygen and prevent re-oxygenation [Forgacs et al., 2004].

Considering toxic and harmful nature of textile industry wastewater, Central pollution control board (CPCB), Ministry of Environment and Forest, Government of India has set minimal national standards (MINAS) for the discharge of effluents generated in textile industry. Because of the difference in the raw materials, dyes, technology and products, the standards of the wastewater emitted by different types of textile units are different. MINAS for dye and dye intermediate, textile, cotton textile (composite and processing) and man-made fiber industries are given in Table 1.3.2.

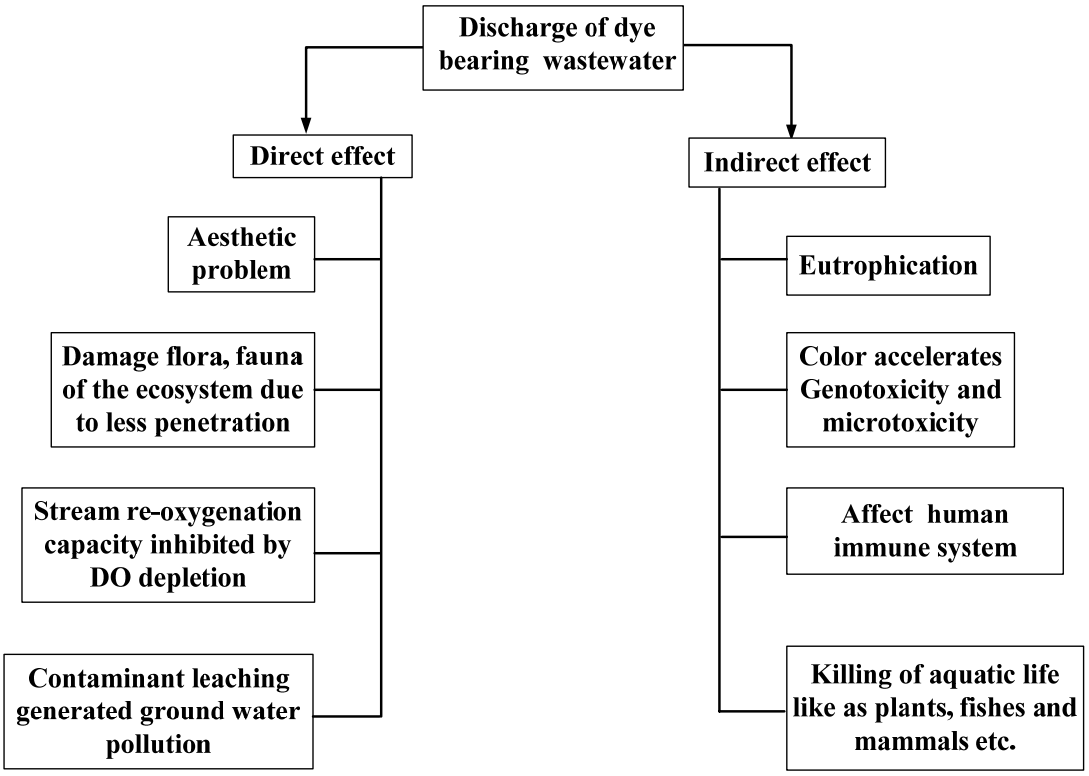

Figure 1.3.1. Schematic representation of direct and indirect effect of textile dye bearing wastewater on the environment.

1.4. METHODS USED IN TEXTILE WASTEWATER TREATMENT: PROBLEM AND PROSPECTIVE

Different treatment technologies have been used for treatment of dye bearing wastewater (Table 1.4.1). These include biological, physical and chemical methods and their various combinations [dos Santos et al., 2007; Ozkan-Yucel and Gokcay, 2010]. Physico-chemical methods such as coagulation with alum, ferric chloride, magnesium chloride and lime [Verma et al., 2011]; adsorption on rice husk [Srivastava et al., 2009a], activated coal fly ash [Lakshmi et al., 2009]; chemical oxidation [Hayati et al., 2011]; advanced chemical oxidation such as UV/H_2O_2, O_3 [Elmorsi et al., 2010]; photocatalytic degradation [Hachem et al., 2001; Daneshvar et al., 2004a;]; Fenton's processes [Martins et al., 2010], etc. are most widely researched methods for textile wastewater treatment. Similarly, various techniques have been reported in literature for removal of triphenylmethane basic dyes such as BG from aqueous solution. These include ozonation [Zhou et al., 2012; Marin et al., 2012], photocatalysis [Chen et al., 2007], adsorption [Huo et al., 2012; Ali, 2012] and coagulation–flocculation [Minhalma et al., 2001; Deng et al., 2011].

Biological treatment methods like as aerated lagoons, trickling filter, activated sludge process, anaerobic filters, sequencing batch reactor (SBR), anaerobic sludge blanket (UASB) reactor, etc. [Chen et al., 2009; Huan et al., 2011] have been reported for treatment of dye bearing effluents. Occasionally, to improve the treatment efficiency pre-treatment strategies like wetlands are also used [Aghaie-Khouzani et al., 2012]. Biological treatment of dying wastewater is cheaper than other methods, but it cannot be applied for treatment of most textile wastewaters due to the toxicity of most commercial dyes to the organisms used in the biological treatment methods [Robinson et al., 2000].

Some of the treatment methods are not effective in removing color from dying wastewater. Physico-chemical methods also have some disadvantages like requirement of higher amount of chemicals, high operation cost and large amount of sludge generation. Advantages and disadvantages of each method have been extensively reviewed in literature [He et al., 2003; Singh and Arora, 2011].

Electrochemical (EC) treatment methods effectively remove the dyes from wastewater and are easy to operate and cost effective [Masion et al., 2000; Szpyrkowicz et al., 2005; Canizares et al., 2006a].

Table 1.3.2. MINAS for dye and dye intermediate industry, textile industry, cotton textile industries (composite and processing) and man-made fiber industry.

Parameter	Concentration not to exceed milligrams per liter (except for pH, temperature and bio-assay)				
	Dye and dye intermediate industry	**Textile industry**	**Cotton textile industries (composite and processing)**	**Man-made fiber industry (Synthetic)**	**Man-made fiber industry (Semi-synthetic)**
pH	6-9	6 - 9	5.5-9.0	-	5.5-9.0
Temperature	Not exceed 5°C above the ambient temperature of the receiving body	-	-	-	-
Color (Hazen Unit)	400	-	-	-	-
Suspended Solids	100	100	100	100	100
BOD (3 days at 27^{o}C)	100	30	150	30	30
COD	-	250		-	-
AOX	-	1	-	-	-
Oil and Grease	10	10	10	-	-
Phenolics as C_6H_5OH	1	1	5	-	-
Sulfide	-	2	2	-	-
Cadmium as Cd	2	-	-	-	-
Copper as Cu	3	-	-	-	-
Mercury as Hg	0.01	-	-	-	-
Nickel as Ni	3	-	-	-	-
Zinc as Zn	5	-	-	-	1
Total Chromium as Cr	2	2	2	-	-
Bio-assay test	90% survival in 96 hours	-	90% survival in 96 hours	-	-
Coliform	-	400 MPN/100 ml	-	-	-

Source: http://www.cpcb.nic.in/dye.pdf , http://www.cpcb.nic.in/Industry-Specific-Standards/Effluent/500.pdf, http://www.cpcb.nic.in/Industry-Specific-Standards/Effluent/412.pdf and http://www.cpcb.nic.in/Industry-Specific-Standards/Effluent/402.pdf.

Table 1.4.1. Various methods for dye bearing wastewater treatment.

Treatment Methods	Method Conditions	Advantages	Disadvantages	Reference
Adsorption	Removal occurred on the Solid surface	Used on wide variety of dyes remove	Difficulty in regeneration and costly disposal off	Mall et al., 2006a
Chemical coagulation/ flocculation	Coagulant/flocculants addition	Good color removal efficiency and economically feasible	Sludge generation	Verma et al., 2012; Rong et al., 2014
Ozonation	Initial alkaline condition at low temperature	Oxygen demanding matter reduces	Higher cost, highly corrosive rate	Robinsons et al., 2001
Fenton Process	H_2O_2-Fe(II) used in oxidation	Decolorization of soluble & insoluble dyes	Sludge generation and handling	Meric et al., 2004; Thomas et al., 2014
Ion exchange	Ion exchange resin	Easy generation	Not effective on all types of dyes	Hai et al., 2007
Membrane filtration	Physical separation	Removal of all type of dyes	concentrated sludge, high cost	Rong et al., 2014
Biological Process	Degradation Microbiological based	Environmental friendly	Slow process, need of nutrient, sludge production	Pakshirajan and Kheria 2012
Electrochemical	Anode cathode materials used for removal	Good removal efficiency	Sludge production, less electrode reliability	Singh et al., 2013a,b,c.

Figures 1.4.1a and b show the number of research publications and citations for various processes employed for the treatment of dye bearing wastewater for last 20 years (1995-2014). It is clear that researchers gave most attention on electrochemical and various advance oxidation processes.

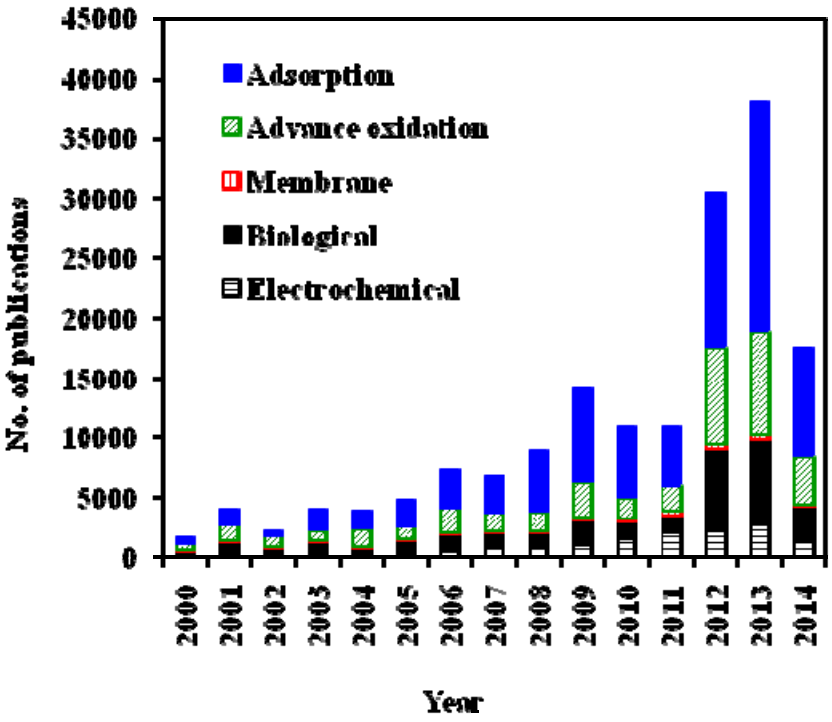

(a)

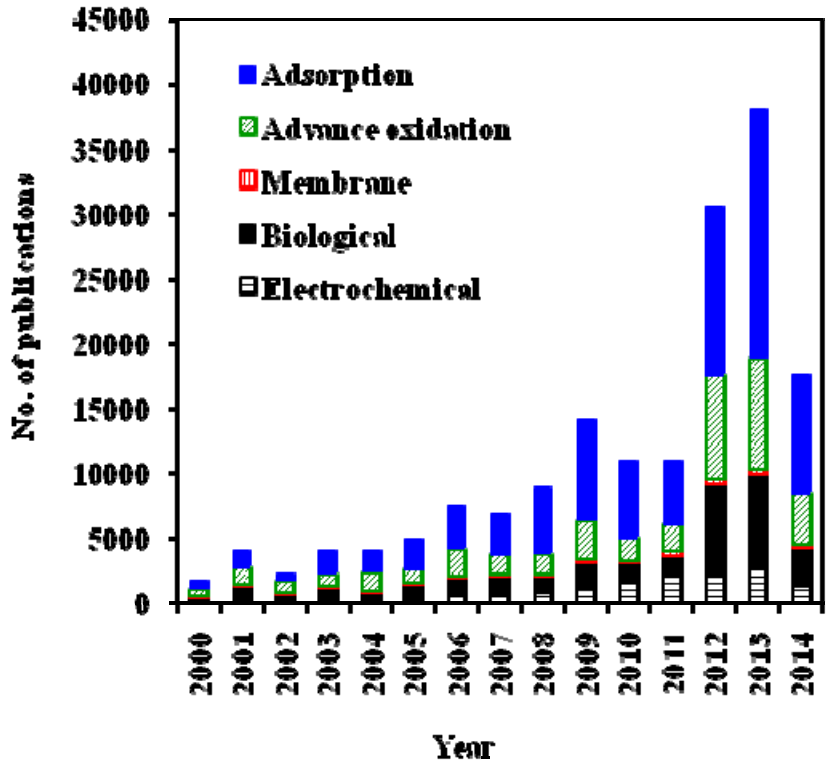

(b)

Figure 1.4.1. (a) Number of research articles published and (b) Number of citations on dye bearing wastewater treatment by adsorption, biological treatment, advanced oxidation and electrochemical process (Scopus database searched on March 30th, 2014).

1.5. ELECTROCHEMICAL TREATMENT

Electrochemical (EC) treatment is considered to be an effective technique for treatment of textile wastewater and has received great attention for treatment of textile dye bearing wastewater in the last one decade [Zhuo et al., 2011]. EC method is comparatively inexpensive and is characterized by its easy operation, reduction in sludge volume and equipment costs.

EC method utilizes metal electrodes as anode and cathode. Anode produces the coagulant via dissolution of electrodes by electrolytic reaction. Finally the coagulant turns into precipitates in the form of metal hydroxides at an appropriate pH level [Coskun et al., 2012]. Electrode potential, surface properties of electrode, type of electrolyte, and type of transient intermediates formed affect the EC degradation of dyes [Keith and Carter, 2013]. Various researchers have extensively been used EC methodology for different kinds of wastewater such as tannery wastewater [Feng et al., 2007], electroplating and chemical mechanical polishing [Adhoum et al., 2004; Drouiche et al., 2007], pulp and paper mill industry wastewater [Mahesh et al., 2006], baker's yeast wastewater [Kobya and Gengec 2012], dairy wastewater [Kushwaha et al., 2011] and slaughterhouse wastewater [Kobya et al., 2006a].

In EC process, metal ions get generated from the dissolution of metal electrodes, hydroxyl ions get generated by the electrolysis of water and hydrogen gas gets evolved at cathode. Generated metal ions interact with hydroxyl ions to form insoluble metal hydroxide that adsorbs pollutant during settling [Singh et al., 2013b,c]. Colloids formed during the EC process and their stability determines the mechanism of the treatment. Stability of the colloids present in the suspension can be explained by the electrokinetic charge (zeta potential). Schematic representation of role of zeta potential in colloids removal during EC process is shown in Figure 1.5.1. Generally the colloids present in wastewater have negative charge and they repel each other [Holt et al., 2002]. This prevents their agglomeration and removal from wastewater by flocculation and settling [Vaghela et al., 2005]. Generally, two mechanisms have been proposed in the literature regarding EC method of treatment by metal electrodes. First involves removal of dissolved matter by electro-coagulation by released metals ions. Second define the opposite charge interaction between positively charge metals ions and negatively charge impurities present in the wastewater [Canizares et al., 2007; Singh et

al., 2013c; Singh et al., 2013d,]. These mechanisms can be better understood by measuring the zeta potential of colloids present in the solution during the EC treatment. Zeta potential study in EC treatment helps in understanding the effect of factors that influences the treatment process.

Local dyers in small towns produce huge amount textile printing dye-bath effluent (DBE) during dying of textiles, woolens, etc. in small dye bath, and discharge them without any treatment to open channels. Our research group previously studied treatment of DBE using SS and Al electrodes separately[Mondal et al., 2012; Mondal et al., 2013] with main focus of these studies being operating parameter optimization. However, measurement of zeta potential and particle size distribution (PSD) of colloids present in the solution during the treatment were not studied.

Yuksel et al. [2013] performed comparative study on EC treatment of a reactive orange 84 dye solution and a textile wastewater by stainless steel (SS) and iron (Fe) electrodes. It was found that the EC process with SS electrodes not only consumed less electrode material and energy but also produced less amount of sludge as compared to Fe electrodes under similar experimental conditions. The operating cost with SS electrodes was about 1.3 times as low as compared to Fe electrode. Thus, the performance SS electrode was found to be much better than Fe because of lower dissolution rate, less operating cost and other operational advantages. Akbal and Camci [2011] reported Al to be more effective than Fe electrode in terms of decolorization efficiencies and operating costs for decolorization of levafix brilliant blue E-B. However, Arslan-Alaton et al. [2009] reported electrocoagulation treatment of simulated reactive dye bath effluent with Al and SS electrodes where SS was found to be more effective as compared to Al. Thus, Al and SS have distinct advantages and disadvantages for treatment of various types of wastewaters depending upon the characteristics (particularly pH) of the wastewater to be treated.

1.6 OBJECTIVES OF THE PRESENT WORK

Based on the research gaps identified in chapter II, following aims and objectives were set for the present work:

1. Multi-step optimization of operating parameters during EC treatment of synthetic textile wastewater (STW) containing basic dyes with aluminum electrode

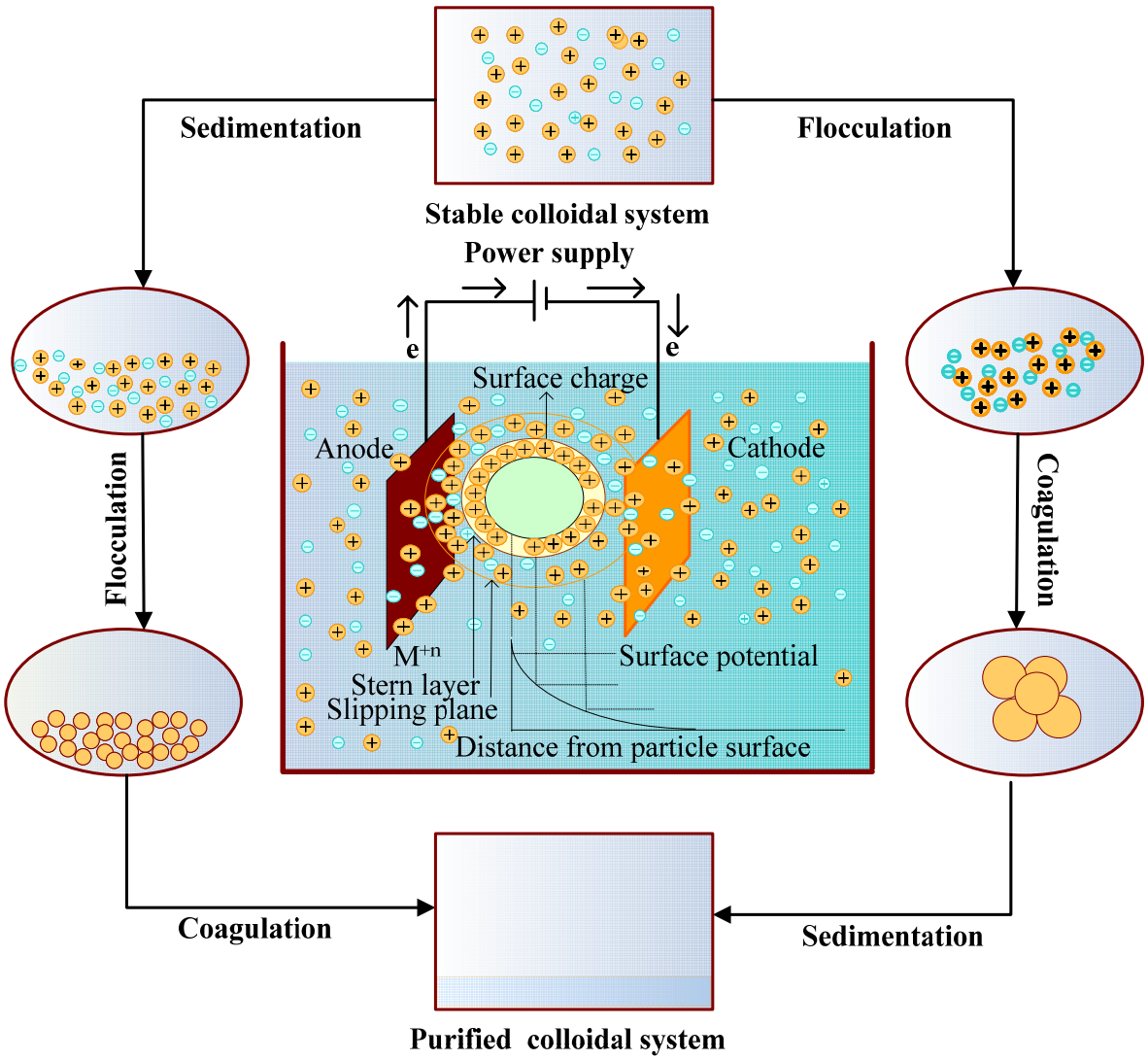

Figure 1.5.1. Electrochemical treatment of dye bearing wastewater.

- To perform multi-step optimization using Plackett-Burman design, Steepest accent/descent method and Box-Behnken design
- To select best values of operating parameters condition among six operating parameters namely current density (j), time (t), electrode gap (g), temperature (T), pH_o and salt concentration (m) for maximizing chemical oxygen demand (COD) and color removal efficiencies.

2. Dye degradation mechanism of basic dye during EC treatment with aluminum electrode

- To study the effect of zeta potential during basic green 4 dye degradation with variation in current density, pH, and initial dye concentration.
- To study the performance in terms of color, COD and total organic carbon (TOC) removal efficiencies; and energy consumption (ENC) and electrode consumption (ELC).
- To identify intermediates formed at various treatment times by mass spectroscopic and chromatographic techniques and to explain degradation mechanism by different possible schemes.

3. EC treatment of actual dye bearing effluent (DBE)

- To perform EC treatment of DBE using aluminum (Al) and stainless steel (SS) electrodes in various anode-cathode combinations in a batch EC reactor.
- To study the effect of operating parameters on the removal efficiency in terms of color, COD, TOC and turbidity; and other performance parameters such as ENC and ELC.
- To study the treatment mechanism via zeta potential study and PSD study at different pH_o values.

4. Recycling and disposal of EC sludge

- To perform physio-chemical and textural characterization, and thermal degradation analysis of EC residues.
- To convert EC sludge generated by aluminum and stainless steel electrodes into nanocomposite (NCMs) and nanomaterials (NMs) by thermally heating method.
- To characterize the NCMs and use them as catalyst for degradation of dyes.

Chapter –2

LITERATURE REVIEW

2.1. GENERAL

Various conventional and newer treatment techniques which include physico-chemical, biological, membrane and advance oxidation including electrochemical methods have been reported in the literature for the treatment of dye bearing wastewater. This is including.

- A critical review of physico-chemical methods for the treatment of dye bearing wastewater has been presented.
- Literature on biological treatment methods has been reviewed.
- Treatment by membrane separation method has been critically reviewed.
- Literature on electrochemical treatment of dye bearing wastewater and its various aspects such as role of zeta potential and sludge reutilization has been reviewed.
- Research gaps in the previous research have been identified and reported at the last section of this chapter.

2.2. PHYSICO-CHEMICAL METHODS

Various physicochemical treatment methods such as filtration, coagulation, flocculation and adsorption can be used to treat dye bearing wastewater. These physicochemical treatment methods can be used in form of pre-treatment, main treatment, post treatment depending upon the characteristics of the dye bearing wastewater [Banerjee et al., 2007; Maiti et al., 2007; Sharma et al., 2010; Bassandeh et al., 2013; Hu et al., 2014]. Table 2.2.1 summarizes various research work done on treatment of actual dye in aqueous solution, synthetic dye wastewater and actual dye bearing effluents by various physico-chemical methods such as coagulation, flocculation, adsorption, ozonation, peroxidation and catalysis [Pandit and Basu 2002; Pandit and Basu 2004; Saroha and Khera 2006; Sharma et al., 2008; Sharma et al., 2009; Maiti et al., 2012].

Coagulation and flocculation are frequently used as main and pre-treatment techniques [Leiknes 2009; Albuquerque et al., 2012] for dye removal by addition of chemicals to change the physical state of wastewater and facilitate their removal by sedimentation/flotation and flocculation mechanism. This technique is applicable for suspended or colloidal form of pollutants only. It has been described that some of the metallic hydrolyzing salts such as ferric chloride and ferric sulphate, aluminum sulphate

and prehydrolysed coagulants like as polyaluminum ferric chloride (PAFCl), polyferrous sulphate (PFS) polyferric chloride (PFCl) and polyaluminum chloride (PAC) at lower temperature give better color removal and produce lower volume of sludge [Verma et al., 2012].It has limitations in removal of soluble dyes and disposal of generated sludge [Zahrim et al., 2010]. Few authors are working on preparation of new generation of chemical coagulants for the textile wastewater treatment. Suwandi et al. [2012] reported coagulant derived from enteromorpha polysaccharides (common fouling green algae) and natural rarasaponin modified kaolin for the dye degradation.

Adsorption process is an attractive process that is generally used as a tertiary treatment method. Adsorption process is one of the efficient methods for removal of various types of contaminants from effluent, especially for moderate and low concentrations effluents and has attracted considerable interest recently [Ko et al., 2002; Sharma et al., 2009; Mui et al., 2010]. Adsorption is one of the most popular technologies used for the treatment of dye bearing wastewater [Karcher et al., 2002; Mall et al., 2007; Patel and Vashi, 2010; Ip et al., 2010a,b]. Granular activated carbon (GAC) along with other commercial adsorbents and low cost-adsorbents such as bagasse fly ash, rice husk ash and activated carbons commercial grade (ACC) have been used for the removal of many dyes from aqueous solution [Mall et al., 2005; Mall et al., 2007; Gupta and Suhas 2009; Mezohegyi et al., 2012]. The usage of the adsorbent depends upon the surface area of adsorbent, high affinity, contact time, pH, capacity for the target compound, particles size, temperature, possibility of adsorbent regeneration, etc. [Robinson et al., 2001, Srivastava et al., 2008]. However, maintenance cost, pre-treatment of wastewater and problems during disposal of spent adsorbents are the major limitations of this technology.

Advanced oxidation processes (AOP) use oxidizing agents such as permanganate (MnO_4), hydrogen peroxide (H_2O_2) and ozone (O_3) for dye degradation [Metcalf and Eddy, 2003]. Among these techniques, ozone treatment is most-developed, however, it has limitation on treatment of disperse and vat dyes [Rajeswari, 2000]. Hence, O_3/UV and H_2O_2/UV are considered as alternate to ultraviolet (UV), ozonation and H_2O_2 alone for dye degradation [Kurbus et al., 2002; Thomas et al., 2014]. Fenton methodology is also an example of AOP which is widely accepted in textile dye wastewater treatment.

Every physicochemical method has some limitations such as ozonolysis is highly expensive, Fenton process is best for color and COD reduction but takes longer time and has sludge handling problems, UV/H_2O_2 is not very effective for color and COD reduction because of problems of UV light penetration, adsorption gives good removal of wide

variety of dye but disposal and regeneration are big problems. Despite these limitations, researchers are still working on these methods for removal of limitations. Some of the authors are working on the combine combination of various technique such as ozonation followed by adsorption on activated carbon [Konsowa et al., 2010], combined coagulation/flocculation and adsorption on activated carbon [Furlan et al., 2010], coagulation and combined, GAC/O_3 oxidation process [Qu et al., 2010], etc. so as to overcome limitations of individual methods.

2.3. BIOLOGICAL METHODS

Biological treatment is considered as one of the techno-economically feasible options for industrial wastewater treatment [Padoley et al., 2011; Azadi wt al., 2012; Gibson et al., 2012; Azadi et al., 2013; Tian et al., 2014]. However, most of industries (especially textile dyes) work in different operating conditions for producing the valuable products (wool, cottons, rayon, etc.) and generate huge amount of waste products. Work on the development of economic, effective and feasible biological technique for the treatment of textile effluent has been also reported [Solis et al., 2012]. However most of the dyes are complex and non-biodegradable in nature. Therefore, it is often difficult to biodegrade the dyes either by aerobic or anaerobic process [Chen et al., 2003]. Reife [1996] reported that some of the insoluble higher molecular weight non-biodegradable complex dye molecules accumulate in biomass and inhibit permeation through biological cell membranes causing potential pollution problem during the disposal of that biomass [Pearce et al., 2003; Solisa et al., 2012]. Despite this, several authors broadly classified the bio-degradation of dye wastewater into three categories: aerobic, anaerobic and aerobic-anaerobic treatment [Robinsons et al., 2001; Forgacs et al., 2004; de santos et al., 2007]. The biodegradation of dyes on the basis of solubility and chemical structure of dyes has been reported. Tables 2.3.1 summarize various studies on biodegradation of dyes. Pagga and Brown [1987] reported on degradation of 87 different dyes including acid, direct, basic, mordant, reactive, etc. by activated sludge. It was reported that acid dyes decolorize 95–100% in 42 days, disperse dyes degrade >90% in one day, reactive dye degrade 74% in 4 days. Singh and Arora [2011] categorized the dyes on the basis of biodegradation like ionic and non-ionic dyes (azo and solvent, disperse, and vat dyes). Dye having –OH or –NH_2 groups undergo rapid biodegradation as compared to –CH_3, –OCH_3, –SO_3H, or –NO_3 and un-substituted chromophores. Microbial consortium (Alcaligenes, Bacillus, and Aeromonas species) has been successfully used for 94.3% BOD (biological oxygen

demand) and 95.7% COD removal of basic green 4 and acid violet 17 dye in an up flow immobilized bioreactor [Quezado et al., 2000]. Aerobic microorganism-aided dye degradation in presence of oxygen has been demonstrated as a safe route for reductive cleavage of azo group by reductase enzyme [Ekici et al., 2003].

Textile effluent treatment with anaerobic method is not very well accomplished; however, some studies have been reported in the literature for treatment with anaerobic method [Pakshirajan and Kheria 2012]. 90% color removal from simulated dye wastewater was achieved in a two-phase upflow packed-bed anaerobic bioreactor in which biodegradation was followed by bio-sorption mechanism [Singh and Arora 2010]. Full-scale combined anaerobic–aerobic system was investigated for decolorization and detoxification of textile effluent containing water soluble and insoluble reactive dyes [Farabegoli et al., 2010] however the main drawback was auto-oxidation of amine in aerobic condition formed during anaerobic condition [Pandey et al., 2007].

Many authors have investigated biodegradation of dyes using fungi, bacteria and algae with low concentration of dyes as higher concentration is toxic for living communities [Mohan et al., 2008; Jadhav et al., 2010; Koupaie et al., 2011]. *Phanerochaete Chrysosporium* (white rot fungi) has been used for biodegradation of azo dyes in non specific oxidative enzyme system [Ali et al., 2008; Kadam et al., 2011]. As compared to fungi and bacteria, yeast has limitation for industrial application due to less rapid growth. Algaes are another source of biodegradation of dye followed by bio-sorption and reductive mechanisms. *Chlorella* and *Oscillatoria sp.* have been successfully used for decomposition of more than 30 azo dyes [Wang et al., 2008; Xin et al., 2012]. Few investigators have worked on the combined anoxic and anaerobic–aerobic sequences for treatment of dye-bearing effluent. Bacterial cultures like as Bacillus subtilise, Bacillus firmus, Aeromonas hydrophila, Pseudomonas pseudomallei and Bacillus sp. strain [Arora et al., 2011]; fungal strains such as Phanerochaete chrysosporium, Cunninghamella polymorpha [Solisa et al., 2012; Hai et al., 2012] and yeast strain such as Candida tropicalis and Pichia anemala [Aghaie-Khouzani et al., 2012] have been used for decolorisation of disperse dye under the anoxic and aerobic conditions [Qu et al., 2010]. Aerobic and anaerobic microorganisms are not able to easily biodegrade the textile dye effluents because of microbial communities toxicity towards nitrogenous compounds derived during dye degradation. Moreover, most of the biological treatment technologies require high operating cost, strict operating conditions and large land area for waste disposal.

Table 2.2.1. Studies on the treatment of dye bearing wastewater by physicochemical methods.

Coagulant/ Adsorbent	Waste water	Experimental design & Operating condition	Process performance	Major Inferences	Refs
Coagulation					
Catalyst with $KAl(SO_4)_2 \cdot 16H_2O$	Cotton textile mill	Jar test apparatus; C_o: original conc. mg/L; pH_o: 6.0; T: 90^oC; t: 4 h.	TGA/DTA; 77.9 & 92.85% and 88.62% & 95.4% COD and color removal.	• Thermolysis with $CuSO_4$, $FeSO_4$, $FeCl_3$, CuO, ZnO and PAC followed with coagulation. • Maximum removal was obtained during coagulation as compared to thermolysis.	Kumar et al., 2008a,b
O_3, powder activated carbon (PAC), H_2O_2 and HCO_3	Synthetic textile	Semi-batch reactor; C_o: 200 mg/L; pH: (3–12); T: (18–70)^oC; ozone doses: (164-493 mg/L).	FTIR. 99% color and 95% COD removal.	• Synthetic textile dyes was fast remove with PAC and ozonation. • Increase, color removal at higher O_3 con due to increase the adsorption of intermediate on the PAC surfaces.	Oguz et al. 2008
Residual bittern	Indigo blue	Jar test apparatus; C_o: 200mg/L; pH_o: 7.3; T: 25^oC; m: 200mg/L; t: 30min.	95% turbidity and 98% color.	• Flocs morphology and zeta potential contribute in dye removal • Adsorption responsible for dye on coagulant surface and removal confirmed by particles size distribution.	Albuquerque et al., 2012
Polyaluminium chloride (PAC), & GAC/O_3	Bio-treated textile wastewater	Batch study; C_o: (5-20) g/L; pH: 8.0 and 5.5; T: (25-50)^oC, m: 25 PAC, 3.1, O_3 and 100 mg/L GAC; t: 10 min.	95.8% turbidity, 97.5% color, 88.1% COD, 68.7% DOC.	• Stepwise coagulation with (polyaluminium chloride) followed by ozonation in presence GAC (GAC/O_3) gives better quality of result.	Qian et al., 2013
Organic polymer flocculant (LA) & Poly-ferric chloride (PFC)	Disperse yellow (DY) and reactive blue (RB)	Jar test analysis; C_o: 40 and 50 g/L; pH: 7.7 ; T: 25^oC, t: 20 min.	Zeta potential analysis; 90% color.	• Maximum color removal efficiency was obtained with PFC and combine LA and dual-coagulant (PFC + LA) both. • Adsorption, bridging and neutralization favored in LA charge in the coagulation.	Rong et al., 2014
Adsorption					
Bagasse fly ash	Orange-G and Methyl Violet	Bench-scale; orbital shaker at 150 rpm;	SEM, TGA, Kinetic	• Surface area, pore, volume and pore size exhibited BFA used as best adsorbent.	Mall et al.,

		C_o:100mg/L; pH_o: 4 & 9.0; T: 30°C; m: 3g/L; t: 4 h.	followed by second-order rate constant.	• Freundlich isotherm best-fits for OG-BFA and Redlich-Peterson isotherm for MV-BFA system.	2006a,b
Bagasse Fly ash (BFA)	Brilliant green	Bench-scale; controlled orbital shaker at 150 rpm; C_o:100 mg/L; pH_o: 3.0; T: 30°C; m: 3g/L; t: 5h.	Kinetic fellow by second-order rate constant.	• Intra-particle diffusion followed by pseudo-second-order kinetics. • BG adsorption onto BFA followed Freundlich and Langmuir isotherm.	Mane et al., 2007
Bagasse Fly ash (BFA); activated carbon commercial (ACC)	Auramine-O (AO)	Batch studies; C_o: 10 mg/L; pH_o: 7.0; t: 3h BFA and 120min ACC; m: 1.0 and 20g/L for both.	Zeta potential analysis determines the colloidal stability.	• Best correlation of adsorption for all the adsorbents with Langmuir isotherm is more favoured. • Adsorption followed pseudo-second order kinetic.	Mall et al., 2007
Fly ash (BFA)	Methylene Blue, Malachite Green, Rhodamine B	Batch study; C_o: (5-20) g/L; pH: (1.-9.0); T: (25-50)°C, m: (0.18–0.61)g/L; t: 80-100 min.	SEM-EDX determines the morphology of adsorbent.	• Malachite green and Rhodamine B shows maximum adsorption 80 min while methylene blue 100 min. • Adsorption followed first order kinetic and exothermic.	Khan et al., 2009
Sagaun Sawdust	Crystal Violet	Batch mode; C_o: (6-12) mg/L; pH_o 7.0; T: 30°C; m: 0.5g/L; t: 30-60 min.	FTIR; SEM analysis help in removal study.	• Adsorption equilibrium followed Langmuir isotherm.	Khattri and Singh 2012
Natural rarasaponin modified kaolin	Malachite green	Batch mode; C_o: 45 g/L; pH: (1.-9.0); T: (25-50)°C, m: (0.1–1) g/L; t: 90 min.	XRD; FTIR, SEM determine the change of reactant.	• Adsorption of MG on kaolin and rarasaponin-kaolin followed pseudo-first-order kinetic.	Suwandi et al., 2012
Polyacrylonitrile /activated carbon	Acid Red 57	Batch system; C_o: (40–150)g/L; pH: (1.-9.0); T: (25-50)°C, t: 90 min.	FTIR, SEM finds out the change of adsorbent.	• At pH 1.0 due to strong electrostatic interactions between dye anion and adsorption site. Process is spontaneous and exothermic.	El-Bindary et al., 2014

Notation: C_o: initial dye concentration; pH_o: initial pH; T: temperature; m: dose of adsorbent or coagulant or catalyst; t: treatment time.

Table 2.3.1. Studies on the treatment of dye bearing wastewater by biological methods.

Species	Dyes/Waste water	Experimental design & Operating condition	Process performance	Major Inferences	Refs.
Anaerobic–aerobic					
Lactobacillus casei	Reactive Black 5	AOMBR; 36 L anaerobic SBR. 18 L aerobic MBR; C_o: 50mg/L; T: 20°C; 48 & 24 h HRT; 2700 & 2100mg/L MLSS anaerobic SBR & aerobic MBR.	92.3 & 5.2% COD; 74.6 & 9.1% color anaerobic SBR & aerobic MBR.	• Anaerobic SBR followed with aerobic MBR, anaerobic SBR gives excellent COD and color RE. • L. lactis have different subspecies and degradation increase after addition of suitable amount of carbon and nitrogen.	You and Teng, 2009
Chlorella vulgaris	Textile wastewater (TW)	Batches of cultures in high rate algae ponds (HRAP); C_o: 0.17 to 2.26 mg/chlorophylla; T: 25°C.	COD (38.3–62.3%); NH_4–N (44.4–45.1%); PO_4–P (33.1–33.3%).	• TW concentration increase in the medium then color removal decrease by *C. vulgaris*. Removel followed by Langmuir and Freundlich isotherms. • Color reduction very fast with *C. vulgaris* as compared to COD, NH_4–N and PO_4–P.	Lima et al., 2010
Mixed cluture	Reactive Red 195	C_o: 800mg/L; pH_o: 7.0-8.5; T: 25°C.	97% color; 90% COD; pseudo-first order kinetic.	• COD/dye ratio determine the oxidation of dye. • ORP conditions determine the color removal efficiency.	Farabegoli et al., 2010
Oscillatoria curviceps	Acid Black 1	10 different cyanobacterial strains; C_o: 100 mg/L; pH_o 7.0-8.5; T:25°C; t: 8days.	FTIR; 84% color removal.	• Degradation ability depends on the polyphenol oxidase laccase, and azo reductase.	Priya et al., 2011
Fungi, Alage, and Bacteria					
Bacterial consortium	Direct Black 22	Batch study; C_o: 100 mg/L; pH: 7.0; T: 45°C; t: 12 h 0.1%, 0.06% (w/v), glucose, and yeast conc.	RSM (CCD)/ HPTLC/91% color removal.	• Mixed bacterial consortium used for dye degradation. • Accuracy and the applicability reflected by experimental and predicted values.	Mohan et al., 2008
Citrobacter sp.	Reactive Red 180	Anaerobic conditions with 4 g/L glucose; C_o: 200 mg/L; pH: 7.0; T: 32°C; t: 36 h.	UV-visible; 95% color removal.	• Color removal with *Citrobacter sp.* followed with biodegradation, rather than adsorption.	Wang et al., 2009
Bacterial	Textile dye	NaCl,bacteriological pep-tone	FTIR; HPLC;	• *Bacterial consortium containin* contian	Jadhav

consortium	Reactive Orange 16	yeast extract, beef extract, agar; C_o: 100 mg/L; pH: 7.0; T: 30°C; t: 48 h.	GC–MS; Cytotoxicity, genotoxicity phytotoxicity.	pseudomonas species. • Biodegradation of dye depends upon the laccase and reductase enzyme.	et al., 2010
Penicillium sp. & Exiguobacterium sp.	Reactive Dark Blue K-R	Batch study; C_o: 200 mg/L; pH: 7.0; T: 37°C; t: 12 h 0.19%, 0.09% 12.5% (w/v), glucose, and yeast.	RSM/CCD, 97%color removal.	• Fungus and bacterium co-cultures strain show the maximum color removal then any single strain. • Synergism strains and co-cultures tolerate high concentration of salinity.	Qu et al., 2010
Sequential anaerobic–aerobic An-SBR; MB-SBBR	Acid Red 18	Three separate lab-scale; C_o: 100 mg/L;T: 24°C; t: 24 h.	SEM; UV-Visible; HPLC/ 82.0% color; 80% COD.	• 80% 1-naphthylamine-4-sulfonate was completely removed in aerobic bio-film reactor. • Increase dye conc. inhibit the growth of the attach bio-flim in MB-SBBRs.	Koupaie et al., 2011
Pseudomonas sp. and Aspergillus ochraceus	Textile dyes (Navy blue)	Rice bran under solid state fermentation; C_o: 200 mg/L; pH: 5.0; T: 30°C; rice bran: 5 g.	92 color and 68% COD removed.	• Reduction with reductase, laccase, and tyrosinase indicate the dye adsorption. • GCMS and HPLC confirmed the different fate of biodegradation of dye	Kadam et al., 2011
Sphingomonas paucimobilis	Methyl Red (MR)	36 L anaerobic SBR/18 L aerobic MBR; C_o: 750 mg/L; T: (5-50) °C; pH: (3-11); t: 24 h.	UV–visible; FTIR; toxicity; 99.63% color.	• MR compound degradation with S. paucimobilis is a nontoxic process. • UV–visible/FTIR confirmed dye removal.	Ayed et al., 2011
Coriolus versicolor,	Dye degradation	Batch scale; GAC layer on membrane module within Fungal MBR; C_o: 50 mg/L;T: 20°C; 3 day HRT.	UV–visible; 85% color obtained.	• HRT, instantaneous membrane flux and amount of GAC-coating was affected color RE with control MBR connected with additional GAC layers.	Hai et al., 2012
Mycelium *(Trichoderma sp.)*	Acid Brilliant Red B	Air lift column reactor; C_o: 50 mg/L;T: 20°C; t: 72h.	100% color removal obtained.	• Settlebility improvements by clogging effect reduction for promote the dye bioaccumulation.	Xin et al., 2012

Notation: C_o: initial dye concentration; pH_o: initial pH; T: temperature; m: dose of fungi, bacteria etc; t: treatment time.
Abbreviations: MBR: Membrane biological reactor; HRT: hydraulic retention time; HPTLC: high performance thin layer chromatography; An-SBR: anaerobic sequencing batch reactor; MB-SBBR: aerobic moving bed sequencing batch biofilm reactor.

2.4 MEMBRANE TREATMENT

Pressure driven membrane technologies work on the sieving and diffusion mechanism for the separation of certain species in a colloidal solution. Species with wide range of molecular weights and sizes can be separated by membranes technologies. Generally, membranes are classified into four types namely reverse osmosis (RO), nanofiltration (NF), ultrafiltration (UF), and microfiltration (MF). In the textile industry, not only pigment rich wastewaters, but also bleaching and mercerizing wastewaters can be filtered and recycled using these filtration methods. The use of different types of membranes depends upon the porosity of filter, specific temperature and chemical composition of wastewater. The utilization of membrane technology for treatment of textile dye bearing wastewater has been also reported [Aouni et al., 2012]. Table 2.4.1 summarizes the literature on the basis of various membrane filtration methods for the treatment of dye bearing textile industry wastewater.

Qin et al. [2007] investigated feasibility of NF technique for the recovery of chemicals from the wastewater of a specific dyeing facility. 99% dye removal was obtained by designed three different NF membranes i.e. NF-70, Desal-5 and NF-40. Ellouze et al. [2012] investigated the combination of nano-filtration process with coagulation–flocculation process for textile wastewater treatment. 100% color, 60% COD and 35% salinity reduction was obtained with nano-filtration process under 10 bar pressure and 40°C temperature under optimal condition. Zheng et al. [2013] studied the effectiveness of submerged nano-filtration (SNF) for the biologically treated textile effluent on the laboratory scale. 99.3% color removal and 91.5% COD reduction was obtained at pressure of 0.8 bar with steady flux of 5.15 L/m^2 of SNF. Similarly, 99% color and 87% COD removal was reported earlier for nano-filtration of 200 mg/L acidic dye solution containing 1000 mg/L NaCl [Al-Aseeri et al., 2008].

Qin at al. [2012] performed comparative study between the RO and NF for water reuse of pre-biologically treated textile effluent using the NF membranes (NF-90) and RO membrane (BW-30). Both membranes removed the color to the desired levels. However, COD reduction with NF-90 was better whereas salinity removal was better with BW-30. It was found that NF-90 exhibited higher permeate flux than BW-30. Cross-flow velocity largely affected the COD removal and permeate flux rate of BW-30 membrane under the same initial flux because of rougher membrane surface as compared to NF-90 membrane. In another study, weaving textile industry wastewater was treated for decolorization, COD and salts concentration using a pilot-scale membrane system. Nano-filtration (NF-270) and

extra-low energy reverse osmosis (RO-XLE) membranes were evaluated under different operating modes namely batch concentrate-recycle mode and continuous mode without concentrate recycle. The average flux values 51.0±17.5 L/m^2/h and 27±6.5 L/m^2h in batch mode and 42±6 L/m^2h and 26±3 L/m^2h in continuous mode for NF-270 and RO-XLE membranes, respectively [Kurt et al., 2012]. Ong et al. [2014] reported a newly developed polyamide-imide hollow fiber NF membrane under the various operating conditions such as pH (3.0, 7.0, 10), temperature solute concentration (100, 500, 1000 mg/L) and (25, 40, 50, 70^oC). The best result of membrane was obtained with average >90% rejections against various dyes and more than 90% of Na_2SO_4 and 80% of NaCl permeate through the membrane.

The feasibility of textile wastewater treatment with membrane technology in different mode of treatment depends upon the nature of contaminated water and quality of the permeate water. Membrane treatment methods such as NF, UF and RO are widely used techniques for chemical recovery and water reuse [Fersi and Dhahbi, 2008; Verma et al., 2012] during the various stage of textile processing under the specific conditions such as chemical composition of wastewater, specific temperature and filter porosity [Yeap et al., 2014]. However, frequent membrane fouling, requirement of different pretreatments depending upon the type of influent wastewaters, high cost, production of concentrated dye bath, etc. are the main drawback of this technology and limit its application [Robinson et al., 2001; Akbari et al., 2006; Ordonez et al., 2014].

2.5. ELECTROCHEMICAL (EC) METHODS OF TREATMENT

EC treatment technology provides a simple, reliable and cost-effective technology for wastewater treatment without additional of any chemicals, and thus reducing the secondary pollution. Metal cations generated during EC process destabilize the colloidal suspension by reducing the negative charge of these colloids and thereby removing the repulsive energy barrier so that these colloids start agglomerating, forming first small groups, then bigger flocs and finally getting removed by settling [Mahesh et al., 2006; Canizares et al., 2006a,b]. A number of EC mechanisms including charge neutralization, double layer compression, bridging agglomeration, flocculation and adsorption, sweep coagulation, electro-flotation and electrochemical oxidation help in overall treatment [Kılıc et al., 2009; Kushwaha et al., 2010].

Table 2.4.1. Studies on the treatment of dye bearing wastewater by membrane treatment methods.

condition	dyes wastewater	Experimental design & Operating condition	Process performance	Major Inferences	Refs.
Polysulfone ultrafiltration membrane (PUF)	Dye wash wastewater	C_o: 100mg/L; pH_o: 6-8; T: 40°C; t: 48h; m: 50mg/L NaCl Batch scale total membrane area of 13.2 cm^2 NaCl, Na_2SO_4, $CaCl_2$ and $MgSO_4$ at 4 bar	UV-visible Spectrophotometry 99% color; 88% COD; 82% TOC; 98% turbidity.	• Hydraulic permeability was 0.48–0.56 m^3m^{-2} day^{-1} at 0.4 MPa and dye retention higher than 96%. • The performance of newly prepared membrane terms of fouling and retention compared with commercial membrane in terms of effect of pH and salt concentration.	Akbari et al., 2006
Nanofiltration	Dye wash wastewater	C_o: 500mg/L; pH_o: 6-8; T: 40°C; t: 48h; m: 50mg/L NaCl Batch scale total membrane area of 465cm^2	99% color; 88% COD; 82% TOC, 98% turbidity.	• NE-70 membrane showed >99% dye removal and better performance in terms of flux and separation than Desal-5 membrane.	Qin et al., 2007
Nanofiltration	Textile wastewater containing	SBR coupled with NF; C_o: 3094mg/L; pH_o: 2.0-11; T: 45°C; pressure: 41 bar NF-270 membrane.	76.2% COD and 90% color removal efficiency.	• The NF shows the color removal yield 85-90% while for SBR used 50% color removal was obtained. • Results were found that percentages of NF rejection higher than 40% imply non acceptable colour removal efficiencies.	Agusti et al., 2010
Reverse osmosis and Nanofiltration	Biologically treated Textile wastewater	Cross-flow permeation tests; C_o: 96–108mg/L; pH_o: 6.5-6.8; T: 25°C; t: 40h; m: 1000 mg/L NaCl BW30 reverse osmosis and NF90 nanofiltration flat-sheet membranes.	SEM, AFM, analysis used for the identification of membrane.	• NF-90 exhibited higher water permeability and more severe flux decline than membrane BW-30 because of its higher porosity and membrane fouling. • Flux performances of membrane depends upon hydrodynamic conditions	Liu et al., 2011
Nanofiltration and Reverse osmosis	Dye wash wastewater	C_o: 600mg/L; pH_o: 2.0-11; T: 45°C; m: 50 mg/L NaCl Batch concentrate-recycle mode and continuous mode ; NF-270 and RO-XLE	Activation energy 6.51±0.53 kJ mol^{-1} and 3.87±0.24	• The feasibility membrane technology for textile wastewater with different mode of treatment depends upon the nature of highly contaminated and high quality of the permeate water.	Kurt et al., 2012

		membranes.	$kJmol^{-1}$	• It was found that, on-site, pilot-scale with NF and RO demonstrated the ability of "high-pressure" membrane processes to remove color, COD, and conductivity.	
Polysulfone (PS) ultrafiltration (UF) membranes	Textile wastewater containing reactive orange 16-(RO16)	NF-270 membrane; MWCO (molecular weight cut-off); C_o: 3094mg/L; pH_o: 9.0; T: 45°C.	SEM and AFM analysis used for the identification of membrane.	• Membranes characteristic i.e. water permeability, porosity, contact angle confirmed by AFM, and SEM analyses • Color rand COD removal efficiencies increased with decreased the flux values of membranes and increase of the evaporation temperature.	Koseoglu-Imer 2013
Nano- filtration	Biologically treated Textile wastewater	Thin-film composite TFC hollow fiber NF membranes, TMP: 8.0 bar. Submerged filtration tests; C_o:120-230 mg/L; pH_o: 6.5-6.8; T: 25°C; t: 40h	99% color and 91.5% COD remove.	• The permeate flux, color removal rate and COD reduction rate affected by the TMP and VCF. • The increase of TMP and/or VCF decreases the water permeability and increase in color and COD reduction rates.	Zheng et al., 2013
Nano-filtration hollow fiber membranesn	Textile wastewater	Lab-scale and pilot-scale studies; batch Mode; C_o: 50mg/L; pH_o: 3.0, 7.0, 10.0; T: 40°C; m: 500 mg/L (NaCl and Na_2SO_4).	99% color and 90% COD remove.	• More than 80% of NaCl and 90% of Na_2SO_4 permeate through the membrane. • The robustness of the membrane was found the satisfactory and stable performance during the lab-scale and pilot-scale evaluations.	Ong et al., 2014

Notation: C_o: initial dye concentration; pH_o: initial pH; T: temperature; m: dose of electrolyte; t: treatment time.

Abbrivations: TFC: thin-film composite; TMP: trans-membrane pressures; VCF: volume concentrating factor; MWCO (molecular weight cut-off); Polysulfone (PS) ultrafiltration (UF) membranes; Polysulfone ultrafiltration membrane (PUF).

Szpyrkowicz [2005a,b] reported the decolorization of three dispersed dyes into two step electrochemical process which consisted of electro-coagulation followed by electro-flotation. Can et al. [2003; 2006] and Kobya et al.[2006b] reported 95% decolorization of Remazol Red 133 and Levafix Orange dyes under the different operating conditions with minimum electrode and energy consumption in acidic and neutral media (pH<6.5). Charge neutralization and precipitation mechanisms helped in the removal of dye with monomeric and polymeric Al species. Similarly, Canizares et al. [2005, 2006] reported 98% Eriochrome Black T (EBT) dye degradation with Al in acidic (6.5<pH) medium by binding the EBT anionic groups ($–SO_3^-$,$–O^-$) to monomeric and polymeric cationic Al-hydroxide via chemisorption process. Canizaries et al. [2006 and 2007] reported the study of colloidal stability in terms of surface complexation or electrostatic attraction mechanism between insoluble metal hydroxides with impurities during the ECT of dye solution by measuring the surface charge in terms of zeta potential. Alinsafi et al. [2005] reported 98% color and 55.3% COD removal for blue reactive dye. Specific electrical energy consumption was found to be ~13.5 kWh/kg at 120 min and with j=12 mA/cm^2. Daneshvar et al. [2006] reported 99% color and 76% COD removal for C_o=50 mg/L at pH_o=5.8 and j=80 m/A^2 with 7.57 kWh/(kg dye) energy consumption. Cameselle et al. [2005] reported a study on the effect of different electrolyte concentration on energy consumption in the following order: NaCl (84 kWh/m^3) < KBr (92 kWh/m^3) < KI (123 kWh/m^3) < $NaHSO_4$ (136 kWh/m^3).

Yuksel et al. [2012; 2013] performed comparative study on EC treatment of a reactive orange 84 dye solution and a textile wastewater by SS and iron (Fe) as sacrificial electrodes. It was found that the EC process with SS electrodes not only consumed less electrode material and energy but also produced less amount of sludge with pH of the medium being more stable as compared to Fe electrodes under similar experimental conditions. The operating cost with SS electrodes was about 0.7 times the cost with Fe electrode. Thus, between SS and Fe, SS because of lower dissolution rate and less operating cost and other operational advantages seems to be much better than Fe. Akbal and Kuleyin [2011] reported Al to be more effective than Fe electrode in terms of decolorization efficiencies and operating costs for decolorization of levafix brilliant blue E-B. However, Akbal and Camcl [2012] reported electro-coagulation treatment of simulated reactive dye bath effluent with Al and SS electrodes where SS was found to be more effective as compared to Al. Thus, Al and SS have distinct advantages and disadvantages

for treatment of various types of wastewaters depending upon the characteristics (particularly pH) of the wastewater to be treated.

Literature of EC treatment of aqueous solution containing various types of dyes is summarized in Table 2.5.1. Studies on the treatment of actual and synthetic textile dye wastewater by electrochemical treatment methods are given in Table 2.5.2.

Very few studied are reported in literature to explain the EC mechanism of dye degradation with Al, Fe and SS electrodes either in solution phase or with the help of solid residue generated at the end of EC process. Mollah et al. [2010] reported the 94.5% orange II dye degradation by the analysis of EC-floc and sludge. Fourier transform infrared spectroscopy (FTIR) and powder X-ray diffraction techniques (PXRD) results indicate that 1402 and 1080 cm^{-1} band of O-H and Al-O- H bending vibrations due to pristine Al-flocs contains hydroxides and oxy hydroxides (boehmite (AlO(OH)), bayerite ($Al(OH)_3$), and diaspore (AlO(OH)) [Vinodgopal et al., 1996] interact with dye molecules in the form of uni-dentate and bi-dentate chelating complex.

Sludge generated with metal electrodes (Al, Fe and SS) during the EC treatment poses a big problem of sludge disposal and reutilization. Considering the same, some of the authors have been working treatment of dye bearing effluent by electro-oxidation method (either direct or indirect mode) in presence of hydroxyl radical intermediate. Therefore, electrochemical oxidation is considered as electrochemical advance oxidation process (EAOPs). As compared to other oxidation methods, anodic oxidation is more attractive treatment method due to the negligible amount of secondary pollution generation. Mohan et al. [2001] and Raghu and Basha [2007] reported 74.05% COD and 100% color removal by direct oxidation of acid red14 and procion black 5B on Ti/RuO_2 electrode surface. Basha et al. [2012] reported 99.17% COD and 35.6 kWh/kg COD specific energy consumption for treatment of dye-bath effluent treatment with $Ti/TiO_2–RuO_2$ electrode. Tavares et al. [2012] confirmed mineralization of methyl red using $Ti/Ru_{0.3}Ti_{0.7}O_2$ and Ti/Pt anodes in presence of different electrotyte ($NaNO_3$, Na_2SO_4, and NaCl). Various active species like $^{\bullet}OH$, $SO_4^{\bullet-}$, $S_2O_8^{2-}$, Cl_2, HOCl and OCl^- contribute in the degradation process.

Table 2.5.1. Studies on the treatment of dye bearing wastewater by electrochemical treatment methods.

Anode – Cathode	dyes wastewater	Experimental design & Operating condition	Reactor & electrode configuration	Process and Removal efficiency	Major Inferences	Refs.
Al-Al	Ramazol red 133	C_o: 250mg/L; pH_o; 6.0; T: 25°C; κ: 750μS/cm; j: 10 mA/cm^2; t_{EC}: 10 min.	Bench-scale; parellel mode; g: 11 mm; A: 78 cm^2; r. s: 200 rpm.	1.4 kg Dye/kg Al and 29 kWh/kg dye/ 98%color.	• pH_o of dye solution and electricity consumed during treatment are important process parameters. • Polymeric species rapidly precipitate dye molecules and $Al(OH)_3$ flocs efficiently trap colloidal precipitates.	Can et al., 2003
Fe-Fe	Orange II	C_o: 100mg/L; pH: 8.0; T: 25°C; m: 3.0g/L NaCl; j: 34.62A/m^2; t_{EC}: 20 min.	Batch mode; monopolar parallel g: 2.0 cm; A: 0.0106 m^2; r. s: 100 rpm; flow rate 3L/h.	98% color; 85% COD removal was obtained	• For dye removal pH optimizes around 8.0 if pH > 8.4 then amount of Fe hydroxide is increased and some OH ions are oxidized therefore this reaction prevent the same proportional of Fe and OH ions. Hence the removal efficiency decreases.	Daneshvar et al., 2003
Fe-SS 304	Acid red 14	C_o: 50mg/L; pH: 8.5; T: 30°C; m: 10 g/L NaCl; j: 80 A/cm^2; t_{EC}: 4.0 min	Batch mode: momopolar and bipolar mode g: 1.0 cm.	80% COD; >90% color with mono polar mode of treatment.	• Monopolar mode shows better removal efficiency then bipolar • Parallel electrode connection gives better RE as compared to series connection	Daneshvar et al., 2004b
Al-Al	Levafix orange	C_o: 250 mg/L; pH_o 6.4; T: 25°C; NaCl: 2g/L; κ: 750 μS/cm; j: 100 A/m^2 t_{EC}: 12 min.	Bench-scale; parellel mode; g: 11 mm; A: 78 cm^2; r. s: 200 rpm.	2.0 kg Al/kg dye and 43 kWh/kg dye 99.9% color.	• DE dependents on the pH_o, μ, j, t and m. • μ, j, t and m increase then DE increase due to sufficient number of aluminium hydroxide interact with dye molecules.	Kobya et al., 2006
Al-Al	Eriochrome Black T	C_o:100 mg/L; pH_o: 4.0; T: 25°C; Na_2SO_4: 3000 mg/L; j: 1.40	Continuous and bench-scale; g: 9 mm; A: 100 cm^2;	99% color removal was obtained.	• At pH<6.0 binding of aluminium hydroxo cations to EBT anionic site increase. • pH~7.0 higher removal efficiency was	Caizares et al., 2006

		mA/cm^2 t_{EC}: 180 min.	flow rate 19 L/h.		obtained by adsorption of EBT on positive charge $Al(OH)_3$ and precipitate was obtained.	
Fe-SS 304	Basic red 46 & Basic blue 3	C_o: 80mg/L; pH: 5.8; T: 25°C; κ: 8.0 µS/cm; m: 50 mg/L NaCl; j: 60 & 80mA/cm^2; t_{EC}: 5.0min.	Batch mode; g: 15 mm; A: 0.0056 m^2; r. s: 400 rpm.	UV-Visible; ENC: 4.70 & 7.57 kWh/(kg dye removed; 75% COD & 99% color.	• Dye degradation increase with increase the j, m and decrease C_o at basic pH range. • Best removal efficiency was obtained with both dyes at 5.5 to 8.5 pH range.	Daneshvar et al., 2006
Fe or Al-SS 304	Acid yellow 23	C_o: 50mg/L; pH: 5.35; T: 25°C; κ: 16.5µS/cm; m: 0.58-1.75g/L NaCl; j: 112.5 A/cm^2; t_{EC}: 5.0 min.	Batch mode: monopolar mode g: 15 mm; r. s: 200rpm.	UV-Visible/ SEEC: 98% color and 69% COD removed.	• SEEC and cell voltage was achieved by increase j and conductivity and cross diction area of electrode and decrease the electrodes distance. • RE depends upon the conc. of ions produced during the electrolysis.	Daneshvar et al., 2007
Al-Al, Fe-Fe	Kaolin suspension; Eriochrome Black T & oil-in-water emulsions	C_o: 0.20g/L; pH: 4.5; T: 25°C; m: 3000mg/L NaCl; j: 0.5 mA/cm^2; t_{EC}: 10 min.	Bench-scale; parallal mode; g: 9.0 mm; A: 100 cm^2; r. s: 250 rpm; flow rate: 50 dm^2/h.	99% color and 78% COD confirmed by colloidal instability of suspension.	• EC mechanism can be explained in terms of the speciation of monomeric and polymeric ionic species. • EC in both aluminum and iron electrodes explained by sweep coagulation and zeta potential contribution.	Canizares et al., 2007
Al-Al	Aniline blue	C_o:100mg/L; pH_o 6.0; T: 25°C; Vap: 11V; t_{EC}: 15min.	Bench-scale; g: 0.5 cm; A: 68 cm^2; r. s:400 rpm.	FESEM/EDX; TGA sludge analysis; 85.5% COD and 97% color.	• Charge neutralization mechanism (monomeric cationic aluminium species) was obtained at pH<6.0. • Sweep coagulation increase at pH>6.0 due to increase amorphous aluminium hydroxide concentration.	Ahlawat et al., 2008
Fe-SS 304	Acid Red 14	C_o: 50mg/L; pH: 4.5; T: 25°C; m: 1.0g/L NaCl; j: 102A/cm^2; t_{EC}: 20	Batch mode, g: 1.0 cm.	RSM CCD/ >91%color removal efficiency.	• Full factorial CCD design help in optimization the operating parameters. • Second-order regression model best fitted for the experimental data.	Aleboyeh et al., 2008

		min.				
A-Al	Bomaplex red CR-L	C_o: 100mg/L; pH: 3.0; T: 25°C; m: 1.5g/L NaCl; j: 0.50mA/cm^2; t_{EC}: 30min.	Batch mode; g: 5.0 mm; A: 1000 cm^2; r. s: 150 rpm.	Experimental design; ENC: 0.607 kWh/kg dye; 99.1%Color.	• Taguchi method and orthogonal array, used for determine the removal efficiency. • ANOVA effect determines optimum and relative magnitude of parameters.	Yildiz et al., 2008
Fe-Fe	Real mercerized and non-mercerized	C_o: original conc mg/L; pH: 11.52; T: 30°C; κ: 15.78 µS/cm; m: 37.5 g/LNaCl; j: 32.5 mA/cm^2; t_{EC}: 210 min.	Batch mode; monopolar parallel; g: 1.5 cm; A: 75.35 cm^2; r. s: 575 rpm.	93.9%, 82.9% 99.5%; 61.6% 66.4% 99.6% COD, turbidity color respectively.	• Experiment design methodology with the satisfactory degrees of fit was found for COD, color and turbidity removal. • EC method optimizes by the RSM and experimental result. It is a strong alterative as compared to conventional physicochemical treatments methods.	Korbahti and Tanyolac 2007, 2008
Fe-Fe	Remazol red 3B	C_o: 0.20g/L; pH: 6.9; T: 25°C; κ: 3,990µS/cm; m: 0.58-1.75g/L NaCl; j: 10.0mA/cm^2; t_{EC}: 10 min.	Batch mode; monopolar parallel g: 11 mm; A: 152 cm^2; r. s: 200 rpm.	Zeta potential/ ENC: 1.7 kWh/m^3; ELC: 0.5 kgFe/m^3; OP: 0.2 €/kg 78% COD; 92% turbidity.	• Zeta potential measurement and help to find out the mechanism of removal with Fe electrodes. • RE increase with increase the pH (7–8) then decreased pH (9–11).	Kobya et al., 2009
Fe-Fe	Reactive black 5	C_o: 100 mg/L; pH: 5.0; T: 20°C; m: 3.0g/L NaCl; j: 4.575mA/cm^2; t_{EC}: 5.0min.	Batch mode; bipolar parallel g: 2.5 cm; A: 0.0218m^2; r. s: 120 rpm.	ENC: 4.96 kWh/kg dye; ELC: 5.32 kWh (kg Fe)$^{-1}$; 98.8% color.	• EC mechanism depends upon the adsorption capacity of the dye molecules by the electrostatic attraction and physical entrapment. • Dye molecules interact with iron hydroxide by adsorption precipitation.	Sengil and Ozacar 2009
Al-Al SS-SS	Reactive dyebath	C_o: original conc mgL^{-1}; pH: 11.5;	Bench-scale; mono polar, g:	ENC: 5.0 Al and	• SS shows the better RE for color then Al. At pH 11–12 the coagulation +	Kabdasli et al.,

(304)	effluent	m: 3.0 g/LNaCl; j: 22mA/m^2; t_{EC}: 30 min.	1.0 cm.	9.0kWh/m^3 for SS and 100%, color removal	adsorption mechanism dominant for color and COD removal and RE followed the pseudo-first order kinetics.	2009
SS-SS, Al-Al	Reactive	C_o: original conc mgL^{-1}; pH: 5.0; T: 25°C; m: >10 g/L NaCl & Na_2SO_4; j: 22 m A/m^2; t_{EC}: 60 & 90 min for SS and Al.	Bench-scale; parallal mode; g: 2.0 mm.	ENC: 3.6 & 1.8 kWh/m^3, 99% & 95% color; 93% & 86% COD for SS & Al.	• COD and color abatement was found very fast in acidic pH range (3-5) for both with Al and SS respectively. • The sludge generating applicability was higher for SS then Al. Hence, SS suitable electrodes for dye bearing effluents.	Arslan-Alaton et al., 2009
Al-Al	Orange II	C_o:10mg/L; pH_o 6.5; T: 25°C; m: 4g/lNaCl; κ: 7.1 µS/cm; j: 160 mA/m^2; t_{EC}: 7.3 min.	FTECA; bipolar mode; g: 6 mm; r. s: 250 rpm; flow rate: 350 mL/min.	FTIR; SEM-EDAX; PXRD /94.5% color removed.	• Decolorisation efficiency increase with j, m and decrease with increase the pH, C_o and flow rate while FTIR determine the EC-flocs containing Al hydroxides/oxy-hydroxides. • PXRD/SEM/EDS confirm amorphous nature of the Al by products.	Mollah et al., 2010
Al-Al	Direct red 81	C_o: 25mg/L; pH_o 6.0; T: 25°C; m: 2g/LNaCl; j: 1.87mA/m^2; t_{EC}: 60 min.	Batch mode; parellel mode; g: 1.5 cm; A: 40 cm^2; r. s: 400 rpm.	FTIR confirmed the change during the treatment; 99% color removal.	• EC precipitate in FTIR spectra with and without dye indicate the presence of azo(1500 and 1411 cm^{-1}) and sulfonate group (1114, 1049, and 617 cm^{-1}) of dye adsorbed on Al(OH) flocs.	Aoudji et al., 2010
Al-Al	Disperse red	C_o: 0.30g/L; pH: 7.6; T: 25°C; κ: 2.1 µS/cm; j: 11.55 mA/cm^2; t_{EC}: 10 min.	Batch mode mono polar or bi-polar mode; g: 1.0 cm; A: 4.59 cm^2.	85.5% SS, 76.2% turbidity, 88.9% BOD_5, 79.7% COD, 93% color.	• COD and BOD_5 reduction can be define by the EC–EF mechanism. • Precipitation and adsorption at pH < 4.0 and pH > 4.0 respectively was obtained.	Merzouk et al., 2010
Al-Al, Fe-Fe	Levafix brilliant blue E-B	C_o: 250mg/L; pH: 5.5; T: 25°C; m: 1.0g/L NaCl; j:	Bench-scale; g: 5 mm; A: 202.5 cm^2.	ENC: 16.9 kWh/$m^3$and OP: 2.921 $	• DE decreased with increasing m due to change the conductivity and ionic strength of aqueous medium.	Akbal and Kuleyin 2010

		100A/m^2; t_{EC}: 20 min.		per m^3; 99% color; 83% COD.	• Reaction between the charge species, kinetics and equilibrium was effected by the ionic strength.	
Al-Al, Fe-Fe	Reactive, Basic	C_o: 100mg/L; pH: 9.7; T: 25°C; m: 1.5g/L NaCl; j: 30 A/m^2; t_{EC}: 5.0min	Bench-scale; g: 8.0 mm; A: 104 cm^2; r. s: 150 rpm.	ENC: 1 kWh m^{-3}/ >95% color.	• RE and ENC results was superior for Fe as compared to Al. • Real textile effluent contains some other auxiliary pollutant which interfaces with EC.	Phalakornkule et al., 2010
Fe-Al, Al-Fe	Crystal violet	C_o: 54mg/L; pH: 9.0; T: 25°C; m: 1420mg/L NaCl; j: 28A/m^2; t_{EC}: 30 min.	Bench-scale; mono polar,; g: 1.1 cm; A: 0.012 m^2; r. s: 400 rpm.	RSM/ UV-Visible/ENC: 0.4WhL^{-1} 100% color	• RSM methodology find out that Fe gives better result than Al. • 95% confidence level reported that pH_o and m showed limited effects whereas j, C_o both was significant.	Durango-Usugaa et al., 2010
Al-SS 304	Acid brown 14	C_o: 50mg/L; pH: 6.4; T: 25°C; m: 0.5g/L NaCl; j: 6.32A/m^2; t_{EC}: 180 & 200 min.	Bench scale (BS) and pilot scale (PS) g: 1.0 & 3.0 cm.	UV-Visible/ ENC: 0.052 & 0.0366 WhL^{-1} 91% & 87% 80% & 64% color and COD	• Al is a better option for EC as compared SS. Color and COD abatement in BS and PS reactor fitted first and zero order kinetic. • RE depends on the conc. of dye for BS reactor while in PS, RE depends on the hydraulic parameters.	Parsa et al., 2011
Al-Al	Reactive Red198	C_o: 0.50g/L; pH_o 5.5 ; T: 20°C; m: 2g/L NaCl; κ: 45 µS/cm; V_{app}: 20V; t_{EC}: 30min.	Batch mode mono polar or bi-polar mode; g: 1.0 cm; A: 484cm^2; r. s: 400 rpm.	ELC 0.052 kg/m^3, ENC 1.303 kWh/m^3, OC 0.25US$ /m/98.6 color 84% COD.	• Dye removal flowed by first order kinetics. • Small different in DE removal efficiency depends upon the nature of the different functional groups of dyes that change properties of dyes.	Dalvand et al., 2011
Fe-SS	Reactive Black 5	C_o: 25mg/L; pH: 9.0; T: 25°C; m: 2.0g/L NaCl & Na_2SO_4; j: 6-7.0 m A/cm^2; t_{EC}: 20 min.	Batch mode; g: 20 mm; A: 44 cm^2; r. s: 400 rpm.	UV-Visible/ ENC: ~29 & 58. KWh/kg dye for NaCl & Na_2SO_4 90% color.	• Azo linkage reduction was obtained by the oxidation of Fe^{2+} as a main mechanism of dye removal. • Vinyl sulphate accumulation and H-Acid removal depends upon the surface complexation reaction.	Patel et al., 2011

Al-Al	Acid black 52, Acid yellow 220; & STW	C_o: 200mg/L; pH: 5; T: 25°C; m: 2.0 g/LNaCl; j: 40 A/m^2; t_{EC}: 30 min.	Batch mode mono polar mode; g: 10 mm; r. s: 200 rpm.	UV–visible/ 92% COD and 95% color	• Removal efficiency increase with increase the j and m. ENC increase with increase the j and decreased from 5668 to 950 kWh/m^3 when m increase from 0 to 2.0 g/L NaCl.	Pajootan et al., 2012
Fe-Steel wool, Fe-SS	Acid Black 1, Reactive Blue 4, Eosin Yellow	C_o: 100 mg/L; pH: 4.5; T: 25°C; m: 1.0g/L NaCl; j: 0.3 A; t_{EC}: 12min.	Bench-scale; A: 28 cm^2 Fe & 591 cm^2 SS plate; r. s: 740 rpm.	UV-Visible/ 99% color confirmed.	• COD and color abatement faster for Fe (28 cm^2)/steel wool cathode (591cm^2) then Fe (28 cm^2)/SS (28 cm^2). • Steel wool cathode increases mixing speed increase the dye removal.	Wei et al., 2011
Al-Al combination	Real textile wastewater	C_o: 0.20g/L; pH: 9.0; T: 25°C; m: 1.5NaCl; j: 50 mA/m^2; t_{EC}: 50 min.	Packed bed reactor; g: 1.6 mm; A: 50 cm^2; Q: 540 mL/min.	XRD analysi of sludge; 99% color; 90% COD.	• XRD analysis of sludge confirmed maghemite formed ferric hydroxide. • COD RE influence by recirculation rate decreasing recirculation flow rate, increase the removal efficiencies.	Wei et al.,2012
Fe-Fe Al-Al	Reactive Red 43	C_o: 50mg/L; pH: 8.5 & 4.5; T: 25°C; m: 1.5 g/LNaCl; j: 36 & 39A/m^2; t_{EC}: 23 &12min.	Bench-scale; mono polar, parellel mode; g: 20 mm; A: 50 cm^2; r. s: 300 rpm.	RSM CCD/ UV-Visible/ TOC/GC-MS/ 99% color, 90.58% Fe 98.3%Al TOC.	• RSM optimize EC process and results evaluated by ANOVA, lack of fit and second order polynomial model. • UV–Visible, TOC and GC–MS results confirmed EC-Fe best pathway of degradation.	Amani-Ghadim et al., 2013
SS-SS, Fe-Fe	Reactive orange 84	C_o: 300mg/L; pH: 7.0; T: 25°C; m: 3000µS/cm; 1.75 g/L NaCl; j: 130 A/m^2; t_{EC}: 30min.	Bench-scale; g: 1.5 mm; A: 78 cm^2; r. s: 400 rpm.	ENC:0.05kWh /m^3, ELC:2.43 kg/m^3,89.7%COD, 91.2% TOC, 94.1% TSS 90.3% turbidity,	• EC performance superior with SS electrodes as compared to Fe electrodes • $Al(OH)_3$ flocs containing polymeric species efficiently trap colloidal impurities and rapidly precipitate out.	Yuksel et al., 2013
Al-Al	Basic green 4	C_o: 100mg/L; pH: 6.2; T: 25°C; m: 1.5g/L NaCl; j: 117.64A/m^2; t_{EC}:	Bench-scale; mono polar; g: 1.0cm; A: 63.75cm^2; r. s:	FTIR, XRD, SEM/EDX, BET, TGA 99.4% color	• Zeta potential study for the BG dye solution was always negative during the treatment. • The maximum removal of the dye was	Singh et al., 2013b

		45min.	600rpm.	82.4% COD, 63.5% TOC; ENC &ELC confirmed.	found at the least negative value of the zeta potential due to the concentration of positively charged colloids in the solution is at a minimum.	
Al-Al	Malachite green	C_o: 125mg/L; pH: 6.5; T: 25°C; m: 1.5g/L NaCl; j: 117.64A/m^2; t_{EC}: 50min.	Bench-scale; mono polar; g: 1.0cm; A: 63.75cm^2; r. s: 600rpm.	UV−visible FTIR; HPLC, GCMS HRMS, 85% COD.	• N-demethylation obtained by the cleavage of conjugated structure and generation of small molecules by cleavage of rings by the interaction of active species. • Hard acid−base interaction between aluminum ions hydroxides and −N $(CH_3)_2$ confirmed by zeta potential.	Singh et al., 2013c
Al-Al, SS-SS, Al-SS, SS-Al	Dye bearing effluent	C_o: original conc mgL^{-1} ; pH: 8.5; T: 25°C; m: 1.5g/L NaCl; j: 117.64 A/m^2; t_{EC}: 150 min.	Bench-scale; mono polar,; g: 1.0cm; A: 63.75m^2; r. s: 600 rpm.	99.90% color, 82.50% COD, 68.8% TOC and 98.8% turbidity and particles size.	• RE at different j and pH with various combination as follow: SS–SS > SS–Al > Al–Al > Al–SS. • ENC and ELC, particles size and zeta potential were obtained in the following order: SS–SS > SS–Al > Al–Al > Al–SS.	Singh et al., 2014
Fe-Fe	Malachite green	C_o: 100mg/L; pH: 8.5; T: 25°C; m: 1.5g/L NaCl; j: 117.64A/m^2; t_{EC}: 60 min	Bench-scale; mono polar; g: 1.0cm; A: 78 cm^2; r. s: 400 rpm.	99% color and 75% COD	• EC mechanism of dye removal depends upon the opposite charge ions generated during anodic dissolution of anode. Electrolysis period increases, increases the concentration of ions and their hydroxide flocs.	Singh et al., 2013d

Notations: C_o: initial/original dye concentration; pH_o: initial pH; T: temperature; m: dose of electrolyte; κ: conductivity; j: current density; t_{EC}: electrochemical treatment time; g: electrode gap; A: effective electrode area; r. s.: stirrer speed.

Table 2.5.2. Studies on the treatment of actual and synthetic textile dye wastewater by electrochemical treatment methods.

Anode – Cathode	dyes wastewater	Operating parameters		Effectiveness of EC process		Refs.
		Experimental conditions	Reactor & electrode configuration	Process performance Removal efficiency	Remarks	
Fe-Fe, Al-Al	Textile	C_o: original conc. mg/L; pH_o: 6.95; T: 25°C; κ: 4.7 mS/cm; j: 200 A/m^2.	Bench-scale; monopolar mode; g: 11 mm; A: 78 cm^2.	76% COD, 65% color.	• Operation cost of Fe and Al was found ~ 0.1 and 0.3 US$ per kg COD. • ELC cost ~50% and 80% of the total cost for Fe and Al.	Bayramoglu et al., 2004
Al-Al	Real textile and synthetic waste water	C_o: original conc mg/L; pH_o: 10.0; κ: 4.7mS/cm; j: 12mA/cm^2 t_{EC}: 105 min.	Bench; parellel mode; g: 20 mm; A: 100 cm^2; flow rate: 370 ml/min.	UV-Visible; RSM; 13.5 ENC: kWh/kg Al; □: 1.1%; 98% color and 38% COD.	• Experimental design and RSM analysis used for determine the color and COD by optimize the pH, j and t. • Short-term respirometry used for determine the biodegradability before and after EC treatment.	Alinsafi et al., 2005
Fe-Fe	Textile	C_o: original conc mg/L; pH_o: 10.6; T: 25°C; κ: 42.6 mS/cm; t_{EC}: 2.0min.	Bench-scale; parellel mode; g: 0.5cm; A: 68cm^2; r.s: 600 rpm.	Zeta potential/ 100% color; 84% COD.	• COD and color removal depends upon time and potential. Ferric hydroxide is responsible for EC treatment determines by zeta potential measurement. • Fe hydroxide stability obtained within the pH range 2.0 < pH< 10.0.	Zaroual et al., 2006
Al-SS	Dye bath effluent	C_o: original conc mg/L; pH_o: 11.5; T: 25°C; m: 3g/L	Bench; mono-polar parellel; g: 3 mm; A: 68 cm^2; r.s: 500	Pseudo-first order 76% color 50% COD for Al; 90% color;	• 5.0 kWh/m^3 ENC_{sp} for Al and 9.0 kWh/m^3 ENC_{sp} for SS. • color and COD RE higher with NaCl as compared to Na_2CO_3	Kabdasli et al., 2009

		NaCl; j: 22 mA/cm^2; t_{EC}: 30min.	rpm.	54% COD for SS.	• pH 11–12 responsible for coagulation and adsorption.	
Al-Al	Dye bearing effluents	C_o: original conc mg/L; pH_o: 6.6; T: 25°C; κ: 750 µS/cm; j: 19.51mA/cm^2 t_{EC}: 102min.	Bench-scale; parellel mode; g: 0.5cm; A: 68cm^2; r.s: 600 rpm.	RSM-CCD TGA/DTA, 0.011 kWh/kg of COD 94% COD 99.7% color.	• DBE treated with Al was optimizing by multi-response analysis for color, COD ENC_{sp} value. • EC and EF mechanism was responsible for color and COD removal. Solid residue study determines sludge used as a fuel.	Mondal et al., 2012
SS-SS	Dye bearing effluents	C_o: original conc mg/L; pH_o; 7.2; T: 25°C; κ: 5.37 µS/cm; j: 15.34mA/cm^2 t_{EC}: 90min.	Bench-scale; parellel mode; g: 1.5cm; A: 68cm^2; r.s: 600 rpm.	RSM, SEM/ EDX; TGA/ DTA; 7.71 kWh/kg COD 91.7% COD 99.8% color.	• ENC, COD and color RE increase with increase in j and t. • FE-SEM/EDAX and TGA results indicate sludge used for fuel briquettes and other organic fuels as fuel in the furnaces.	Mondal et al., 2013
Al-Al; SS-SS	Synthetic textile wastewater	pH_o; 4.0, 8.0; T: 25°C; m: 2.0; 1.0g/L j: 97.2;111A/m^2; t_{EC}: 120, 105 min Al-Al/SS-SS.	Bench-scale; monopolar mode; g: 1.0 cm; A: 180 cm^2; r.s: 600 rpm.	RSM-BDD/ 46.87%, 98.61% for Al and 54.37%, 83.89% for SS COD and color removal	• RSM find out BBD model most effective for DBE analysis. • 0.8815, 0.8995 for COD, 0.9494, 0.8243 for color and 0.9331, 0.8805 for ENCsp coefficient of determination R^2value was obtained for Al and SS respectively.	Bhatnagar et al., 2013
Al-Al	Synthetic textile wastewater (STW)	C_o: original conc mg/L; pH_o; 5.5; T: 25°C; κ: 750 µS/cm; j: 185.30A/m^2 t_{EC}: 190min.	Bench-scale; parellel mode; g: 1.0cm; A: 68cm^2; r. s: 500rpm.	FESEM/EDX, TGA-DTA/ 70.5% COD; 98.2% color.	• Plackett–Burman (PB) design, steepest accent/descent and finally BBD was utilized to evaluate the optimum electrochemical conditions. • EC and EF found as a main mechanism for COD and color removal.	Singh et al., 2013a

Notations: C_o: initial/original dye concentration; pH_o: initial pH; T: temperature; m: dose of electrolyte; κ: conductivity; j: current density; t_{EC}: electrochemical treatment time; g: electrode gap; A: effective electrode area; r. s.: stirrer speed.

2.5.1. Role of zeta potential in EC treatment

Colloidal suspensions exhibit surface charge or zeta potential due to their dipolar attributes and ionic characteristics. Colloidal stability and interaction are determined by zeta potential measurement. The nature of zeta potential measurement depends upon the both particle and suspension formulation. Colloidal suspension destabilize by the interaction of aluminum and iron matrix during the electrolysis due to reduction of attractive or repulsive forces, enabling the particles to aggregate and lowering the energy barrier [Holt et al., 2002; Canizaries et al., 2006].

Charge neutralization, double layer compression, bridging and adsorption are the major EC mechanism which depends upon the chemical and physical properties of solution and nature of coagulant and pollutant. Zeta potential measurement under the different operating conditions of EC determine the charged of colloidal particles. Very few studied are reported in literature during the EC mechanism with Al, Fe and SS respectively. Canizares et al. [2007] reported the behavior of zeta potential for Eriochrome Black T (EBT) dye removal with both Al and Fe electrodes. Both exhibited similar behavior in different pH, although the efficiency were not similar and depended upon the speciation of dissolved metals i.e. dose of amorphous (monomeric and polymeric) metal species. Charge neutralization mechanism followed with lower doses of Al by the binding interaction of opposite charge species adsorbed on cationic surface of aluminum hydroxide as compared to iron hydroxide [Canizares et al., 2006]. Kobya et al. [2009] evaluated the possible mechanism of textile wastewater treatment with Fe^{+2} and Fe^{+3} at different pH. Iso-electric point was observed at pH= 6.0. However, the potential value remain negative all over the experiment and pH of the solution did not change during the course of experiment due to some pH buffering capacity exhibited by iron hydroxide during the EC treatment [Holt et al., 2005; Zaroual et al. 2006].

2.5.2. Sludge Reutilization

Electrochemical (EC) method is one of the recently developed simple, cost effective and reliable methodologies having very short treatment time. Despite less generation of EC sludge as compared to conventional coagulation and biological methods, still this sludge contains the electrode material which needs to be disposed off. However, sludge disposal is a one of the biggest challenge for wastewater treatment. Many methods, direct and indirect, are used for the disposal and decomposition of sludge such as sludge settling, sedimentation, incineration, etc. Some of the technologies like thermal decomposition suggest using the sludge as fuel in boilers/incinerators. Use of nano-

materials, such as nano-sized metal oxides which exhibit higher reactivity due to their surface sites properties, as catalysts has increased recently in industrial wastewater treatment [Zhou et al., 2011; Chen et al., 2013; Pouran et al., 2014]. However, application of nano-sized metal oxide in wastewater treatment is widely acceptable. Therefore, a simple, versatile and environmentally friendly methodology is required for preparation ofnano sized metal oxides. Several sustainable methods are already reported in literature for the preparation of nano oxides [Liu et al., 2011; Matos et al., 2011].

Some of investigators are also working on preparation of useful material from different solid wastes [Fan et al., 2008; Kargbo 2010]. Fan et al. [2008] reported arsenate removal using adsorbent prepared from municipal solid waste. Sewage sludge-based composite materials have been used as an adsorbent for interacting with NO_2 [Pietrzak and Bandosz, 2008]. Municipal sludge has been used for biodiesel production proposing a promising technique for replacement of petroleum-based diesel fuel [Kargbo 2010]. But nano materials (NM) and nano-composite materials (NCMs) preparation from solid waste (sludge) is a scientific and engineering challenge. Very few studies are reported for coagulant derived useful materials. Shon et al. [2010] reported the preparation of titanium oxide (TiO_2), aluminum oxide (Al_2O_3) and ferric oxide (Fe_2O_3) from the coagulant derive sludge heated at different higher temperature range [Shon et al., 2007; 2009].

2.6. RESEARCH GAP

It is known from the literature review that a number of EC mechanisms help in treatment of dye bearing effluent during EC treatment, however, the magnitude of the zeta potential essentially determines the stability of the colloids present in wastewater [Espinosa-Jimenez et al., 2002]. Despite its high importance, only scarce studies are reported in the literature explaining the removal mechanism of EC process with relation to zeta potential [Zaroual et al., 2006; Canizares et al., 2007; Singh et al., 2013b]. Based on these research gaps, present study focuses on explaining the effect of various parameters such as current density (j), initial dye concentration (C_o), and initial pH (pH_o) in relation to zeta potential for the EC degradation of BG dye with aluminum electrode.

Review of the literature shows that very few studies are available in open literature which try to elucidate mechanism of degradation of chemical structure of organic dye into smaller one during degradation processes [Chen et al., 2007a, b; Dowling et al., 2007; Oturan et al., 2008; Andersen et al., 2009; Chen et al., 2010; Du et al., 2011; Wu et al., 2011; Sun et al., 2013; Zhou, et al., 2013] (Table 2.6.1). Most of these studies are, however, based on catalytic degradation, biological degradation and advance oxidation processes.

Thus, step-by-step EC mineralization mechanism has not been reported and the schemes of degradation mechanism have not reported earlier in open literature. On the basis of above considerations, one of the major objectives of the present study was to perform step-by-step EC mineralization of BG during EC treatment with aluminum electrode. To the best of our knowledge, this is the first study that elucidates the mineralization mechanism of a dye during EC treatment.

Local dyers in small towns produce huge amount textile printing dye-bath effluent (DBE) during dying of textiles, woollens, etc. in small dye bath, and discharge them without any treatment to open channels. Our research group [Mondal et al., 2012, 2013] previously carried out parametric optimization of parameters for EC treatment of DBE using SS and Al electrodes separately. However, there was a further need to study the treatment of DBE with SS and Al in different anode-cathode combinations (Al–Al, Al–SS, SS–SS and SS–Al). It is also important to study the change in zeta potential and colloid particle size distribution (PSD) of colloids in the solution during the treatment. In continuation with our previous studies and available literature, it was aimed to perform EC treatment of DBE using aluminum (Al) and stainless steel (SS) electrodes in various anode-cathode combinations in a batch EC reactor.

Despite small amount of sludge generation in the EC method as compared to conventional coagulation and biological methods, still the sludge containing the electrode material needs to be disposed off. Only scarce studies are reported on preparation of useful material from different solid wastes but not with EC sludge. Nano-composite materials (NCMs) possessing meso- and micro-pores have received much attention in wastewater treatment in recent years. A study of literature on preparation of NCMs shows that there is a probability of conversion of EC residues to NCMs which can further be used as catalysts for dye degradation.

All these research gaps need to be filled with future studies. The main aim and detail objectives of this present study (as given in Chapter I) have been formulated based upon the research gaps identified in the literature (as discussed above).

Table 2.6.1. Literature of various degradation studies on Basic Green (BG) in different wastewaters.

Process used in study	Experimental conditions	Analytical studies	Remarks	Ref.
Multi–residue method	Liquid–liquid extraction in different conc. of sample in different conditions.	LC–MS	m/z (329; 314; 313; 285; 251; 237)	Dowling et al., 2007
Cation exchange (solid phase extraction)	C_o: 0.25mg/L; pH: 4.5; T: 25^oC; m: 0.05 mol/L ammonium acetate.	HPLC; MP-SPE	Separation of BG dye from mixed dye without mass data	Chen et al., 2007
UV induced photodegradation on (TiO_2) nanaoparticle	C_o: 50 mg/L; pH: 7.0; T: 25^oC; m: 0.05g/L TiO_2; t: 24hr.	HPLC–MS	m/z (329.26; 315.18; 301.22; 287.05)	Chen et al., 2008
Oxidation pathway with electro–Fenton (Fe^{3+}catalysed)	C_o: 0.5 mg/L; pH: 3.0; T: 25^oC; m: 0.2g/L Fe^{3+}; j: 250mA/cm^2; t: 540min.	HPLC; GC–MS; ion exchange	m/z (239; 225; 197; 166; 137; 126; 93;	Oturan et al., 2008
Anaerobic treatment (Shewanella NTOU1)	C_o: 50 mg/L; pH: 6.6; T: 35^oC; m: 0.5g L^{-1} t: 5.0 h.	GC–MS	m/z (330; 253; 239; 210; 165; 126)	Chen et al., 2010
Biodegradation (Pandoraea pulmonicola YC32)	C_o: 100mg/L; pH: 7–10; T: 35^oC; m: 106 mg/L of P. pulmonicola cells; t: 210min.	HPLC; GC–MS	m/z (330; 329; 315; 301; 284; 225)	Andersen et al., 2010
Biodegradation by *sphingomonas sp.* CM9	C_o: 100mg/L; pH: 7.0; T: 30^oC; m: 50 mg/L; t: 24h.	HPLC-MS; GC–MS	m/z (92; 91; 65)	Wu et al., 2011
Aerobic Biodegradation (Pseudomonas sp. strain DY1)	C_o: 800mg/L; pH: 6.6; T: 30^oC; m: 2g/L; t: 24h.	UV–visible; GC–MS; LC–MS	m/z (347; 226; 212; 198; 167;121)	Du et al., 2011
Capillary electrophoresis with extraction procedure	C_o: 30mg/L; pH: 4.0; T: 25^oC; m: 50 mM buffer H_3PO_4; V_{ap}: 23V	HPLC	Only based on separation of BG-4 from fish liver by HPLC	Sun et al., 2013
Ultrasonic assisted ozone oxidation	C_o: 35.85mg/L; pH: 5.29; T: 20^oC; m: 75 mM of O_3; Q: 12 L/h	HPLC-MS–MS	m/z (329.4; 315.4; 301.3; 287.5; 225)	Zhou et al., 2013

Notation: C_o: initial dye concentration; m: amount of species/electrolyte concentration added; V_{ap}: Voltage applied; j: applied current density; t: treatment time; Q: flow rate; g: electrode gap; A: electrode surface area; m/z molecular mass.

Abbreviation: MP-SPE: molecularly imprinted solid-phase extraction; Response Surface Methodology (RSM).

2.7. BRIEF DISCRETION OF EC TREATMENT TECHNOLOGY

The major screened-off areas in the ECT are electro-coagulation (EC), electro-flotation (EF) and electro-oxidation (EO).

2.7.1. Electro-flotation (EF)

A simple process in which buoyant gases bubbles generated during electrolysis take pollutant materials to the surface of liquid body is EF process. Bubbles of hydrogen and oxygen, generated by electrolysis of water move upwards in the liquid phase. A layer of foam, containing gas bubbles and floated particles is formed at the surface of water [Kushwaha et al., 2010, 2011]. The rate of flotation depends on several parameters such as surface tension between the water particles and gas bubbles; the bubble size distribution and bubble density; size distribution of the particles; the residence time of the solution/liquid in the EC cell and the flotation tank; the particle and gas bubble zeta potentials; and the temperature, pH of the solution [Singh et al., 2014].

2.7.2. Electro-oxidation (EO)

Decomposition of organic materials through EO treatment means the oxidation of organic pollutants present in wastewater to give carbon dioxide, water or other oxides. The electrochemical oxidation of wastewater is achieved in two ways. First, by direct anodic oxidation, in which organic compounds are adsorbed at the electrode and oxidized at the surface of the electrode or by indirect oxidation in which some oxidizing agents are generated electrochemically that may cause oxidation of organic species present in the solution [Kushwaha et al., 2010].

Organic pollutants are adsorbed at the surface of anode in direct anodic oxidation process, where active oxygen (adsorbed hydroxyl radicals) or chemisorbed "active oxygen" is accountable for the oxidation of adsorbed organic pollutants. The mechanistic outline for the oxidation of organic matter on oxide anode (MO_X) as suggested by Panizza and Cerisola [2009] is given below [Arslan et al, 2000; Panizza and Cerisola 2007, 2008]:

$$H_2O + MO_X \longrightarrow MO_X[OH] + H^+ + e^- \qquad (2.7.1)$$

The adsorbed hydroxyl radicals may form chemisorbed active oxygen.

$$MO_X[OH] \longrightarrow MO_{X+1} + H^+ + e^- \qquad (2.7.2)$$

The liberated chemisorbed active oxygen is responsible for the oxidation process.

During the EO treatment process, two types of oxidation are possible. In one way, toxic and non-biocompatible pollutants are converted into bio-degradable organics, so that further biological treatment can be initiated. In contrast, in other way pollutants are oxidized to water and CO_2 and no further purification is necessary.

Martinez–Huitle and Ferro [2006] has postulated that indirect oxidation process may lead to the formation of strong oxidant such as hypochlorite/chlorine, ozone, and hydrogen peroxide by following chemical reaction:

$$H_2O + Cl^- \longrightarrow HOCl + H^+ + 2e^- \quad (2.7.3)$$

High voltage can tune a possibility of the formation of hydrogen peroxide and other molecules in the following way-

$$H_2O \longrightarrow OH, O, H^+, H_2O_2 \quad (2.7.4)$$

These oxidants oxidize many inorganic and organic pollutants in the bulk solution [Szpyrkowicz et al., 2001; 2005a, b].

2.7.3. Electro-coagulation (EC)

Alike simple coagulation, EC is the process of destabilization of colloidal particles present in wastewater and can be achieved by two mechanisms. In the first one is, an increase in ionic concentration, gives rise to reduction in the zeta potential/adsorption of counter-ions on colloidal particles to neutralize the colloidal particle charge, while in the other, by well known sweep flocculation mechanism [Duan et al., 2003; Kushwaha et al., 2010].

EC processes start when electrodes directly connected to electric power source generate coagulants at the anode and hydrogen gas generated at cathode via electrodes dissolution [Muthukumar et al., 2006; Murthy et al., 2007; Merzok et al., 2010; Murthy and Parmar 2011].

Generally EC process performance depends upon the chemistry of wastewater especially in terms of conductivity and particle size, pH and chemical constituent. Three main mechanisms are takes place i.e. (1) electrode surfaces reactions (electro-dissolution reaction) in electrolyte; (2) coagulants formation; (3) pollutants adsorbed on the coagulants and removed by flotation or sedimentation.

Electro-dissolution and electrolysis reaction of different electrode combination was described at anode and cathode. Metal cations (at anode) and OH ions (at cathode) react to form of various monomeric and polymeric species and ultimately get converted into $Al(OH)_3$ and $Fe(OH)_3$ coagulants through complex reactions.

Different monomeric, polymeric and ionic species play crucial role in the removal efficiency. The interaction rate between dye molecules and hydrolysis products depends upon the pH and ions present in the colloidal suspension. At the same time, zeta potential measurements give the support on the same type of interaction in terms of zero point charge (zpc) in the treatment solution. The soluble hydroxide and oxy-hydroxide

monomeric species polymerize into insoluble amorphous species. On the basis of this observation, in literature two main interaction mechanisms precipitation and adsorption have been suggested at separate pH range (low and high) for both electrodes, respectively [Singh et al., 2013a, b and c; 2014]. At higher pH, like charge species concentration increases in the colloidal suspension and decrease the removal efficiency. However, "sweep flocs" of freshly formed amorphous hydroxides, $Al(OH)_3$ and $Fe(OH)_3$, rapidly adsorbed and immobilise the dye and other colloidal particles. Hence, they are easily removed from the solution by flotation and sedimentation mechanism.

Chapter – 3

EXPERIMENTAL

This chapter deals with the description of the materials and experimental methods adopted for electrochemical (EC) treatment of synthetic textile wastewater (STW) containing basic dyes, aqueous solution containing basic green 4 (BG) dye and an actual dye bearing effluent (DBE).

3.1. MATERIALS

All the chemicals used in this study were of analytical grade. Basic green 4 (BG-4), basic orange (BO-30) and basic violet (BV-16) were purchased from Yogesh dyestuff product Ltd., India. Reagents mercuric sulphate (Hg_2SO_4) and silver sulphate (Ag_2SO_4) were obtained from Himedia laboratories, India. Potassium dichromate ($K_2Cr_2O_7$), sulfuric acid (H_2SO_4), sodium chloride (NaCl) and sodium hydroxide were obtained from Ranbaxy chemicals Ltd., India. Carboxy methyl cellulose (CMC), starch, sodium carbonate (Na_2CO_3) sodium bicarbonate ($NaHCO_3$), hydrochloric acid (HCl) and nitric acid (HNO_3) were obtained from S.D. fine chemicals, India. Di-chloromethane (CH_2Cl_2), acetic acid (CH_3COOH), acetophenol acetonitrile (CH_3COOCN) and formic acid (HCOOH) were purchased from Merck, India.

Millipore water was obtained from a Milli–Q water ion exchange system and was used for the preparation of all analytical standards and for the eluent preparation and sample dilution in chromatography. All solvent employed in chromatography were of high performance liquid chromatograph (HPLC)–grade. The aluminum (Al) and stainless steel (SS) sheet used as electrode materials were procured from the local suppliers.

3.2. WASTEWATER

Three types of wastewaters namely STW containing three basic dyes, aqueous solution containing basic green 4 dye and actual DBE were used in present study. The STW was synthetically prepared using basic orange 30, basic violet 16 and basic green 4 dyes as per the method reported in the literature using chemicals (Table 3.2.1) which are commonly found in textile mill wastewater [Korbahti and Tanyolac, 2008; Singh et al., 2013a]. For studying the dye degradation mechanism of basic green 4 dye, stock solution containing 1000 mg/L of dye was prepared. The desired concentration of dye

solution was prepared by dilution the stock solution with distilled water [Singh et al., 2013b,c]. The characteristic of basic green 4 is given in Table 3.2.2. DBE used in the present study was collected from local dyer in Roorkee.

Table 3.2.1. The composition of synthetic textile wastewater.

Pollutant	Concentration (mg/L)
Carboxy Methyl Cellulose	150
Starch	1500
Acetic acid	500
Basic orange	50
Basic violet	50
Basic green	50
NaOH	660
H_2SO_4	357
NaCl	500
Na_2CO_3	1000
$NaHCO_3$	2000
Glucose	2062

Table 3.2.2. Characterization of the basic green 4 (BG) dye.

Characteristic name	Value
Color index name	C.I. Basic Green 4 (BG)
Color index number	C.I.42000
CAS number	569-64-2
Chemical Class	Acrylic, cationic dye
Chromophore	Triaryl methane
Common name	Aniline green; Victoria green B; Malachite green
Water solubility at 293 K (g/l)	60
pH value	5.4
Molecular formula	$C_{23}H_{25}ClN_2$ (chloride)
Molecular weight (g/mol)	364.911 g/mol (chloride)
λ_{max} (nm)	619

3.3. EXPERIMENTAL METHODOLOGY

Perspex made EC batch reactor of 1.5 L capacity (130 mm×130 mm×210 mm) was used in the experiments. Most of the experiments were carried out with two Al electrodes only, however, for treatment of DBE, Al and SS plate electrodes were used in parallel connection as various anode-cathode combinations. Each electrode was having 108 mm×108 mm×130 mm dimension with total submerged area being 63.75 cm^2. Electrode gap of 1.0 cm was maintained between the electrodes for providing sufficient movement space to the liquid/solid particles between the electrodes. The electrodes were connected to a digital dc power supply (0–20 V, 0–5 A) equipped with potentiostatic or galvanostatic operational options. Agitation of the solution was done using magnetic stirrer. The schematic diagram of the laboratory scale experimental set-up in the electrochemical degradation studies is shown in Figure 3.3.1.

All EC experiments were conducted in thermostatically controlled cuboid batch reactor with 1.5 L capacity at the specified conditions. Two electrodes (Al and SS) with different anode-cathode combinations such as Al–Al, Al–SS, SS–SS and SS–Al have been used in this study. A magnetic stirrer with 600 rpm speed was used for stirring the solution during treatment. The pH of the solution was adjusted by adding 0.1 N NaOH or 0.1 N H_2SO_4, respectively. Reaction time (t) was measured from the time when power supply was switched on. Current density (j) was maintained constant during each experimental run. After the desired treatment time, the treated solution was centrifuged at 2000 rpm for 20 min and the supernatant was used for determination of residual color, COD, TOC and turbidity concentration. After the experiment, the electrodes surface was washed with acetone and followed by dipping in HCl (35%) and hexamethylene tetra amine ($(CH_2)_6N_4$) (2.9%) for 5 min after each run to remove the impurities from electrode surface after which it was dried and reweighed.

Energy consumption (ENC) is an extremely important parameter of an EC process and is directly proportional to current passed and electrode dissolution during the EC treatment. ENC (kWh/m^3) was calculated using the following equation:

$$\mathrm{ENC} = \frac{UIt_{EC}}{V} \qquad (3.3.1)$$

Where, U is the cell voltage (V), I is the current (A), t_{EC} is the time (s) of electrocoagulation and V is the volume (m^3) of wastewater treated.

SEC is an extremely important parameter of an EC process and is directly proportional to current passed and electrode dissolution during the EC treatment. SEC (kWh/kg COD removed) was calculated using the following equation:

$$SEC = \frac{UIt_{EC} \times 1000}{\left(COD_o - COD_{t_{EC}}\right)V} \quad (3.3.2)$$

Where, U is the cell voltage (V), I is the current (A), t_{EC} is the time (h) of electrocoagulation, V is the volume (L) of wastewater treated, COD_o is the initial COD of the solution in mg/L and COD_t is the COD in mg/L at time t.

Theoretical amount of anodic dissolution (ELC_t) was calculated using Faraday's law [Singh et al., 2013b; Ghosh et al., 2008]:

$$ELC_t = \frac{It_{EC}M_w}{ZFV} \quad (3.3.3)$$

Where, ELC_t is the theoretical metal consumption (kg/m^3), M_w is the molecular weight of anode (g/mol) in the EC reactor, Z is the chemical equivalence and F is the Faraday's constant (96,500 C/mol). Actual or experimental amount of anodic dissolution (ELC_e) was calculated by weighing the anode before and after experiment.

Current efficiency (CE) was calculated using the following equation [Singh et al., 2013b, Singh et al., 2014].

$$CE = \frac{ELC_e}{ELC_t} = \frac{ELC_e}{\left(ZFV\right)/\left(It_{EC}M_w\right)} \quad (3.3.4)$$

Where, ELC_e is the actual or experimental amount of anodic dissolution (kg/m^3) which was calculated by weighing the anode before and after experiment, ELC_t is the theoretical metal consumption (kg/m^3) which was calculated using Faraday's law, M_w is the molecular weight of anode (g/mol) in the EC reactor, Z is the chemical equivalence and F is the Faraday's constant (96485.3 C/mol).

3.4. SLUDGE GENERATION

In EC treatment, some amounts of solid residues (sludge and scum) also get generated. Despite small amount of sludge generation in the EC method as compared to conventional coagulation and biological methods, still the sludge containing the electrode material needs to be disposed off. Therefore studies are required on disposal or reutilization of these residues. The sludge generated with Al and SS electrodes have different characteristic. Sludge generated during EC treatment were collected after the experiments, dried in oven for removal of moisture then stored in desiccators for performing various physico-chemical analyses later. Thermogravimetric analysis gives the information regarding potential use of sludge as a fuel in the boilers/incinerators for recovering energy. There is a potential of preparation of nano materials (NMs) and nano-composite materials (NCMs) from the non-decomposable part of sludge as identified in chapter II. Preparation of NCMs was done as follows. 5 g of the solid waste was taken in a silica crucible and heated in a muffle furnace from 100°C and gradually increasing the temperature in steps of 100-300 °C up to 1000^{o}C. Finally, the samples were furnace cooled and coded as follows according to the calcination temperature.

Figure 3.4.1 gives various paths that have been used in the present work for carrying out various studies as per objectives given in chapter 1.

3.5. ANALYTICAL AND CHARACTERIZATION METHODS

To understand the dye degradation mechanism and treatment efficiency, various physico-chemical analysis and characterization of treated wastewater and solid residues was done using various techniques (Table 3.5.1) details of which are described briefly in subsequent paragraphs.

3.5.1. UV -visible spectrophotometer

Double beam UV visible spectrophotometer (HACH, DR 5000, USA) designed on split-beam for multiple analyate analysis with accuracy of ±1 nm and resolution of 0.1 nm and having multi wavelength scanning facility from 190-1100 nm was used for various analysis. Chemical oxygen demand (COD) and color of initial and treated samples was determined using digestion unit (DRB 200, HACH, USA).

Dye concentration was determined (λ_{max}) by measuring the absorbance of unknown sample at wavelength of maximum absorbance and then comparing the value to previous drawn calibration plot of absorbance versus known concentrations. The

change in λ_{max} determined by UV-visible spectral analysis during the treatment helped in determining the structural changes in dye with time during the EC treatment process and thus helped in the understanding the dye degradation mechanism.

Turbidity of initial and final sample was measured by turbidity meter (2100P, HACH).

The percentages of removal efficiencies of each factor were calculated using the following relationship:

$$\text{Removal efficiency (\%)} = \frac{(C_o - C_f)100}{C_o} \qquad (3.5.1)$$

Where, C_o is the initial (mg/L) and C_f the final (mg/L) value of COD, color and turbidity.

3.5.2. High performance liquid chromatography

The concentration of intermediate compounds at different time interval formed during the EC treatment of basic green 4 dye degradation was analyzed by HPLC supplied by water India Ltd. HPLC system consists of the mobile phase, separation column and detector. The separation in the column is achieved by the partitioning of solute between the mobile phase and stationary phase held on the solid support. HPLC system used in the present study was equipped with C18 reverse phase column having 5 μm column, 150 mm × 4.6 mm internal diameter (ID) and ultra-violet (UV) detector. The mobile phase was prepared for liner gradient elution. The gradient was set as follows: 60% acetonitrile in H_2O (0.1% HCOOH) for 3.5 min followed by a 10 min linear gradient by 80% acetonitrile (0.1% HCOOH). Mobile phase and analytic samples filtered through 0.2 μm pore size membrane (PTFE) filter were used in HPLC system. The analysis was carried out in the mobile phase flow rate at 1.0 ml/min for liner gradient. Wavelength in the UV detector was kept at 610 nm for the measurement of basic green 4. A calibration curve was prepared for basic green 4 and was used to evaluate the experimental data.

Figure 3.3.1. Experimental setup for electrochemical treatment.

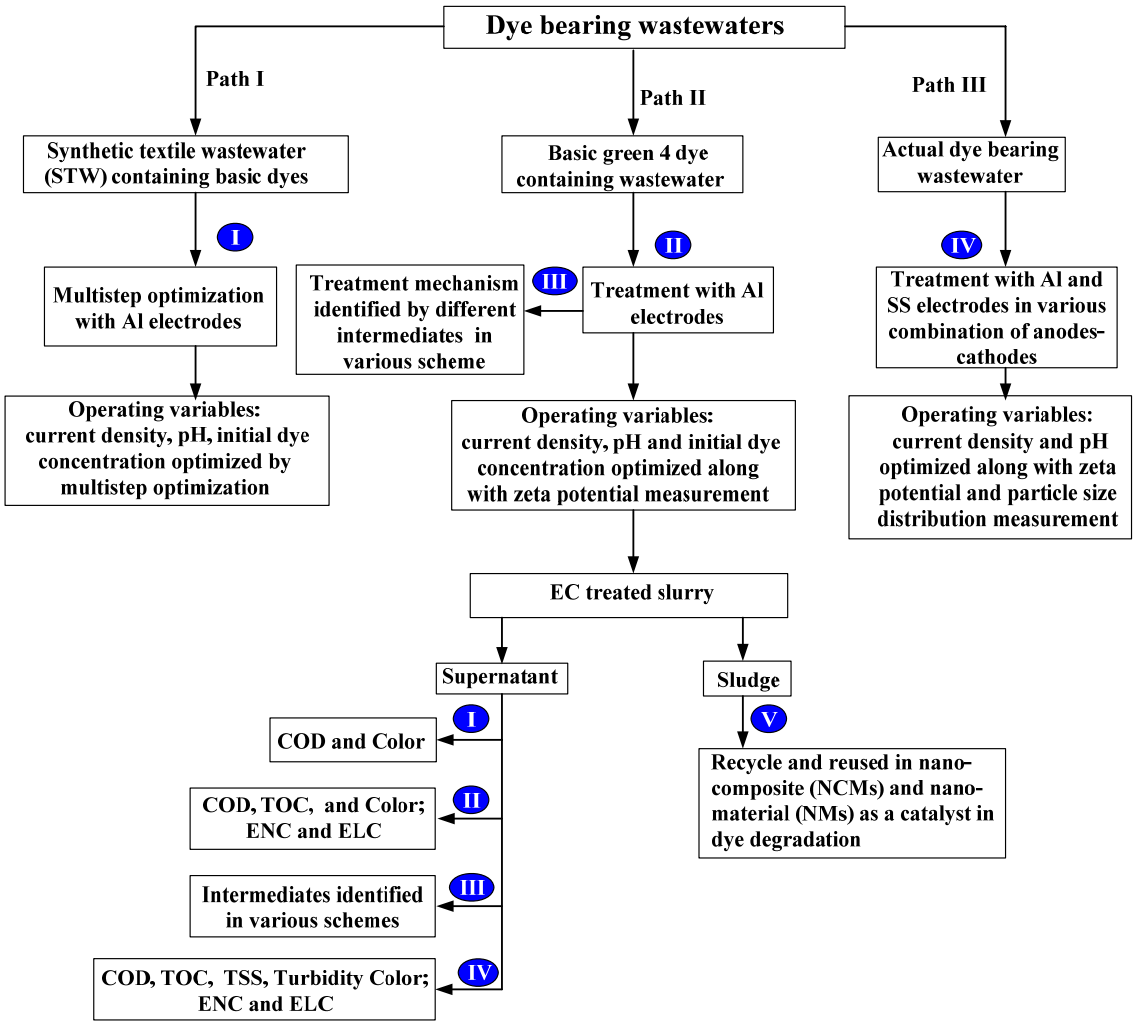

Figure 3.4.1. Flow diagram of various studies in the present work.

Table 3.5.1. Summary of various analytical and characterization techniques used in present study.

Characterization techniques	Chapter IV					
	4.1	4.2		4.3	4.4	
		4.2.1	4.2.2		4.4.1	4.4.2
Spectrophotometers	√	√		√	√	√
HPLC			√			
COD analyzer	√	√		√	√	√
TOC analyzer		√		√		
Turbidity meter				√		
HPLC			√			
GCMS			√			
HRMS			√			
FESEM/EDAX	√	√		√	√	√
TGA/DTA				√	√	√
XRD		√			√	√
BET		√		√	√	√
TEM					√	√
AFM					√	√
XPS					√	

3.5.3. Total organic carbon (TOC) analyzer

Total organic carbon (TOC) analyzer (TOC–V–CSN 39208967, Shimadzu) equipped with an auto sampler and non dispersive infra-red (NDIR) detector was used in the present study. Instrument measured total carbon (TC) and inorganic carbon (IC) directly and the TOC was determined by the instrument through subtraction of IC from TC values. TOC estimation process involved catalytic oxidation of the sample followed by quantification of the CO_2 formed through NDIR detector.

TOC analysis is based on a combustive and NDIR gas analysis method. For TC estimation, high purity zero air is supplied as carrier gas to the combustion tube at the rate of 150 ml/min. Combustion tube consist of quartz tube filled with oxidation catalyst (platinum catalyst), maintained at 680 ^{o}C. After combustion, carrier gas carries the sample combustion products first through dehumidifier, where the gas is cooled and dehydrated, thereafter through halogen scrubber, where chlorine and other halogen compounds get removed. Effluent gas is detected in terms of CO_2 through NDIR gas analyzer to estimate TC. Potassium hydrogen phthalate was employed as standard for TC calibration.

For estimating ICs (carbonates, bicarbonates and dissolved CO_2 in water), sample was injected into the inorganic carbon reactor vessel where the carrier gas flows in the form of tiny bubbles through a solution sample acidified by IC reagent (25% phosphoric acid). Only the IC gets decomposed to CO_2, which is then detected by NDIR detector. Sodium carbonate and sodium bicarbonate were used as standards for IC calibration.

Each sample was injected thrice, which was validated by the apparatus only when the standard deviation was less than 3%. TOC values used for analysis were average of at least two measurements.

3.5.4. Thermo-gravimetric analysis (TGA)

Thermal analysis of the solid residue was carried out by using a thermal analyzer (TA) instrument. Thermogravimetric (TGA), differential thermogravimetric (DTG) and the derivatives thermal (DTA) analysis were carried out from the data and the plot obtained from the instrument (Perkin Elemer Pyris Diamond) having a flow rate of 200 ml/min, in the temperature range from room temperature to 1000^{o}C with heating rate of 10^{o}C/min. Aluminum was used as a reference material. The continuous weight loss of a sample during TGA under oxidative (air or oxygen) and inert gas

atmospheres is a function of temperature (or time) and is governed by the thermal event (volatilization) or chemical reaction (combustion).

3.5.5. Spectroscopic Analysis

3.5.5.1. Fourier transformation infra red (FTIR) spectroscopy: In Infra red spectroscopy, finger-print region provides valuable information regarding sample composition by determining the functional groups present in samples. FTIR spectrophotometer (Nicolet Avtar 370, Thermo-scientific Instruments Corporation, USA) equipped with EZ-OMNIC software was used for the analysis of dye solution at different time interval and solid residue generated after the treatment. Pellet (pressed–disk) technique was used over a spectral wave number range of 400-4000cm^{-1}. The samples (solution and solid residue) were prepared using the potassium bromide (KBr) disc method.

3.5.5.2. Mass spectroscopy: Molecular mass of intermediates formed during EC degradation of basic green 4 dye was determined by gas chromatography–mass spectroscopy (GCMS) and high resolution mass spectroscopy (HRMS). Gas chromatography mass spectrometer (GC-MS) separated, identified and quantified the complex mixtures of chemicals by the analysis of the hundreds of relatively low molecular weight compounds. Sample was injected into the GC where it was vaporized and swept onto a chromatographic column by the carrier gas. At the last, compounds elute from ion source column and get converted to ions. A Perkin–Elmer Auto system–XL gas chromatograph interfaced to a turbo mass selective mass detector in DB–5 fused silica capillary column (30 m×0.25 μm internal diameter) of 5% diphenyl/95% dimethyl–siloxane. The split–split less injector mode was used with injector temperature (280^{o}C) and split flow 10 mL/min. Helium was used as carrier gas with flow rate of 1 mL/min. Mass spectra were obtained in m/z range of ≈50–500 at 70eV. The temperatures corresponding to the inlet line and ion source were set at 240 and 280^{o}C, respectively.

3.5.5.3. X-Ray Photoelectron Spectroscopy: X-Ray photoelectron spectroscopy (XPS), also known as ESCA (electron spectroscopy with chemical analysis) is a surface sensitive quantitative spectroscopic technique that measures the elemental composition at the parts per thousand range. XPS spectra are obtained by irradiating a material with a beam of X-rays while simultaneously measuring the kinetic energy by the number of electrons that escape from the top 0 to 10 nm of the material and analyzed. XPS

requires high vacuum (P~10^{-8}millibar) or ultra-high vacuum (P<10^{-9}millibar). A typical XPS plot consists of a number of peaks drawn as number of electrons detected versus the binding energy of the electrons. These set of peaks represent characteristic binding energy value which directly identify element present on the surface of material being analyzed.

XPS of sludge sample (Sludge at 0 ^{o}C and 800 ^{o}C) samples were recorded in Thermo Fisher Scientific Multilab 2000 spectrometer using AlKα radiation (1486.6 eV) as an X-ray source operated at 150 W (12 kV and 12.5 mA). Binding energies reported here were calculated with reference to C1s at 284.6 eV having a precision of ± 0.2 eV. All the spectra were obtained with pass energy of 25 eV and step increment of 0.05 eV. For XPS analysis, powder samples were made into 8 mm diameter pellets, mounted on the sample holder and kept into preparation chamber with ultrahigh vacuum (UHV) at 10^{-9} Torr for 5 h in order to desorb any volatile species present on the sample surface. After this time period, samples were placed into analyzer chamber with UHV at 10^{-9} Torr.

3.5.6. Microscopic Analysis

3.5.6.1. Field Emission Scanning Electron Microscope (FE-SEM) and Energy-Dispersive X-ray analysis (EDX): Scanning electron microscope (SEM) is often the preferred basic tool for analytic microscopy. SEM generates an image of largely magnified by electrons. Energy Dispersive X-ray (EDX) provide the information about the elemental composition of sample surface and backscattered X-rays gives the information for mapping the elemental features at the surface of the materials and rapid discrimination in multiphase samples. Field emission scanning electron microscope (FE-SEM) (QUANTA 200-FEG) was used to examine the surface topography. The elemental analyses of the solid sample at various locations were analyzed with EDX accessory (FEI-TECNAI 300 kV digital). The sample were first grounded to make the samples homogeneous and then spread on the sample holders in such a manner to produce flat surfaces. After this, the samples were gold coated using sputter coater (Edwards S150) to provide conductivity to the samples, and then the images of FE-SEM were taken at an acceleration voltage of 20 kV under low vacuum. The error in the content of elements determined using this method is between 5 and 10%.

3.5.6.2. Transmission Electron Microscope (TEM): The transmission electron microscope (TEM) was used for the microstructure analysis of the samples with atomic scale resolution by using the high energy electron beam transmitted through a very thin

sample to image. Electromagnetic lenses are used to focus the electrons and image is observed on a fluorescent screen. TEM micrographs of samples were recorded on FEI-TECNAI 300 kV digital TEM equipped with EDAX facility having resolution of 0.19 nm by scanning the dried grid at different magnifications under the electron microscope. Carbon-coated copper grid G-200 (size 3.05 mm) were used for preparing the sample by applying a drop of the colloidal sample Excess amount of colloidal solution was removed by tissue paper and then the grid was placed in a dark room for 30 min for evaporate the remaining moisture. Selected area electron diffraction (SAED) patterns were recorded to obtain the crystallographic information from the selected regions of the sample. The diffraction spots orientations and planar spacing were indexed by using a ratio method and different rings were used for determining the Miller indices.

3.5.6.3. Atomic Force Microscope (AFM): Atomic force microscope (AFM) is a scanning probes microscope and does an extremely fine probe profiling of the surface by measuring the deflection of the cantilever. 2D and 3D images of samples at magnifications over one million times were obtained by the drop casting method using tapping mode of AFM supplied by M/s Molecular Tools and Devices for Nanotechnology (NT-MDT). AFM was equipped with NOVA software for image analysis.

3.5.7. Surface Area and Pore Size Distribution Analysis

Pore size distribution, porosity and pore surface area of solid samples were determined using liquid nitrogen adsorption–desorption isotherms measured at temperature of 77 K with Micromeritics ASAP 2020 apparatus. Brunauer-Emmett-Teller (BET) [Barret et al., 1951; Iglesias et al., 2011] surface area was calculated using the following relation:

$$\frac{p}{v(p_o - p)} = \frac{1}{v_m C} + \frac{(C-1)p}{v_m C p_o} \qquad (3.5.2)$$

Where, p_o is the saturated vapour pressure at (-200^{o}C), v is the volume of gas adsorbed at the equilibrium pressure, and v_m is the liquefaction (Q_1) of nitrogen gas.

Pore size distribution analysis was done by using Barrett-Joyner-Halenda (BJH) method [Barret et al., 1951; Singh et al., 2013b]:

$$\ln\left(\frac{p}{p_o}\right) = -2\sigma v \cos\left(\frac{\theta}{r_k R}\right) \qquad (3.5.3)$$

Where, σ is the surface tension, θ is the wetting angle, R is the gas constant and r_k is the Kelvin's radius. Before the analysis, the sample was degassed at 300^oC for about 6 h. The surface area was obtained using BET model for adsorption data in a relative pressure range of 0.05 to 0.30. The total pore volume was calculated from the amount of N_2 vapor adsorbed at a relative pressure of 0.99.

3.5.8. Scattering Analysis

3.5.8.1. Dynamic Light Scattering (DLS) or Zeta Potential Analysis: Dynamic light scattering (DLS) technique was employed for determining the zeta potential and particle size distribution (PSD) of colloids present in the solutions. Malvern Nano Zetasizer (Z–S 90, UK) was used to measure the colloidal suspension stability during EC processes using a non-invasive technique.

3.5.8.2. Powder X-ray diffraction (PXD): Powder X-ray diffraction (PXD) patterns were recorded on a Bruker AXS D8 Advance powder X-ray diffractometer operating at 40 kV and 30 mA using Cu Kα radiation (λ = 1.5418 Å) in the angular range 10–90^o. The data were recorded at a scan rate of 0.02°/step and 0.5 s per step. The observed PXD patterns were analyzed by comparing with the powder diffraction files available in the joint committee on powder diffraction standards (JCPDS) database.

3.6. EXPERIMENTAL STRATEGY DURING EC TREATMENT OF STW

3.6.1. Placket–Burman (PB) design

Placket–Burman (PB) design has been used previously for screening and evaluating the important variables that influence the response of a particular process [Liu et al., 2010; Myers and Montgomery 2002; Singh et al., 2013a]. A total (n) of six parameters (current density (j), time (t), electrode gap (g), temperature (T), initial pH (pH_o) and salt concentration (m)) were investigated using PB design to identify the variables that significantly affect the COD and color removal efficiency. Each variable was represented at two levels, high and low, denoted by (+) and (-) signs, respectively. Table 3.6.1 illustrates the factors under investigation as well as levels of each factor used in the experimental design. Table 3.6.2 shows the PB matrix used for EC treatment of STW.

3.6.2. Path of steepest ascent/descent

The initial estimate of the optimum operating conditions for any system by PB design is far from the actual optimum. Therefore, variables that significantly influenced

the desired responses were optimized by performing experiments as per steepest ascent/descent method [Myers and Montgomery, 2002; Loukas, 2001].

3.6.3. Optimization by Box-Behnken (BB) design

The minimum and maximum ranges of these three variables namely; j (117.64-196.07) A/m^2, t (120-240) min and pH_o (3.5-5.5) identified using PB design and the path of steepest ascent/descent were taken as input parameters for Box-Behnken (BB) design. A total of 17 experiments were conducted as per BB design (Table 3.6.3).

Table 3.6.1. Levels and units of the factors used in the Plackett-Burman design.

Factors	Units	Level	
		Low (-)	High (+)
A. Current density	A/m^2	117.6	588.23
B. Time	Min.	60	180
C. Gap	cm	1	3
D. Temperature	^oC	30	50
E. pH	-	3	10
F. Salt	g/l	0	2

Table 3.6.2. Plakett-Burman matrix used for EC treatment of STW.

Std. order	A	B	C	D	E	F
1	1	-1	1	-1	-1	-1
2	1	1	-1	1	-1	-1
3	-1	1	1	-1	1	-1
4	1	-1	1	1	-1	1
5	1	1	-1	1	1	-1
6	1	1	1	-1	1	1
7	-1	1	1	1	-1	1
8	-1	-1	1	1	1	-1
9	-1	-1	-1	1	1	1
10	1	-1	-1	-1	1	1
11	-1	1	-1	-1	-1	1
12	-1	-1	-1	-1	-1	-1

Table 3.6.3. Box-Behnken (BB) matrix used for EC treatment of STW.

Std. order	Run	j (A/m^2), X_1	t (min), X_2	pH_0, X_3
1	4	117.64	150	4.5
2	16	196.07	150	4.5
3	1	117.64	210	4.5
4	11	196.07	210	4.5
5	6	117.64	180	3.5
6	3	196.07	180	3.5
7	10	117.64	180	5.5
8	14	196.07	180	5.5
9	13	156.85	150	3.5
10	9	156.85	210	3.5
11	7	156.85	150	5.5
12	5	156.85	210	5.5
13	17	156.85	180	4.5
14	12	156.85	180	4.5
15	2	156.85	180	4.5
16	15	156.85	180	4.5
17	8	156.85	180	4.5

Chapter –4

RESULTS AND DISCUSSION

This chapter presents the results and discussion concerning to electrochemical (EC) treatment of dye bearing wastewater from aqueous solution using aluminum (Al) and stainless steel (SS) electrodes. This chapter has been sub-divided into the following four sections as per the objectives given in section 1.6:

- EC treatment of synthetic textile wastewater (STW) containing basic dyes with Al electrode
- Dye degradation mechanism of basic dye during EC treatment with aluminum electrode
- EC treatment of actual dye bearing effluent (DBE) with various combination of Al and SS electrodes
- Recycling and disposal of EC sludge

4.1 EC TREATMENT OF SYNTHETIC TEXTILE WASTEWATER (STW) CONTAINING BASIC DYES WITH ALUMINUM ELECTRODE

This section of the present study aimed to investigate the effectiveness of Al electrode for the treatment of synthetic textile wastewater (STW) in terms of COD and color removal efficiencies. A multi-step procedure was applied to screen and optimize the factors. First, Plackett–Burman (PB) was employed to screen most significant three factors among a largest number of parameters. Afterwards, method of steepest ascent and Box-Behnken (BB) design were used to determine the optimum levels of the factors that significantly influence the COD and color removal efficiencies.

4.1.1. Characterization of synthetic textile wastewater (STW) [Singh et al., 2013a]

The synthetic textile wastewater **(**STW) prepared as per method given in section 3.2 was analysed for its physico-chemical parameters as per standard methods [APHA, 2005] and the methods described in Chapter 3. The wastewater was dark brownish red in color and had very low transparency. The characteristic of the wastewater are shown in Table 4.1.1.

Table 4.1.1. Characteristics of synthetic textile wastewater.

Parameter	Value
Chemical oxygen demand (mg/L)	2900
Color (Pt-Co)	1440
Turbidity, NTU	18
pH	9.7
Total solids (mg/L)	12.38
Dissolved oxygen (mg/L)	5.1
Total volatile solids (mg/L)	4990
Total suspended solids (mg/L)	120
Non-volatile solids (mg/L)	7390
Chloride (mg/L)	413
Conductivity (mS/cm)	6.1

4.1.2. Screening of the parameters by Plackett–Burman (PB) design

PB design was utilized to assess the significant parameters. A total (n) of six parameters (current density (j), time (t), electrode gap (g) , temperature (T), pH (pH_o) and salt concentration (m)) were investigated using PB design to identify the variables that significantly affect the COD and color removal efficiency. Each variable was represented at two levels, high and low, denoted by (+) and (-) signs, respectively (Table 4.1.2).

Responses (COD and color) were measured in terms of removal efficiency. The main effects plot is most useful when there are several factors (Figure 4.1.1). Changes in the level-means can be compared to deduce which factors highly influence the response. The factors which have greatest slope in absolute terms in Figure 4.1.2 can be considered as the most influential parameters. First-order model linear equation was used to elucidate the most important factors by PB design:

$$y = \beta_o + \sum_{i=1}^{n} \left(\beta_i X_i \right) \tag{4.1.1}$$

Where, y represents the response (i.e. COD or color removal efficiencies), β_o is the model intercepts, β_i is the linear coefficient, X_i is the level of the independent variable, and n is the number of involved variables. Regression analysis was further done to find out parameters which were significant at 5% level ($P < 0.05$). Regression coefficients and their

significance for the response of PB design are given in Table 4.1.2. Following equations obtained from PB design represents the effect of the tested parameters (in terms of actual values) for the two responses [Sahan et al., 2010]:

$$\%\text{COD removal efficiency} = 50.108 + 4.058\ j + 7.225\ t - 0.775\ g + 1.942\ T - 6.558\ pH_o + 1.108\ m \quad (4.1.2)$$

$$\%\text{Color removal efficiency} = 87.917 + 1.250\ j + 2.083\ t - 0.083\ g + 1.250\ T - 2.750\ pH_o - 0.415\ m \quad (4.1.3)$$

The vertical line in the Pareto chart of standardized effects (Figure 4.1.2) shows the 95% confidence interval for responses, percent COD and color removal [Amini et al., 2008; Luna et al., 2010]. Figure 4.1.3 shows the interaction plot of various parameters for COD and color removal. If the lines are parallel in the interaction graph, then it implies that there is no interaction between the factors. Non-parallel lines in the interaction plot indicate existence of an interaction between the factors. The greater the difference between the slopes of the lines of two factors in the range tested, the greater is the interaction [Kim et al., 2003].

Table 4.1.2 and Figures. 4.1.1 and 4.1.2 showed that the factors *j, t* and pH_o were the most significant variables of the COD and color removal. Other factors are not significant for COD removal and were not further considered.

Table 4.1.2. Regression coefficient and their significances for responses (COD and Color) in the Plackett–Burman design.

Terms	**level**		**COD**				**Color**			
	(-1)	**(+1)**	**Effect**	**Coeff.**	**T**	**P-Value**	**Effect**	**Coeff.**	**T**	**P-Value**
Constant				50.10	53.23	0.000		87.91	193.26	0.000
Current density (A/m^2)	39.21	196.0	8.11	4.05	4.31	0.008	2.50	1.25	2.75	0.040
Time (min)	60	180	14.45	7.22	7.67	0.001	4.16	2.08	4.58	0.006
Gap (cm)	1	3	-1.55	-0.77	-0.82	0.44	-0.16	-0.08	-0.18	0.86
Temperature (^oC)	30	50	3.88	1.94	2.06	0.09	2.50	1.25	2.75	0.040
pH_o	3	10	-13.11	-6.55	-6.97	0.001	-5.50	-2.75	-6.05	0.002
Salt concentration (g/l)	0	2	2.21	1.10	1.18	0.29	-0.82	-0.41	-0.92	0.40

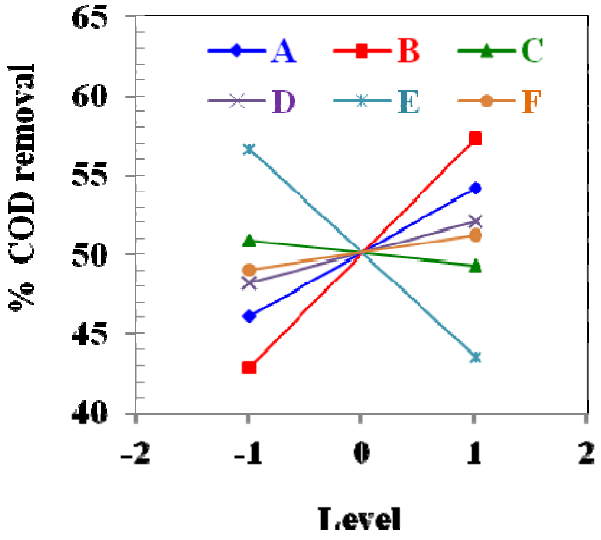

(a)

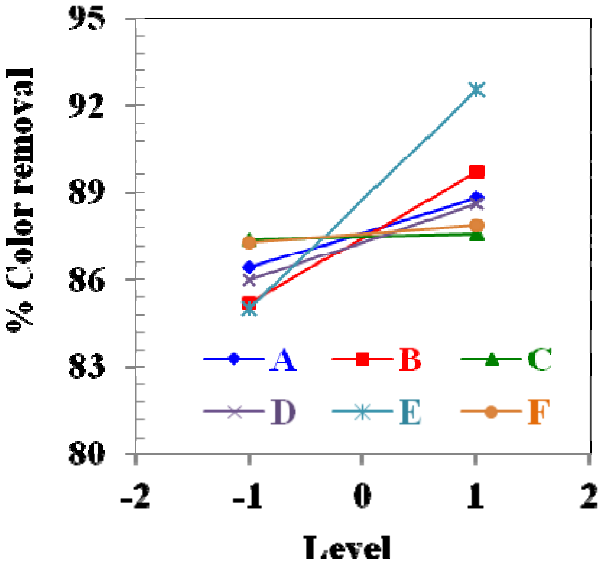

(b)

Figure 4.1.1. Main effects plot for (a) %COD and (b) color removal.

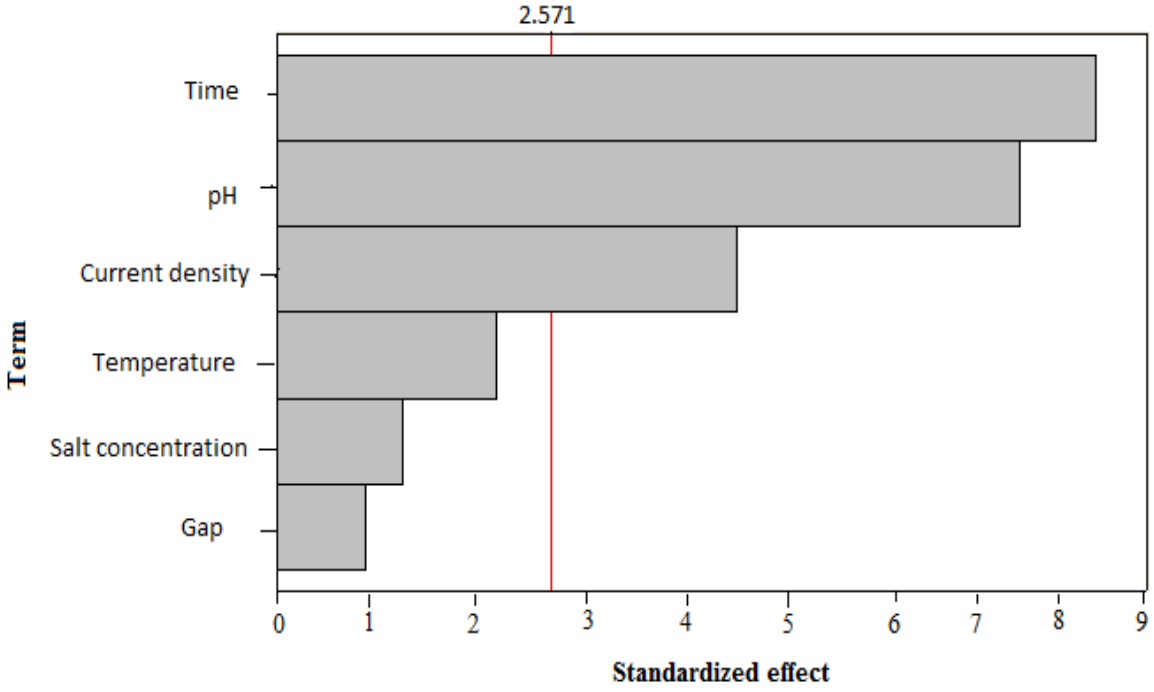

(a)

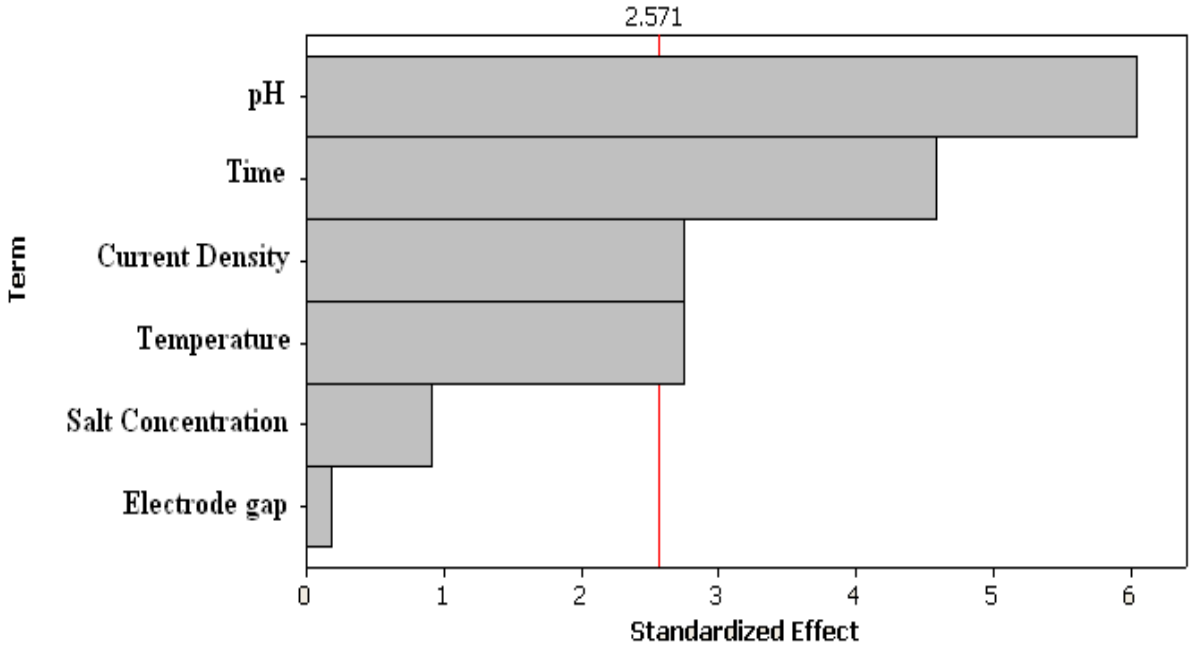

(b)

Figure 4.1.2. Pareto chart of standardized effects for the Plackett–Burman design for response (a) COD removal and (b) color removal.

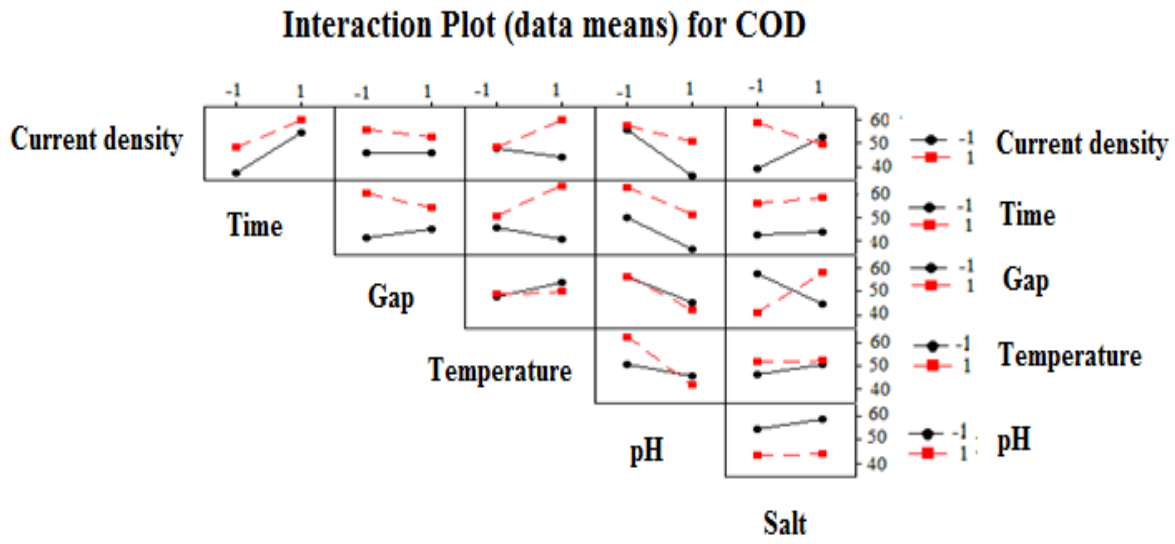

(a)

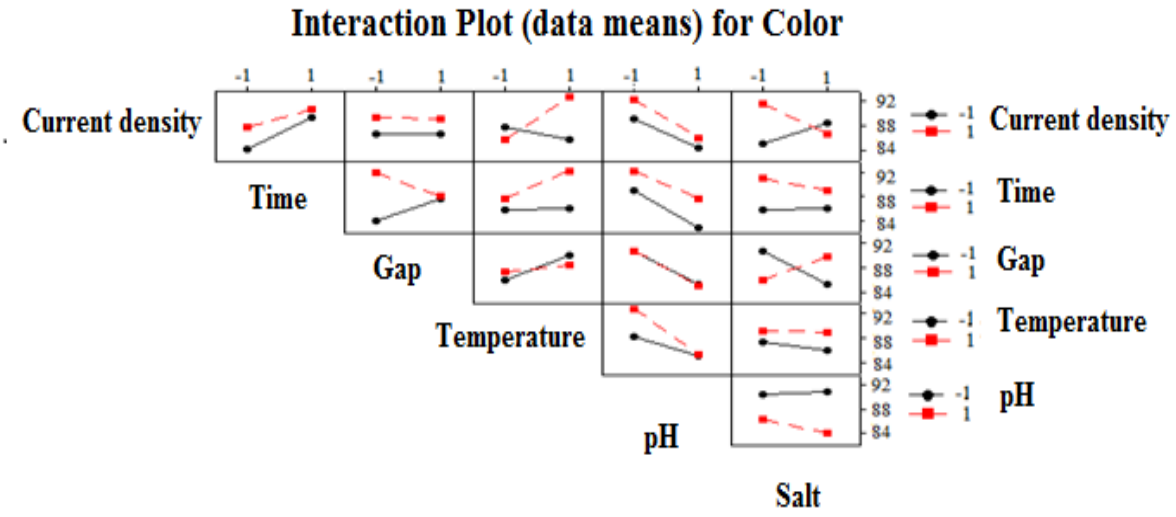

(b)

Figure 4.1.3. Interaction plot (data means) for the Plackett–Burman design for response (a) COD removal and (b) color removal.

4.1.3. Method of steepest ascent/descent

PB design helped in finding out the most significant variables affecting COD and color removal efficiency; however, optimum levels of the selected variables were still unknown. The method of steepest ascent was applied for moving sequentially along the path of steepest ascent/descent, that is, in the direction of the maximum increase/decrease in the response [Myers and Montgomery, 2002; Loukas, 2001]. Initial experiment was carried out at j=117.64 A/m^2, pH_o=6.5, and t=120 min (Table 4.1.2). Thereafter, the path of steepest ascent/descent was employed to find out the plateau by increasing the j and t and by decreasing the pH_o of STW [Kobya et al., 2006; Sahan et al., 2010]. Results of the experiments performed by applying this method are shown in Table 4.1.3. It may be seen that the highest COD and color removal efficiencies were obtained at j=156.86 A/m^2, pH_o=4.5, and t=180 min. Based on these results, range of variables for BB design were chosen as: j=117.23-196.07 A/m^2, t=120–24 min and pH_o=3.5–5.5.

Table 4.1.3. Experimental design of steepest ascent and corresponding response.

Experiment no.	Current density (A/m^2)	pH_o	Time (min)	Response	
				COD (%)	Color (%)
0	117.64	6.5	120	50.56	88.45
0+1Δt	137.25	5.5	150	60.15	90.35
0 +2Δt	156.86	4.5	180	69.25	96.35
0 +3Δt	176.50	3.5	210	65.50	95.25
0 +4Δt	196.07	2.5	240	62.55	98.22

4.1.4. Response surface methodology

To determine the optimum values of various parameters, experiments were carried out as per BB design matrix given in Table 4.1.4. Results of sequential model sum of squares and model summary statistics (Table 4.1.5) were used to choose a quadratic model for representing COD removal and a linear model for representing color removal. The analysis of variance (ANOVA) was tested using Fishers' statistical analysis and the results are given in Table 4.1.6 for COD and color removal.

4.1.4.1. Effects of j, t and pH_o on COD removal (Y_1) and color removal (Y_2)

For COD removal, model F value of 24.32 implies that the quadratic model is significant. The smaller is P-value, the bigger is the significance of the corresponding factor [Ponselvan et al., 2009]. The results obtained by the ANOVA showed that P-value for lack-of-fit (0.4086) was not significant ($P > 0.05$) (Table 4.1.6). Fitting of the quadratic model was good (coefficient of determination (R^2) = 0.737) and only 26.30% of total variance was not explained by the model [Kumar et al., 2008]. ANOVA result obtained from RSM quadratic model (Table 4.1.6) indicate that j is highly significant, whereas t, pH_o, j^2, t^2 and j × t are also significant term. "Adeq Precision" measures the signal to noise ratio which is desired to be greater than 4. For the present study, this value was 18.17 indicating adequate signal. For COD removal, the final quadratic equation in terms of coded factors is given below:

$$Y_1 \text{ (COD removal)} = 65.38 + 6.07X_1 + 3.00X_2 + 1.76X_3 - 4.00X_1^2 - 2.08X_2^2 - 0.49X_3^2 - 1.95X_1X_2 + 1.50X_1X_3 - 0.83X_2X_3 \quad (4.1.4)$$

The ANOVA for the liner model fitted for Y_2 is given in Table 4.1.5. The model F-value of 7.01 implies that the liner model is significant. The ANOVA values (Table 4.1.6) obtained show that the model terms j, t, and pH_o are significant. The liner equation in terms of coded factors for Y_2 is as given below:

$$Y_2 \text{ (Color removal)} = 92.12 + 3.28X_1 + 2.37X_2 + 0.94\ X_3 \quad (4.1.5)$$

Table 4.1.4 shows the actual and predicted values of Y for COD and color removal of STW by EC process using aluminum electrodes. It is seen that the developed model is adequate because the residuals for the prediction of each response are minimum, and the predicted and actual values are close to each other.

In the EC treatment, electro-dissolution, electro-coagulation, electro-flocculation, electro-flotation and electro-oxidation, may take place simultaneously in the EC reactor. First, electro-dissolution of aluminum takes place on anode electrode surface generating Al^{+3} ions. Simultaneously, water reduction at cathode generates oxygen and hydrogen.

$$\text{Anode: } Al \rightarrow Al\ (aq)^{3+} + 3e- \quad (4.1.6)$$

$$\text{Cathode: } 3H_2O + 3e- \rightarrow 3/2\ H_2 + 3OH^- \quad (4.1.7)$$

$Al(aq)^{3+}$ and OH^- ions generated by electrode reactions (4.1.6) and (4.1.7) react to form various monomeric species such as $Al(OH)^{2+}$, $Al(OH)_2^+$, $Al_2(OH)_{24}^+$, $Al(OH)_4^-$, and polymeric species such as $Al_6(OH)_{15}^{3+}$, $Al_7(OH)_{17}^{4+}$, $Al_8(OH)_{20}^{4+}$, $Al_{13}O_4(OH)_{24}^{7+}$, $Al_{13}(OH)_{34}^{5+}$, which may get transformed into $Al(OH)_3$ depending upon the pH [Canizares et al., 2005; Kobya et al., 2006].

Table 4.1.4. Experimental and predicted value of response Y (COD and Color) removal by EC treatment.

Std. order	Run	j (X_1)	t (X_2)	pH_o (X_3)	%COD reduction		%Color reduction	
					$Y_{1obs.}$ (%)	$Y_{1pred.}$(%)	$Y_{2obs.}$ (%)	$Y_{2pred.}$(%)
1	4	117.64	150	4.5	47.35	48.50	82.34	86.80
2	16	196.07	150	4.5	64.50	64.25	92.45	93.35
3	1	117.64	210	4.5	58.25	57.75	90.50	91.53
4	11	196.07	210	4.5	67.35	66.50	96.12	98.08
5	6	117.64	180	3.5	54.25	54.88	88.76	88.24
6	3	196.07	180	3.5	62.50	63.13	90.32	94.78
7	10	117.64	180	5.5	56.00	54.88	89.15	90.10
8	14	196.07	180	5.5	70.50	71.13	98.08	96.65
9	13	156.85	150	3.5	58.45	56.63	92.00	89.14
10	9	156.85	210	3.5	65.12	64.38	94.24	93.87
11	7	156.85	150	5.5	62.15	62.63	90.36	91.04
12	5	156.85	210	5.5	65.50	66.38	95.67	95.74
13	17	156.85	180	4.5	64.00	65.00	93.23	92.44
14	12	156.85	180	4.5	63.47	65.00	94.15	92.44
15	2	156.85	180	4.5	67.18	65.00	95.05	92.44
16	15	156.85	180	4.5	65.35	65.00	96.00	92.44
17	8	156.85	180	4.5	66.00	65.00	92.00	92.44

Table 4.1.5. Adequacy of the model tested using 'sequential model sum of squares' and 'model summary statistics' for COD and color removal.

Source	Sum of squares	Degree of freedom	Mean square	F value	Prob >F	Remark
Sequential Model Sum of Squares						
COD						
Mean	65952.03	1	6595.03			
Linear	391.38	3	130.46	12.49	0.0004	
2FI	26.86	3	8.95	0.82	0.5111	
Quadratic	92.61	3	30.87	13.23	0.0029	Suggested
Cubic	7.84	3	2.61	1.23	0.4086	Aliased
Residual	8.50	4	2.13			
Total	66479.22	17	3910.54			
Color						
Mean	1.453E+005	1	1.453E+005			
Linear	137.74	3	45.91	7.01	0.0048	Suggested
2FI	21.72	3	7.24	1.14	0.3790	
Quadratic	38.19	3	12.73	3.53	0.0767	
Cubic	15.93	3	5.31	2.29	0.2206	Aliased
Residual	9.29	4	2.32			
Total	1.445E+005	17	8558.15			
Model summary statistics						
COD						
Liner	3.23	0.7424	0.6829	0.5640	229.86	
2FI	3.30	0.7933	0.6693	0.3673	333.53	
Quadratic	1.53	0.9690	0.9292	0.7372	138.67	Suggested
Cubic	1.46	0.9839	0.9355		+	Aliased
Color						
Liner	2.56	0.3082	0.5299	0.6180	154.19	Suggested
2FI	2.52	0.7155	0.5448	-0.0140	226.00	
Quadratic	1.90	0.8868	0.7413	-0.2088	269.41	
Cubic	1.52	0.9583	0.8333		+	Aliased

Table 4.1.6. Results of regression analysis of the second-order polynomial model for optimization of COD removal.

Source	Coefficient estimate	Sum of squares	Degree of freedom	Mean square	F-value	Prob.>F	Remark
COD removal							
Model		510.85	9	56.76	24.32	0.0002	significant
Intercept	65.38						
X_1	6.07	294.40	1	294.40	126.13	< 0.0001	Highly significant
X_2	3.00	72.24	1	72.24	30.95	0.0008	significant
X_3	1.76	24.75	1	24.75	10.60	0.0139	significant
X_1^2	-4.00	67.44	1	67.44	28.89	0.0010	significant
X_2^2	-2.08	18.30	1	18.30	7.84	0.0265	less significant
X_3^2	-0.49	1.02	1	1.02	0.44	0.5297	not significant
X_1X_2	-1.95	15.13	1	15.13	6.48	0.0383	less significant
X_1X_3	1.50	8.97	1	8.97	3.84	0.0908	not significant
X_2X_3	-0.83	2.76	1	2.76	1.18	0.3132	not significant
Residual		19.34	7	2.33			
Lake of fit		7.84	3	2.61	1.23	0.4086	not significant
Pure error		8.50	4	2.13			
Cor Total		527.19	16				
Color removal							
Model		137.74	3	45.91	7.01	0.0048	significant
Intercept	92.44						
X_1	3.28	85.94	1	85.94	13.12	0.0031	
X_2	2.37	44.79	1	44.79	6.84	0.0214	
X_3	0.94	7.01	1	7.01	1.07	0.3196	
Residual		85.13	13	6.55			
Lake of fit		75.84	9	8.43	3.63	0.1135	not significant
Pure error		9.29	4	2.32			
Cor Total		222.87	16				

X_1: j (A/m^2); X_2: t (min); X_3: pH_o.

Charge neutralization of the negative charged colloidal matter present in the solution by positively charged monomeric and polymeric aluminum ions helps in aggregation of neutralized colloid particles which ultimately get removed by settling [Kobya et al., 2006; Aleboyeh et al., 2008]. Similarly, generated flocs of $Al(OH)_{3(s)}$ have large surface areas, which help in rapid adsorption of soluble compounds by trapping of colloidal particles [Basha et al., 2012]. Hydrogen gas generated at the cathode helps in floatation of less dense colloidal particles present in the solution. These particles form a scum layer at the top of the solution which can be skimmed off. Similarly, chloride ions present in the wastewater may form various chlorine species (Cl_2, HOCl and ClO^-) in the solution depending upon the pH. These chlorine species help in indirect oxidation of the organic material present in the wastewater [Kushwaha et al., 2011]. During EC treatment, combinations of these mechanisms help in the removal process.

Three-dimensional response surface graphs for COD and color removal efficiency are shown in Figure 4.1.4. and Figure 4.1.5. It may be seen that the COD and color removal efficiency (Figure 4.1.4a and 4.1.4b) increased with an increase in j and t. It is known that the COD and color removal efficiency directly depends on Al^{3+} ions concentration produced by the aluminum electrodes. Concentration of Al^{3+} ions increases with an increase in the value of j and t due to higher dissolution of electrode, and these result in high COD and color removal efficiency via charge neutralization for $pH_o < 6$ [Canizares et al., 2005].

Figure 4.1.5a and 4.1.5b show the effect of pH_o on the COD and color removal efficiency. It may be seen from these figures that, for any constant j, the effect of pH_o is very marginal. As seen, only at higher j values, there is marginal increase in COD and color removal efficiency with an increase in pH_o. This marginal increase may be due to the evolution of hydrogen gas generated at the cathode [Can et al., 2006]. Hydrogen gas helps in floatation of the bigger size EC floc generated by charge neutralization and aggregation mechanism [Kobya et al., 2012].

4.1.4.2. Optimum condition: The optimum values of j, t and pH_o, as per the analysis of response curves and the fitted model, were found to be 185.30 A/m^2, 190 min, and apporiximately 5.0, respectively. At the optimum condition, the COD and color removal efficiencies were found to be 70.50% and 98.2%, respectively. Confirmation experiments showed removal efficiencies within 95% confidence interval of the predicted value.

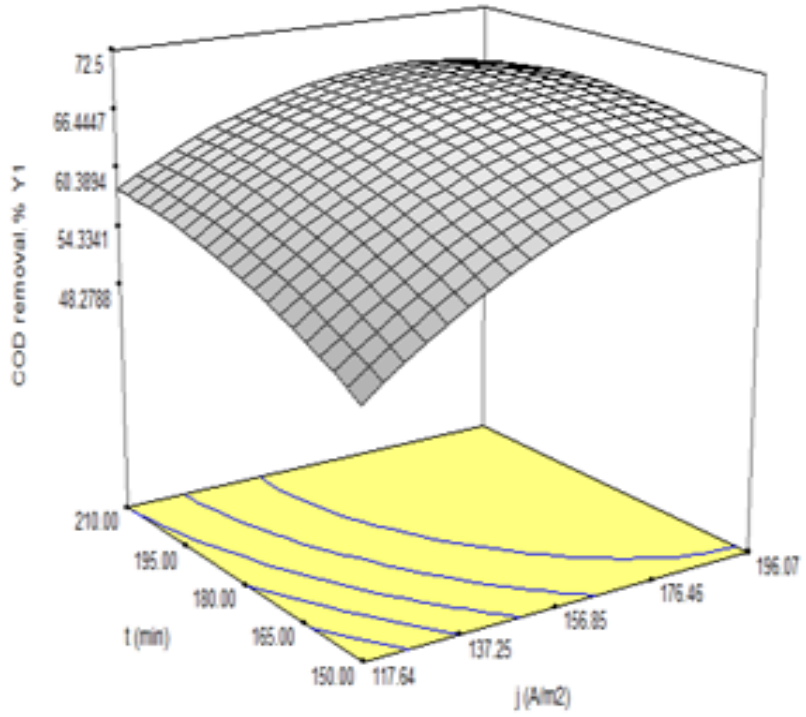

(a)

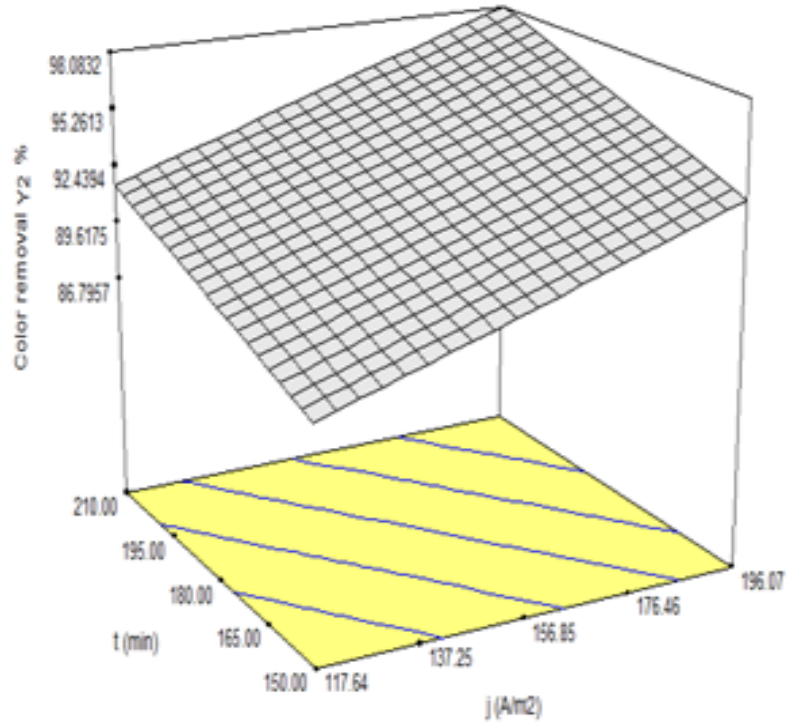

(b)

Figure 4.1.4. Three-dimensional response surface graphs for the EC treatment of STW (a) COD removal vs t and j at pH_o ~5.0; (b) Color removal vs pH_o and j at t 190 min.

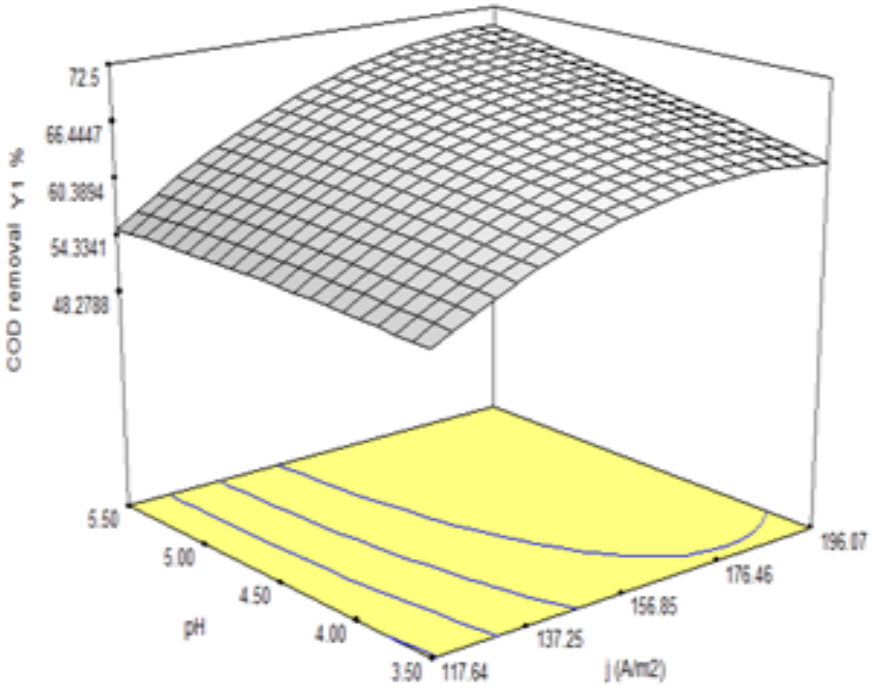

(a)

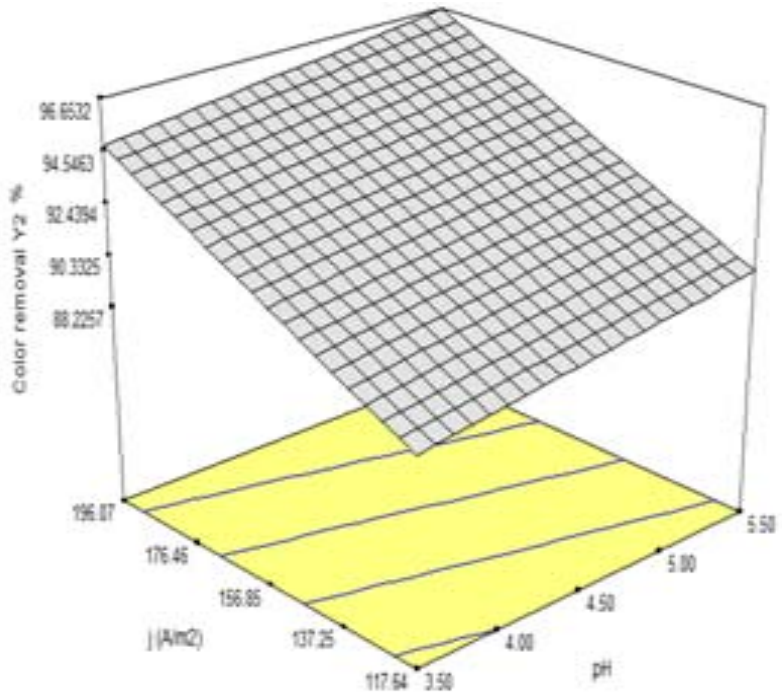

(b)

Figure 4.1.5. Three-dimensional response surface graphs for the EC treatment of STW (a) COD removal, Y_1 (%) vs pH_o and j at t 190 min; and (b) Color removal, Y_2 (%) vs t and j at pH_o ~5.0.

4.2. DYE DEGRADATION MECHANISM OF BASIC DYE DURING EC TREATMENT WITH ALUMINUM ELECTRODE

Very few studies are available in open literature which try to elucidate mechanism of degradation of chemical structure of organic dye into smaller one during degradation processes. Most of these studies are, however, based on catalytic degradation, biological degradation and advance oxidation processes. No study was reported in the literature (before this study) [Singh et al., 2013b,c] on mineralization of any dye during EC treatment. Therefore, studies were conducted for understanding the EC degradation mechanism of a triphenylmethane dye namely basic green 4 (BG) commonly known as malachite green with aluminum electrode.

First, mechanistic study of EC treatment of BG dye with aluminum electrodes was studied through zeta potential measurement, and the characterization of generated solid residues by Fourier transform infrared spectroscopy (FTIR), X-ray diffraction (XRD), scanning electron microscopy (SEM), energy dispersive spectroscopy of X-rays (EDX), etc. Variations in electrode and energy consumptions with respect operating parameters were studied as principal cost parameters. In the second part, step-by-step EC mineralization of BG was studied during EC treatment with aluminum electrode in the present study. Each step of degradation was determined by various spectroscopic and chromatographic methods. The intermediates were identified by mass spectroscopic techniques. COD and decolorization efficiencies were determined to understand step-by-step mineralization of BG. The degradation mechanism has been explained by different possible schemes.

This section has been divided into following subsections:

- Mechanistic study through zeta potential measurement
- Mechanistic study through characterization of solid residues
- Step-by-step EC mineralization of dye

4.2.1 Mechanistic study using zeta-potential measurement

4.2.1.1 Speciation of aluminum ions and contribution of zeta potential during EC treatment: The speciation of aluminum depends on the total concentration of aluminum and pH in an aqueous solution. Aluminum metal ions get hydrolysed in water. In the primary shell, water molecules are in direct contact with the central metal ion whereas they are loosely held in the secondary hydration shell [Duan and Gregory 2002]. Effectively, depending on pH and the metal ion concentration, these water molecules are progressively replaced by hydroxyl ions in the hydration shell giving a lower positive charge [Martinez–

Huitle and Brillas, 2009]. The stability constants help in determining the percentage of Al^{3+} hydrolytic products at various pH [Canizares et al., 2005; Ahlawat et al., 2008]. Ionic monomeric hydrolysis can be represented by following successive deprotonation reactions [Wesolowski et al., 1994; Duan and Gregory, 2002].

$$Al^{3+} + H_2O \rightarrow Al(OH)^{2+} + H^+ \qquad K_1 = 4.95 \qquad (4.2.1)$$

$$Al(OH)^{2+} + H_2O \rightarrow Al(OH)_2^{+} + H^+ \qquad K_2 = 5.6 \qquad (4.2.2)$$

$$Al(OH)_2^{+} + H_2O \rightarrow Al(OH)_3 + H^+ \qquad K_3 = 6.7 \qquad (4.2.3)$$

$$Al(OH)_3 + H_2O \rightarrow Al(OH)_4^{-} + H^+ \qquad K_4 = 5.6 \qquad (4.2.4)$$

$$Al(OH)_3 \leftrightarrow Al^{3+} + OH^- \qquad K_S \qquad (4.2.5)$$

The speciation diagram of Al^{3+} ions drawn using above stability constants is presented in Figure 4.2.1a. The speciation diagram indicates that in the acidic range, the predominant species are the monomeric cationic hydroxo-aluminum species. An increase in pH leads to the coexistence of monomeric species along with increase in the amount of polymeric cationic species [Duan and Gregory 2003; Can et al., 2003]. For pH close to neutrality, the predominant species are the aluminum hydroxide precipitates. Still further increase in the pH in the alkaline range leads to the dissolution of the precipitates to form monomeric anionic hydroxo-aluminum. Thus, aluminum hydrolysis involves formation of monomeric, oligomeric and polymeric ionic species, and ions precipitates [Gao et al., 2002; Ahlawat et al., 2008].

Zeta potential measurements help in understanding the role of electrostatic interaction between aluminum species and the dye molecules. However, determining the zeta potential without varying the pH is almost meaningless. It is well known that solutions of most materials exhibit an isoelectric point that is a solution pH where the net charge on the particles is zero [Canizares et al., 2006; Srivastava et al., 2006a,b; Huo and Yan, 2012]. At isoelectric point, flocculation of particles present in the solution is highly possible.

The variation of zeta potential of the aluminum-water solution (without BG dye) in the EC reactor with time at various pH is given in Figure 4.2.1b. It may be seen that zeta potential becomes more negative with time at any pH indicating release of positive charge species into the solution. It may also be seen that an increase in pH from 3.2 to 6.2 leads to shift in zeta potential towards less negative side i.e. towards neutral side. This indicates that with an increase in pH, the overall quantity of cations released by the electrodes decreases. However, further increase in pH beyond 6.2 shifts the zeta potential towards more negative side. This is due to the formation of aluminum hydroxide precipitates which

are heavier particles and settle easily. While sinking they sweep down the remaining impurities in the water [Chen et al., 2006]. Generally two distinct mechanisms: charge neutralization of negatively charged colloids by cationic hydrolysis products (changes obtain towards more acidic pH) and sweep coagulation of the colloidal impurities by the amorphous hydroxide precipitate help in treatment process [Can et al., 2006]. The relative importance of these mechanisms depends on factors such as pH change and increase in coagulant dosage with an increase in treatment time during EC process [Terrazasa et al., 2010; Basha et al., 2012].

4.2.1.2. Effect of initial pH (pH_o): pH is considered as one of the most important operating parameter that determines the performance of EC process [Bayramoglu et al., 2004; Aoudj et al., 2010; Akbal and Kuleyin, 2011]. Also, type of electrode material and initial pH (pH_o) determine the change in pH of the suspension during the process. Figures 4.2.2 and 4.2.3 show the effect of pH_o on COD, TOC and color removal efficiencies.

Figure 4.2.2a,b show that when the pH of the dye solution was increased from 3.2 to 6.2, COD and TOC removal efficiency first increased. Maximum COD and TOC removal efficiencies of 82.2% and 62%, respectively, were achieved at optimum $pH_o \approx 6.2$. Further increase in pH from 6.2 to 12.2 led to decrease in COD and TOC removal efficiencies.

Figure 4.2.3b shows the variation in zeta potential of the solution with treatment time for wastewater having different pH_o. It may be seen that at any time, t, the negative value of zeta potential decreases with an increase the pH from 3.2 to 6.2, however, negative value of zeta potential increases with an increase the pH from 6.2 to 12.2. For treatment time of 45 min, the minimum zeta potential value of –15.2 mV was achieved at pH=6.2. Thus, least number of positive colloids and maximum number of aluminum hydroxide flocs were present in the solution at pH=6.2. The value of zeta potential for untreated BG solution was –6.2 mV at its natural pH 5.4. At low pH, cationic soluble species Al^{3+} and $Al(OH)^{2+}$ are predominant. However when pH is increased, these monomeric and polymeric aluminum species get converted to insoluble amorphous $Al(OH)_3$ through complex polymerization/precipitation mechanism [Can et al., 2003; Aleboyeh et al., 2008]. It may be seen in Figure 4.2.2a that at pH≈6.2, aluminum forms solid aluminum hydro-oxide $Al(OH)_3(s)$ [Kobya et al., 2006]. At this pH, BG molecules get trapped and adsorbed on the large surface area of the flocs of $Al(OH)_3(s)$ and get removed by the process of sweep coagulation [Bayramoglu et al., 2004].

It may be seen in Figure 4.2.3a that the decolorization efficiency continuously increased with an increase in pH. Thus, though the COD and TOC removal efficiencies decreased with an increase in pH beyond 6.2, however, decolorization efficiency continuously increases for pH>6.2 also. It may be noted that BG itself act as an acid-base indicator [Chen et al., 2009]. It has been reported earlier that for BG dye, some decolorization efficiency is observed by change in pH alone. This is due to the structural changes affected in the dye-molecules at higher pH [Mall et al., 2006; Mane et al., 2007]. The chromatic form of BG molecules changes to a leuco-form at alkaline pH due to chemical transformation and this increases the decolorization efficiency [Schneider et al., 2006; Chen et al., 2009; Srivastava and Sinha, 2004].

4.2.1.3. Effect of current density (j): Figures 4.2.4a,b and 4.2.5a show that the percentage COD, TOC and color removal increases with an increase in j from 39.21 to 117.64 A/m^2. Figure 4.2.5a also shows the effect of variation in current density on the decolorization efficiency. The removal percentage increased from 64% at 32.91 A/m^2 to 99.8% at 117.64 A/m^2. At higher j, more aluminum cations are generated in solution and rate of formation of $Al(OH)_3$ increases. Beyond j=117.64 A/m^2, no substantial improvement in decolourization efficiency was detected. It is well known that the current density determines the coagulant production rate which in turn influences the dye removal by the EC processes [Bayramoglu et al., 2004; Yılmaz et al., 2008].

It may be seen in Figures 4.2.4a,b and 4.2.5a that the maximum COD, TOC and color removal efficiencies were achieved within 45 min of treatment and marginal change was observed thereafter. The removal of COD and TOC occurs due to the interaction of Al ions and dye molecules forming insoluble metal-dye complex through EC mechanism [Daneshvar et al., 2006; Murugananthan and Raju, 2010]. It may be noted that Al^{3+} ions released from anodic dissolution and turn into aluminum-hydroxide, which is a good adsorbent and helps in the treatment process [Aoudj et al., 2010; Kobya and Gengec, 2012; Kobya et al., 2013].

Zeta potential became more negative with an increase in j value from 32.91A/m^2 to117.64 A/m^2. Figure 4.2.5b shows that the potential value increases in a regular way. For j=117.64 A/m^2, potential changed from –9.2 mV at 5 min to –16.2 mV at 45 min. With an increase in the j value, positive floc formation increases which in turn increases the negative value of zeta potential. Since BG molecules are also positively charged, therefore, the removal seems to be due to neutral aluminum hydroxides which remove the colloids physically by sweep coagulation [Zaroual et al., 2006].

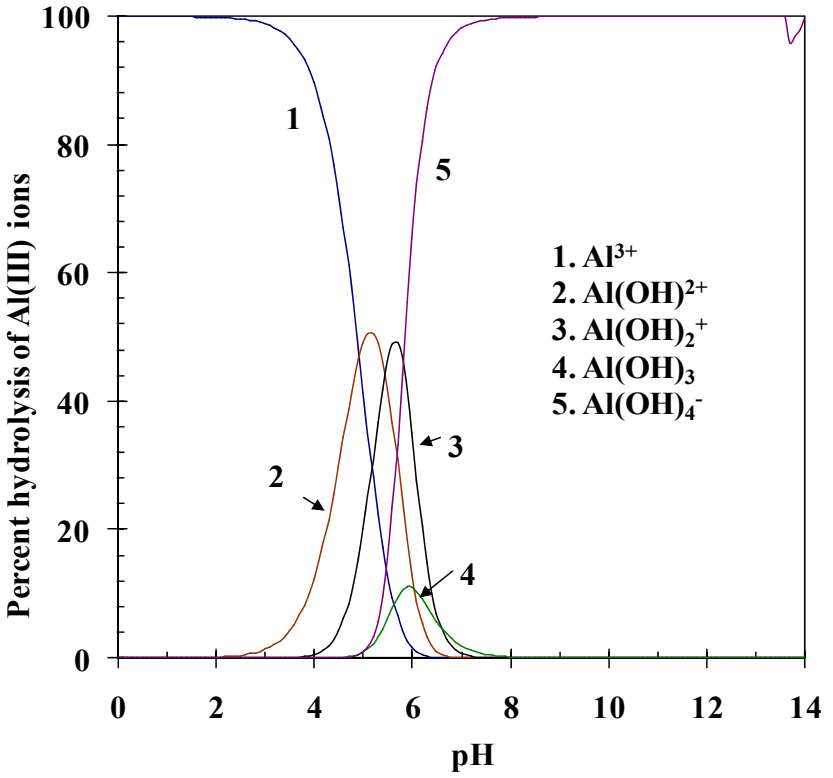

(a)

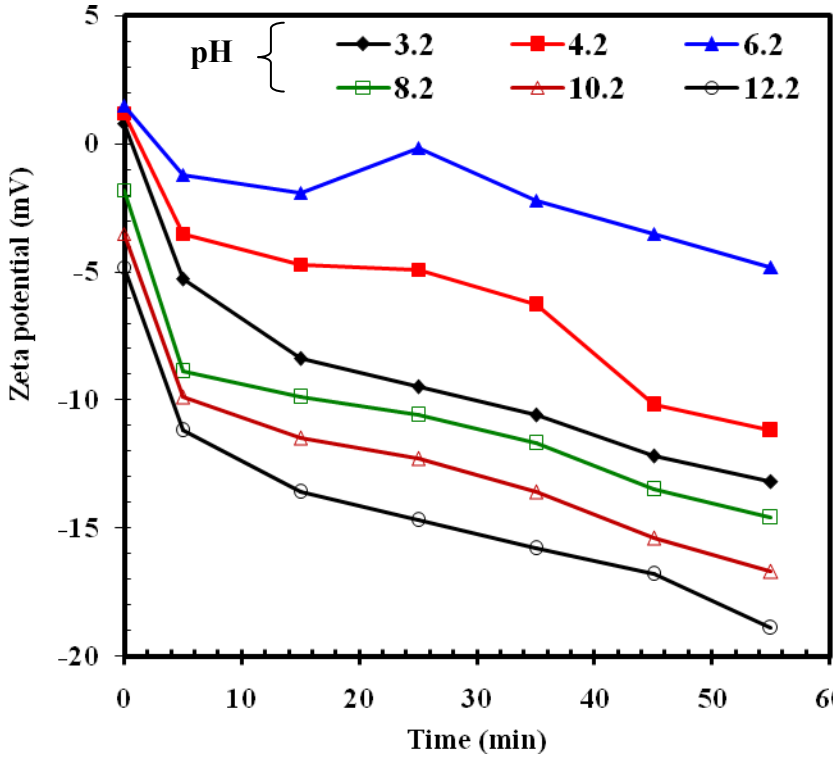

(b)

Figure 4.2.1. (a) Speciation diagram of Al(III), (b) Zeta potential of solution at different pH during EC treatment of pure water by aluminum electrodes.

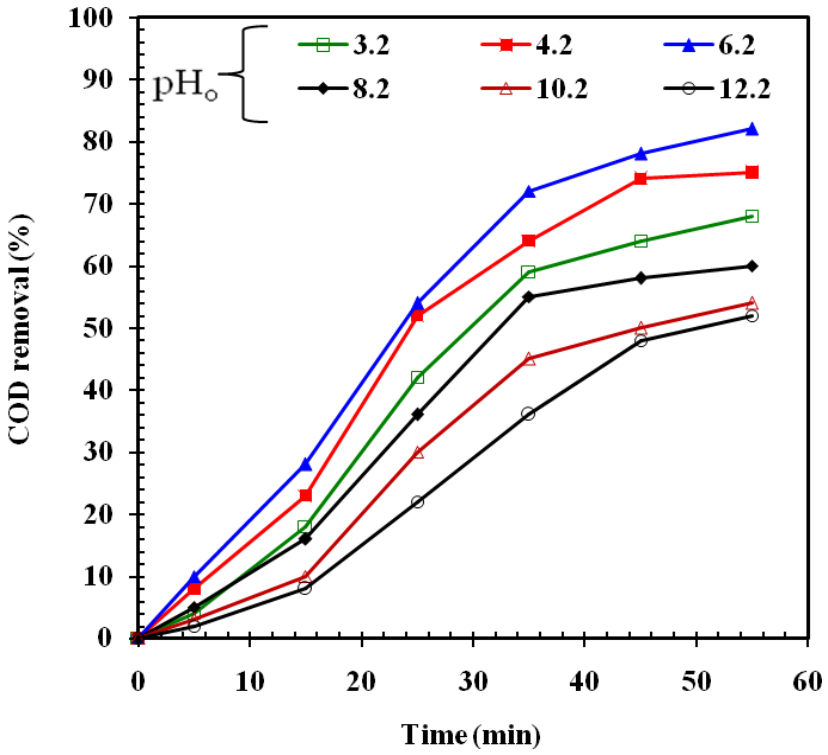

(a)

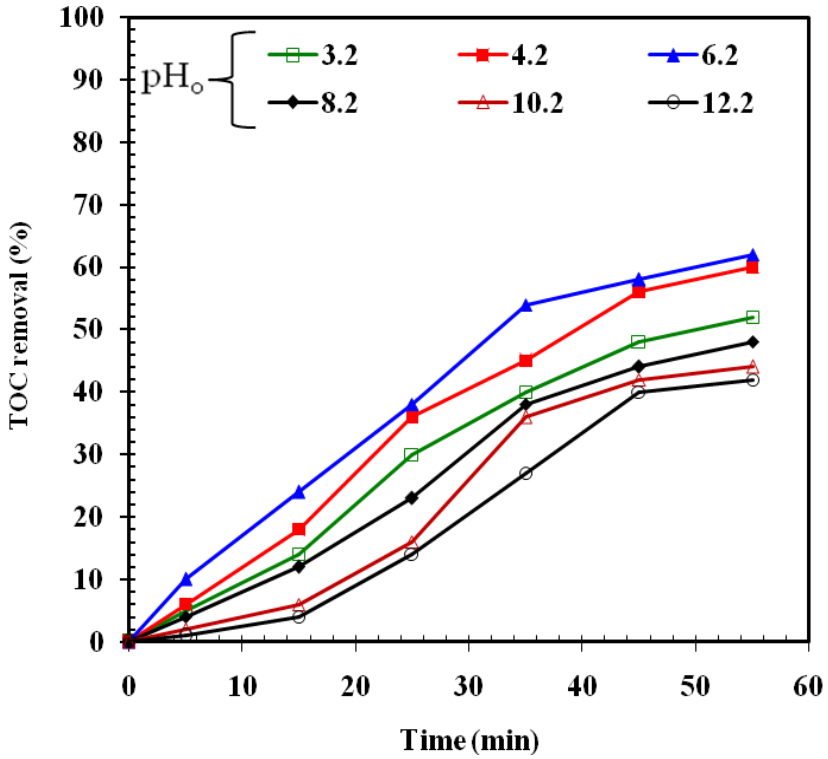

(b)

Figure 4.2.2. Effect of pH_o on removal efficiency of BG in term of (a) COD; (b) TOC (C_o: 100 mg/L; NaCl: 1.5 g/L; j: 117.0 A/m^2; temperature: 25 ^{o}C; electrode gap.

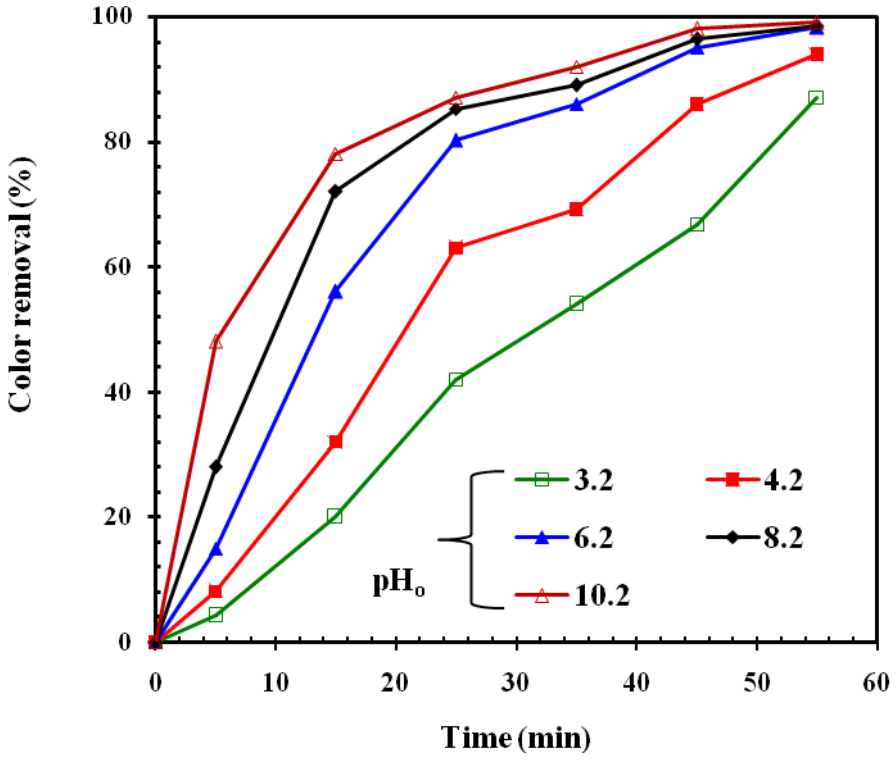

(a)

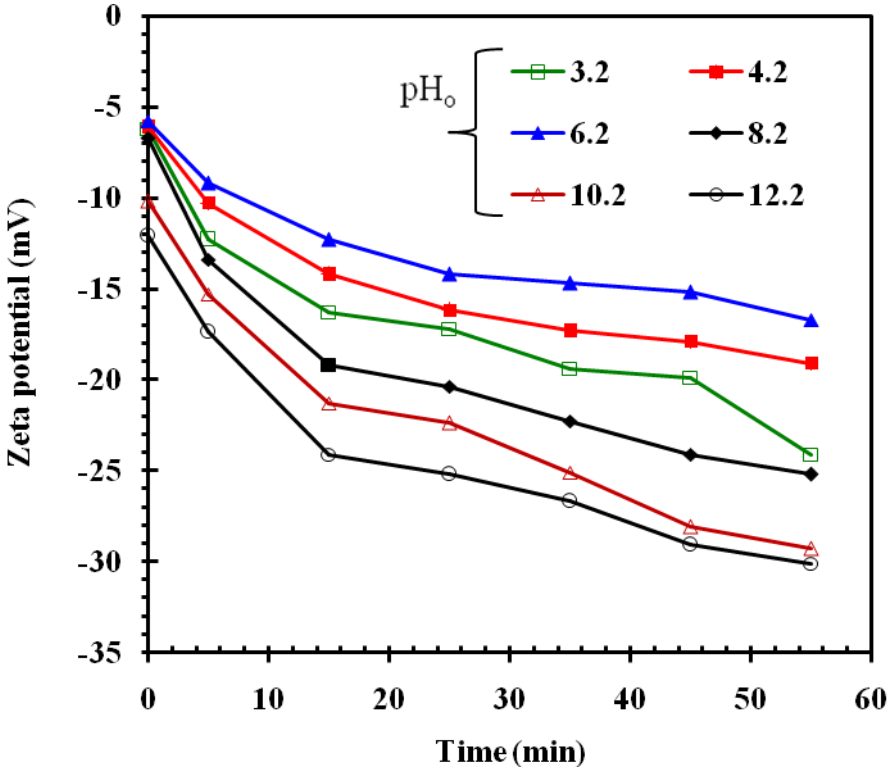

(b)

Figure 4.2.3. Effect of pH_o on removal efficiency of BG in term of (a) color and (b) variation of zeta potential. (C_o: 100 mg/L; NaCl: 1.5 g/L; j: 117.0 A/m^2; temperature: 25 ^oC; electrode gap.

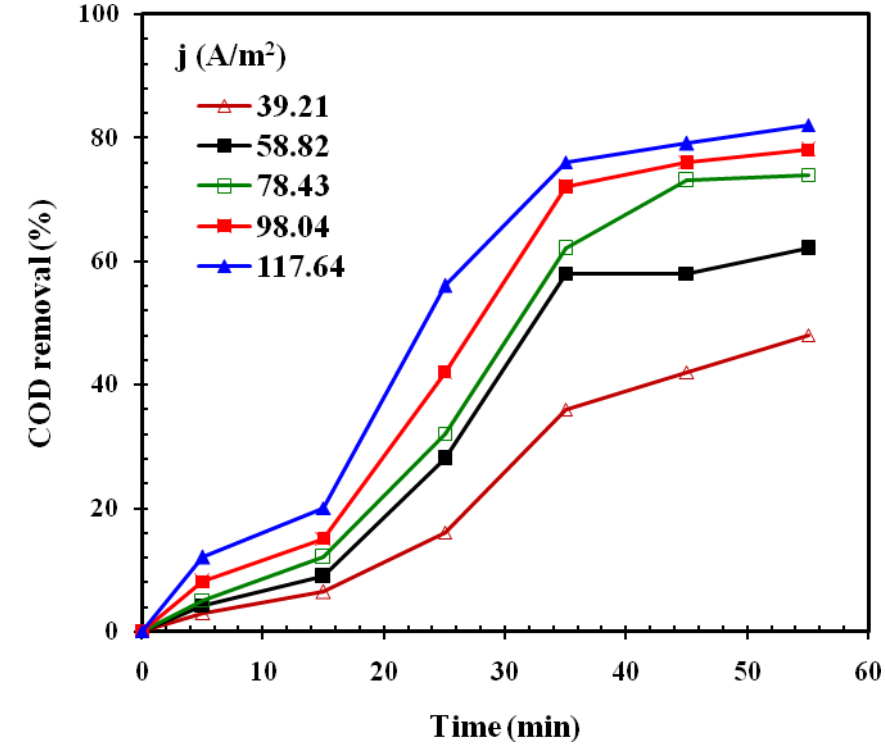

(a)

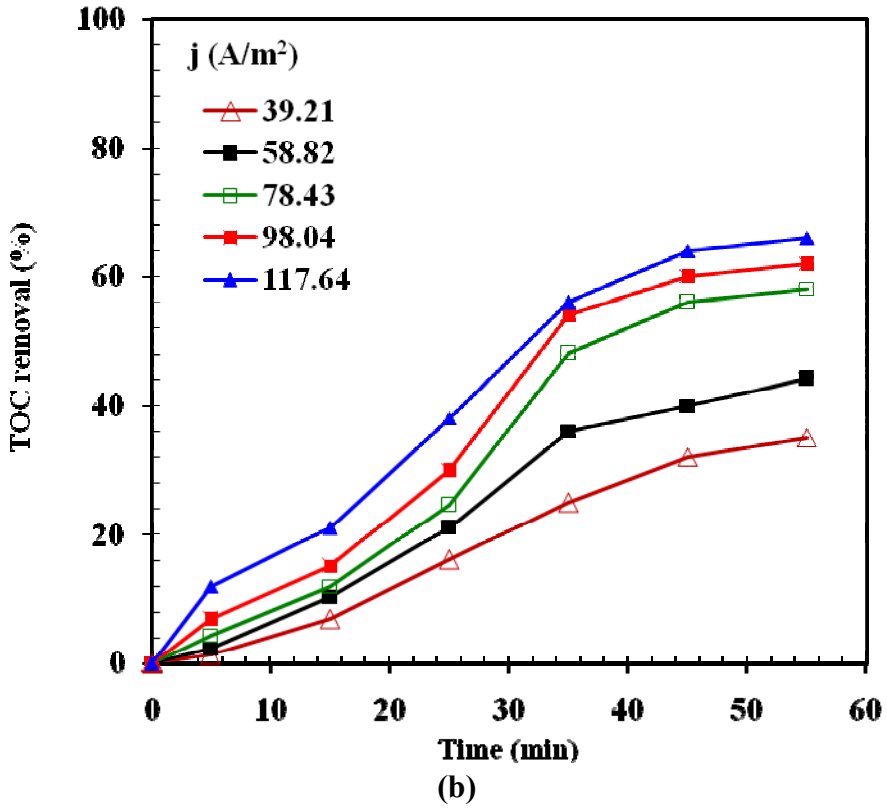

(b)

Figure 4.2.4. Effect of j on removal efficiency of BG in term of (a) COD and (b) TOC (C_o: 100 mg/L; NaCl: 1.5 g/L; pH_o: 6.2; temperature: 25 ^oC; electrode gap: 1 cm).

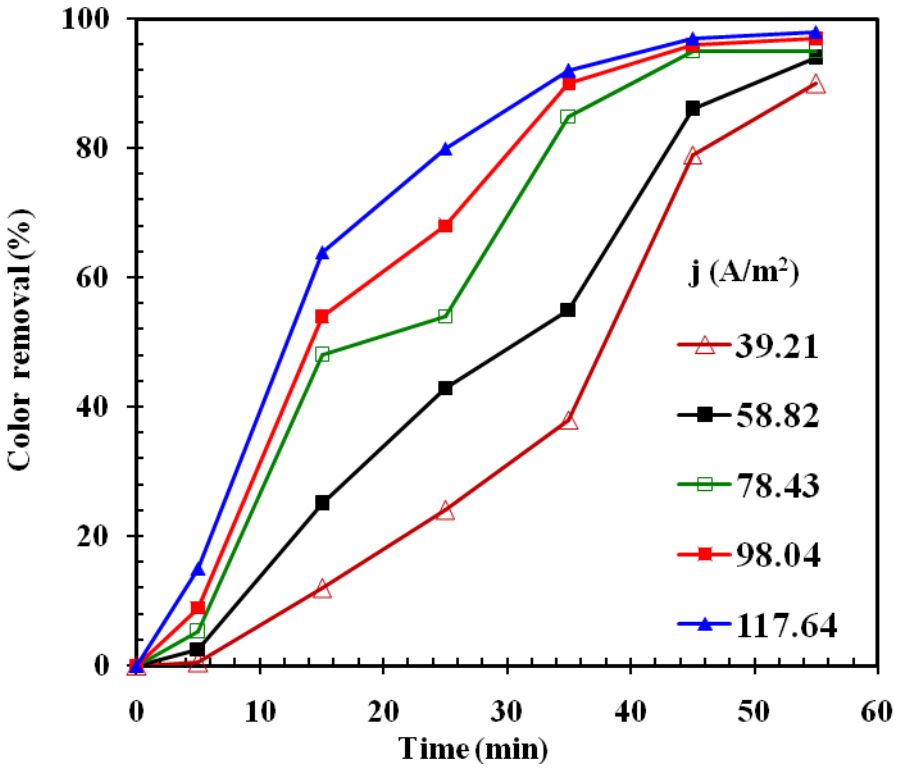

(a)

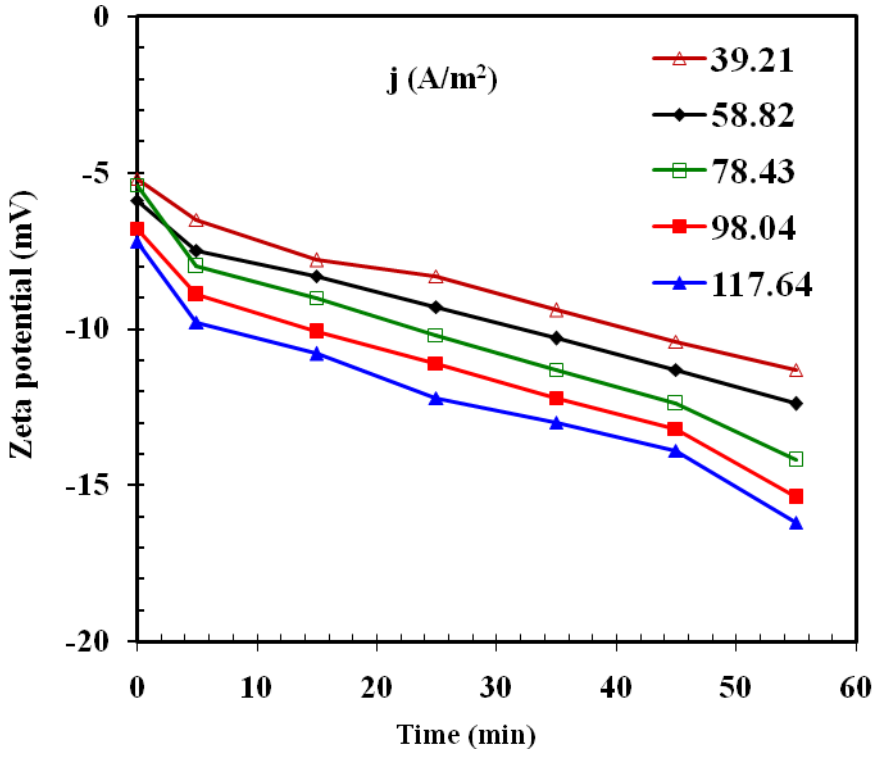

(b)

Figure 4.2.5. Effect of j on removal efficiency of BG in term of (a) color and (b) variation of zeta potential. (C_o: 100 mg/L; NaCl: 1.5 g/L; pH_o: 6.2; temperature: 25 ^oC; electrode gap: 1 cm).

4.2.1.4. Effect of initial dye concentration (C_o): Figure 4.2.6a,b show that the COD and TOC removal efficiencies decreased from 82.4 to 58% and from 63.5 to 44%, respectively, with an increase in C_o from 100-500 mg/l. Similarly, decolorization efficiency decrease from 99% to 72% when the dye concentration was increased from 100 to 500 mg/l (Figure 4.2.7a). The behaviour of zeta potential of the BG at different concentrations of the cationic dye solution is represented in Figure 4.2.7b. At constant j and pH, the amount of dye molecules increases, and therefore, zeta potential becomes more negative (–16.2 to –28.6 mV) with an increase the concentration from 100 to 500 mg/l. At constant j and pH_o, number of netural $Al(OH)_3$ flocs released are constant [Drouiche et al., 2007, 2009; Mollah et al., 2010]. It is known that the dye removal takes place by adsorption onto aluminum hydroxide. At higher C_o number of aluminum hydroxide particles available to capture excess dye molecules are less, therefore, the removal efficiency decreases [Kobya et al., 2003; Drouiche et al., 2009]. Furthermore at higher C_o, the repulsion between approaching particles is large enough so that they remain away from one another and exist in a state of dispersion. Therefore, the removal efficiency decreases with an increase in rise C_o [Aoudj et al., 2010].

4.2.1.5. Energy and electrode consumption: Effects of pH_o, C_o and j on energy consumption (ENC) in kWh per kg of COD removed are shown in Figure 4.2.8. The amount of aluminum released includes both dissolved aluminum and precipitated as $Al(OH)_3$. Experimental values of electrodes consumed were determined by weighing the electrode before and after experiment. Effects of pH_o, C_o and j on experimental (actual) value of electrode consumption (kg/kg COD removed) are shown in Figure 4.2.8. At constant j and C_o, the energy consumption increased with an increase pH. The values of the energy consumption increased from 0.92 kWh/kg COD removed to 1.7 kWh/kg COD removed with an increase in pH from 3.2 to 12.2 (Figure 4.2.8). Similarly, the Al dissolution also increased with an increase the pH from acidic to basic range. The energy and electrode consumptions increased from 1.2 to 2.58 kWh/kg COD and 0.06 to 0.16 kg Al/kg COD removed with an increase in j from 39.21 to 117.64 A/m^2 (Figure 4.2.8b). This trend is obvious owing to the fact that energy consumption and electrode dissolution are directly proportional to the j. It may be seen in Figure 4.2.8c that the energy and electrode consumption showed an inverse relationship with C_o. With an increase in C_o from 100 to 500 mg/L, the values of energy and electrode consumptions decreased from 2.48 to 1.3 kWh/kg COD removed and 0.15 to 0.08 kg Al/kg COD removed, respectively (Figure 4.2.8c).

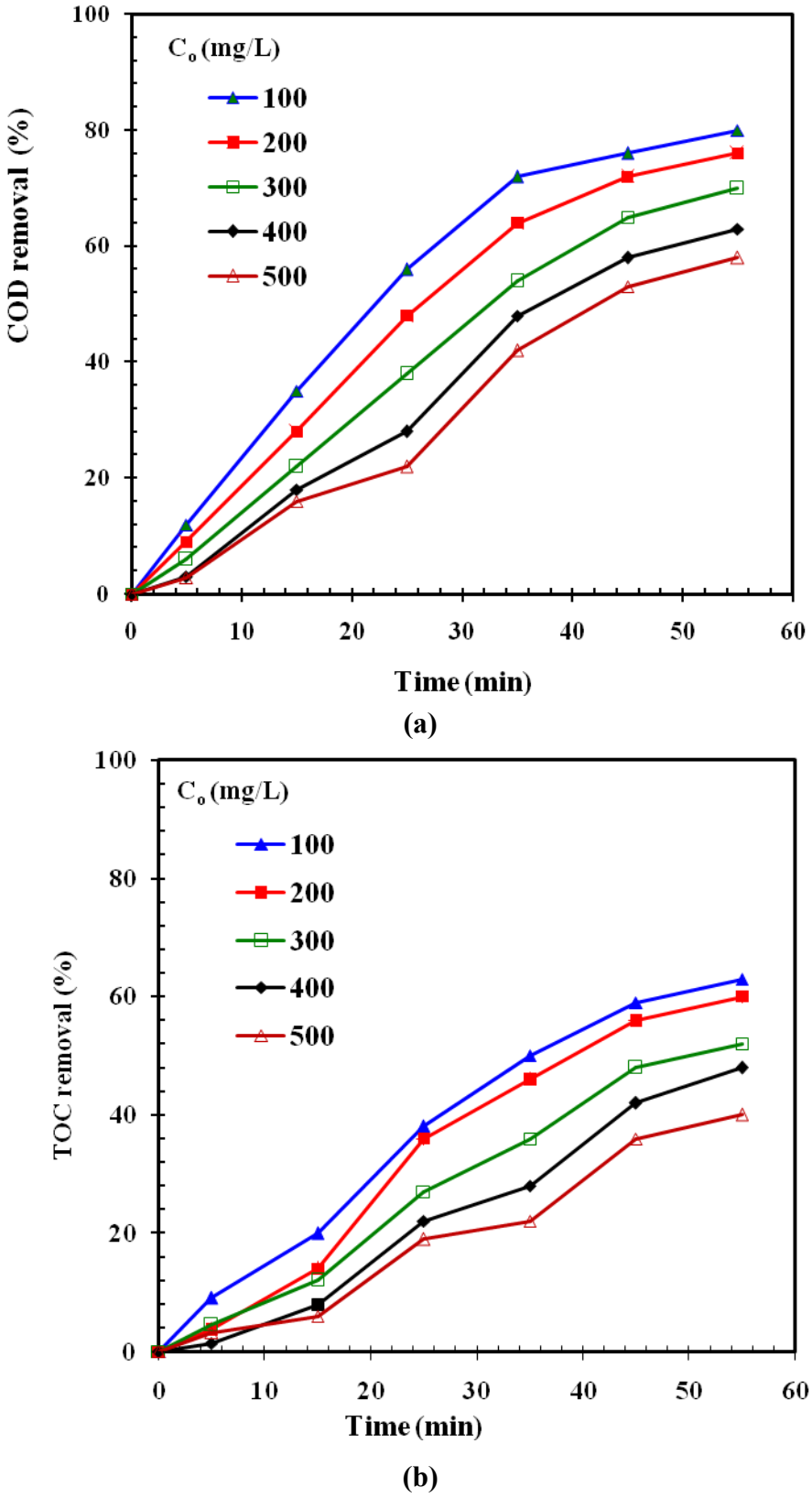

Figure 4.2.6. Effect of C_o on removal efficiency of BG in term of (a) COD; (b) TOC (j: 117.0 A/m^2; NaCl: 1.5 g/L; pH_o: 6.2; temperature: 25 ^oC; electrode gap: 1 cm).

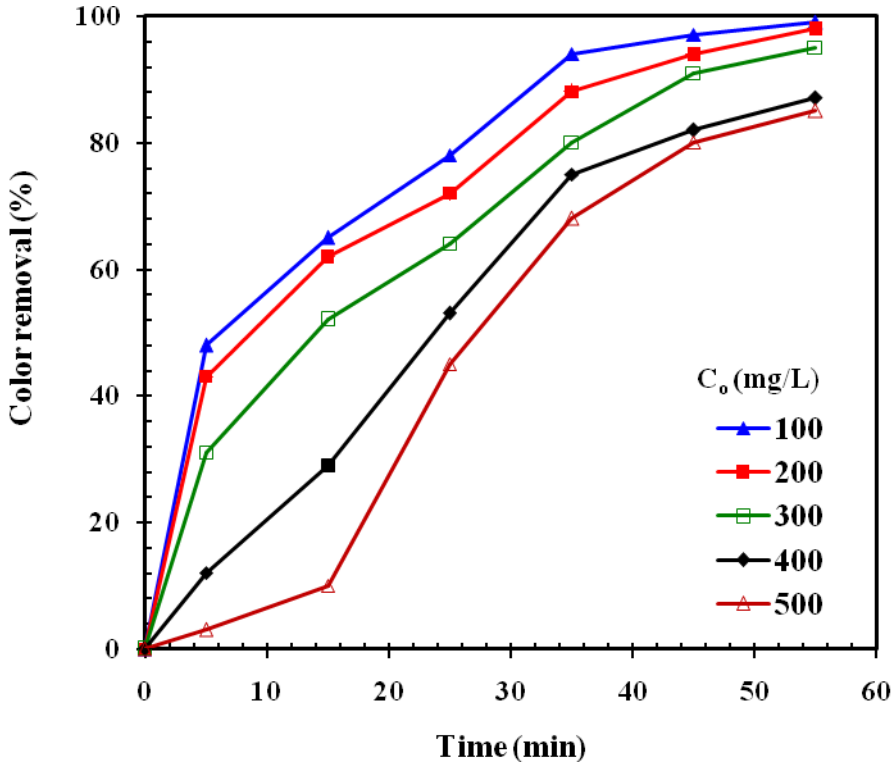

(a)

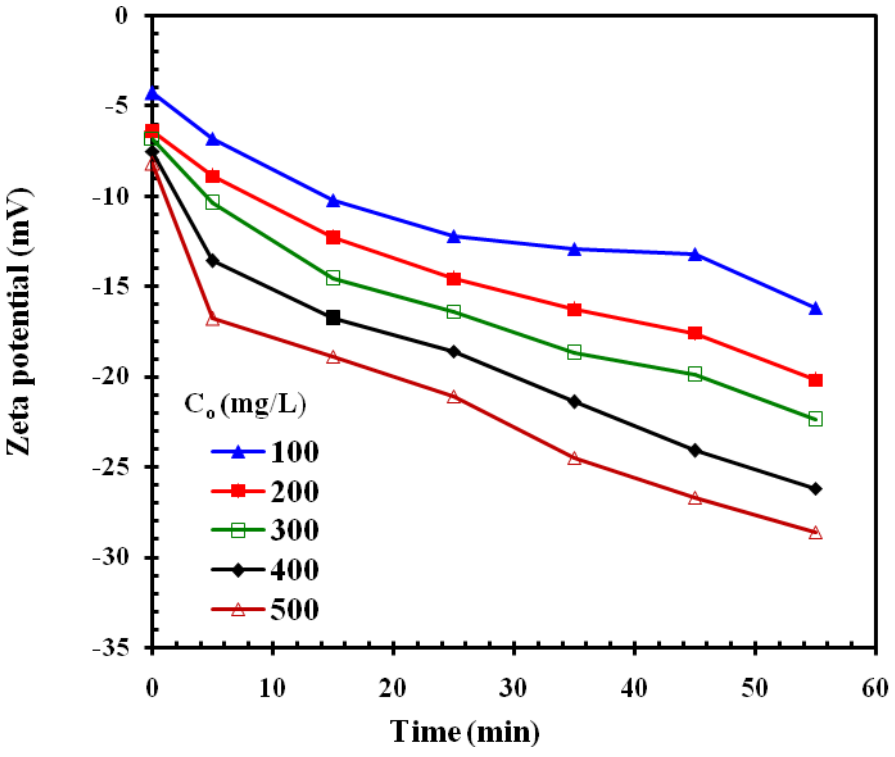

(b)

Figure 4.2.7. Effect of C_o on removal efficiency of BG in term of (a) color and (b) variation of zeta potential (j: 117.0 A/m^2; NaCl: 1.5 g/L; pH_o: 6.2; temperature: 25 ^{o}C; electrode gap: 1 cm).

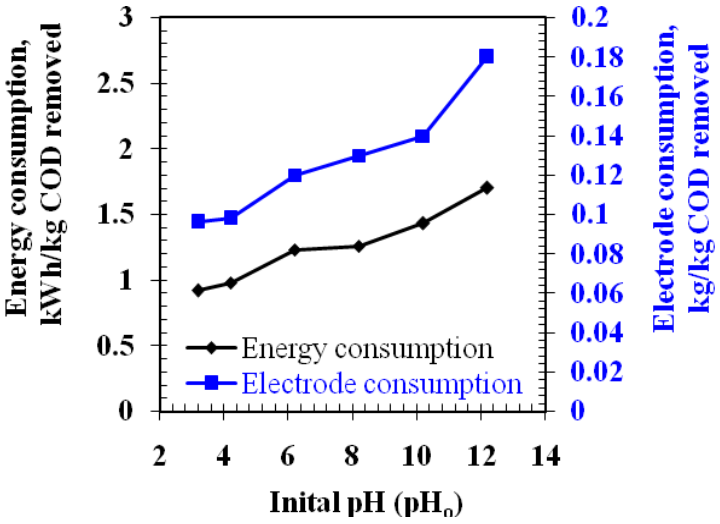

(a)

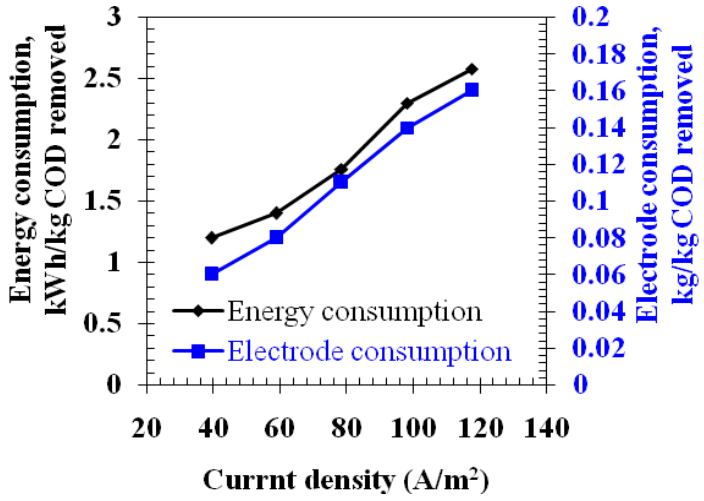

(b)

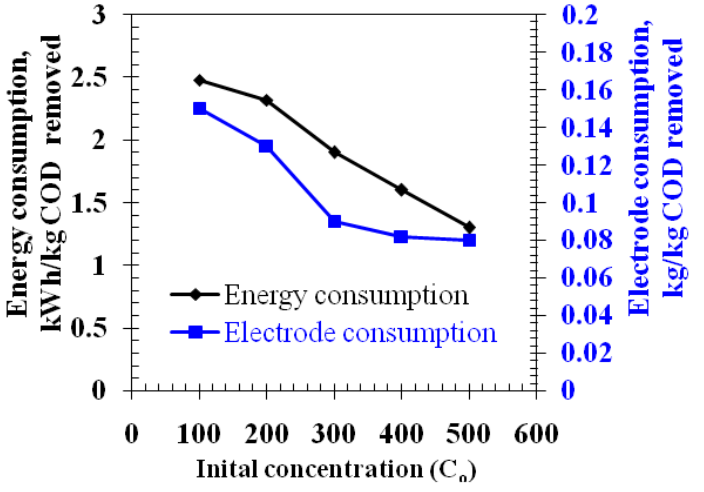

(c)

Figure 4.2.8. Variation of energy and electrode consumption after 45 min of treatment time with (a) initial pH_o, (b) j, and (c) C_o (temperature: 25 ^oC; electrode gap: 1 cm).

Specific energy consumption decreased at high C_o due to the fact that aluminum hydroxide flocs available at constant j were better utilized and were able to adsorb more amount of dye molecules at higher C_o. the cell voltage slightly increased with an increase in C_o.

4.2.2. Mechanistic Study through Characterization of Solid Residues

4.2.2.1. Fourier Transforms Infrared (FTIR) Spectroscopy: FTIR helps in understanding the removal mechanism. Figure 4.1.9a shows FTIR spectrum of sludge generated during treatment of BG dye with aluminum electrodes coded as [Sludge-(BG+Al)]. To better understand the types of flocs generated, experiment was carried out without any dye i.e. with pure water only. Sludge generated in this experiment coded as [Sludge-(Al alone)] was also characterized by FTIR. These spectra are shown in Figure 4.1.9a. The differential spectrum of Sludge-(BG+Al) and Sludge-(Al alone) is shown in Figure 4.1.9b designated by sludge. In addition, FTIR spectra of pure BG dye and scum obtained during treatment of dye is shown in Figure 4.1.9b. A comparative assessment of various strong, broad and sharp peaks is given in these spectra is given in Table 4.1.1. Peaks at ≈1110, ≈1080 and ≈1400 cm^{-1} in scum and sludge are assigned to Al-O-Al, Al-O-H and O-H bending vibrations, respectively [Parshetti et al., 2006; Drouiche et al., 2009]. The presence of these bands indicates that most of the Al generated in EC contains oxy-ether, hydroxides and oxy-hydroxides. These spectra also show broad band between 3100 and 3700 cm^{-1} indicating presence of both free and hydrogen bonded –OH groups in EC residues.

Peak at 3435 cm^{-1} in Figure 4.1.9a of sludge (aluminum alone) indicates the presence of -OH group while peak at 3438 and 3446 cm^{-1} in Figure 4.1.9 indicates the presence of N–H stretching due to the formation of secondary amine in pure dye and scum. After degradation the peak of N–H stretching (3472–3422 cm^{-1}) completely convert into primary amine shown in Figure 4.1.9a and 4.1.9b (sludge dye with aluminum). Some characteristics peaks of BG dye in the finger print region (1500 to 500 cm^{-1}) show the presence of mono and para benzene substituted derivatives of dye [Mall et al., 2005]. The peak at 1593–1587 (s) and 1375–1377 (s) cm^{-1} is due to C=C stretching of benzene ring, and peak at 1170.20 cm^{-1} shows C–N stretching vibrations. These peaks give the perception of the structure of BG [Mane et al., 2007a, b]. Data generated from the FT–IR as shown in Table 4.2.1 provide the information regarding the partial destruction of BG molecules during EC.

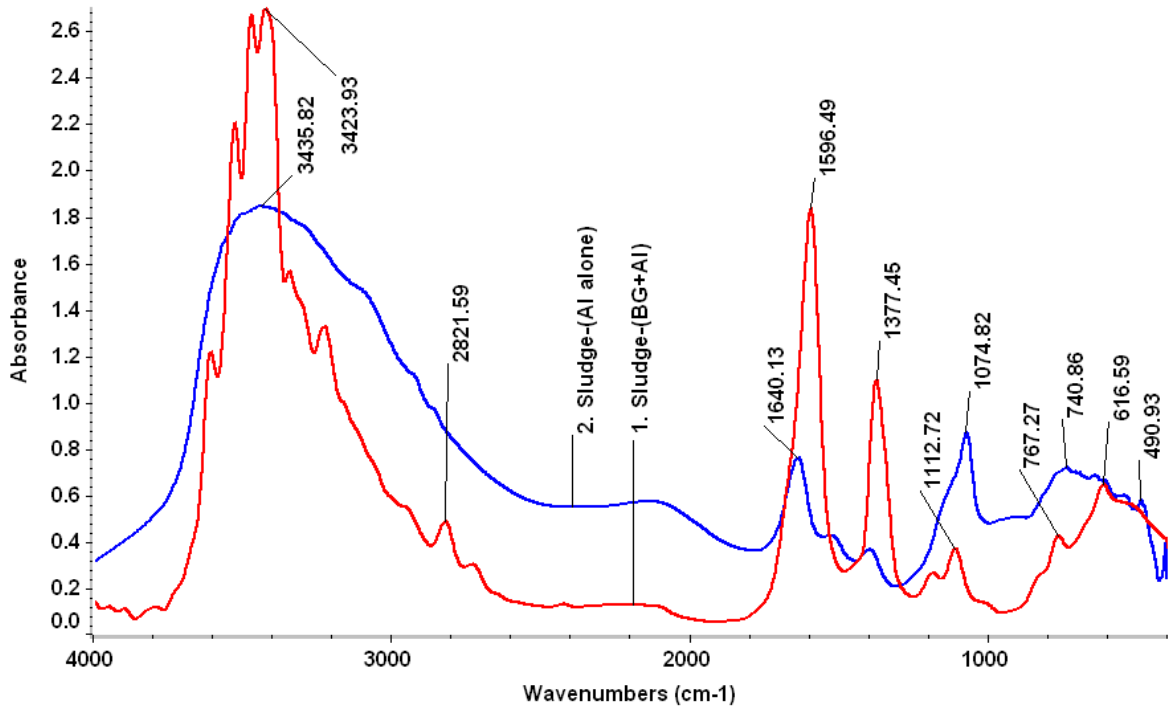

(a)

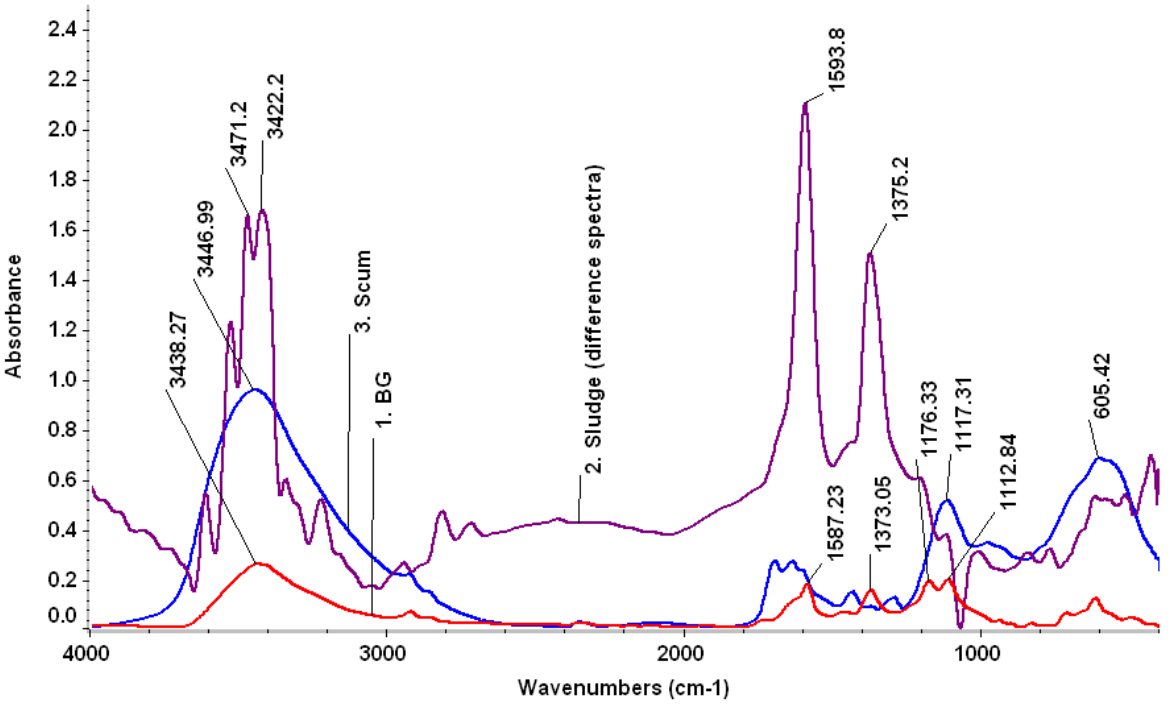

(b)

Figure 4.2.9. FTIR spectrum of (a) Al sludge [Sludge-(Al alone)] and sludge generated during treatment of BG dye with aluminum electrodes [Sludge-(BG+Al)] (b) BG dye, scum and sludge (differential spectra of spectrum in figure (a)).

Table 4.2.1. FTIR characterization of BG dye and Al by product with and without the presence of the dye in EC process.

Band assignments	Pure dye	EC run with dye		Sludge without dye
		Scum	Sludge	
O-H stretching				3334–3668 (br)
O-H bending				1640 (br)
Primary amine-(NH_2)			3420 (br)	
C=C aromatic skeletal	1587 (br), 1373 (sh)	1587 (br), 1373 (sh)	1598 (br), 1375 (sh)	
Phenyl ring C–H and C=C stretching	2996–2821 (br),	2996–2821 (br),	2980–2879 (s),	
–N-H stretching, bending	3438(br)	3446 (br)		
N-C stretching	1176(w),	1171(w),	1165(w),	
Ortho and Para derivatives		767–740(w), 650-610(w)	767–740(w), 650-610(w)	
Al-O-Al		1117 (br)	1112 (br)	1119 (br)
Al-O-H bending		1080 (br)	1080 (br)	1074 (br)

s: strong, br: broad, w: weak, sh: shoulder

4.2.2.2. XRD characterization: The powder X-ray diffraction (XRD) analysis of the EC residue were carried out in Cu-Kα radiation source filtered with a graphic monochromators (λ = 1.5406 Å). The incident ω angle was from 10 to 100^o with 0.050^o step-width and 180s step time. X-ray diffractograms of Al sludge without dye, and scum and sludge generated during treatment showed very broad and diffused diffraction peaks i.e. amorphous and very poorly crystalline in nature (Figure 4.2.10). Use of ICDD (International Centre for Diffraction Data) database and powder indexing software indicated the presence of boehmite (AlO(OH)), bayerite ($Al(OH)_3$), akdalaite ($Al_2O_3)_4{\cdot}H_2O$), and diaspore (AlO(OH)) in these diffractgrams [Mollah et al., 2010]. FTIR and XRD analysis of the EC residues the presence of be aluminum hydroxides and aluminum oxy–hydroxides in these residues.

4.2.2.3. Scanning electron microscope and energy dispersive X-ray analysis: SEM/EDX analysis was performed to evaluate the surface and structural features of the sludge and scum during the EC process as shown in Figure 4.2.11. SEM image shows surface texture of the scum to be hard and that of the sludge to be amorphous in nature. Surface of scum and sludge contain pores of varying sizes.

EDX analysis was used to evaluate the elemental composition (Table 4.2.2) in solid EC residue. Sludge generated during treatment of water with and without dye contained 18.06% and 16.56% carbon, 37.75% and 43.99% oxygen, 32.25% and 37.91% aluminum, 2.32% and 0.40% chlorine, 1.11% and 1.14% sodium by mass, respectively. Scum contained 31.19% carbon, 29.32% oxygen, 24.13% aluminum, 5.67% chlorine and 4.27% sodium. Thus, scum contains higher amount of carbon, whereas sludge contained higher amount of aluminum. This means that the treatment by EC occurred by a combination of electro-floatation, sweep coagulation and aggregation [Ahlawat et al., 2008]. Small organic molecules generated by the degradation of dyes molecules are collected on the surface of solution by electro-flotation, in the form of a layer of gas bubbles with floated particles called scum.

Table 4.2.2. EDX analysis determine the elemental composition in EC generated solid residue.

Elements Analysis	Scum with dye	Sludge with dye	Sludge without dye
	Scum-(BG+Al)	Sludge-(BG+Al)	Sludge-(Al alone)
Elements Analysis			
Carbon (%)	21.16	13.56	28.19
Oxygen (%)	39.5	39.58	34.32
Aluminum (%)	34.25	38.91	24.32
Chlorine (%)	1.92	1.40	7.67
Sodium (%)	2.11	1.14	6.277

4.2.3. Step-by-step EC mineralization of dye

4.2.3.1. Theortical Background: During EC treatment method, the various chemical reactions occur on anode and cathode. These reactions depend on the nature of anode material and chemical structure of dye molecules. The mechanism of EC degradation of BG involves mainly processes such as electro-coagulation, electro-oxidation, electro–floatation, etc. which may occur individually or simultaneously depending upon the operating conditions. In electro-coagulation, in–situ formation of coagulants occurs on anodic dissolution of electrode material. Simultaneous evolution of hydrogen takes place on the cathode which removes pollutant through flotation. Main anodic reactions are as follows:

$$Al \rightarrow Al^{3+} + 3\ e^{-} \quad (4.2.6)$$

($E^{o}(Al^{3+}/Al)$= –1.66 V versus SHE (pH acidic range)

$$Al^{3+} + 3H_2O \rightarrow Al(H_2O)_3(s) + 3\ H^{+} \quad (4.2.7)$$

$$nAl(H_2O)_3\ (s) \rightarrow Al_n(H_2O)_{3n} \quad (4.2.8)$$

Main cathodic reactions are as follows:

$$H_2O + 3\ e^{-} \rightarrow 3/2\ H_2 + 3\ OH^{-} \quad (4.2.9)$$

Aluminum and hydroxyl ions are generated during electrode reaction in equation (4.2.6) and (4.2.8) to give different monomeric and polymeric species at low and higher pH, respectively [Panizza and Cerisola, 2005; Khandegar and Saroha, 2012; Singh et al., 2013c]. During EC treatment, oxidation of dye molecules takes place via the active species already present in the solution [Panizza and Cerisola, 2006]. Electrochemical advance oxidation processes (EAOPs) are used for destruction of dyes through oxidation by $^{\bullet}OH$ radicals generated at the surface of metal anode at high oxygen over–voltage during H_2O decomposition [Martinez–Huitle and Ferro, 2006; Panizza and Cerisola, 2009] The electrolyte, the electrode potential, and structural abnormalities and/or transient intermediates all affect the mineralization process [Keith and Carter, 2013] The main reaction involved during the EC treatment are shown as follows:

$$2H_2O \rightarrow O_2 + 4\ H^{+} + 4\ e^{-} \quad (4.2.10)$$

$$2\ Cl^{-} \rightarrow Cl_2 + 2\ e^{-} \quad (4.2.11)$$

$$Cl_2 + H_2O \rightarrow HOCl + HCl \quad 4.2.12)$$

$$HOCl + OH^{-} \rightarrow OCl^{-} + H_2O \quad (4.2.13)$$

$$O_2\,(g) + 2\ H^{+} + 2\ e^{-} \rightarrow H_2O_2 \qquad E^{o}\ (O_2/\ H_2O_2) = 1.23\ V \quad (4.2.14)$$

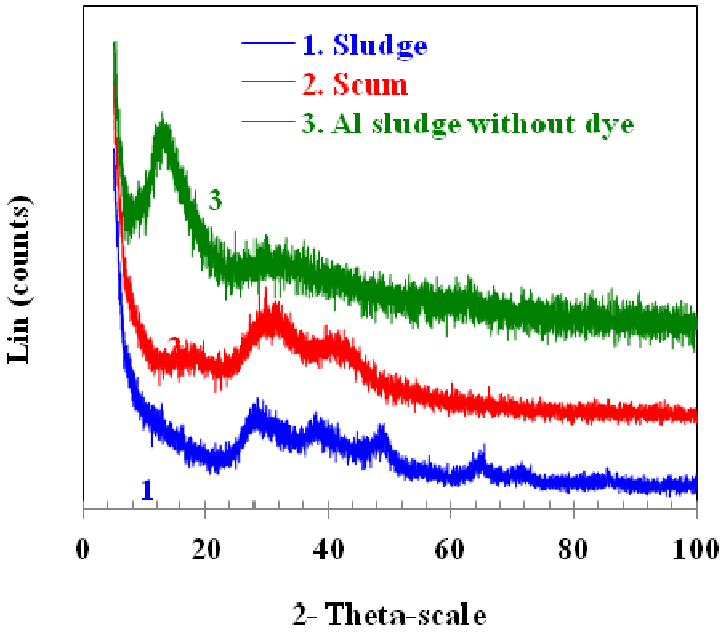

Figure 4.2.10. XRD diagram of scum and sludge obtained during EC treatment of BG dye bearing aqueous solution, and of the sludge obtained from Al electrode during EC treatment of pure water without dye.

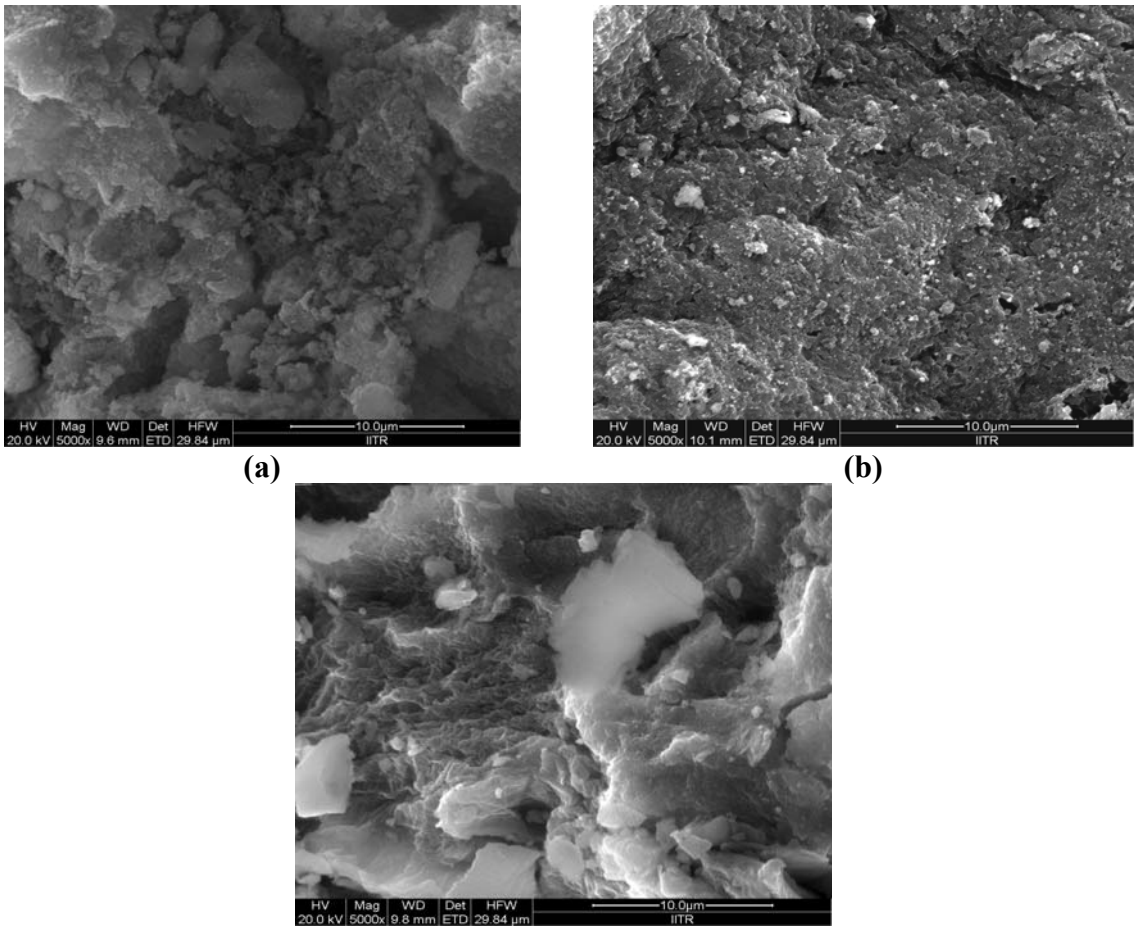

Figure 4.2.11. FE-SEM pattern of EC residue (a) sludge without dye (b) scum and (c) sludge with dye.

Molecular oxygen converts into active oxygen via cathodic reaction.

$$4\ H_2O + 2\ O_2\,(aq) + 4e^- \rightarrow 2\ H_2O_2 + 4\ OH^- \quad (4.2.15)$$

$$Al^{+3} + 2\ H_2O_2 \rightarrow [\text{monomeric/polymeric Al cationic species}] + {}^{\bullet}OH + OH^- \quad (4.2.16)$$

($^{\bullet}OH$, $E^o(^{\bullet}OH/\ H_2O)$=2.80 V versus SHE

$$Al(H_2O) \rightarrow Al(^{\bullet}OH) + H^+ + e^- \quad (4.2.17)$$

Ozone may also get produced if either anodic potential goes to 1.51 V or by the oxidation of evolved oxygen [Pletcher and Walsh, 1993; Raju et al., 2008].

$$4\ H_2O + 2\ O_2 \rightarrow O_3 + 2\ H^+ + 2\ e^- \quad (4.2.18)$$

At the time of electrolysis, a number of oxidants such as nascent oxygen, ozone, hydrogen peroxide, free chlorine and free radical such as $^{\bullet}OH$ and $^{\bullet}OCl$ may get produced [Szpyrkowicz et al., 2000]. On the basis of above reactions, solution may contain cocktail of various oxidants. It is too difficult to find out the actual quantitative amount of each oxidant. Oxygen and ozone are weak oxidant, and it is presumed that hydrogen peroxide and $^{\bullet}OH$ are main oxidants [Rodgers et al., 1999; Canizares et al., 2005; Mondal et al., 2013] which are responsible for the degradation of dyes and other organic compounds.

4.2.3.2. UV–visible analysis: EC degradation before and during treatment (at various treatment time) was studied using UV–visible analysis (200–800 nm). Intense green color of BG is shown by an absorption band at λ_{max}=619 nm (extinction coefficient=$10^5\ M^{-1}cm^{-1}$) in the UV–visible spectrum (Figure 4.2.12). The intensity of peak at λ=619 nm decreased with an increase in treatment time. The absorption at 619 nm became almost zero after 50 min of EC treatment indicating the absence of auxochrome groups –N(CH_3) responsible for the color of the BG dye. Peak at 253 nm shifts towards lower wavelength (209 and 185 nm) indicating the presence of the mono aromatic rings in the solution after 50 min of treatment. The presence of new absorption wavelength at 365 nm provides the information of poly conjugated triphenylmethane aromatic ring [Behnajady et al., 2008]. This change in position of spectral peaks to shorter wavelength, generally termed as hypsochromic shift, is due to N–de–methylating process [Montanaro and Petrucci, 2009]. This shift can also occur because of change in solvatochromic parameters such as solvent polarity.

4.2.3.3. FTIR analysis: Figure 4.2.13 shows FTIR spectra of EC reactor solutions collected at different time during the treatment. At time t=0 min, FTIR spectrum of pure BG dye shows a broad band between 3000 and 3700 cm^{-1} with peak at 3445 cm^{-1}. This

band is due the presence of tertiary amine group and N-H bending in the dye molecule. This may also be due to the presence of OH groups due to the hydrogen bonding of dye in the solution. A peak at 2914 cm^{-1} is due to -CH_3 stretching [Mall et al., 2005]. Peak at 1630 cm^{-1} is due to N-H in-plane bending. During initial phases of treatment ($t \leq 30$ min), a large number of peaks are observed between 3100 and 3650 cm^{-1}. These are due to the presence of a number of hydroxyl groups that get generated during the initial phases of treatment generated by the interaction of H_2O_2 (generated on cathode shown in equation 4.2.14) and aluminum ion concentration (on anode shown in equation 4.2.6) during EC treatment (shown in equation 4.2.16). These peaks also indicate presence of inter and intra molecular hydrogen bonding between the dye and water molecules [Mollah et al., 2010]. Peaks within the range 3100 to 3450 cm^{-1} may also be due to the conversion of attached tertiary amine functional group of dye into primary amines. Conversion of tertiary amine group to secondary and primary amines is shown by emergence of peak at ≈1350 cm^{-1}. Increase in absorbance at ≈1610 cm^{-1} may be due to C=O stretching of lactones [Mohan, 2004]. These peaks may also be due to presence of –NH deformation and aromatic rings. A number of peaks in the range of 400-650 cm^{-1} show the presence of mono- and para-substituted derivatives of benzene ring at the end of EC treatment. After treatment for 50 min, most of peaks observed earlier in the range of 3100 and 3650 cm^{-1} disappeared and only a flat broad peak was observed indicating utilization of OH groups for EC treatment of BG dye. Similarly, peak intensity at ≈1610 cm^{-1} got decreased indicating oxidation and conversion of C=O and –NH groups, and aromatic rings. It may, however, be seen in the Figure 4.2.13 that the intensity of peak at ≈2105 cm^{-1} goes on increasing with treatment time. This peak is due to alkyl CN stretching. This may be due to the conversion of aromatic ring structure to small aliphatic CN groups.

4.2.3.4. Intermediate Identification through HPLC Analysis: HPLC analysis of the sample was carried out at various treatment time and the chromatograms are shown in Figure 4.2.14 for detection at 619 nm. The peak area below the retention time of BG (≈8.8 min) was found to decrease with treatment. It may be seen that a number of new peaks appeared in the chromatograms taken at various treatment time. Thus, it seems that many new degradation species were formed in the solution during the treatment process. Because of short life of the intermediates and non-availability of standards, it was difficult to identify the intermediates with HPLC analysis. Therefore, further analysis of samples was

done in HRMS and GCMS to identify the intermediates formed during the treatment process [Richardson et al., 2000; Boyd, 2011]. Similar strategies of analysis have been reported earlier for UV–visible light induced photodegradation of malachite green [Chen et al., 2013] and basic violet–4 [Chen and Lu, 2007] through photocatalytic degradation with TiO_2 catalyst.

4.2.3.5. Intermediate Identification through HRMS Analysis: HRMS spectral analysis was further used to identify the N–de–methylated intermediates. HRMS analysis of solution (Figure 4.2.15) after 10 min of treatment showed presence of various intermediates during BG degradation. Table 4.2.3 shows various compounds identified using HRMS spectra.

4.2.3.6. GCMS Analysis: GCMS mass spectra of solution at various treatment times are shown in Figure 4.2.16 and Table 4.2.4 presents the intermediates fragmentation pattern (A'–D', a–h, a'–d' and f', g', 1–3 and I–XIII) and intermediates compounds identified in GCMS spectra. According to mass analysis, these intermediates were ascribed as follows: A (m/z 329.2009) as BG with λ_{max} (619 nm); B (m/z=315.1885) as (N, N–dimethyl–N'–methyl–4,4'–diaminotriphenylcarbenium) (DMDTC); C (m/z=301.1454) as (N–methyl–N'–methyl–4,4'–diaminotriphenylcarbenium) (MMDTC) and C' might be the C isomer; D (m/z=284) as (N–methyl–4,4'–diaminotriphenylcarbenium) (MDTC); E (m/z=268) as (4,4'–diaminotriphenylcarbenium) (DTC). Intermediate F and I, with m/z=284 and 239.1185 as (N,N,N,N–tetramethyl–diminodiphenylepoxide) (TDDE), (N,N–dimethyl–aminodiphenylepoxide) (DDE), respectively, represented cleavage of the central carbon. Two other peaks d and e were also found with m/z=225.1031 and 209.1088 as N–methyl–4, 4'–diaminobenzophenone (MDBP), 4, 4'–bis–aminobenzophenone (BP). These provide information about the further degradation of epoxides intermediate F and I into small and easily degradable organic molecules.

During GC–MS analysis most abundant peaks were identified as: N, N–dimethylparaaminobenzenzoic acid (DABc): m/z=166 and 60.8%, N, N–dimethylparaaminobenzaldehyde (DABz): m/z=148 and 100%, N–methylparaaminobenzaldehyde (MABz): m/z=132 and 68.8%, N–dimethylparaaminobenzene (DAB): m/z=121 and 98.8% found at the middle of treatment. Aminobenzene (AB): m/z=93 and 72%, ethylamide (EAs): m/z=71 and 66.2% ethylamine (EAs): m/z=44 and 100% were found at the end of treatment time.

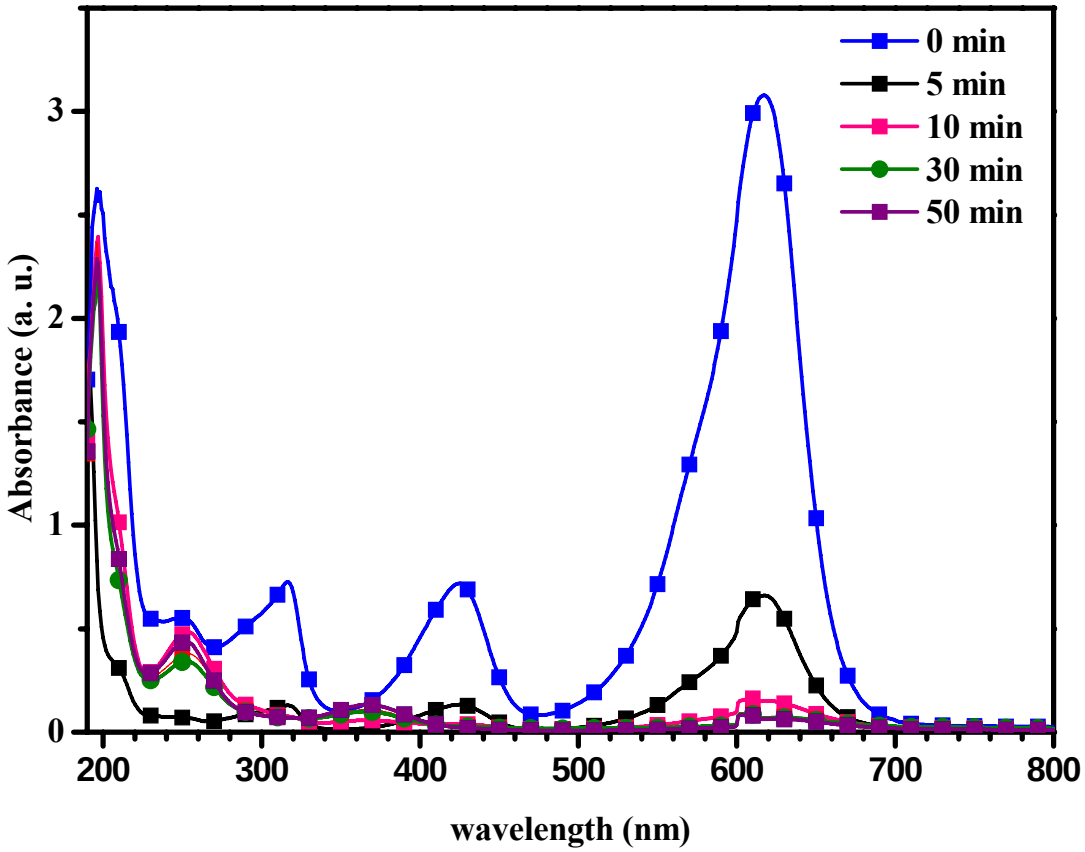

Figure 4.2.12. UV–visible spectra of basic green 4 at different time intervals during the EC treatment.

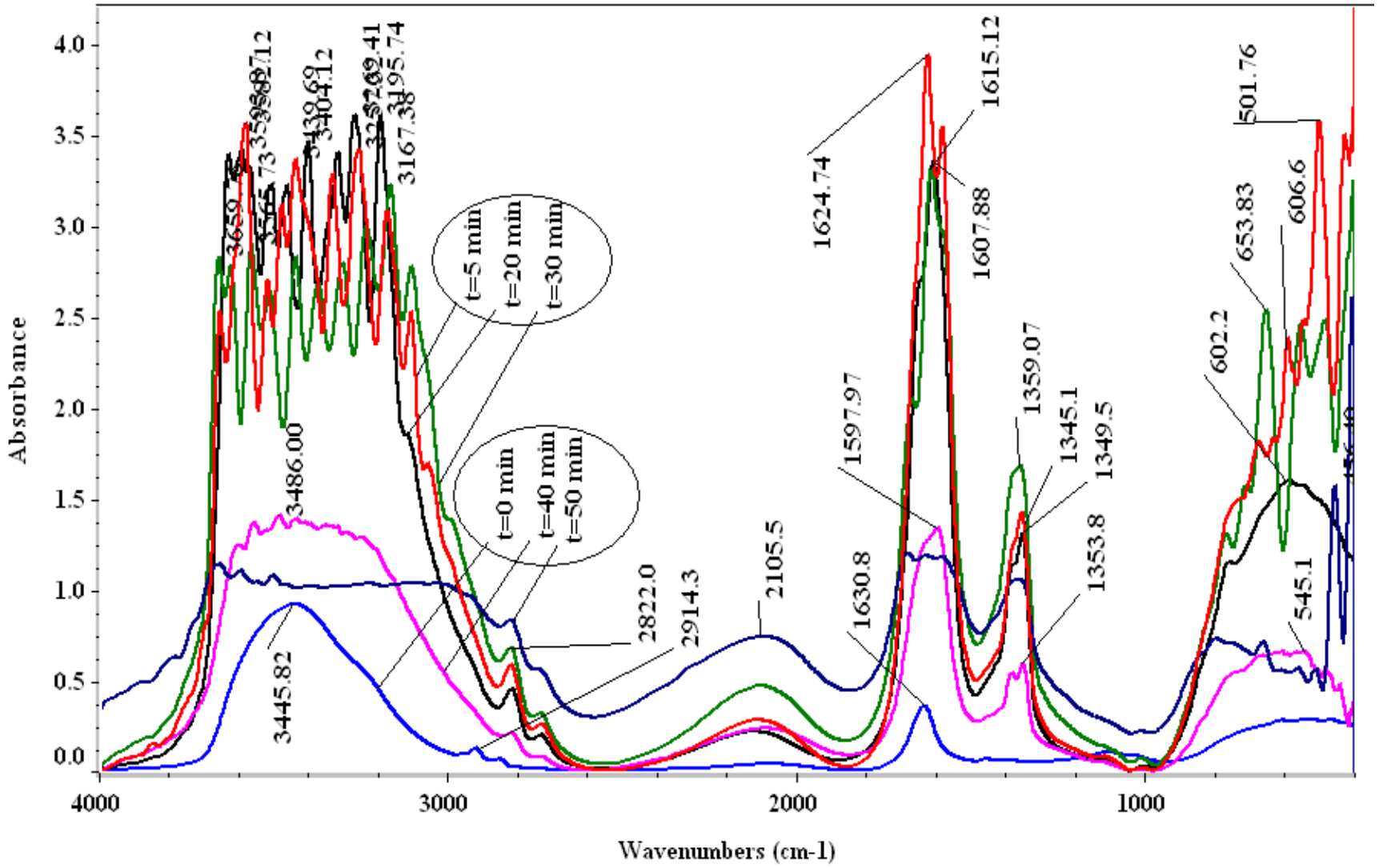

Figure 4.2.13. FTIR spectra of basic green 4 at different time intervals during EC treatment.

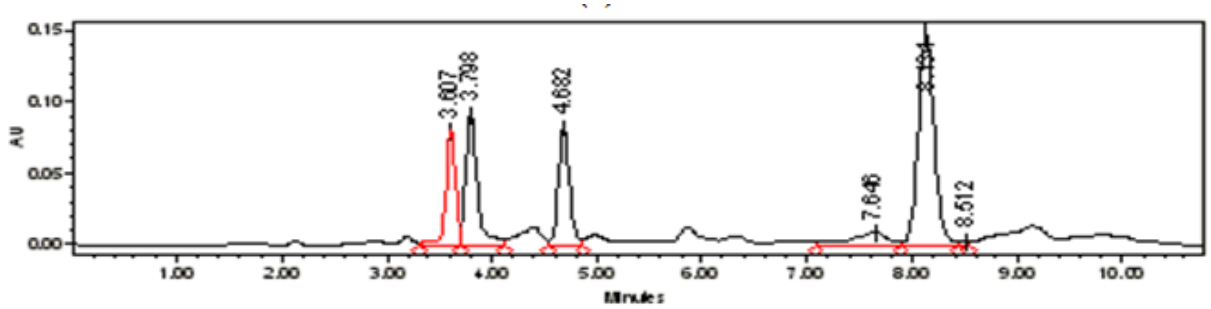

(a) 10 min

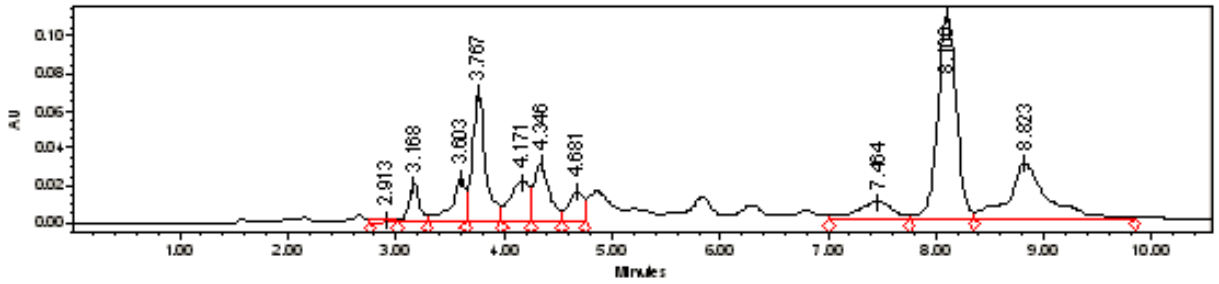

(b) 20 min

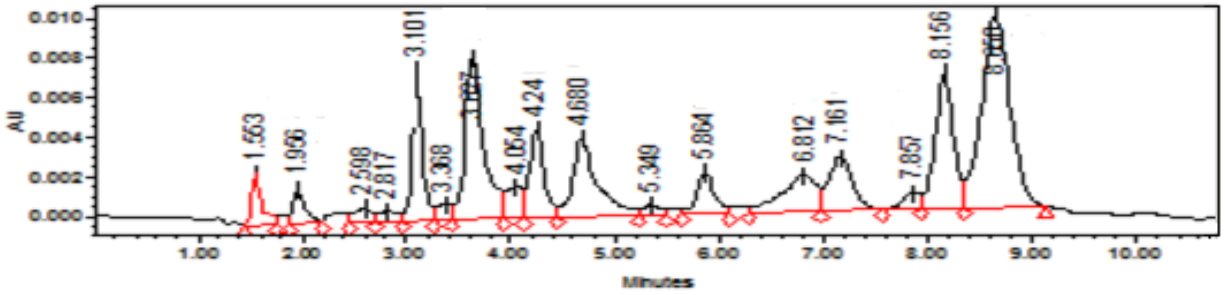

(c) 30 min

Figure 4.2.14. HPLC analysis at various time at λ=619 nm.

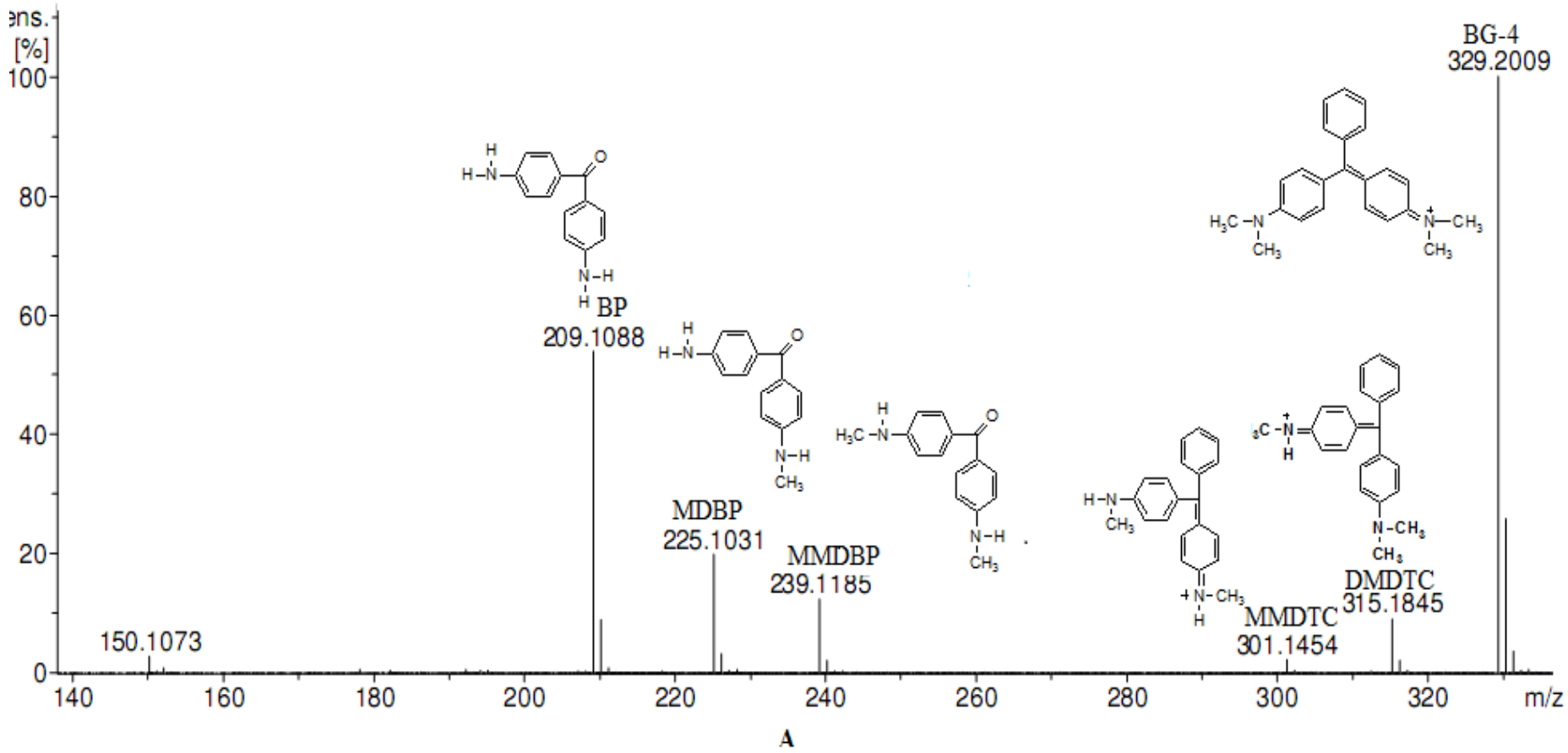

Figure 4.2.15. HRMS analysis of solution after 20 min of treatment.

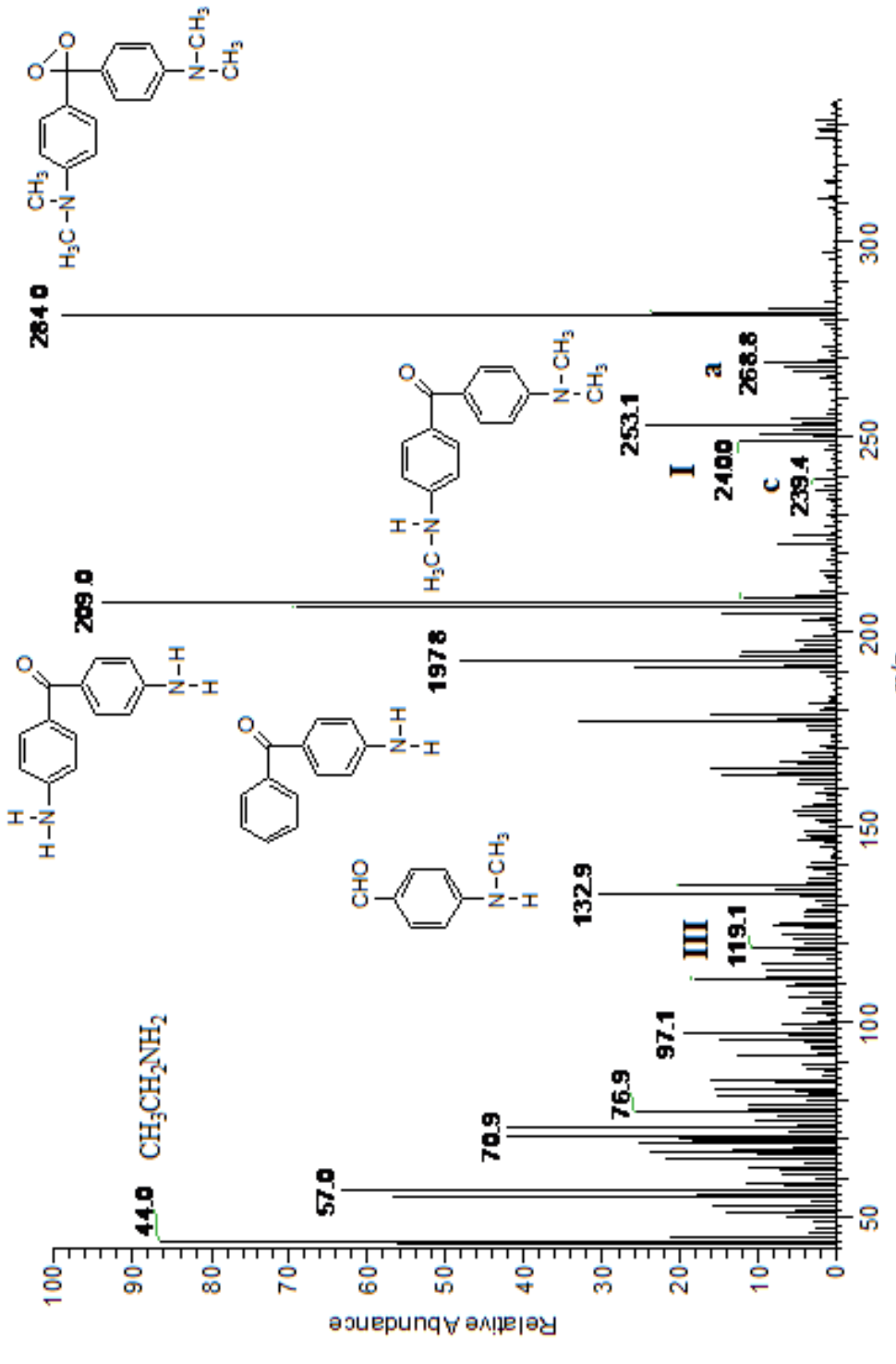

(a) 20 min

Figure 4.2.16. GC–MS analysis at different time (a) 20 min, (b) 30 min, and (c) 50 min [Continued to next page]

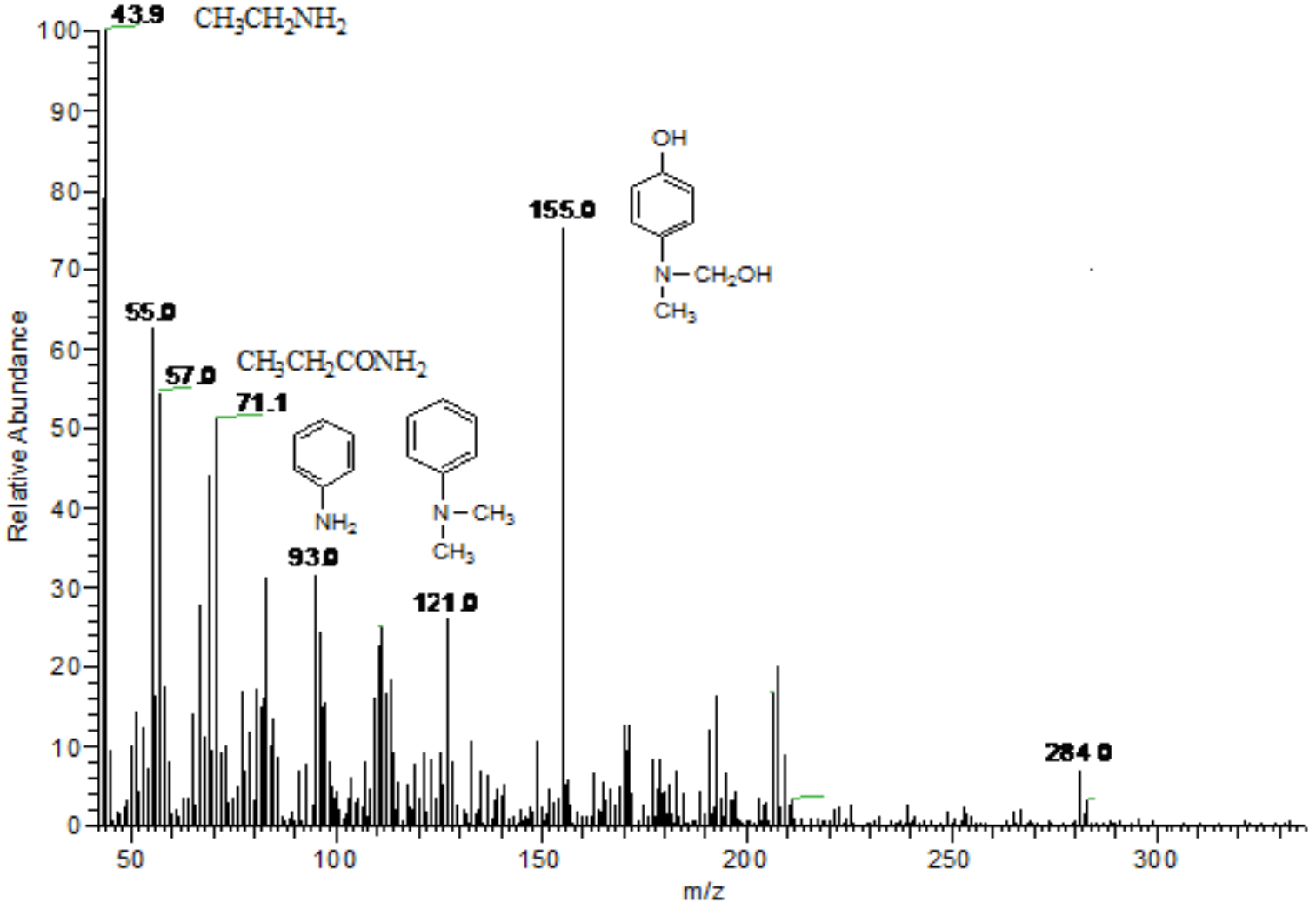

(b) 30 min.

Figure 4.2.16. GC–MS analysis at different time (a) 20 min, (b) 30 min, and (c) 50 min [Continued to next page]

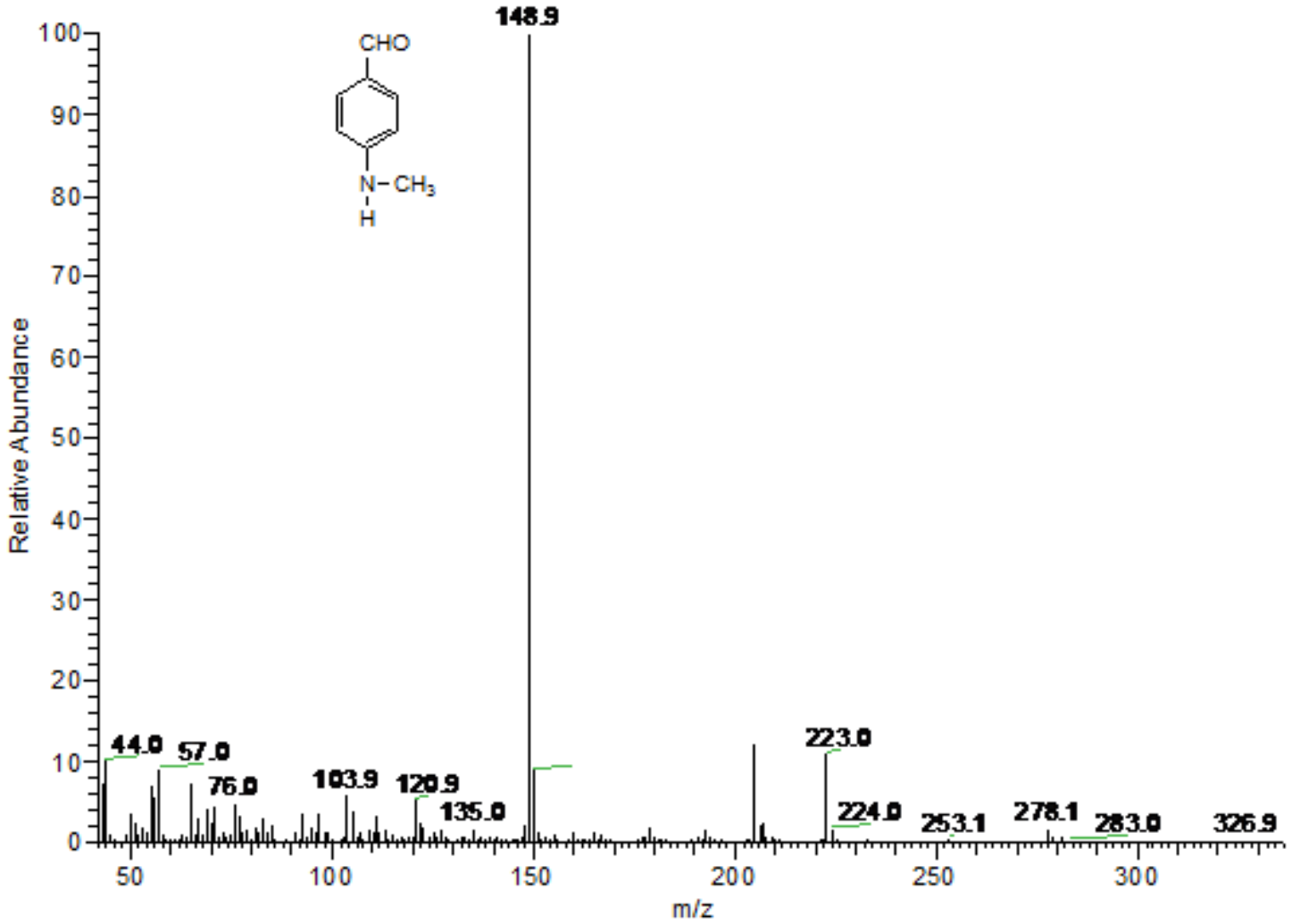

(c) 50 min

Figure 4.2.16. GC–MS analysis at different time (a) 20 min, (b) 30 min, and (c) 50 min.

Table 4.2.3. Analysis of HRMS spectra.

S.No.	N–de–methylating intermediates	abbreviation	MS peaks (m/z)
A	N,N,N',N'–tetramethyl–4,4'–diaminotriphenylcarbenium	BG	329.2009
B	N,N–dimethyl–N'–methyl–4,4'–diaminotriphenylcarbenium	DMDTC	315.1845
C	N–methyl–N'–methyl–4,4'–diaminotriphenylcarbenium	MMDTC	301.1454
C’	N,N–dimethyl–4,4'–diaminotriphenylcarbenium	DDTC	315.1845
D	N–methyl–4,4'–diaminotriphenylcarbenium	MDTC	nil
E	4,4'–diaminotriphenylcarbenium	DTC	nil
F	N,N,N',N'–tetramethyl–4,4'–diaminodiphenylepoxide	TDDE	nil
I	N,N–dimethyl–4–aminodiphenylepoxide	DADE	nil
c	N–methyl–N’–methyl–4,4'–diaminobenzophenone	MMDBP	239.1185
d	N–methyl–4,4'–diaminobenzophenone	MDBP	225.1031
e	4,4'–bis–aminobenzophenone	BP	209.1088

Table 4.2.4. Analysis of GC–MS spectra

S.No.	N–de–methylation intermediates	abbreviation	m/z value
A’	N,N–dimethyl–N’–hydroxymethyl–N’–methyl–4,4'–diaminotriphenylcarbenium	DHMDTC	-
B’	N,N–dimethyl–N’–hydroxymethyl –4,4'–diaminotriphenylcarbenium	DHDTC	331
B’’	N–methyl–N–hydroxymethyl–N’–methyl –4,4'–diaminotriphenylcarbenium	MHMDTC	331
C’	N–methyl –N’–hydroxymethyl–4, 4'–diaminotriphenylcarbenium	MHDTC	-
C’’	N–hydroxymethyl –N’–methyl–4,4'–diaminotriphenylcarbenium	HMDTC	-
D’	N–hydroxymethyl –4,4'–diaminotriphenylcarbenium	HDTC	-
a	N,N,N’,N’–tetramethyl–4,4'–diaminobenzophenone	TDBP	268
b	N,N,–dimethyl–N’–methyl–4,4'–diaminobenzophenone	DMBP	253
c	N–methyl–N’–methyl–4,4'–diaminobenzophenone	MMDBP	239
d	N–methyl–4,4'–diaminobenzophenone	MDBP	225
e	4,4'–bis–aminobenzophenone	BP	209
a’	N,N–dimethyl–N’–hydroxymethyl–N’–methyl–4,4'–diaminobenzophenone	DHMDBP	284
b’	N,N–dimethyl–N’–hydroxymethyl–4,4'–diaminobenzophenone	DHDBP	268
c’	N–methyl–N’–hydroxymethyl–4,4'–diaminobenzophenone	MHDBP	-
d'	N–hydroxymethyl–4,4'–diaminobenzophenone	HDBP	-
f	N,N–dimethyl–4–aminobenzophenone	DABP	225
g	N–methyl–4–aminobenzophenone	MABP	209
h	4–aminobenzophenone	ABP	197
f’	N–methyl–N–hydroxymethyl–4–aminobenzophenone	MHABP	241
g’	N–hydroxymethyl–4–aminobenzophenone	HABP	227
1.	N,N–dimethyl–para–aminophenol	DAP	-
2.	N–methyl–para–aminophenol	MAP	121
3.	4–aminophenol	AP	-
I	Benzene	B	78
II	Benzoic acid	BA	-
III	N,N–dimethylaminobenzene	DAB	121
IV	N,N–dimethyl paraaminobenzoic acid	DABA	-
V	N–methyl paraaminobenzoic acid	MABA	-
VI	N,N–dimethyl paraaminobenzaldehyde	DABz	148
VII	N–methyl paraaminobenzaldehyde	MABz	-
VIII	Amino benzene	AB	93
IX	4–aminobenzoic acid	ABc	-
X	Ethyl amide	EAs	71
XI	Acetic acid	AAc	60
XII	Acetamide	AMs	59
XIII	Ethyl amine	AAn	44

4.2.3.7. Electrochemical Degradation of BG 4

4.2.3.7.1. Degradation pathways: According to literature review [Richardson et al., 2008] N–de–alkylation process occurs by the formation of radical on central nitrogen, while the destruction of conjugated structure occurs by the generated radical on central carbon [Liu et al., 2000; Oturan et al., 2008]. Therefore, the overall mineralization of BG involves two degradation pathways, namely N–de–methylation and destruction of chromophore structure resulting from different radicals, either carbon centred and nitrogen centred. These two degradation pathways (shown in different Figures later on) are due to the multiple sites available for •OH attack, generated during EC treatment, on BG dye and its byproducts [Oturan et al., 2008; Ayed et al., 2011; Chen et al., 2010]. Anodic oxidation of electrodes generates electrons which react with the positively charged dimethyl amine group within the dye molecule yielding the cationic dye radical. After the formation of cationic dye radical, hydrolysis and deprotonation processes occur [Chen et al., 2007; Liu et al., 2011]. Literature reported on the degradation of triphenylmethane dye via various methods [Oturan et al., 2008; Chen et al., 2010]. These studies help to understand the formation of N–methylamino moiety because of the electrophilic attack on nucleophilic nitrogen through the hydroxymethylamino derivatives as intermediates.

Intermediates (A'–D'; a'–d' and f', g), 1' and 2' are genarted during N–methylation of BG through the formation of hydroxymethylamino derivatatives via the interaction of active oxygen species and N,N–dimethyl or N–methyl groups [Chen et al., 2007]. Interface interactions between auxochrome group of dye molecules and active species generated during EC generate many intermediates. Intermediates, as indentified in (Figure S4 given in supporting information), shows that c (MMDBP): m/z=239.1185, d (MDBP): m/z=225.1031, e (BP): m/z=209.1088 are obtained via the formation of intermediate F and its degradation through hydroxymethylamino derivatives.

4.2.3.7.2. N–de–methylation of BG: In acidic and near neutral condition, maximum number of monomer aluminum cationic species and electrons are generated during anodic dissolution via equations 4.2.6 and 4.2.10. BG receives these electrons from colloidal suspension through electron mobility from anode to cathode via the positive dimethylamine group. This converts the dye molecule into cationic radicals. N–de–methylated intermediate and methanol are obtained by the interaction of H_2O molecules on methyl group of dimethylamine of cationic dye radical. O_2 generated during cathodic reaction of H_2O (via equation 4.2.10) and reduces it into H_2O_2 (via equations 4.2.14 and 4.2.15). The $OH^{\bullet}$ radical, which is a strong initiator for degradation of the dye molecules,

gets generated through indirect reaction of Al^{3+} and H_2O_2 shown in equation 4.2.16. The intermediate of N–de–methylated derivatives of dye i.e. B: mono N–de–methylated (DMDTC), C: di N–de–methylated (MMDTC) and C': DDTC; D: tri N–de–methylated (MDTC) are formed during 10 min of the EC treatment. N–de–methylated process continues until the formation of complete de–methylation intermediate E: DTC as shown in Figure 4.2.17. Figure 4.2.18 shows that the carbon centred radical generated via the transfer of electron in conjugated structure, reacts with oxygen molecule leading to the formation of F: TDDE through path I and I: DDE through path II. F: TDDE and I: DDE are reactive and highly unstable intermediates and their expected destruction mechanism is represented in schemes Figure 4.2.19 and Figure 4.2.20. Intermediates c (MMDBP), d (MDBP) and e (BP) get formed via the same process of electron attack, hydrolysis or deprotonation through the degradation of epoxide F: TDDE (Figure 4.2.19). Similarly, degradation of intermediate I: DDE leads to formation of compound h and other intermediates in Figure 4.2.20. Mass of intermediates defined in above text and Figure of degradation also confirmed from the Figure 4.2.15 and 4.2.16 along with Tables 4.2.3 and 4.2.4 respectively.

4.2.3.7.3. Destruction of conjugated structure: All the intermediates described in schemes 4.2.17–4.2.20 further get degraded into small aromatic compounds which get easily mineralized into small molecules as shown in Scheme 4.2.21 and Figure 4.2.16. These smaller molecules are given in Table 4.2.4 and these include molecules such as I(B), II(BA), III(DAB), IV(DABA),V(MABA), VI(DABz), VII(MABz), VIII (AB) and IX (ABc), X(EAs), XI(AAc), XII(AMs), XIII(AAs), and 1, 2, 3 which get further mineralized to $NO_3^-$and CO_3^{-2} [Prevot et al., 2001; Chung et al., 2011]. GCMS analysis provided information regarding above described schemes and path. The most abundant peaks of intermediates were identified as: IV(DABA): m/z=166; VI(DABz): m/z=148;VII(MABz): m/z=132; VIII (AB): m/z=93; X(EAs): m/z=71; XIII(AMs): m/z=44; and III(DAB): m/z=121 at 60.8%, 100%, 68.8%, 66.2%, 100%, 72% and 98.8%, respectively, giving evidence regarding formation of different intermediates. The peaks in GCMS give evidence of the conversion of large aromatic ring derivatives into small aromatic derivatives by possible Figures as described in this study.

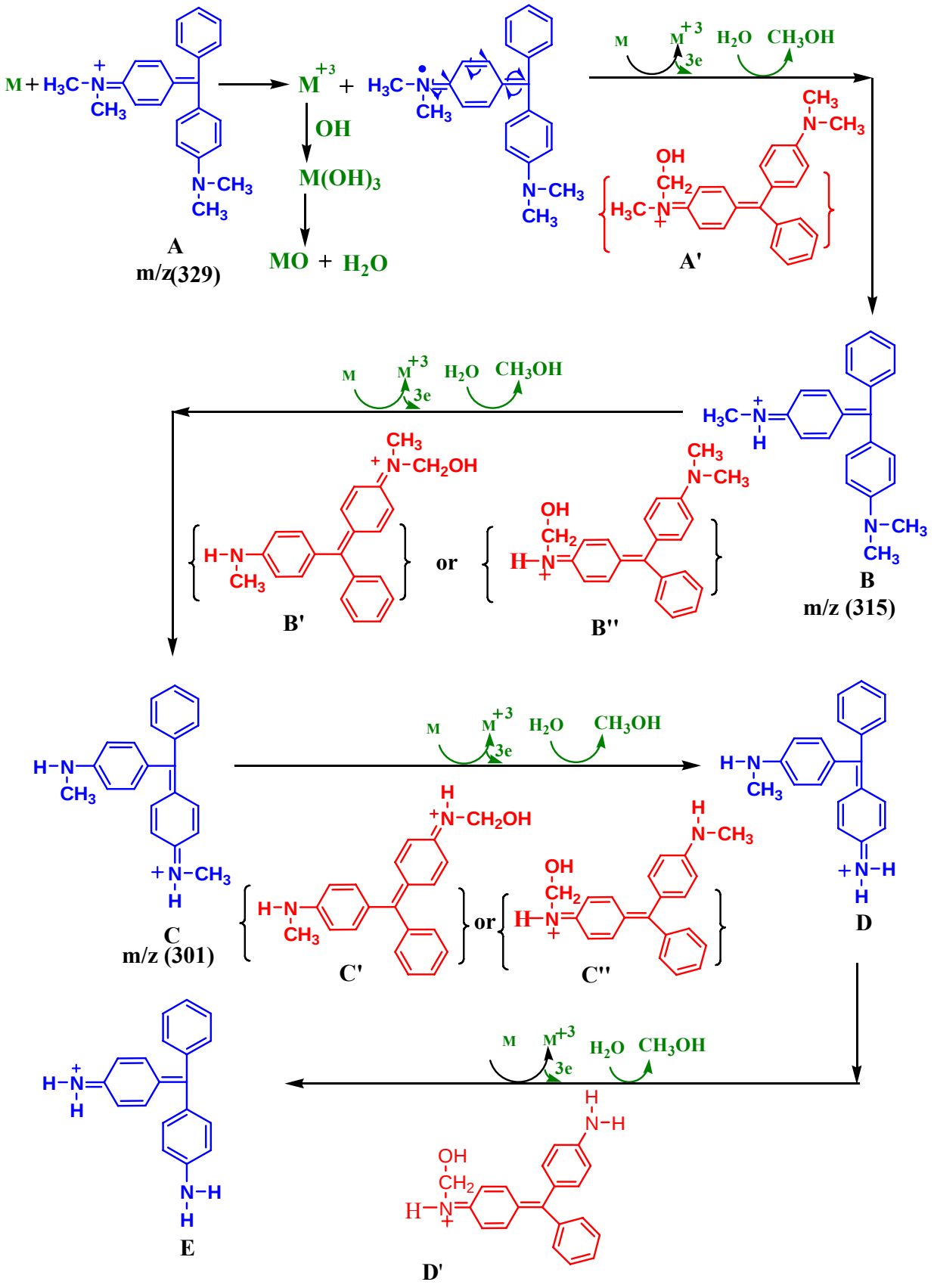

Figure 4.2.17. N–demethylation pathway of BG dye during EC treatment based on different intermediates identified by mass analysis.

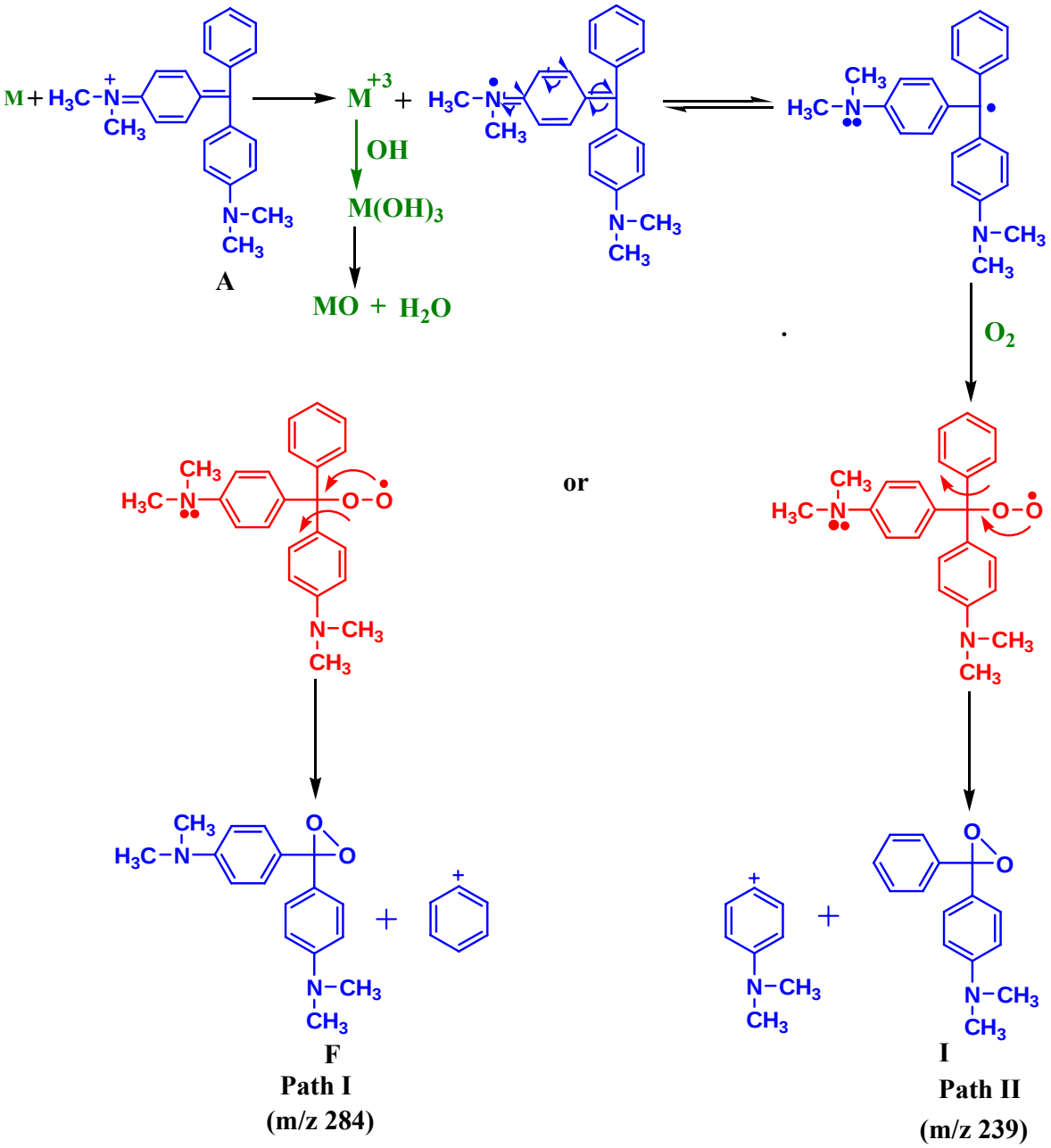

Figure 4.2.18. Destruction of conjugated structure of the BG dye during EC treatment based on different intermediates identified by mass analysis.

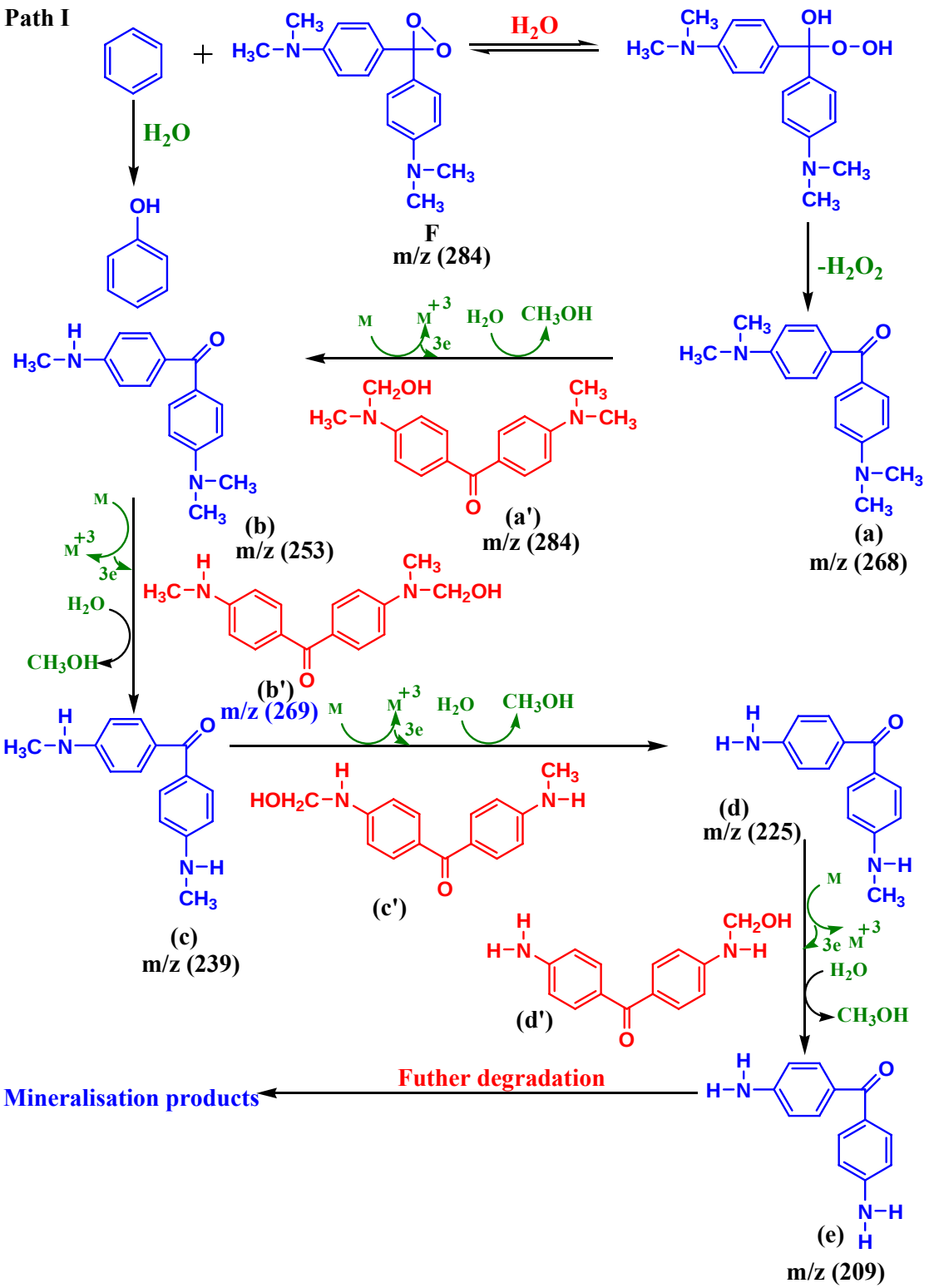

Figure 4.2.19. Destruction of TMDBP derivatives based on different intermediates identified by mass analysis.

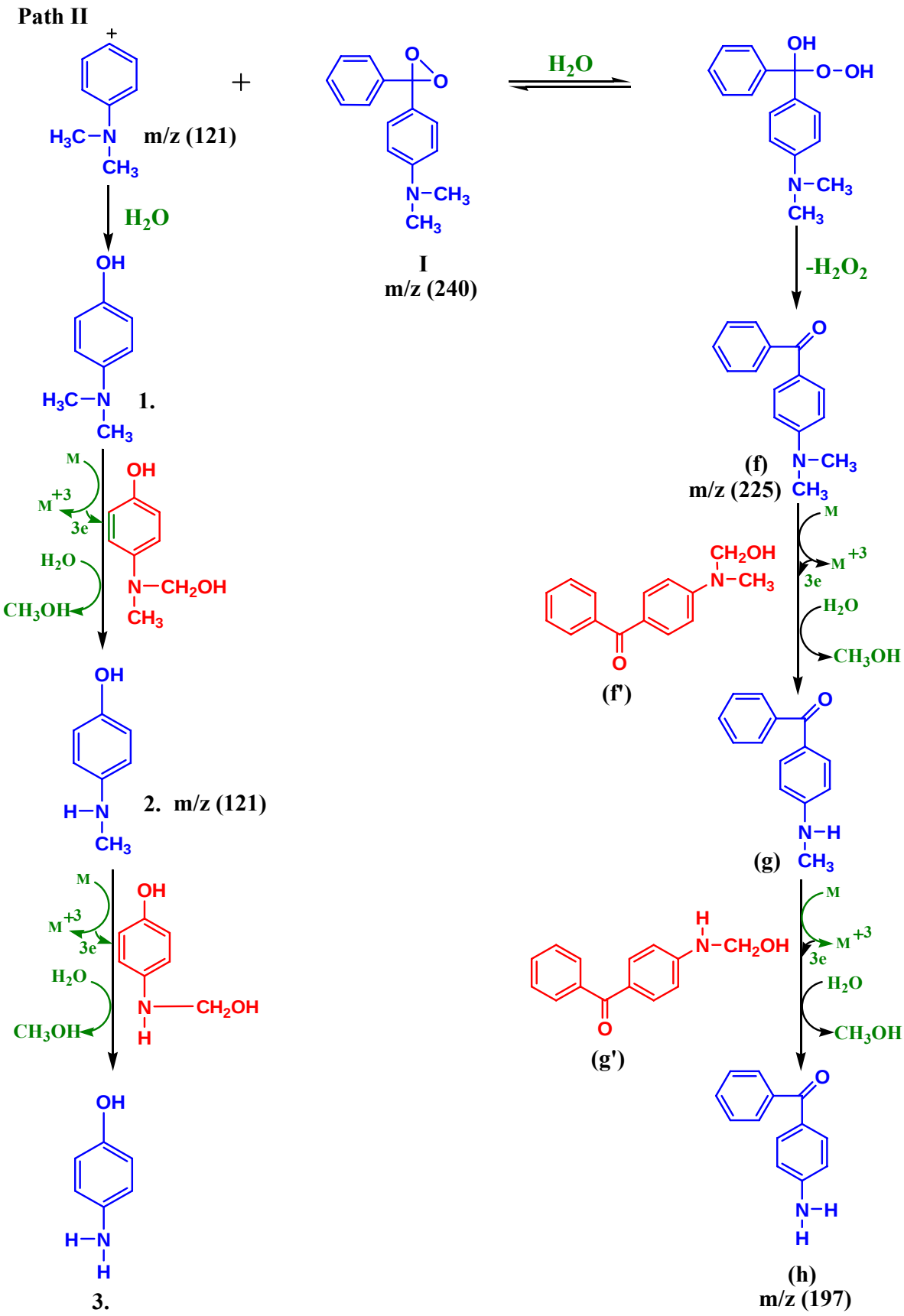

Figure 4.2.20. N–demethylation pathway of DADE derivatives based on different intermediates identified by mass analysis.

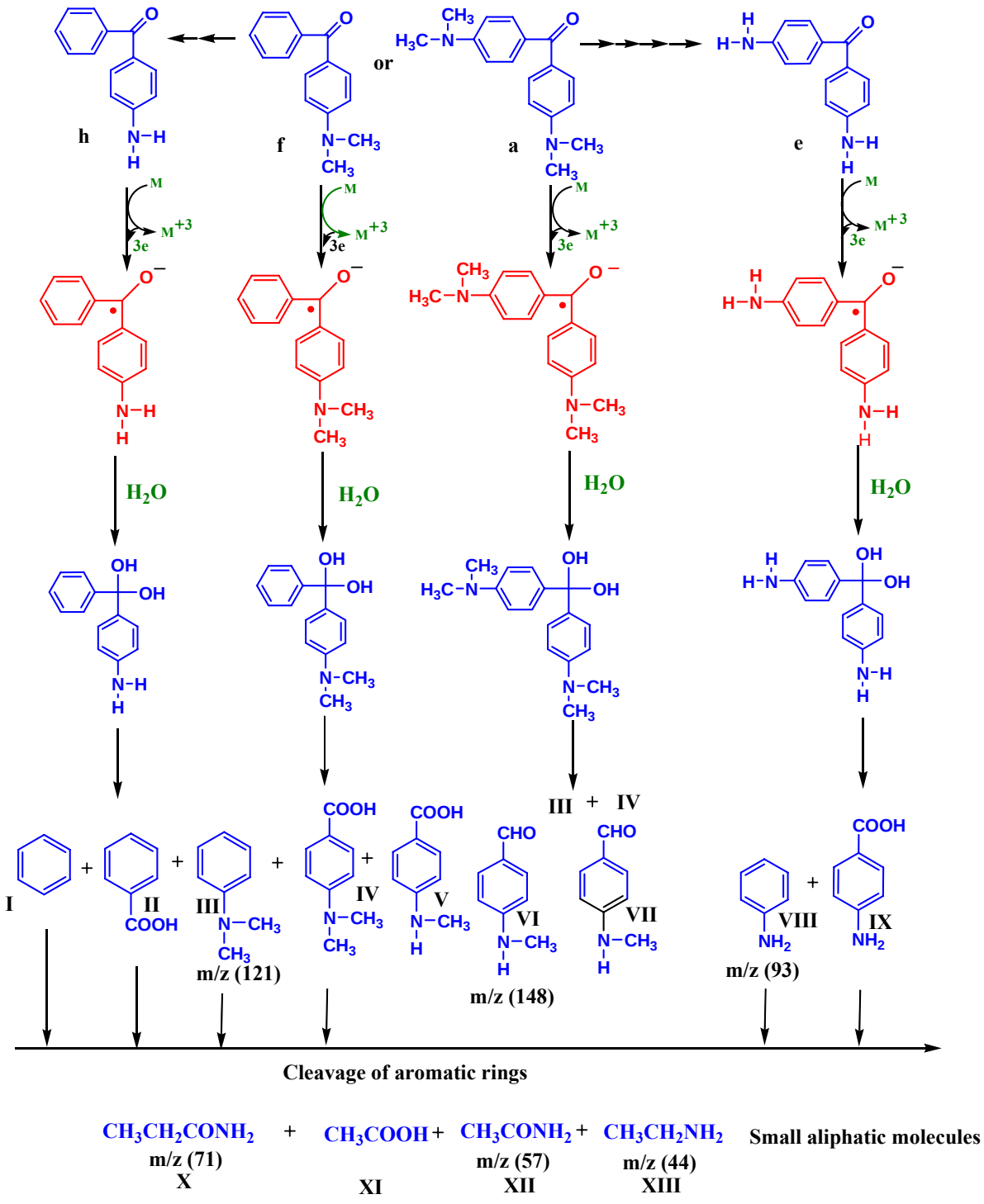

Figure 4.2.21. Successive pathway of mineralization formation into small molecules based on different intermediates identified by mass analysis.

4.3. ELECTROCHEMICAL TREATMENT OF DYE BEARING EFFLUENT

Local dyers in small towns produce huge amount textile printing DBE during dying of textiles, woollens, etc. in small dye bath, and discharge them without any treatment to open channels. The main aim of the present study was to perform EC treatment of DBE using aluminum (Al) and stainless steel (SS) electrodes in various anode-cathode combinations in a batch EC reactor. The effect of j, pH_o, electrode material and treatment time has been studied on the removal efficiency in terms of color, COD, TOC and turbidity. Energy consumption (ENC) and metal ion dissolution or electrode consumption (ELC) has also been estimated during the treatment. DBE removal mechanism has also been justified via zeta potential study and PSD study at different pH_o values. Physio-chemical analysis of sludge has also been studied for understanding the removal mechanism of DBE. Thermo-degradation analysis and pore size distribution of residues were determined for proposing their potential further application.

4.3.1. Characteristic of DBE wastewater

The main characteristics of the DBE obtained from local dye bath/textile printers in Roorkee, India are given in Table 4.3.1.

Table 4.3.1.Characteristic of DBE before and after EC treatment with different combination of electrodes at optimum conditions.

Parameters	Before treatment	After treatment			
		SS/SS (%)	SS/Al (%)	Al/Al (%)	Al/SS (%)
COD (mg/L)	4890	82.50	70.40	68.62	56.65
Color (Pt-Co unit)	397000	99.0	94.50	96.35	88.5
Conductivity (µm)	6.42	0.82	0.98	1.24	1.63
Total solid (g/L)	13.65	0.32	1.35	4.13	6.78
Total suspended solid (TSS) (g/L)	2.86	0.18	0.35	0.63	1.08
pH	9.98	11.89	12.56	8.2	8.9
Na (g/L)	1.2	0.28	-	0.34	-
Cl (g/L)	9.6	0.38	-	0.68	-

4.3.2. EC mechanism with aluminum and stainless steel metal electrodes

The main reactions occurring during the EC are as follows [Daneshvar et al., 2006; Lakshmanan et al., 2009; Kobya et al., 2013]:

4.3.2.1. Anode Reactions

4.3.2.1.1. Al/Al and Al/SS combinations

$$Al(s) \xrightarrow[3e^-]{\text{Oxidation}} \underset{E_o(1.66)\ V}{Al^{+3}\ (aq)} \xrightarrow[nH_2O]{\text{hydrolysis}} Al(H_2O)_n^{(3-n)} \qquad (4.3.1)$$

4.3.2.1.2. SS/SS and SS/Al combinations

$$Fe(s) \xrightarrow[2e^-]{\text{Oxidation}} \underset{E_o(0.44)\ V}{Fe^{+2}\ (aq)} \xrightarrow{\text{hydrolysis}} Fe(OH)_2(aq) \qquad (4.3.2)$$

$$Fe(s) \xrightarrow[3e^-]{\text{Oxidation}} \underset{E_o(0.44)\ V}{Fe^{+2}(aq)} \xrightarrow{\text{hydrolysis}} \underset{E_o(-0.771)\ V}{Fe^{+3}(aq)} \longrightarrow Fe(OH)_3\ (aq) \qquad (4.3.3)$$

$$Fe(s) \xrightarrow[3e^-]{\text{Oxidation}} \underset{E_o(0.37)\ V}{Fe^{+3}(aq)} \xrightarrow{\text{hydrolysis}} Fe(OH)_3\ (aq) \qquad (4.3.4)$$

4.3.2.2. Cathode Reactions

$$2H_2O \xrightarrow{2e^-} H_2 + 2H\bar{O} \qquad (4.3.5)$$

$$H_2O \xrightarrow{3e^-} 3/2\ H_2 + 3H\bar{O} \qquad (4.3.6)$$

Concentration of ferrous and ferric ion generation and their concentration depends on pH and DO during iron electro-coagulation. Generated Fe^{2+} decrease with an increase in pH and DO concentration due to rapid oxidation of Fe^{2+} to Fe^{3+} [Lakshmanan et al., 2009].

4.3.2.3. Secondary Reactions

Sodium chloride is used as an electrolyte and chloride anions get generated during the EC treatments which oxidize into Cl_2 (g) by following reaction [Akbal and Kuleyin 2011; Yuksel et al., 2013]:

$$2\ Cl^- + 2\ e^- \rightarrow Cl_2 \qquad (4.3.7)$$

Chlorine gas (Cl_2) hydrolyzes in water according to the following reaction to form hypochlorous acid (HOCl) [Deborde et al., 2008]:

$$Cl_2 + H_2O \leftrightarrow HOCl + Cl^- + H^+ \qquad (4.3.8)$$

Hypochlorous acid is a weak acid which dissociates in aqueous solution to form ClO^-:

$$HOCl \leftrightarrow ClO^- + H^+ \quad (4.3.9)$$

Thus chlorine, depending on the pH, forms various chlorine species (Cl_2, HOCl and ClO^-) in the EC reactor. Hypochlorous acid and hypochlorite are the main chlorine species present in water in the pH range 6–9. These species can indirectly oxidise the organic material present in the DBE. Since, Cl_2 hydrolysis is almost complete at pH<4, therefore, it can usually be neglected under typical drinking water treatment conditions (pH 6-9). In addition to these major chlorine species, other chlorine intermediates, including trichloride (Cl_3^-), chlorine hemioxide (Cl_2O), and H_2OCl^+ species may also get produced in the wastewater depending upon pH [Arotsky and Symons1962]. ClO^-, which is dominating at higher pH, has been reported as better oxidant among all chlorine species [Deborde et al., 2008; Cherney et al., 2006]. Other secondary reactions such as direct oxidation of dye molecules in presence of SO_4^{2-} (strong oxidant) may also occur if anodic potential is sufficiently higher.

4.3.2.4. EC treatment mechanism

Generally EC process performance depends upon the chemistry of wastewater especially in terms of conductivity and particle size, pH and chemical constituent. The treatment in EC process involved three main mechanisms with Al and SS electrodes: (a) electrode surfaces reactions of electrolyte; (b) coagulants formation in solution phase; (c) pollutants forming soluble colloidal suspension get adsorbed on the coagulants and get removed by flotation or sedimentation.

Different monomeric, polymeric and ionic species play crucial role in the removal efficiency. The interaction rate between dye molecules and hydrolysis products depends upon the pH and ions present in the colloidal suspension. At the same time, zeta potential measurements give the support on the same type of interaction in terms of zero point charge (zpc) in the treatment solution [Sharp et al., 2006; Verma et al., 2011; Singh et al., 2013b]. In the literature, two main interaction mechanisms of precipitation and adsorption have been suggested for separate pH range for both electrodes combination [Kobya et al., 2006a; Lakshmanan et al., 2009]. At low pH (<6.0 and <8.0 for Al and Fe, respectively), flocculation reactions can be explained [Kobya et al., 2006a,b]. At high pH (>6.0 and >8.0 for Al and Fe, respectively), adsorption mechanism can be explained [Rajkumar et al., 2003; Ahlawat et al., 2008; Singh et al., 2013b].

4.3.2.4.1. Precipitation and flocculation/flotation mechanism

Dye + monomeric Al/Fe → (dye monomeric Al/Fe)(s) (pH <6.0 and <8.0 for Al/Fe) (4.3.10)

Dye + polymeric Al/Fe → (dye polymeric Al/Fe)(s) (pH <6.0 and <8.0 for Al/Fe) (4.3.11)

4.3.2.4.2. Adsorption

Dye + $Al(OH)_3/Fe(OH)_3$ (s) → (particles) (pH >6.0 >8.0 for Al/Fe) (4.3.12)

Dye polymeric Al/Fe)(s) + $Al(OH)_3/Fe(OH)_3$ (s) → (particles) (pH >6.0 >8.0 for Al/Fe) (4.3.13)

4.3.3. Effect of current density

Current density (j) is an important parameter for controlling the electro-dissolution, potential between the pollutant and coagulant particles, interaction between the particles, etc. [Wang et al., 2008]. The effect of j on DBE treatment efficiency during EC treatment was investigated within the range from 39.215 to 156.86 A/m^2 at 9.5 pH and 3.5 mS/cm conductivity of DBE. Figures 4.3.1 and 4.3.2 represent the percentage color and COD removal at different j during EC treatment with four different anode-cathode combinations of electrodes. Color and COD removal increased with an increase in the j value from 39.215 to 156.86 A/m^2 as shown in Figures 4.3.1a, b and 4.3.2a. However, very little change in removal efficiency was obtained with further increase in j beyond 156.86 A/m^2 (Figure 4.3.2b). This may be due to the fact that at appropriate j, sufficient coagulants get generated via anodic dissolution and they interact with OH ions to form respective principates (Equations 4.3.1-4.3.6) so as to remove impurities by the adsorption and flotation (precipitation) mechanism [Cotillas et al., 2013]. For j=117.64 A/m^2 after 120 min of electrolysis, 98.2% color and 64.7% COD removal was obtained with SS–SS, 96.7% and 44.7% with Al–Al, 97.9% and 56.1% with SS–Al, 91.4% and 38.5% with Al–SS electrode combinations. SS–SS and SS–Al electrode combinations gave approximately 82% COD and 99.8% color removal after 150 min of electrolysis at 117.4 A/m^2. TOC and turbidity removal efficiencies at different j values with various combinations of electrodes are reported in Figures 4.3.3a and 4.3.3b. 68.4% TOC and 98.5% turbidity was removed at optimum j with SS–SS electrode combination after 150 min of electrolysis. For 150 min treatment time, increase in j had no effect on removal efficiency. Therefore, 150 min of electrolysis was sufficient at j=117.64 A/m^2 at which 68% TOC and 99.8% turbidity removal was obtained with SS–SS, 64.25% TOC and 92.35% turbidity removal was obtained with SS–Al, 58.23% TOC and 95.32% turbidity removal was obtained with Al–

Al, and 43.14% TOC and 89.12% turbidity removal was obtained with Al–SS electrode combination.

Zeta potential measurement at different j values with different electrode combinations at different electrolysis time help to understand the treatment mechanism by EC process. Original DBE was found to have pH≈9.5 and zeta potential≈ -28.6 mV. It may be seen in Figures 4.3.4 and 4.3.5 that the actual value of zeta potential changes from more negative value (-28.6 mV) to less negative or positive value for EC treatment of DBE with all anode-cathode combinations. Comparison of zeta potential values obtained after 150 min of treatment show that the zeta potential values are higher (i.e. less negative or positive value) for higher j value. Treated DBE was found to have zeta potential -6.1 mV for Al–Al, -1.2 mV for Al–SS, 5.2 mV for SS–SS and 3.6 mV for SS–Al combination after 150 min of electrolysis time. These results show that the metal cationic species increase with an increase the j value and interact with negatively charged impurities [Akbal and Camcl, 2012].

Comparison of the result for j=117.16 and 156.86 A/m^2 in Figures 1c, 1d, 2c and 2d shows that the color and COD removal efficiencies and the value of zeta potential at t=150 min follow the following order for various anode-cathode combinations:

SS–SS > SS–Al > Al–Al > Al–SS

Above results show that the higher value of j produces higher amount of metallic cationic species which in turn increased color and COD removal efficiencies because of which zeta potential of the treated DBE moves toward positive value. Also, EC equivalent masses of iron (17.37 mg/A min) is almost three times higher than that of aluminum (5.59 mg/A min) i.e. the SS electrode produces more iron coagulants than aluminum when same amount of electric charge is passed through these electrodes [Kobya et al., 2014]. Therefore, SS-Al and SS-SS systems have higher treatment efficiencies than Al-Al and Al-SS systems. It may be noted that the effect of j was studied at pH≈9.5 where aluminum exist in form of $Al(OH)_4^-$ ions and Fe exists in the form of $Fe(OH)_4^-$ ions. It may also be noted that the DBE itself contains very high amount of chloride. During EC process, chlorine gas gets generated at anode (via reaction 4.3.7) and forms other chlorine species (HOCl and ClO^-) depending upon pH via reactions 4.3.8 and 4.3.9. At high pH> 9, ClO^- (formed via reaction 4.3.9) is the dominating among all chlorine species has very high oxidation potential. It helps in the treatment of DBE at high pH by direct oxidation [Thakur et al., 2009].

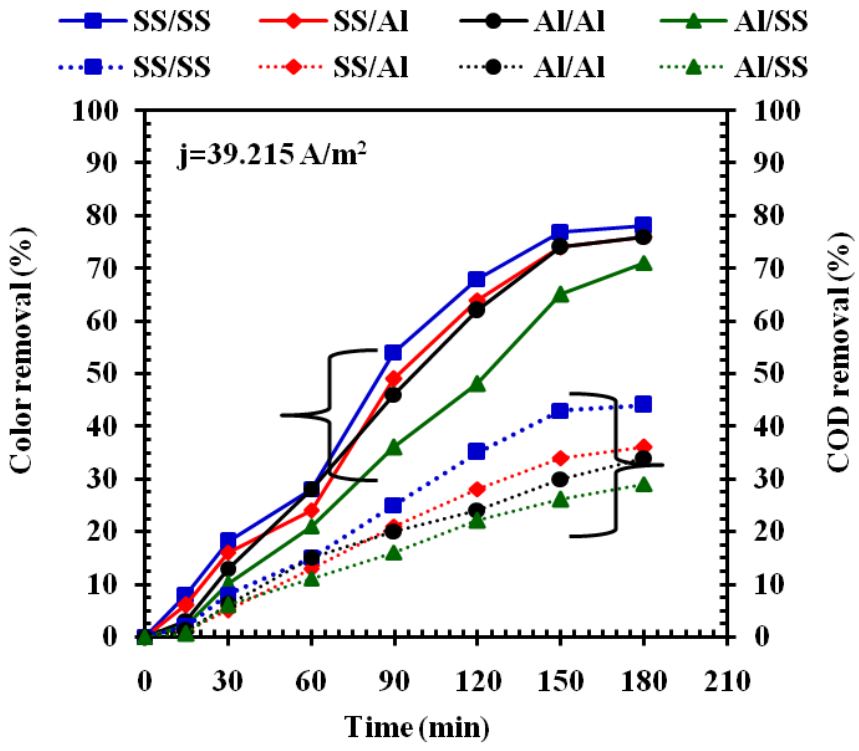

(a)

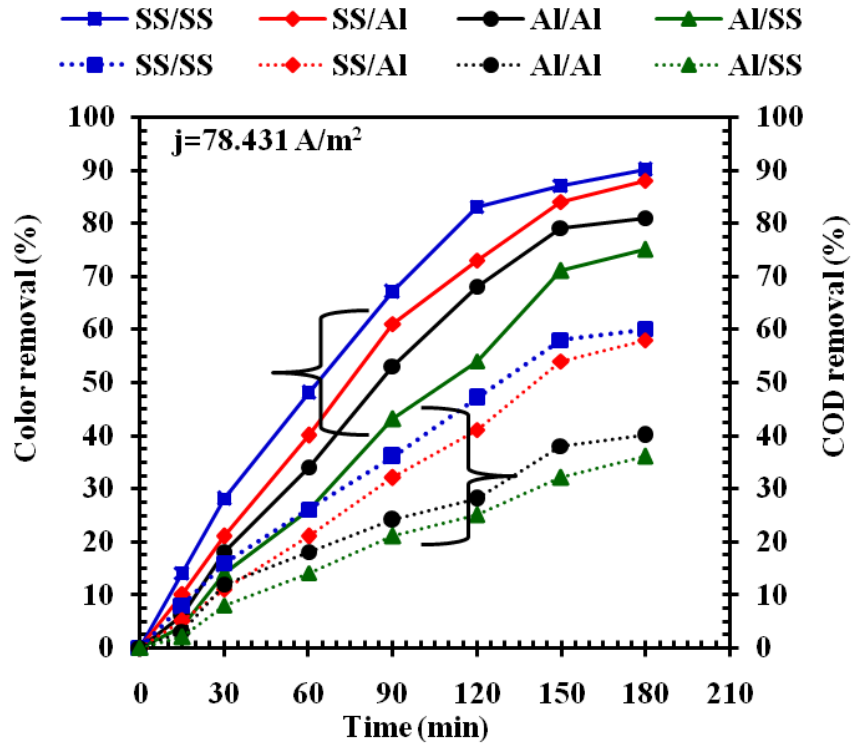

(b)

Figure 4.3.1. Effect of current density (j=39.215 and j=78.431 A/m^2) and time on color and COD removal for different anode-cathode combinations.

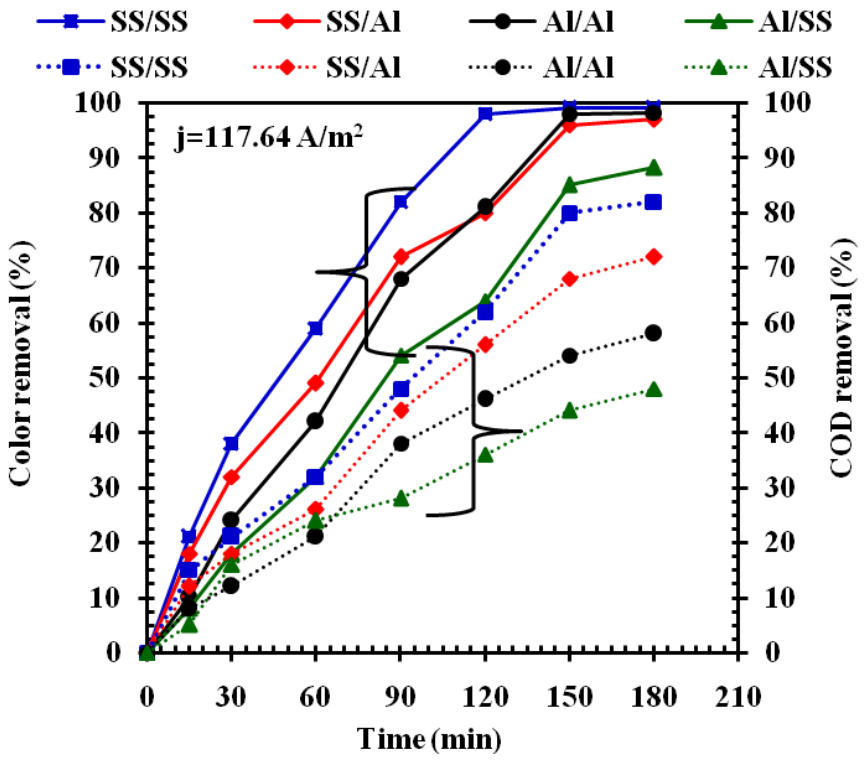

(a)

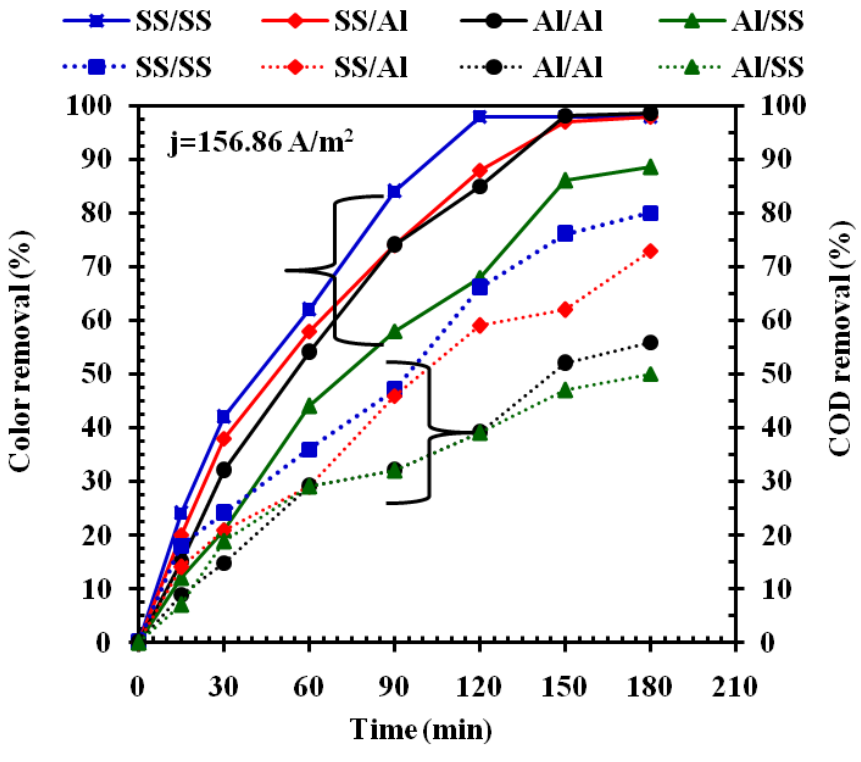

(b)

Figure 4.3.2. Effect of current density (j=117.64 and j=156.86 A/m^2) and time on color and COD removal for different anode-cathode combinations.

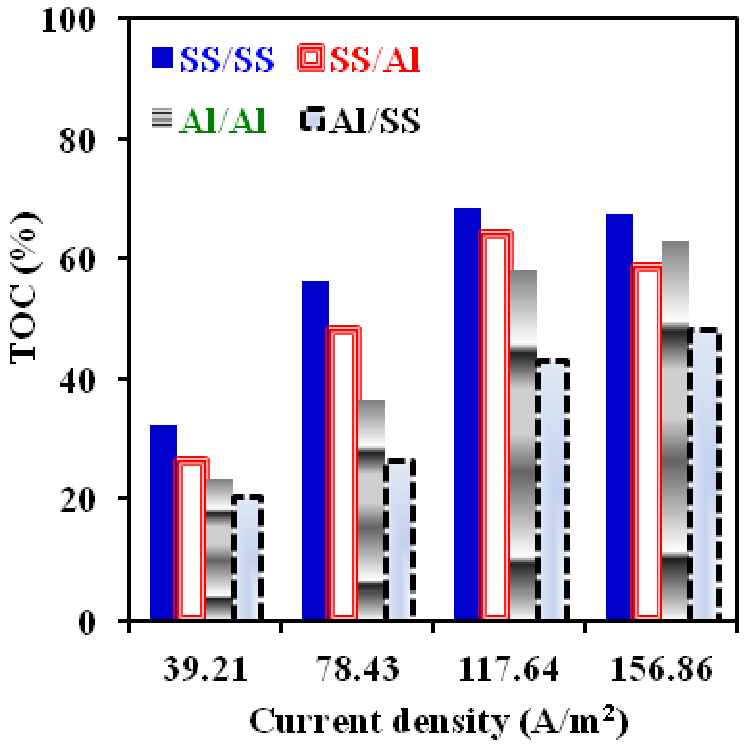

(a)

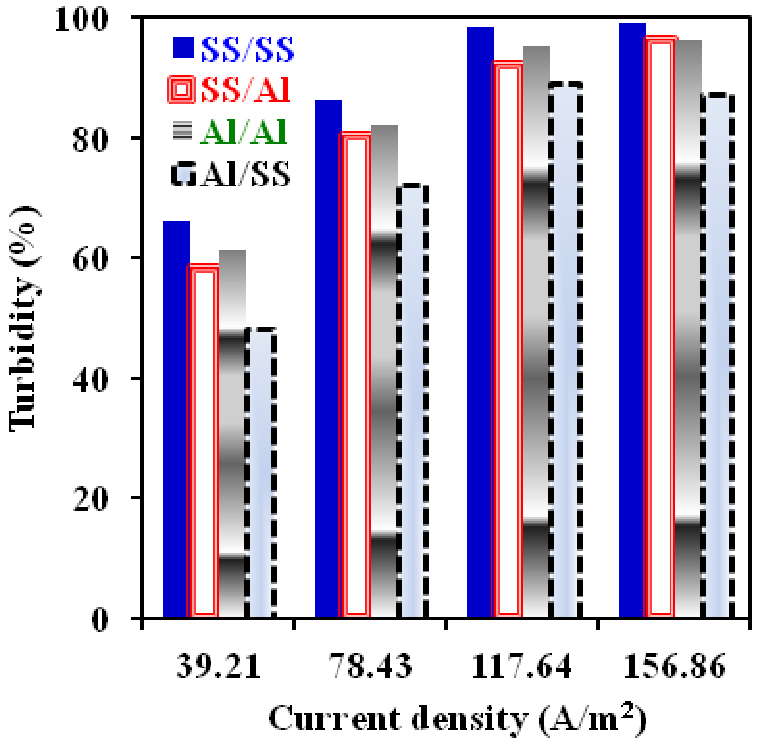

(b)

Figure 4.3.3. Effect of current density on (a) TOC removal and (b) turbidity removal with various anode-cathode combinations at t=150 min and pH=9.5.

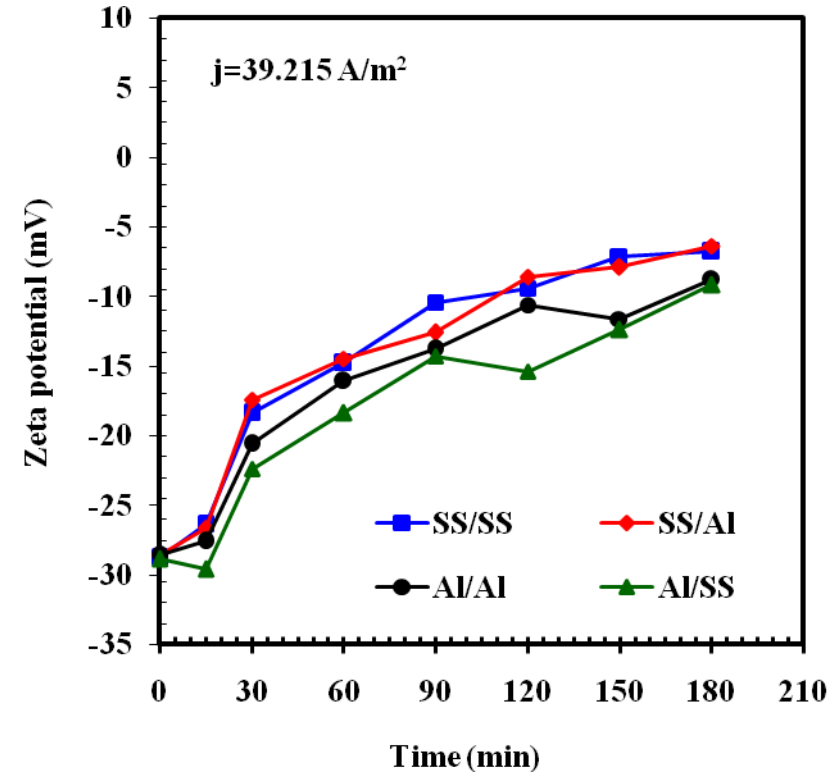

(a)

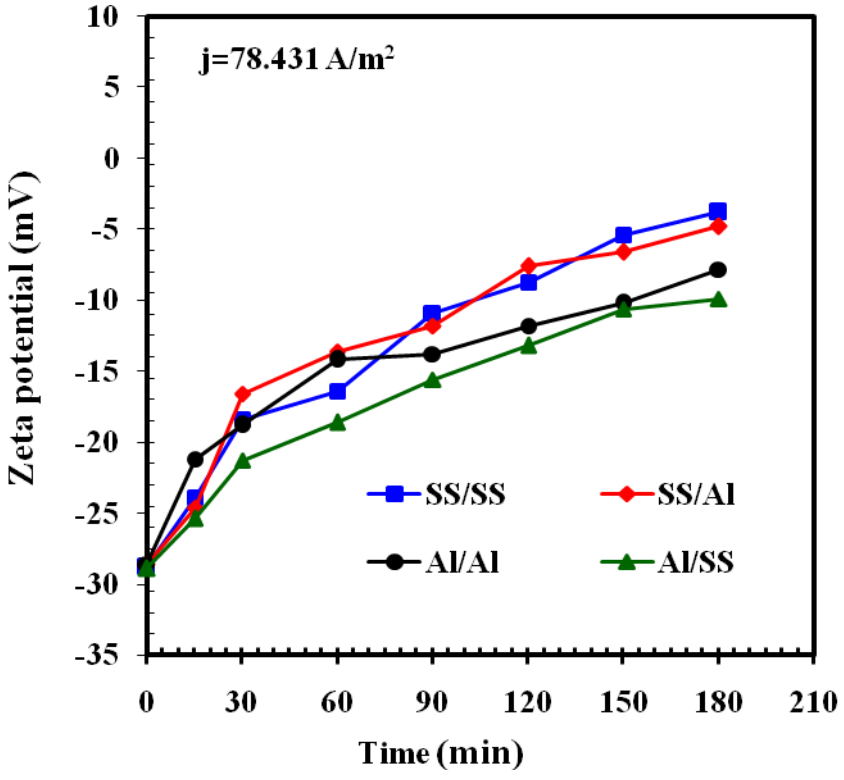

(b)

Figure 4.3.4. Effect of current density (j=39.215 and j=78.431 A/m^2) and time on zeta potential for different anode-cathode combinations.

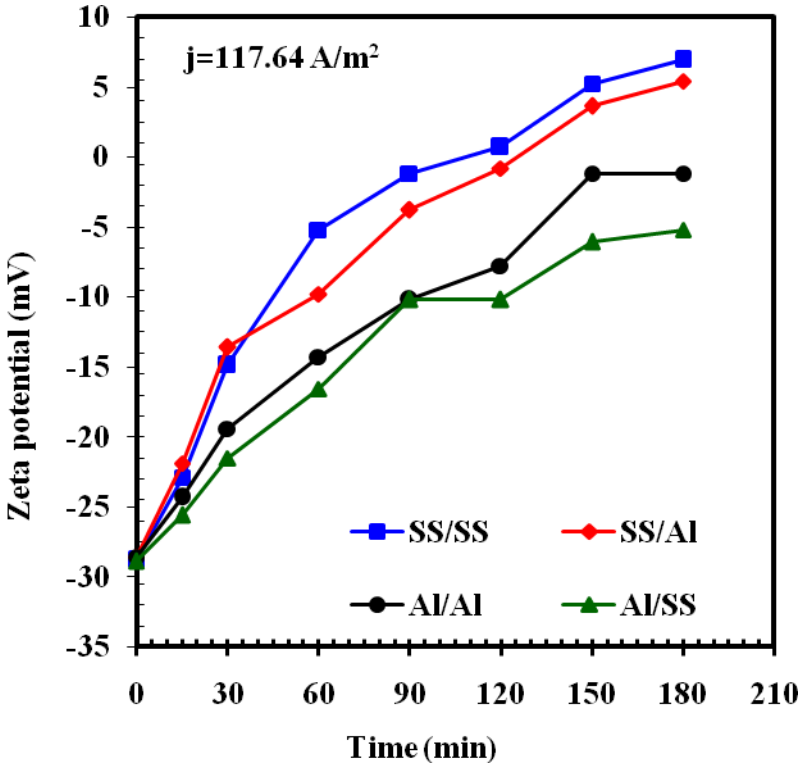

(a)

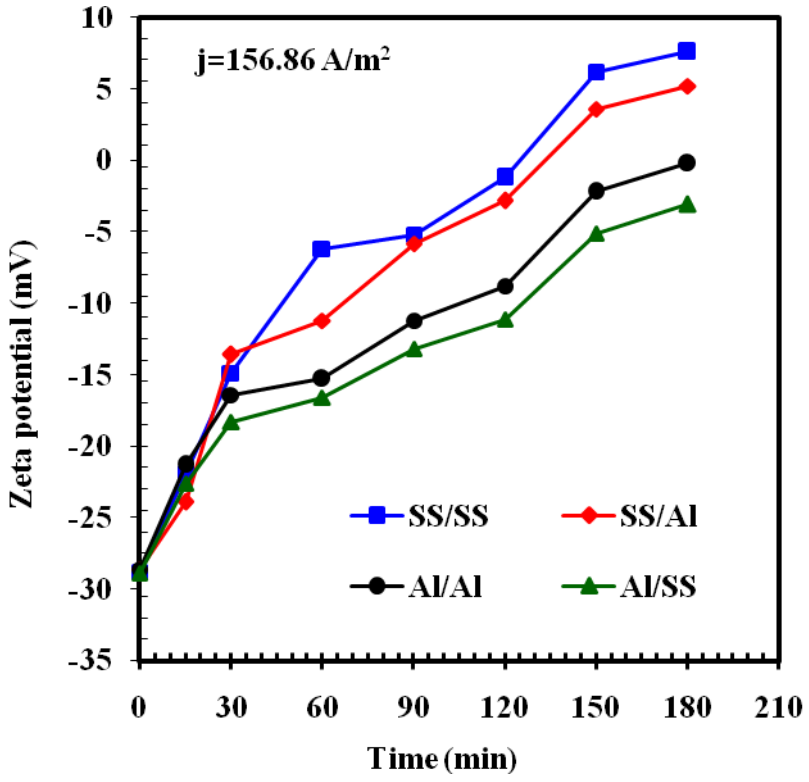

(b)

Figure 4.3.5. Effect of current density (j=117.64 and j=156.86 A/m^2) and time on zeta potential for different anode-cathode combinations.

Figures 4.3.6a,b variation of SEC and CE with j for various anode-cathode combinations. After 150 min of treatment and for j=117.64 A/m^2, SEC values were found to be 4.71 and 4.24 kWh/kg COD for SS-SS and SS–Al, 3.84 and 3.35 kWh/kg COD for Al–Al and Al-SS, respectively. Generally, CE values were ≥100% i.e. ELC_e were found to be higher than ELC_t in the present study indicating insignificant passivation of electrodes. Higher amount of electrode consumption as compared to theoretical amount may be because of dessoultion of cathodic electrode materials at high (>9.5) solution pH and high current densities [Banerjee et al., 1999; Kobya et al., 2014]. Also the hole and pit formation on the surface of electrode referred to as corrosion pitting also causes higher metallic loss on the electrode surface. This mass loss also gets calculated as the metal dissolved by the electro-chemical process and increases the CE values [Singh et al., 2014]. Overall SS–SS electrode combination was found to have highest removal efficiencies (99.8% color, 82.4% COD, 68.5% TOC and 96% turbidity removal) for j=117.64 A/m^2 at 150 min treatment time. Corresponding SEC value with SS–SS combination was 4.71 kWh/kg COD.

Considering electrocoagulation as the surface process, the degradation kinetics can be represented in term of heterogeneous rate constant (k_h) by the following equation:

$$r = -\left(\frac{V}{A_e}\right)\frac{d[COD]}{dt} = k_h[COD] \qquad (4.3.14)$$

Also inside the batch electrocoagulation reactor, the COD removal rate is proportional to the concentration of the organic pollutant and the amount of corresponding hydroxides formed [Mohan et al., 2002; Balasubramanian et al., 2009]. Since the generation of ferric and aluminum hydroxide can be assumed constant for a given current density, therefore, the kinetics for COD removal can be represented by the pseudo first-order kinetic model as:

$$-\frac{d[COD]}{dt} = k[COD] \qquad (4.3.15)$$

Where, k the pseudo first-order reaction rate constant (min^{-1}) and is related to k_h by the following equation:

$$k_h = k\left(V/A_e\right) \qquad (4.3.16)$$

Rearranging equation (17) and integrating the equation gives:

$$COD_t = COD_o e^{-kt} = COD_o e^{-k_h\left(A_e/V\right)t} \qquad (4.3.17)$$

Values of k and k_h were determined from ln(COD/COD$_o$) versus time plots (Figures 4.3.7 and 4.3.8) at various j values. The rate constants (k and k_h) and R^2 values for COD removal for various anode-cathode combinations at various j values are given in Table 4.3.2. It may be observed that k values increase with increase in j values. Also, values of k are much higher for SS electrodes than for Al electrodes indicating higher COD removal rate for SS electrodes.

Table 4.3.2. Values of pseudo-first order rate constant (k) and correlation coefficient (R^2) for COD removal at various current densities.

Anode-cathode combination	Current density (j=A/m^2)			
	39.21	**78.43**	**117.64**	**156.86**
	Pseudo-first order rate constant (k), min^{-1}			
SS/SS	3.6×10^{-3}	5.3×10^{-3}	9.0×10^{-3}	9.8×10^{-3}
SS/Al	2.7×10^{-3}	5.0×10^{-3}	6.9×10^{-3}	7.3×10^{-3}
Al/Al	2.1×10^{-3}	5.0×10^{-3}	3.0×10^{-3}	4.5×10^{-3}
Al/SS	2.0×10^{-3}	2.5×10^{-3}	3.6×10^{-3}	3.8×10^{-3}
	Heterogeneous rate constant (k_h), cm/s			
SS/SS	6.65×10^{-4}	4.97×10^{-4}	1.66×10^{-3}	1.81×10^{-3}
SS/Al	4.99×10^{-4}	9.23×10^{-4}	1.27×10^{-3}	1.36×10^{-3}
Al/Al	3.9×10^{-4}	9.23×10^{-4}	5.54×10^{-4}	8.31×10^{-4}
Al/SS	3.69×10^{-4}	4.62×10^{-4}	6.65×10^{-4}	7.02×10^{-4}
	Correlation coefficient (R^2)			
SS/SS	0.98	0.99	0.98	0.96
SS/Al	0.98	0.98	0.98	0.98
Al/Al	0.98	0.99	0.98	0.98
Al/SS	0.99	0.98	0.98	0.97

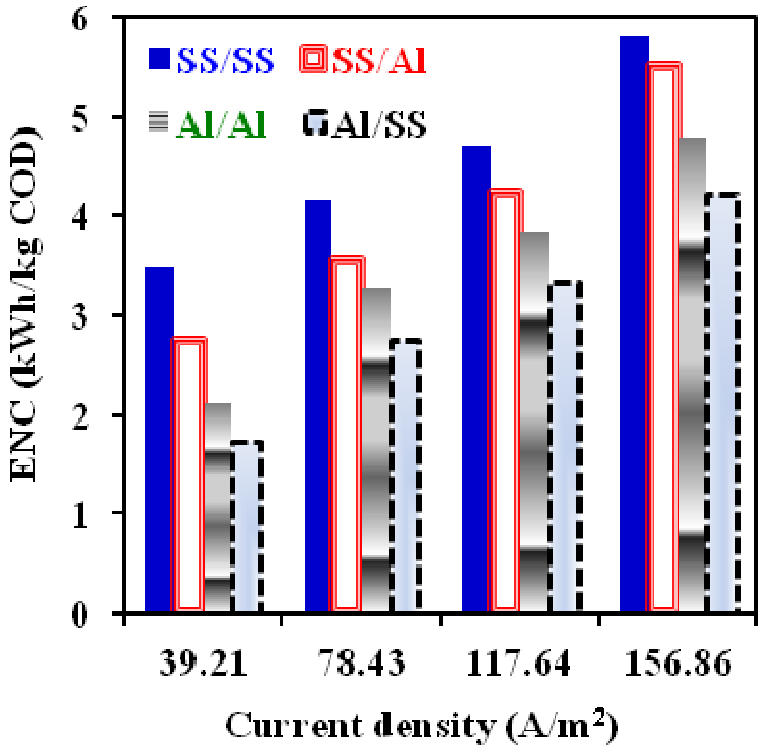

(a)

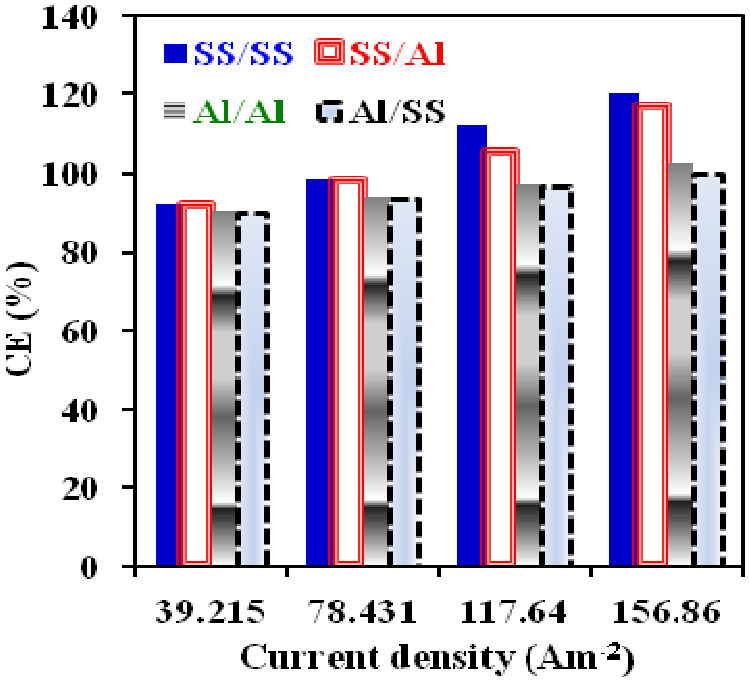

(b)

Figure 4.3.6. Effect of current density on (a) energy consumption (ENC) and (b) electrode consumption (ELC_e) with various anode-cathode combinations at t=150 min and pH=9.5.

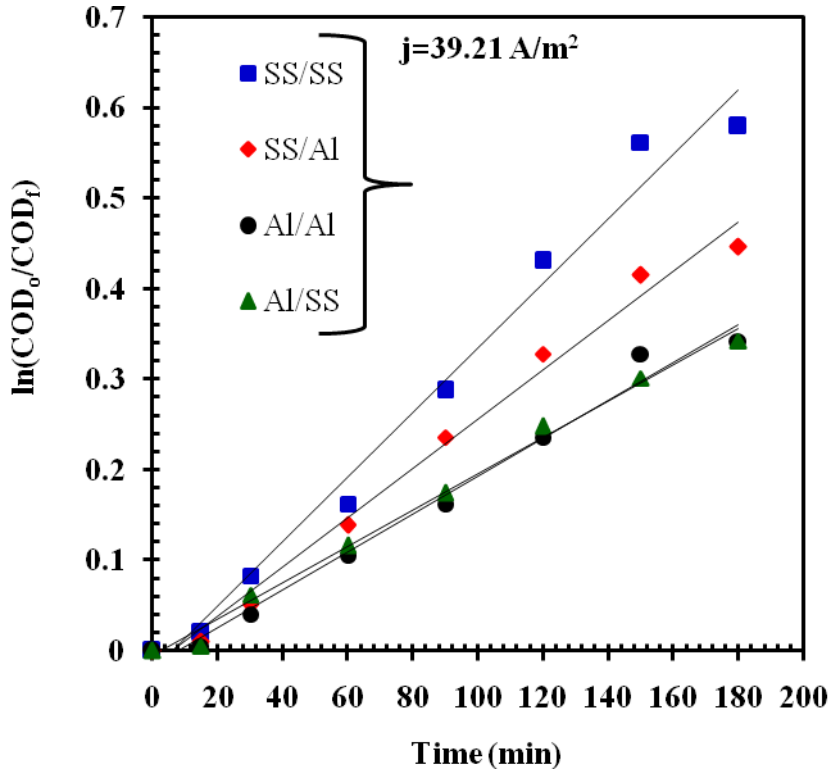

(a)

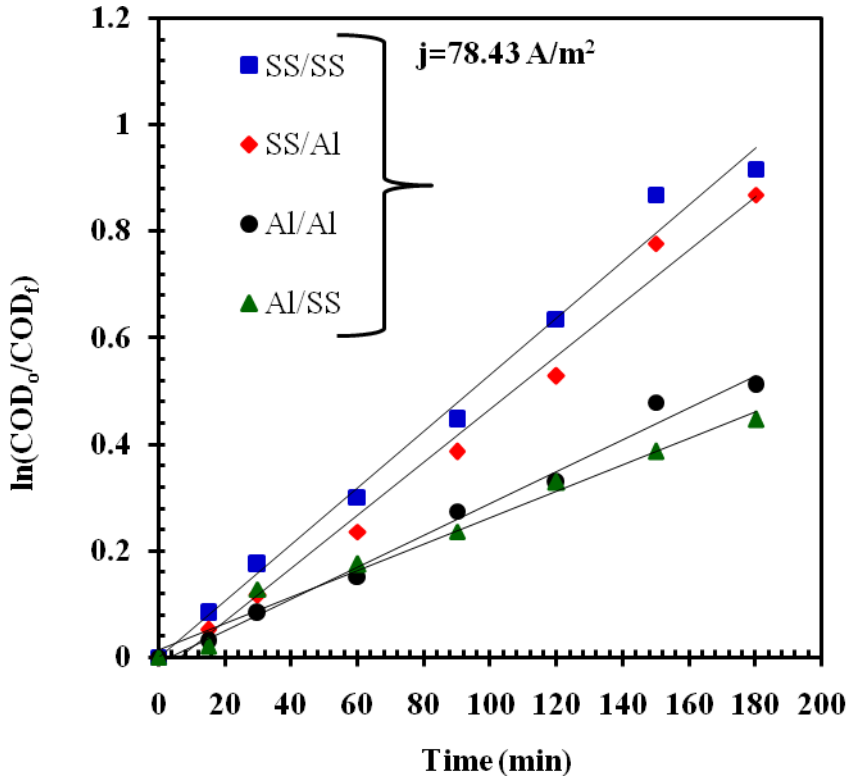

(b)

Figure 4.3.7. Linear pseudo-first-order kinetic plot for COD removal from by different combination of electrodes at different current densities (j=39.21 and 78.43 A/m^2).

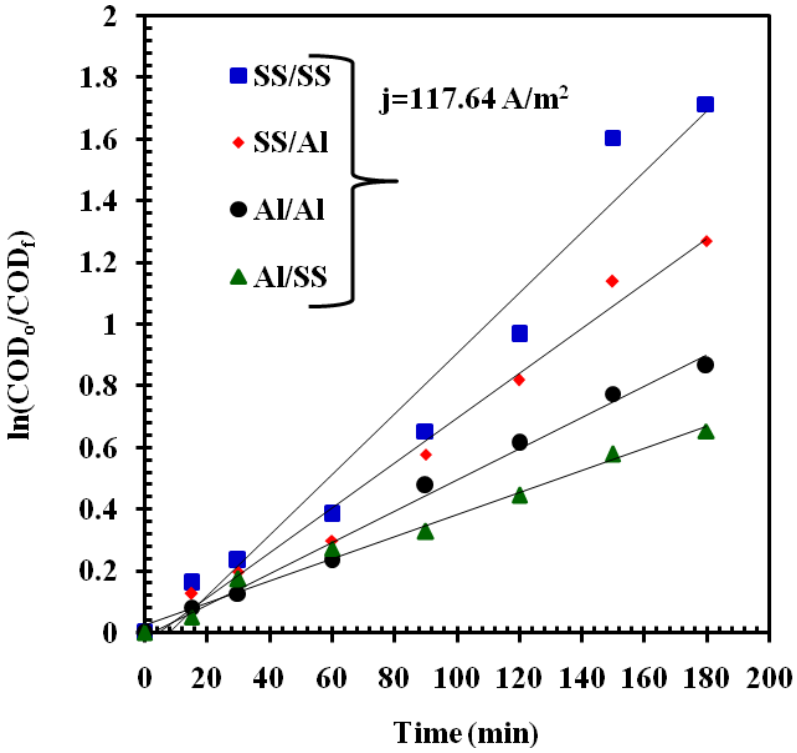

(a)

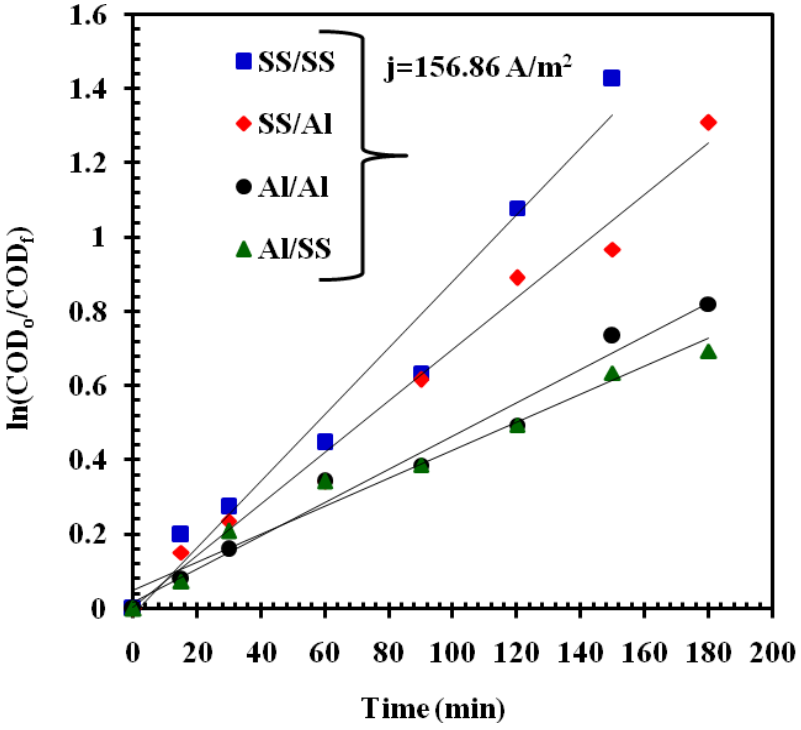

(b)

Figure 4.3.8. Linear pseudo-first-order kinetic plot for COD removal from by different combination of electrodes at different current densities (j=117.64 and 156.86 A/m^2).

4.3.4. Effect of pH

EC process performance and the treatment efficiency are directly influenced by the pH. The effect of pH on various parameters is reported in Figure 4.2.9. Figure 4.2.9a shows the effect of pH on color and COD removal efficiencies with various combinations of electrodes. For Al–Al and Al–SS combinations, COD and color removal efficiencies increased with an increase in pH from 3.5 to 6.5, while for SS–SS and SS–Al combination, COD and color removal efficiencies increased to maximum within the range pH 6.5 to 8.5. Maximum color and COD removal efficiencies were found to be: 95% and 66% for Al–Al, 86% and 52% for Al–SS at pH 6.5, 99% and 82% for SS–SS, 96% and 74% for SS–Al at pH 8.5, respectively. Beyond pH~6.5 and pH~8.5, the removal efficiencies decreased for Al–Al and Al–SS; and SS–SS and SS–Al combinations, respectively (Figure 4.2.9a). Figure 4.2.9b shows the plot between initial and final pH change during the EC treatment at different pH. A marginal increase in pH was found for all anode-cathode combinations.

Untreated DBE effluent has a zeta potential of –28.6 mV. Figures 4.2.10a and 4.2.10b show the value of zeta potential and particle diameter for DBE treated at different pH with various anode-cathode combinations. It may be observed in Figure 4.2.10a that the treated DBE had less negative or positive value of zeta potential for all combinations.

Values of zeta potential of treated DBE increased during the treatment because of the charge neutralization reaction of negative charged colloids species present in the DBE with the positive metal ions released into the solution from various anodes (Figure 4.2.10a).

For Al–Al and Al–SS combination of electrodes, zeta potential was found to be positive in nature at optimum pH value of 6.5. Beyond the optimum pH, zeta potential of decreases for experiments carried out with Al as anode. The increase in color and COD removal was constant and further decreased after increase in pH beyond the optimum pH. For experiments carried out at $2.5 \leq pH \leq 6.5$, an increase in pH increases the cationic species (Al^{3+} and $Al(OH)^{2+}$) which increase the color and COD removal efficiencies. In case of Al as anode, for pH >6.5, aluminum exist in form of $Al(OH)_4^-$ ions. This reduces the color and COD removal efficiencies because of increase in repulsion between the same charge particles in colloidal DBE effluent. Similarly, for pH~8.5, the speciation of SS as anode [Duan and Gregory 2003; Lee et al., 2006] illustrates that various cationic and hydroxide species (Fe^{2+}, Fe^{3+}, $Fe(OH)^{2+}$ and $Fe(OH)_2$ etc.) increase the removal efficiency by the charge neutralization mechanism and sweep coagulation mechanism (Figure 4.2.10a).

Particle size distribution (PSD) of colloids present in DBE was determined by dynamic light scattering (DLS) measurement. It is known that the smaller particles move quickly than the larger particles because of which smaller particles show larger fluctuation in the intensity of scattered light whereas the larger particle give smaller fluctuations [Beckett, and Le 1990; Perret et al., 1994; Gregory et al., 2006]. In EC treatment, the particle size increased with an increase the pH from 2.5 to 8.5 with SS as anode and 6.5 with Al as anode (Figure 4.2.10b). Particle diameters and color and COD removal efficiency follow the following order for various anode-cathode combinations:

SS–SS > SS–Al > Al–Al > Al–SS

At optimum pH, charge neutralization and sweep coagulation by respective hydroxides allow the different particles at come together by van der Waals interaction and adsorption mechanism, respectively. These mechanisms increase the particle size at optimum pH. These particles later on settle to the bottom and cause highest color and COD removal efficiencies (Figures 4.3.9a and 4.3.10b). Thus, floc formation and settling are directly related to particle diameter [Mondel et al., 2012].

Similarly, TOC and turbidity removal percentage at different pH value with various combinations of electrodes are reported in Figure 4.3.11a and Figure 4.3.11b. 68.4% TOC and 98.5% turbidity removal was observed for SS-SS electrode combination after 150 min of electrolysis at pH=8.5. For 150 min treatment time, increase in pH had no effect on removal efficiency. Therefore, 150 min of electrolysis was sufficient at pH=8.5, 68.8% TOC and 98.8% turbidity removal was observed with SS–SS; and 92.25% TOC and 62.65% turbidity was obtained with SS–Al combination. Similarly, 56.23% TOC and 91.32% turbidity removal was observed with Al–Al; and 48.14% TOC and 87.32% turbidity removal was observed with Al–SS electrode combination at optimum pH≈6.5.

Figure 4.3.12 shows variation of ENC and current efficiency (CE) with pH for various anode-cathode combinations. After 150 min of treatment and for pH=8.5, SEC values were found to be 3.81 kWh/(kg COD) and 3.28 kWh/(kg COD) for SS-SS and SS–Al, respectively; and for pH=6.5, ENC values were found to be 3.68 kWh/(kg COD) and 3.51 kWh/(kg COD) for Al–Al and Al-SS, respectively. CE values were found to be higher for SS electrodes as compared to that for Al electrodes. This is due to higher electrochemical equivalent mass of iron as compared to that of aluminum. SEC and CE values increase with an increase in the pH value due to increase in anode dissolution

Overall, at low pH (<6.0 and <8.0 for Al and Fe, respectively), charge neutralization of colloids by monomeric and polymeric cationic species followed by flocculation and

settling or floatation is helping in the treatment process. At pH~6.0 for Al and pH~8.0 for Fe, treatment efficiencies get enhanced by another mechanism where metal hydroxide ($Al(OH)_3$ and $Fe(OH)_3$) remove the colloids by adsorption onto their surface and subsequent settling. At high pH (>9), ClO^- (formed via reaction 4.3.9) removes COD by direct oxidation of the colloidal matter present in DBE.

4.3.5. Surface morphology of sludge

Surface and elemental features of sludge generated with various anode-cathode combinations of electrodes obtained after EC treatment are shown in Figure 4.3.13. Surface of sludge was found to be amorphous in nature with a number of pores (as shown in SEM images). EDX analysis was done so as to find element composition in various anode-cathode combinations sludge [Kushwaha et al., 2010]. Sludge of SS-SS and SS–Al contain 34.28% and 32.15% iron, 20.15% and 19.16% carbon, respectively (Table 4.3.3). Sludge of Al–Al and Al–SS contain 33.29% and 33.21% aluminum, 26.24% and 24.26% carbon, respectively. Thus, the results indicate that SS–SS and Al–Al combination having higher amount of metals as compared to SS–Al and Al–SS combination. Carbon content in SS–SS and Al-SS sludge was found to be higher than the others.

Table 4.3.3. EDX analysis of sludge generated by the EC process with various anode-cathode combinations of electrodes.

Elements	SS-SS	SS–Al	Al–Al	Al–SS
Iron	34.28%	32.15%	-	2.11%
Aluminum	-	1.35%	33.29%	33.21%
Carbon	20.15%	19.16%	26.24%	24.26%
Oxygen	31.58%	31.48%	35.28%	34.05%
Sodium	2.24%	3.13%	2.68%	2.88%
Chlorine	3.92%	3.60%	1.63%	2.53%
Chromium	4.20%	4.15%	-	-
Nickel	4.21	4.18%	-	-

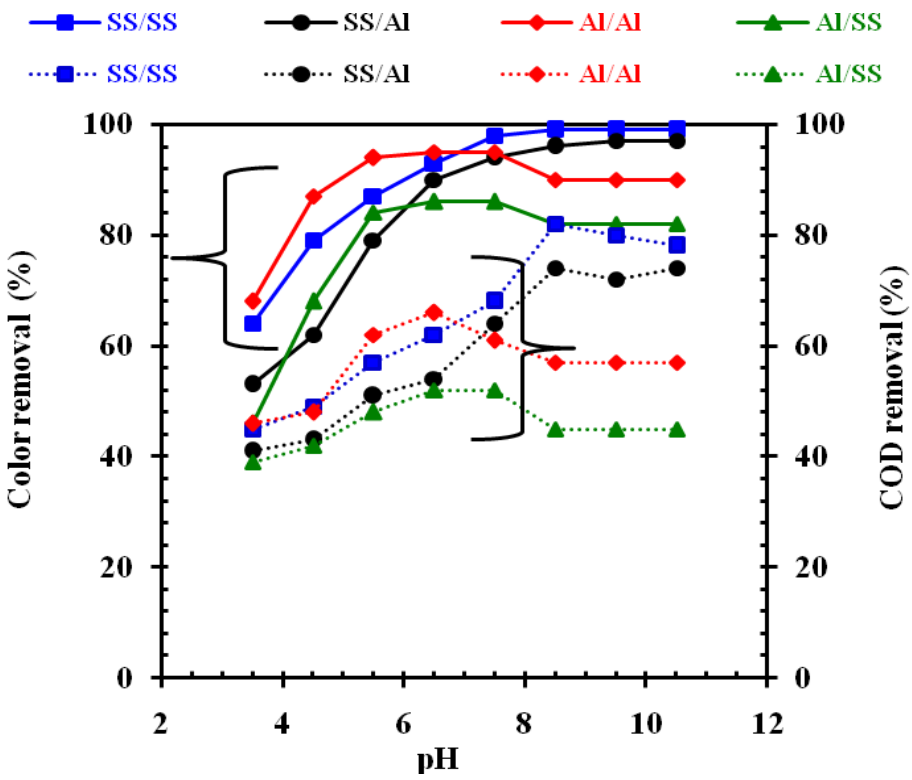

(a)

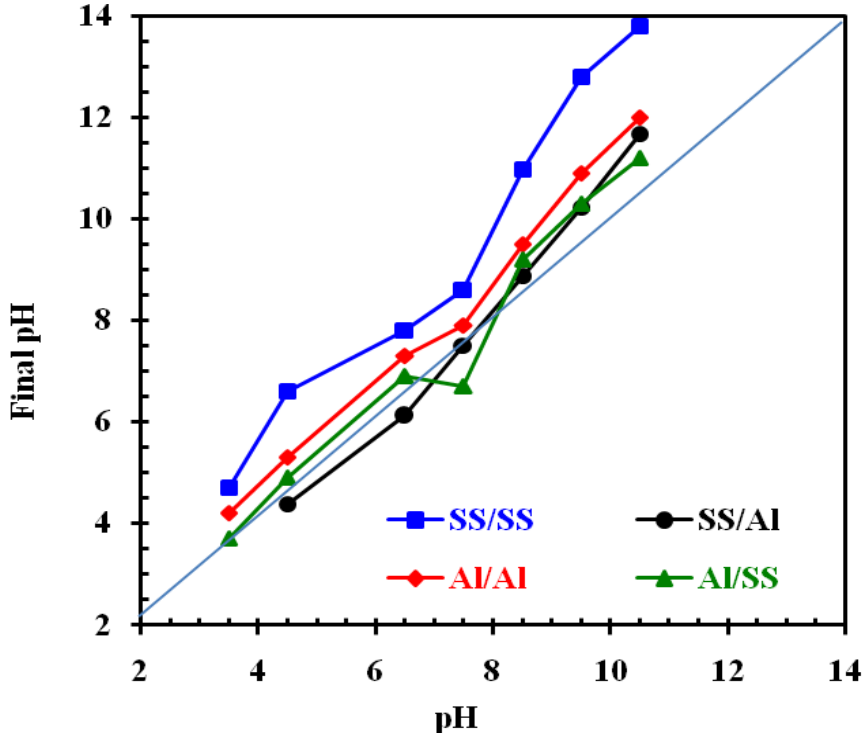

(b)

Figure 4.3.9. Effect of pH on (a) color and COD removal efficiencies, (b) final pH for various anode-cathode electrode combinations at t=150 min and j=117.64A/m^2

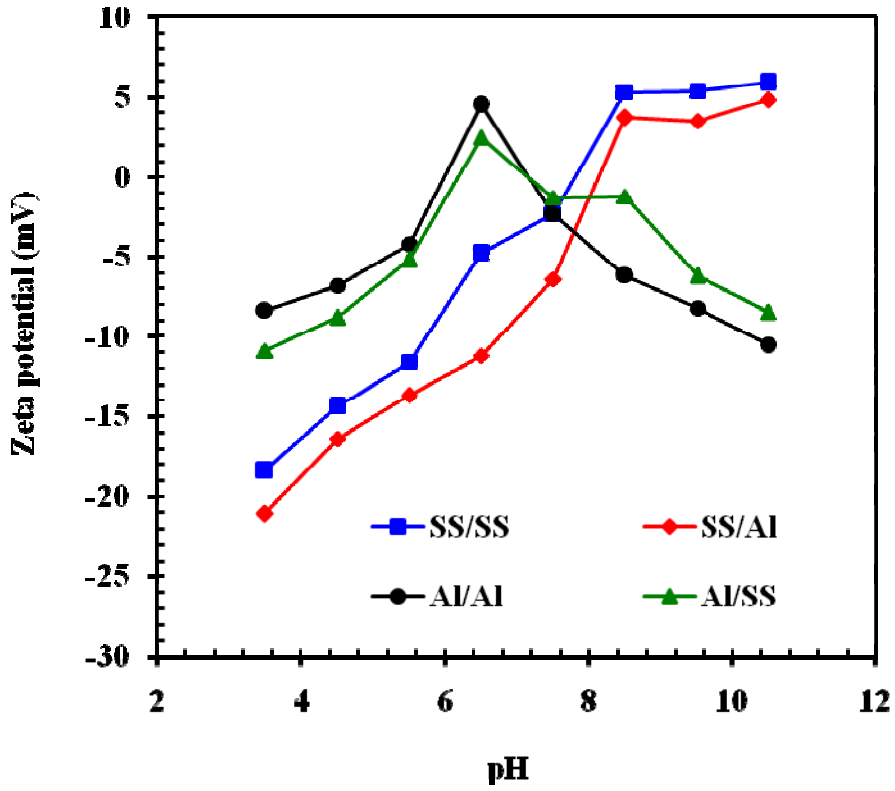

(a)

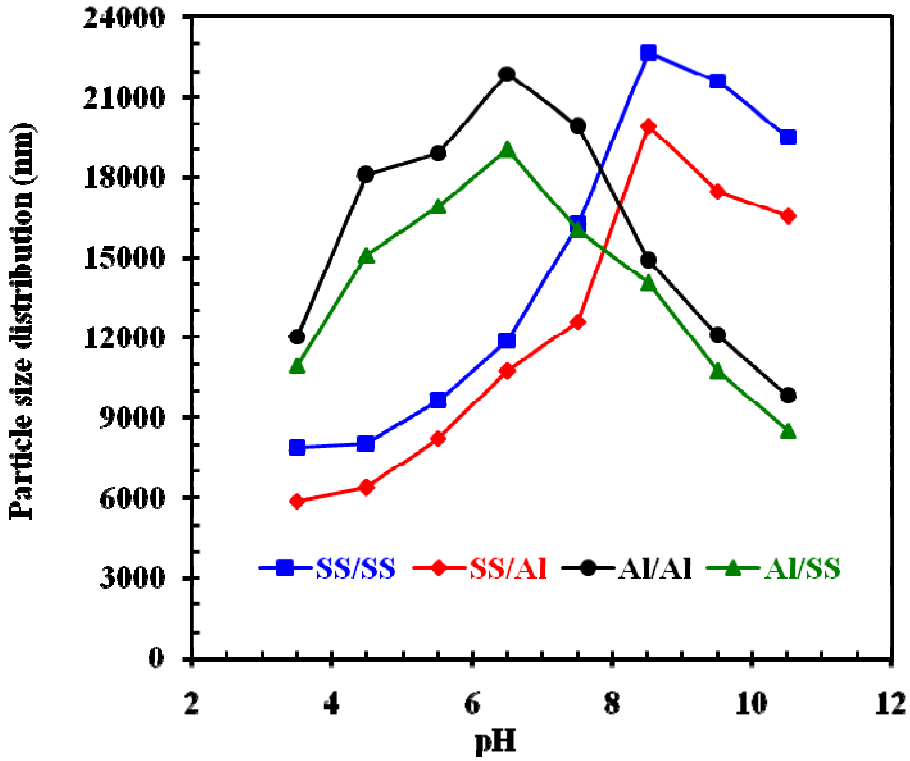

(b)

Figure 4.3.10. Effect of pH on (a) zeta potential and (b) particle diameter for various anode-cathode electrode combinations at t=150 min and j=117.64A/m^2.

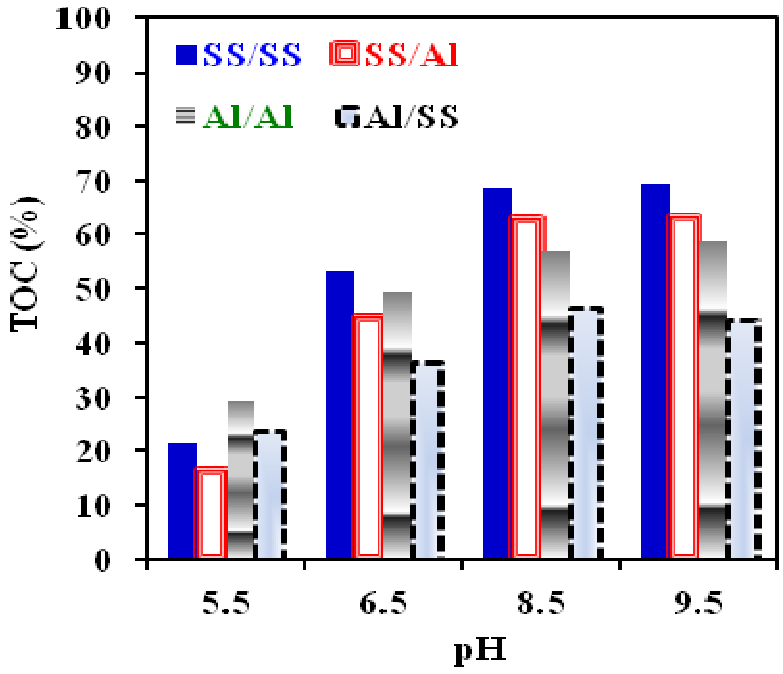

(a)

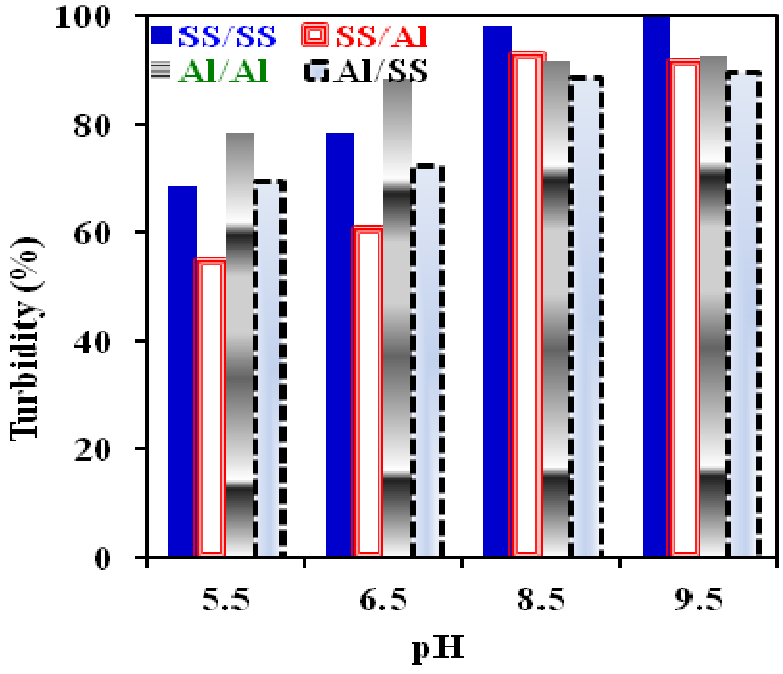

(b)

Figure 4.3.11. Effect of pH on (a) TOC removal, (b) turbidity removal with various anode-cathode combination at t=150 min and j=117.64A/m^2.

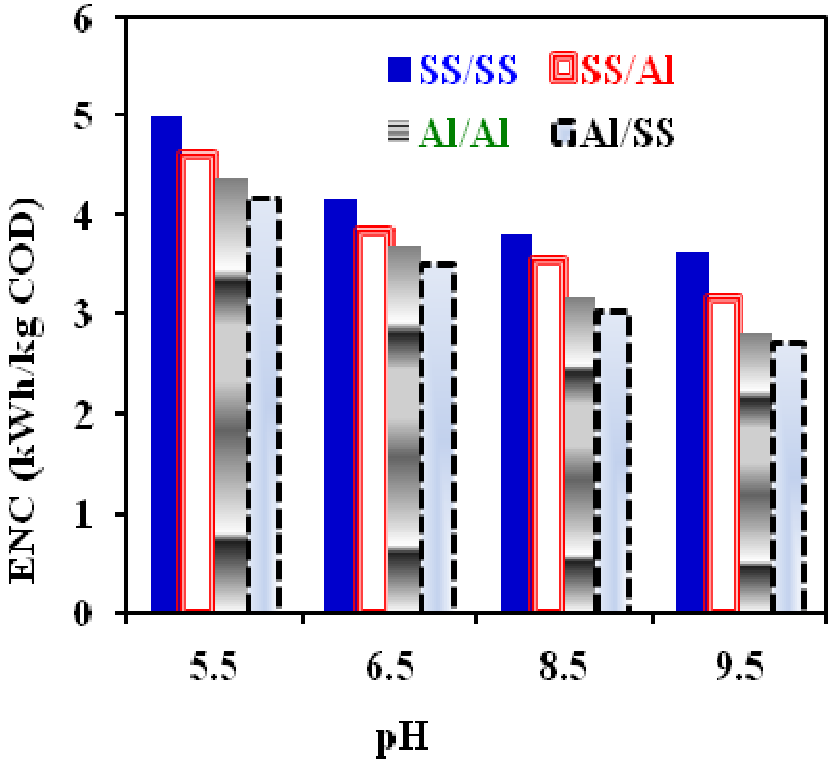

(a)

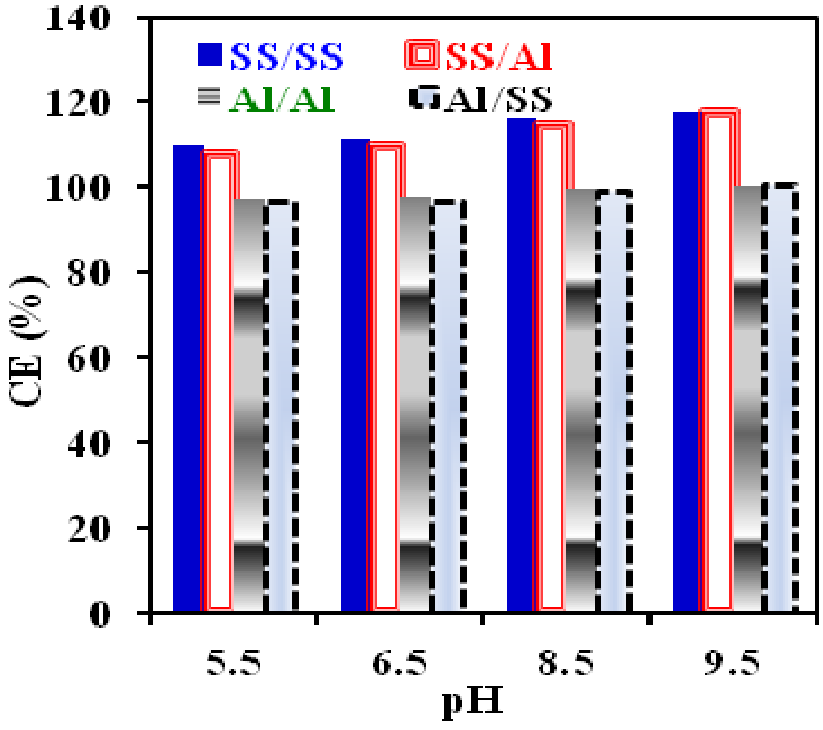

(b)

Figure 4.3.12.Effect of pH on (a) energy consumption and (b) current efficiency (CE) with various anode-cathode combinations at t=150 min and j=117.64A/m^2.

4.3.6. Textural analysis of sludge

Textural analysis of various sludge generated with various anode-cathode combinations are shown in Figures 4.3.14 and 4.3.15. Figures 4.3.14a and 4.3.14b show volume of nitrogen adsorbed with relative pressure for SS-SS and SS-Al; and Al-Al and Al-SS, respectively, during adsorption (A) and desorption (D). N_2 adsorption (A)–desorption (D) isotherms of different types of sludge exhibit H1-type hysteresis loop with a type IV isotherm curve, which indicate the mesoporous structure of different sludge based on the IUPAC classification [Barret and Joyer, 1951]. H_2 type hysteresis loop corresponds to ink-bottle pores and reduction of the pore volume occurs due to percolation effect caused by small impurities settled within the mesoporous. Figures 4.3.15a and 4.3.15b show variation of pore volume and pore area with pore diameter, respectively. Table 4.3.4 shows the textural properties of the various types of sludge. The order of BET surface area of different combination of electrodes was found to be in the following order: Al–Al (389.7 m^2/g) > Al–SS (372.7 m^2/g) > SS–SS (272.2 m^2/g) >SS–Al (196.9 m^2/g).

The internal structure and structure heterogeneity of sludge can be determined in terms of pore size distribution with the help of Barret-Joyer-Halenda (BJH) analysis [41]. Industrial application of the EC generated sludge is likely to be highly dependent upon its pore size distribution analysis. BJH pore volume was found to be in the following order: SS–Al (0.386 m^3/g) > Al–SS (0.325 m^3/g) > SS–SS (0.292 m^3/g) > Al–Al (0.280 m^3/g). Similarly, BJH pore diameters were found to be in the following order: SS–Al (66.95 Å) > SS–SS (43.72 Å) > Al–SS (33.60 Å) > Al–Al (32.80 Å) respectively. IUPAC classifies various types of pores based on pore diameter (d) as: super-micropores (d < 7Å) < ultra-micropores (7 Å < d < 20 Å) < micropores (d < 20 Å) < mesopores (20 Å < d < 500 Å) < macropores (d > 500 Å). Based on textural analysis, it can be said that all the anode-cathode combinations sludge are meso-porous in nature.

4.3.7. Thermo-gravimetric analysis of sludge

Thermal degradation characteristics of sludge generated after EC treatment of DBE by various anode-cathode combinations was analysed by thermal analysis [Mondal et al., 2012; Singh et al., 2013a,b]. TGA/DTA analysis give qualitative and quantitative results regarding thermal degradation nature, energy content, etc. which help in deciding their possible usage as fuel in boilers and furnaces. Thermographs of sludge obtained in air environment at 10^{o}C/min various sludge are shown in Figure 4.3.16, and the main results are shown in Table 4.3.4. TGA (Figure 4.3.16a) illustrate the quantitative analysis of mass change due to change in chemical composition of sludge during oxidation; DTG (Figure

4.3.16b) and DTA curve (Figure 4.3.16c) shows range of exothermic peaks associated with thermally induced oxidation. Table 4.3.4 shows the values of weight loss with temperature, peak temperature and enthalpy change, etc. Analysis of Figure 4.3.16a shows 10-21% thermal degradation in samples because of loss of moisture and some volatile matter up to a temperature of 210^{o}C. Sludge of different electrode combinations showed major degradation zone between 220–450^{o}C. Zones of maximum degradation for various anode-cathode combinations sludge with corresponding weight loss were: 200–360^{o}C and 400–980^{o}C with 11.31 and 10.18% weight loss for SS–SS; 200–210 and 210 980^{o}C with 30 and 8.5% weight loss for SS–Al; 220–400 and 430-950^{o}C with 24.5 and 7.5% weight loss for Al–Al; and 210–350^{o}C and 400–930^{o}C with 16.8 and 15.71% weight loss for Al–SS (Figure 4.3.16a). Rate of maximum weight loss (Figure 4.3.16 b) was found to be 0.20 and 0.167 mg/min at 220^{o}C and 350 ^{o}C for SS–SS, 0.23 mg/min at 260^{o}C for SS–Al, 0.32 mg/min at 300^{o}C for Al–Al and 0.58 mg/min at 319^{o}C for Al–SS. DTA curve in Figure 4.3.16c shows different exothermic peaks of different electrodes sludge and results are shown in Table 4.3.4. Total weight losses were found to be 68.6%, 62.6%, 69.9% and 70% for SS-SS, SS-Al, Al-Al and Al-SS, respectively. DTA analysis predicted that heating value of different electrode sludge to be: 2.73 MJ/kg, 2.80 MJ/kg, 1.28 MJ/kg and 1.45 MJ/kg for SS–SS, SS–Al, Al–Al and Al–SS respectively.

Overall comparison of sludge characteristics based on textural and thermo-gravimetric analysis shows that the sludge has very less heating value as compared to Indian coal (18.8 MJ/kg). However, pore surface area of the sludge is more than many of the low cost adsorbents like bagasse fly ash (156.9 m^2/g) [Rameshraja et al., 2012], rice husk ash (36.44 m^2/g) [Srivastava et al., 2006], fertilizer plant waste carbon (357 m^2/g) [Mall et al., 2006] etc., and some of the commercial adsorbents like commercial activated carbon (174.2 m^2/g) [Rameshraja et al., 2012], zironia (87-320 m^2/g) [Kumar et al., 2011], alumina (143 m^2/g) [Srivastav et al., 2009], etc. Because of the good surface area, sludge can be directly used as an adsorbent, however, leaching of elements can be an issue. Since the sludge also contain a number of metals like iron, aluminum, etc., therefore, these sludge can be used for making nano-materials out of them by heat treatment [Shon et al., 2009]. These nano-materials can further be used as catalysts for other applications.

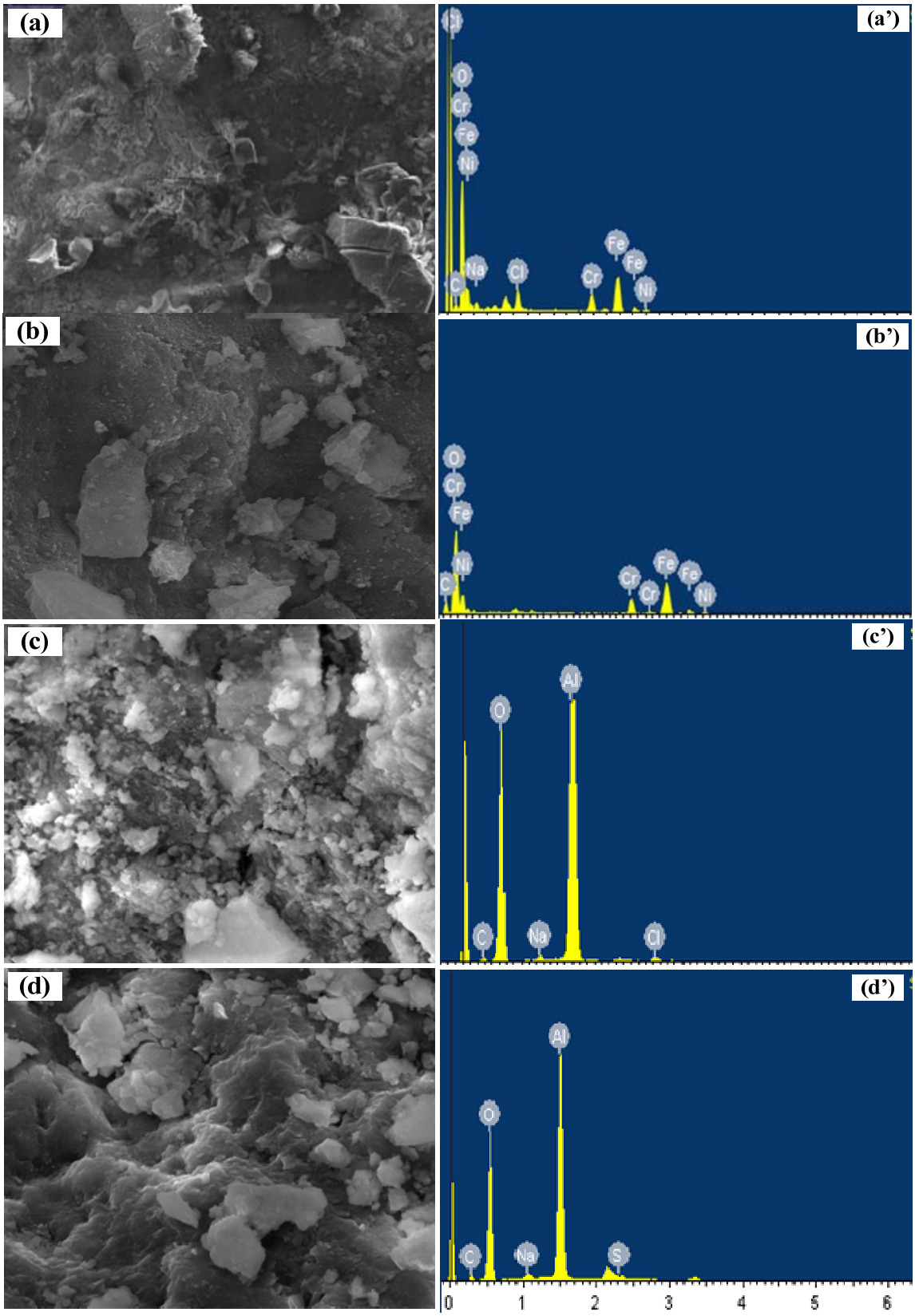

Figure 4.3.13. FE-SEM/EDX analysis of (a & a') SS/SS; (b & b') SS/Al; (c & c') Al/Al and (d & d') Al/SS electrodes sludge after treatment of DBE effluent at current 3 A; electrode gap 1 cm and optimum pH of each electrodes.

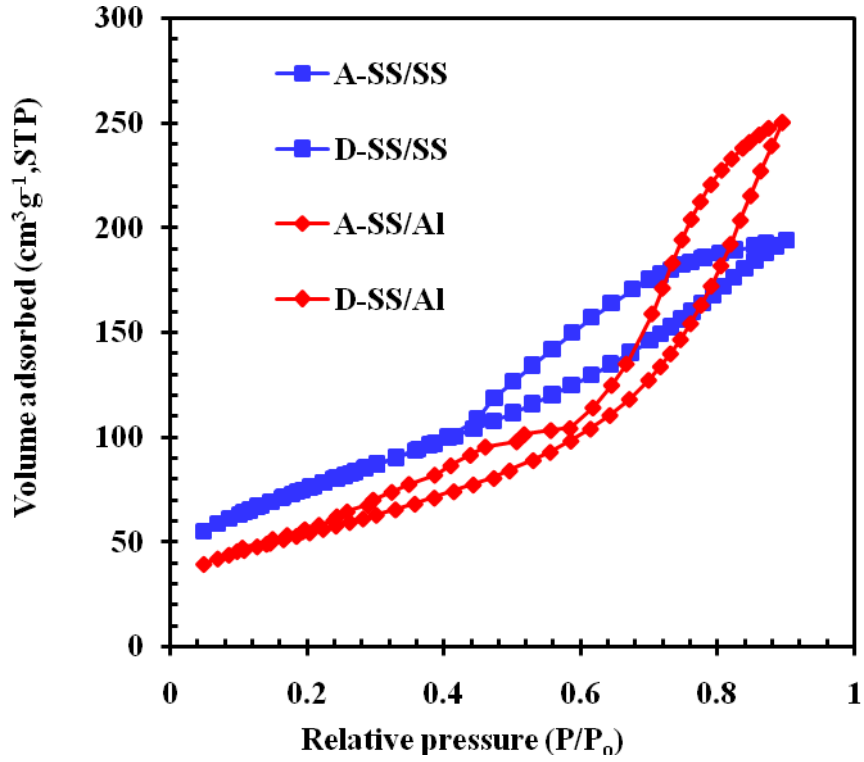

(a)

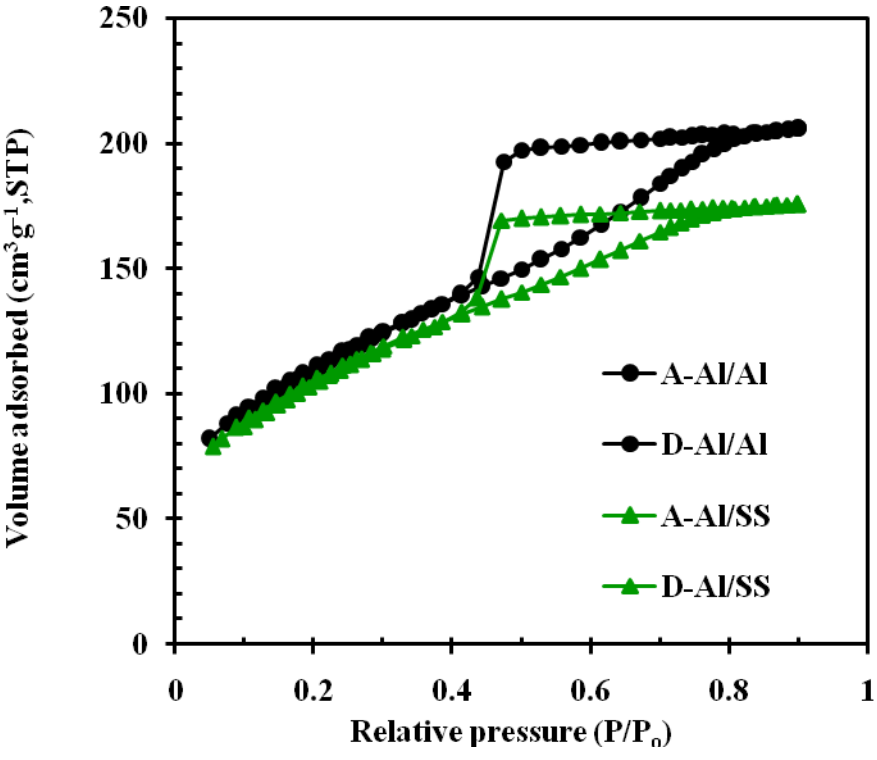

(b)

Figure 4.3.14. (a) Nitrogen adsorption (A) and desorption (D) isotherms for SS-SS and SS-Al, and (b) nitrogen adsorption (A) and desorption (D) isotherms for Al-Al and Al-SS.

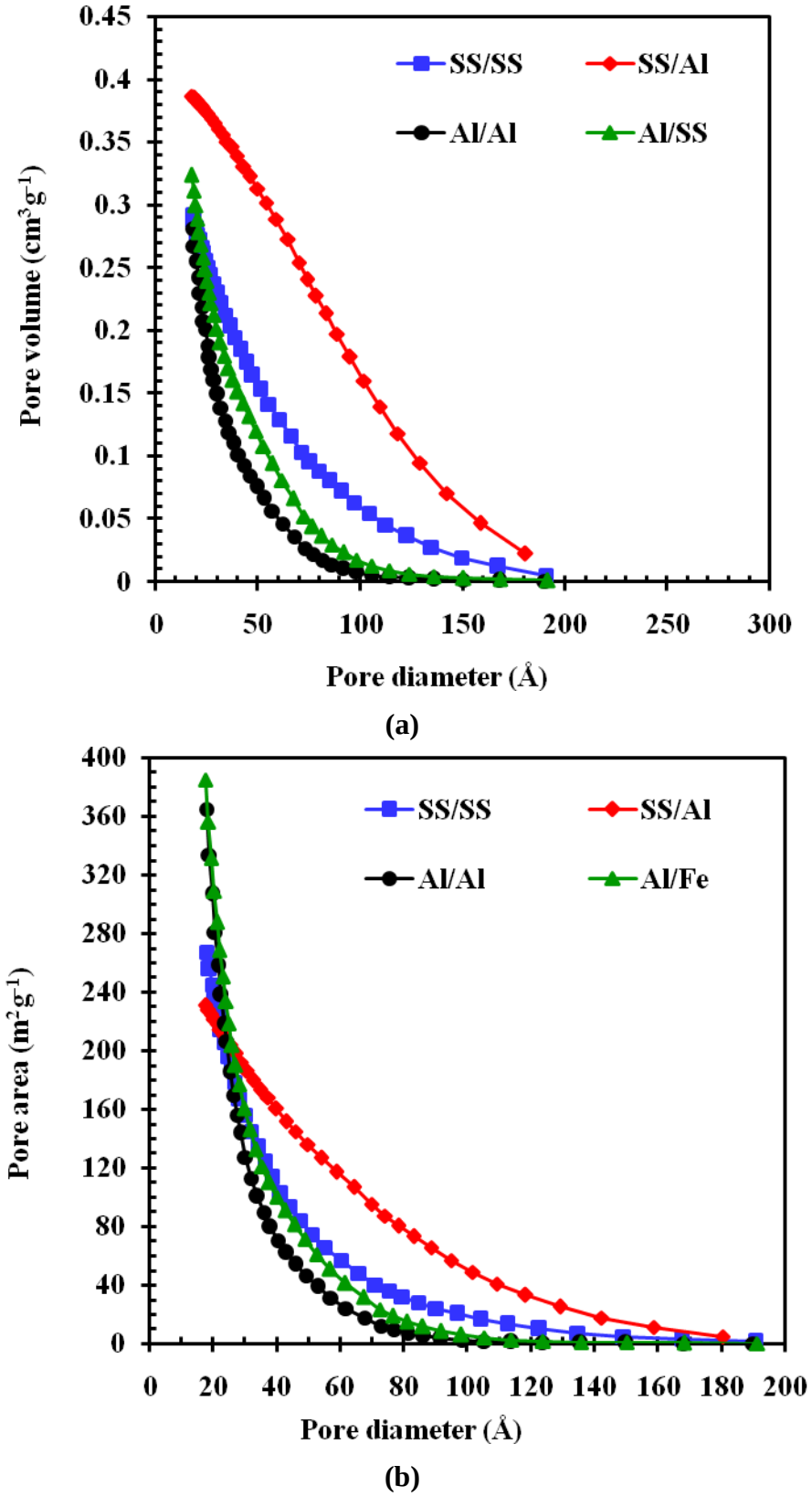

Figure 4.3.15. (a) Pore volume and (b) pore area distribution of SS-SS, SS-Al, Al-Al and Al-SS sludge.

Table 4.3.4.Textural and thermal degradation properties of the solid residue generated by the EC process of different combination of electrodes.

Parameters	Sludge of different combination			
	SS/SS	**SS/Al**	**Al/Al**	**Al/SS**
Textural properties				
BET surface area (m^2/g)	272	196.95	389.69	372.66
BJH surface area (m^2/g)	267.28	230.82	364.95	385.03
BJH pore volume (m^3/g)	0.292	0.386	0.280	0.3254
BJH pore diameter (Å)	43.72	66.95	32.80	33.60
TGA analysis				
Drying range (^oC)	25-100	25-100	25-100	25-100
Moisture (%)	17.26	20.9	20.11	13.21
Degradation range (^oC)	300-450	300-460	350-456	300-480
	850-1000		870-920	820-950
Temperature T_{max} (^oC) at which maximum rate of weight loss	220 & 350	260	300	319
Maximum rate of weight loss (mg/min)	0.20 & 0.167	0.323	0.329	0.58
DTA analysis				
Exothermic reaction temperature range (^oC)	200-260 300-400	220-260	350-420	335-390
Exothermic energy, ΔH (MJ/kg)	-2.73	-2.80	-1.28	-1.45

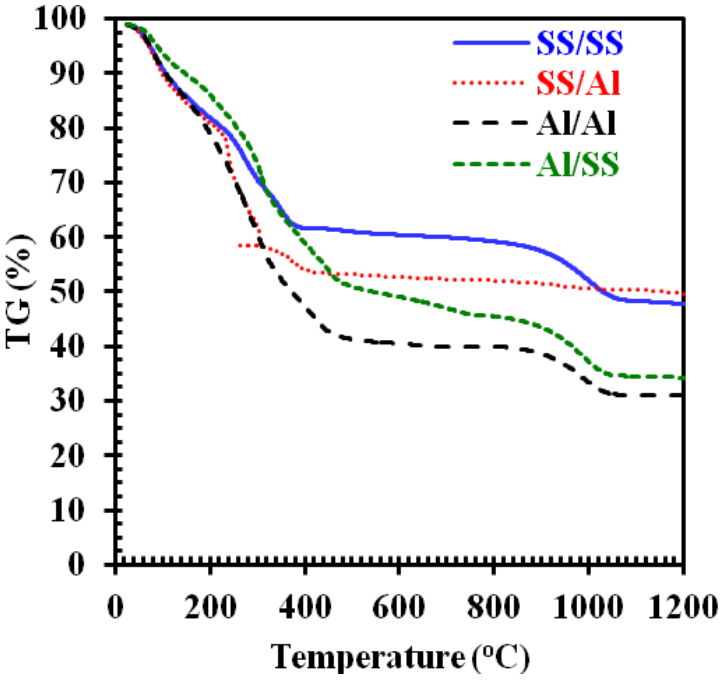

(a)

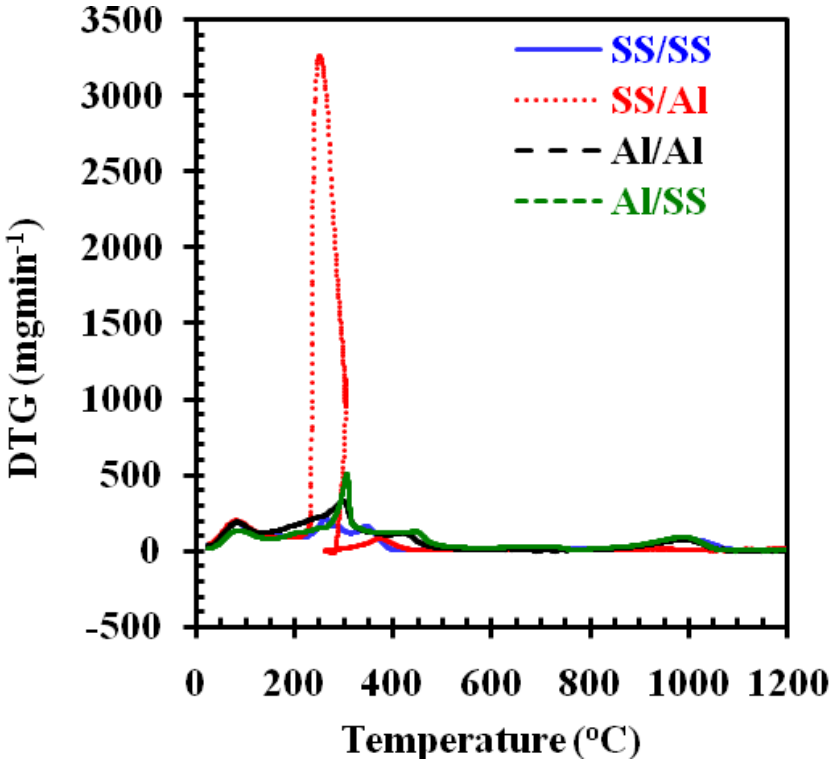

(b)

Figure 4.3.16. Variation of (a) TGA, (b) DTG, and (c) DTA graphs of SS-SS, SS-Al, Al-Al and Al-SS sludge generated after EC treatment of DBE (continued to next page).

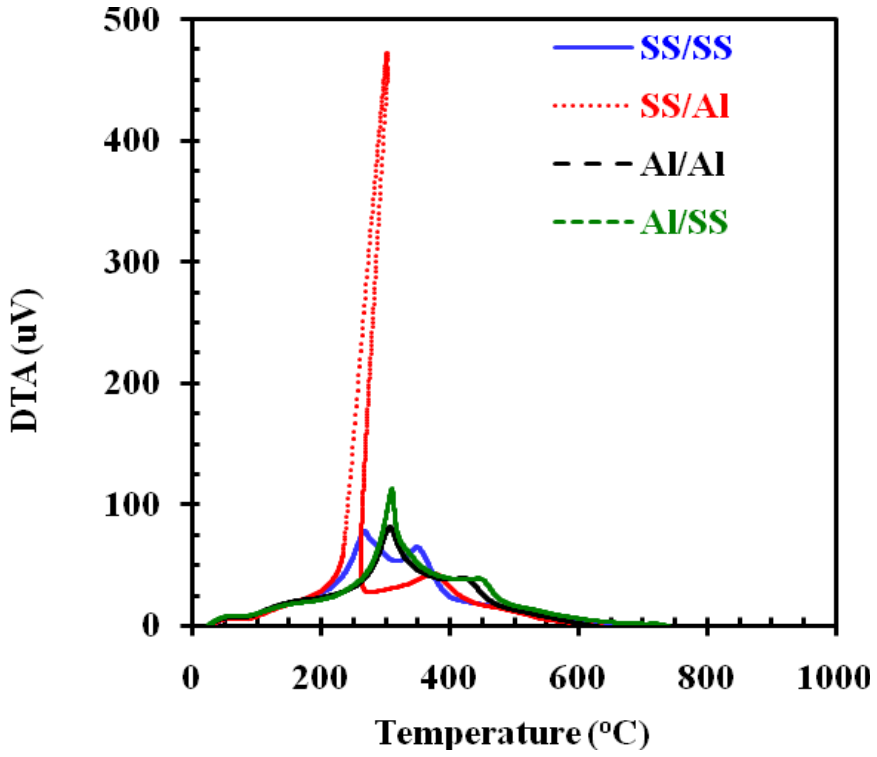

(c)

Figure 4.3.16. Variation of (a) TGA, (b) DTG, and (c) DTA graphs of SS-SS, SS-Al, Al-Al and Al-SS sludge generated after EC treatment of DBE.

4.4. RECYCLING AND DISPOSAL STUDIED OF EC SLUDGE GENERATED BY STAINLESS STEEL AND ALUMINIUM ELECTRODES

4.4.1 Characterisation of nanocomposite materials (NCMs) prepared by the conversion of stainless steel electrode EC sludge

Solid waste (sludge) generated during EC treatment of basic green 4 dye wastewater treatment with stainless steel (SS) electrode was recycled by heting the solid waste at different temperatures under controlled condition to produce nano composite materials (NCMs) that exhibited high stability, superior adaptability and sustainability in dye wastewater treatment. Schematic representation of the preparation of iron oxide NCM from EC solid waste is shown in Figure 4.4.1.

4.4.1.1. Thermogravimetric analysis

Thermogravimetric analysis, TGA and DTA thermograms of S(Fe-0) and S(Fe-8) are shown in Figure 4.4.2. Three oxidative weight loss zones can be observed in the TGA of S(Fe-0). First zone with 16.73% weight loss was from 20 to 200^{o}C due to loss of light weight molecules and moisture from the sample. 21.03 % weight loss was obtained between 200 and 550^{o}C due to oxidative degradation of organic contaminants in sample by the evolution of CO_2 (450–1000°C) and CO (200–500°C) in second oxidative degradation zone (Table 4.4.2). Last but the least weight loss zone (3.6%) occurred at higher temperature above 600 and up to 1000^{o}C (Figure 4.4.2). Residue left at higher temperature is the weight of the ash bearing iron NCM. Thermogram of S(Fe-8) (Figure 4.4.2) showed negligible (1.76%) mass change and indicated its high thermal stability because of its pure composite nature. Color of the EC sludge changed from grey to dark brown after incineration because of the removal of organic impurities at lower temperature.

4.4.1.2. Powder X-ray diffraction (PXD) analysis

Analysis of the powder X-ray diffraction (PXD) patterns indicates the formation of crystalline phases only in those samples which were heated at 600^{o}C and above (Figure 4.4.3). On further heating up to 1000^{o}C, no further change in the PXD patterns was observed suggesting that no additional phase evolution took place except that the particle size and crystallinity of the sample was increased as evidenced by narrowing of the peak widths and increase in the peak intensity.

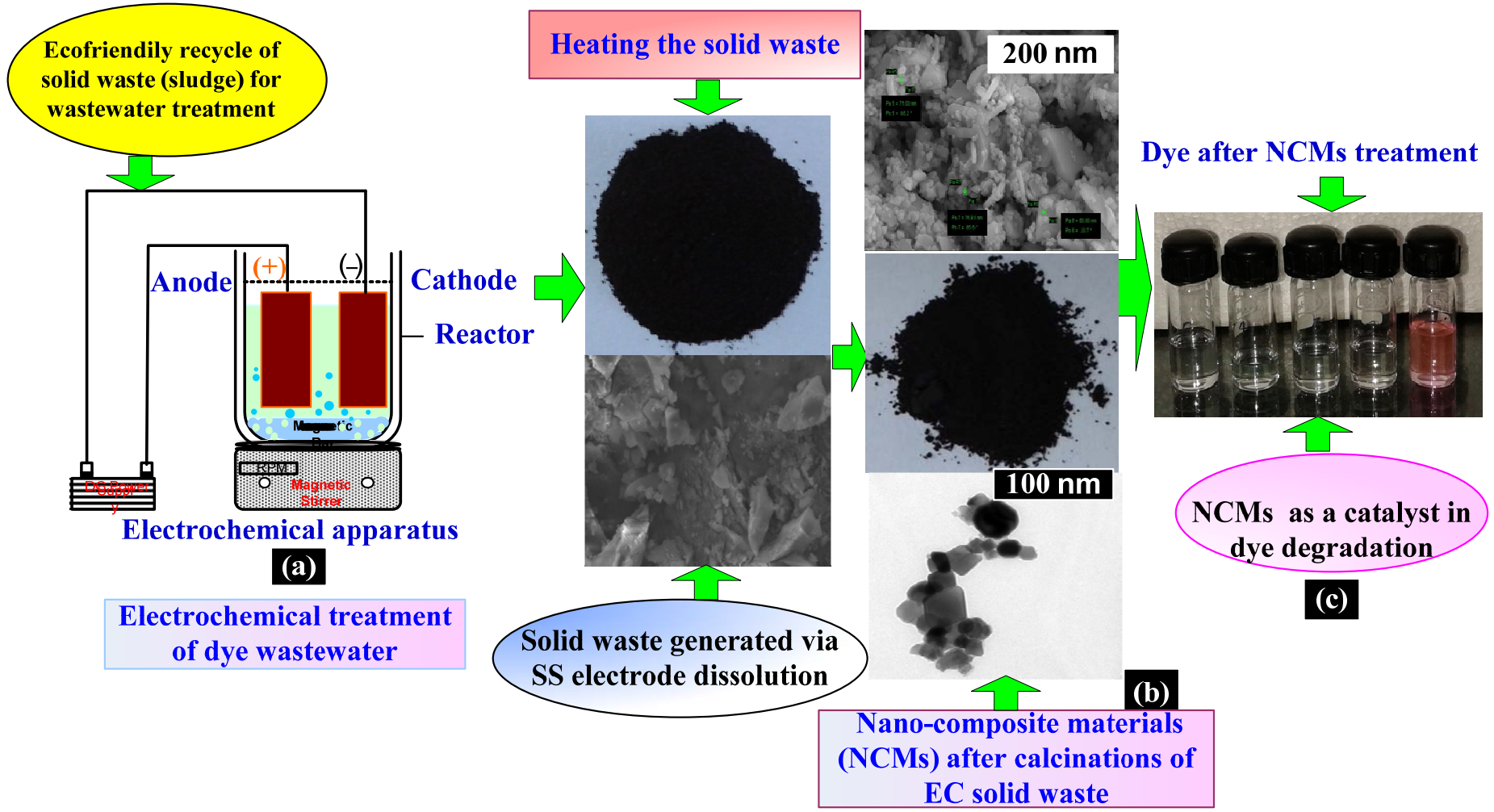

Figure 4.4.1. Schematic representation of NCMs from basic green 4 dye treated EC sludge.

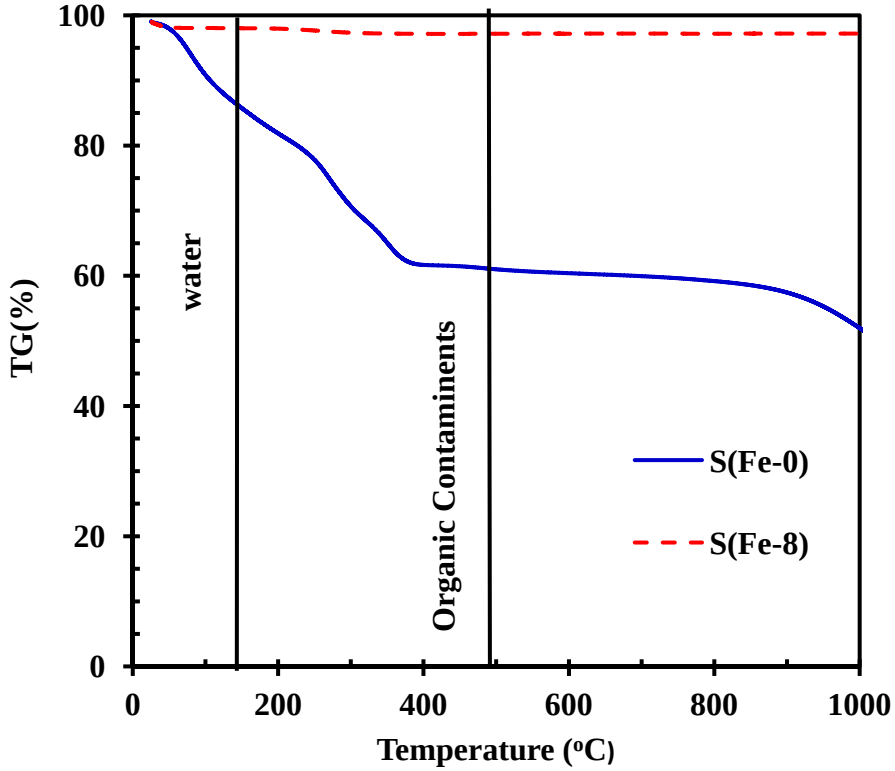

(a)

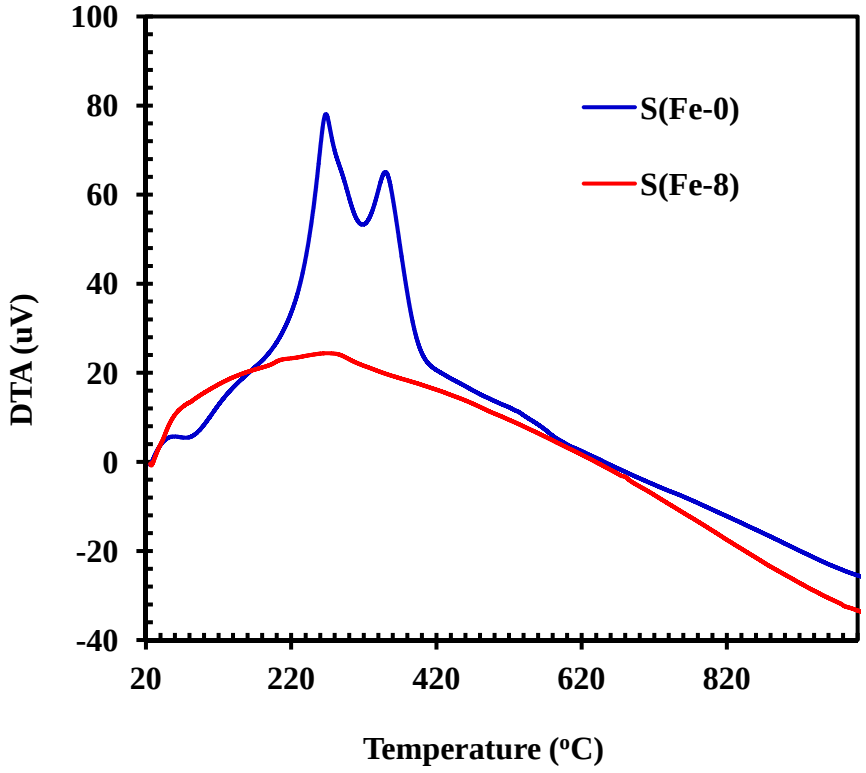

(b)

Figure 4.4.2. Thermogravimetric (a) TGA (b) DTA analysis of electrochemical sludge of S(Fe-0) and S(Fe-8).

Table 4.1.1.Thermal degradation and Textural analysis of the EC generated sludge of S(Fe-0), and final S(Fe—8) sample.

Parameters	S(Fe-0)	S(Fe-8)
TGA analysis		
Drying range(^{o}C)	20-100	-
Moisture (%)	16.29	-
Degradation range (^{o}C)	200-250, 350-550	-
T_{max}(^{o}C) maximum weight loss temperature	190, 300 & 450	-
Maximum rate of weight loss (mg min^{-1})		
DTA analysis		
Exothermic reaction temperature range (^{o}C)	200-300 & 350-400	350-400
Texture analysis		
BET surface area(m^2 g^{-1})	272.39	4.34
BJH surface area (m^2 g^{-1})	267.28	4.22
BJH pore volume (cm^3 g^{-1})	0.292	0.0057
BJH pore diameter (Å)	43.72	54.18
Average pore width (Å)	43.97	51.10

Phase analysis of the PXD pattern obtained at 800^{o}C shows presence of hexagonal Fe_2O_3 (α- Fe_2O_3, JCPDS-PDF #33-0664) type phase with corundum structure admixed with trevorite $NiFe_2O_4$-type (JCPDS-PDF #10-0325) cubic phase. The data of PXD pattern of Fe_2O_3 and $NiFe_2O_4$ was given in Table 4.4.2. All the peaks observed in the PXD pattern arising due to the α–Fe_2O_3 type phase were indexable in the $R\bar{3}c$ space group. A least-square refinement of the lattice parameter gave the refined parameter as a = 5.022(1) Å, c = 13.672(9) Å [Losocha annd Lewinski, 1994]. The cell parameters were slightly smaller than those reported for pure hexagonal α–Fe_2O_3 phase (a = 5.035 Å, c =13.748 Å) [Cherepy et al., 1998; Kucheryavy et al., 2013]. This reduction in the cell parameter could be due to the incorporation/doping of smaller Cr^{3+} (ionic radii 0.615 Å) in place of Fe^{3+} (ionic radii 0.645 Å) in the octahedral site of α-Fe_2O_3 giving a composition $(Fe_{2-x}Cr_x)O_3$ [Shannon, 1976]. However, the possibility of a small amount of Ni substitution in the octahedral site of α-Fe_2O_3 giving a composition $(Fe_{2-x-y}Cr_xNi_y)O_3$ cannot be ruled out on the basis of EDX data. The phase identity and (*hkl)* indexing of hexagonal α-Fe_2O_3 and

cubic $NiFe_2O_4$ along with respective crystal structures are shown in Figures 4.4.4 and 4.4.5. A similar least-square refinement of the lattice parameter gave a = 8.318(2) Å, which is slightly smaller than that observed for pure $NiFe_2O_4$ (8.339 Å) [Shannon, 1976]. Here again, the reduction in the cell parameter could largely be due to the replacement of octahedral Fe^{3+} (at the 8*a* and 16*d* sites) by Cr^{3+} giving $Ni(Fe_{2-x}Cr_x)O_4$. The 16c tetrahedral site is believed to be mostly occupied by Ni^{2+}. However, a slight excess Ni was evidenced by EDX data. This extra Ni could be sitting at the 16*d* octahedral site and imparting only a little effect on the cell parameter. The possibility of Ni^{2+} replacement by Fe^{2+} at the tetrahedral site can be ruled out due to the fact that this would lead to an increase in the cell parameter due to much larger ionic radii of the Fe^{2+} (0.78 Å) as compared to Ni^{2+} (0.69 Å) [Shannon, 1976].

Elemental analysis of original sludge analysis by EDX showed the presence of Fe, Cr, Ni metals along with oxygen (Table 4.4.3). The elemental ratio of Fe/Cr/Ni in the electrochemical sludge as shown by EDX replicated the composition of the stainless steel electrode well within experimental errors. The elemental analyses of the 800°C heat treated sample shows different compositions (Figure 4.4.6) at different crystallites, which is also expected from the phase analysis of the PXD patterns (Figure 4.4.3). Among the two different sets of compositions obtained, the total metal to oxygen ratio is about 0.66 in one case and is much higher in the other (Figure 4.4.6). The metal to oxygen ratio of 0.66 matches very well with the Fe_2O_3 type phase, while the higher metal to oxygen ratio will corroborate with $NiFe_2O_4$-type phase (metal to oxygen ratio = 0.75). It must be mentioned that, the amount of Ni present in the crystallites corresponding to Fe_2O_3 was much smaller than in those corresponding to $NiFe_2O_4$ (Figure 4.4.7). However, the amount of Cr present in both type of crystallites were substantial (6-14 atomic %) and the amount of Cr present in $NiFe_2O_4$ type crystallite was almost double to that present in Fe_2O_3 type crystallite. This probably indicates that in both α–Fe_2O_3 and $NiFe_2O_4$ phase, octahedral Fe^{3+} has been replaced by Cr^{3+} giving rise to a contraction in the cell parameters of the iron oxide NCMs. This is also in corroboration with the PXD studies and refined lattice parameter results.

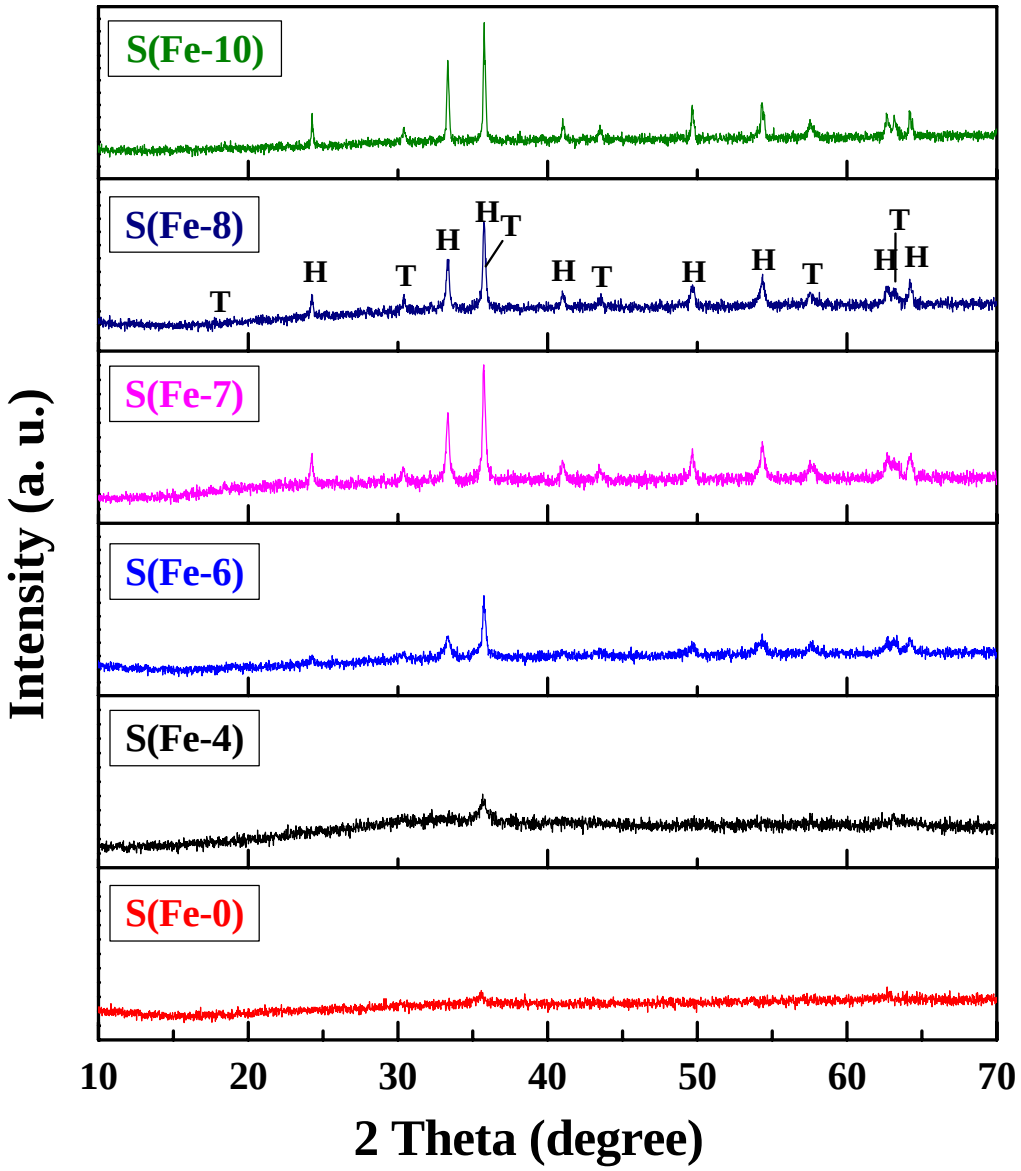

Figure 4.4.3. PXD patterns of thermally treated electrochemical sludge: Original sludge [S(Fe-0), sludge calcined at 400^{o}C [S(Fe-4)], 600^{o}C [S(Fe-6)], 700^{o}C [S(Fe-7)], 800^{o}C [S(Fe-8)], and 1000^{o}C [S(Fe-10)]. On sample S(Fe-8), 'H' indicates hexagonal Fe_2O_3-type phase and 'T' indicates trevorite $NiFe_2O_4$- type phase.

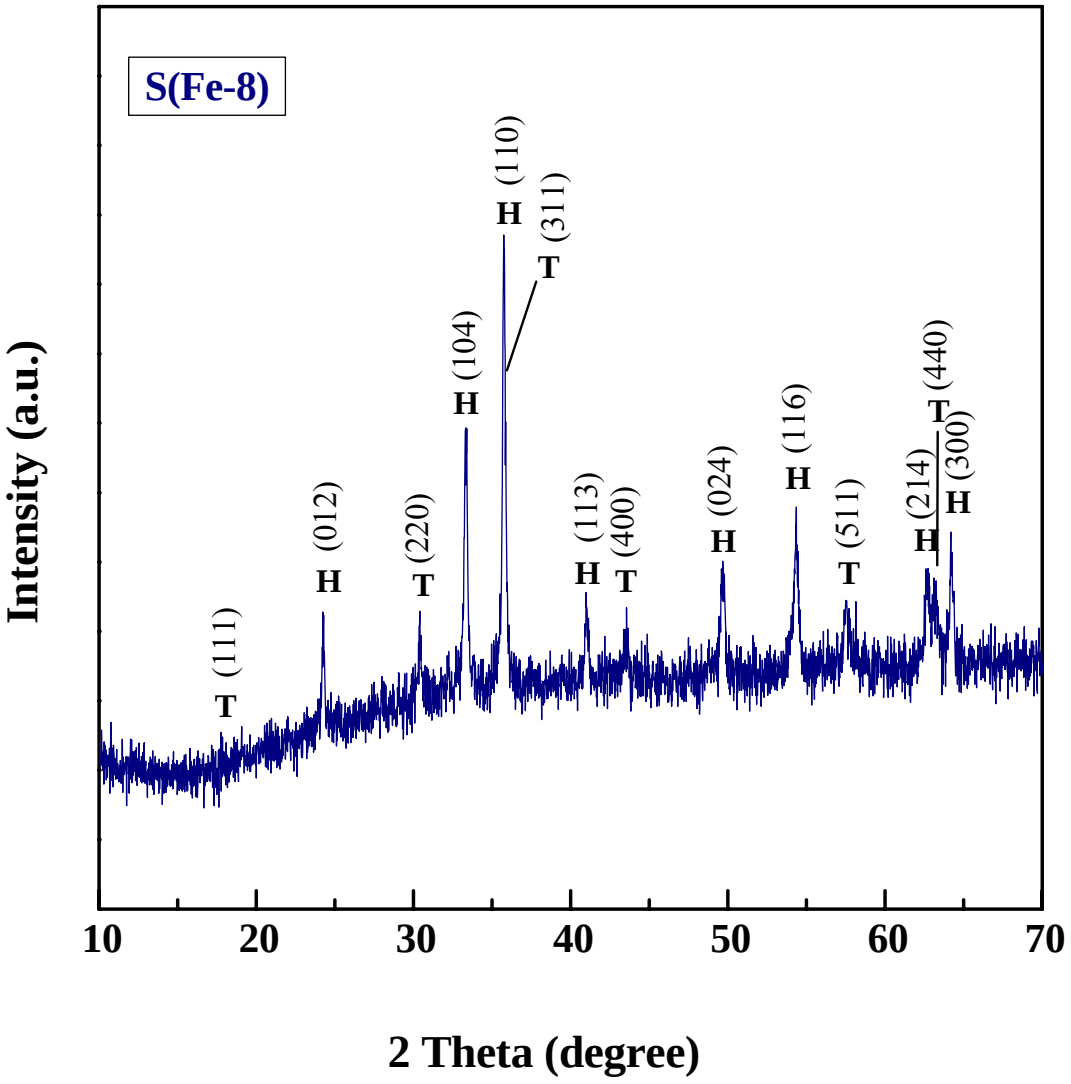

Figure 4.4.4. Indexed PXD pattern of S(Fe-8) sample represented (H) hexagonal α-Fe_2O_3-type phase and (T) cubic trevorite $NiFe_2O_4$- type phase.

Table 4.4.2. Powder XRD data for Fe_2O_3 and $NiFe_2O_4$.

h	***k***	***l***	d_{obs}**(Å)**	d_{obs}**(Å)**	I_{obs}
		Fe_2O_3			
0	1	2	3.6640	3.6695	24.29
1	0	4	2.6860	2.6874	33.35
1	1	0	2.5090	2.5110	33.78
1	1	3	2.1990	2.1993	41.04
0	2	4	1.8340	1.8347	49.71
1	1	6	1.6880	1.6874	54.34
2	1	4	1.4820	1.4814	62.68
3	0	0	1.4500	1.4497	64.23
		$NiFe_2O_4$			
1	1	1	4.8100	4.8022	18.44
2	2	0	2.940	2.9407	30.42
3	1	1	2.5040	2.5078	35.86
4	0	0	2.0794	2.0794	43.52
5	1	1	1.6010	1.6007	57.56
4	4	0	1.4710	1.4703	63.20

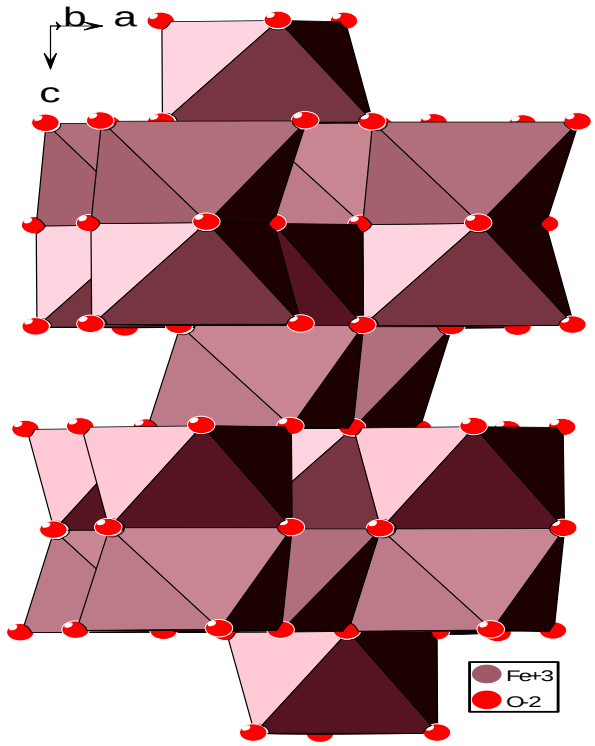

(a)

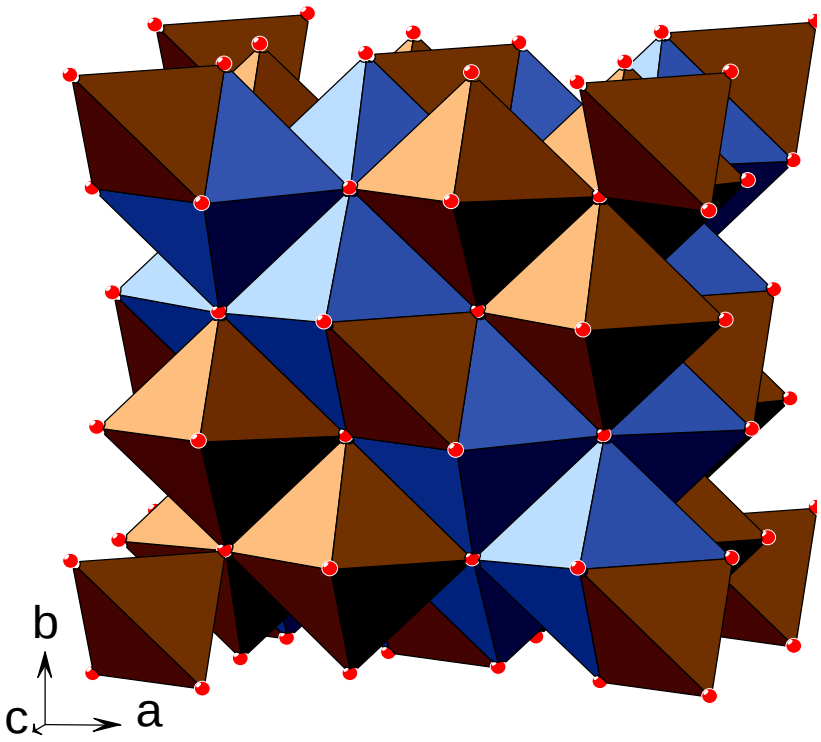

(b)

Figure 4.4.5. (a) Hexagonal α-Fe_2O_3-type phase and (b) cubic trevorite $NiFe_2O_4$- type phase I crystal structures of iron oxide nano composite material.

Table 4.4.3. EDX analysis of sludge samples at different temperature.

Name of elements	S (Fe -0)	S (Fe-4)	S (Fe-6)	S (Fe-7)	S (Fe-8)
O, Weight (%)	33.51	25.66	38.84	35.66	40.97
O, Atomic (%)	54.76	47.22	62.07	58.33	70.45
Fe, Weight (%)	38.85	46.21	36.55	46.21	46.30
Fe, Atomic (%)	16.06	24.37	16.73	24.37	22.81
Cr, Weight (%)	9.90	12.99	10.55	12.99	12.73
Cr, Atomic (%)	4.98	7.36	5.19	7.36	6.73
Ni, Weight (%)	5.21	6.41	4.67	6.41	6.96
Ni, Atomic (%)	2.32	3.22	2.03	3.22	4.38
C, Weight (%)	6.64	5.69	4.59	2.38	0.78
C, Atomic (%)	14.44	13.96	9.78	3.27	1.23
Na, Weight (%)	2.25	3.08	2.12	1.08	0.64
Na, Atomic (%)	2.56	3.88	2.68	1.98	1.14
Cl, Weight (%)	3.92	2.43	1.05	0.98	0.32
Cl, Atomic (%)	2.89	2.13	2.32	1.32	0.89

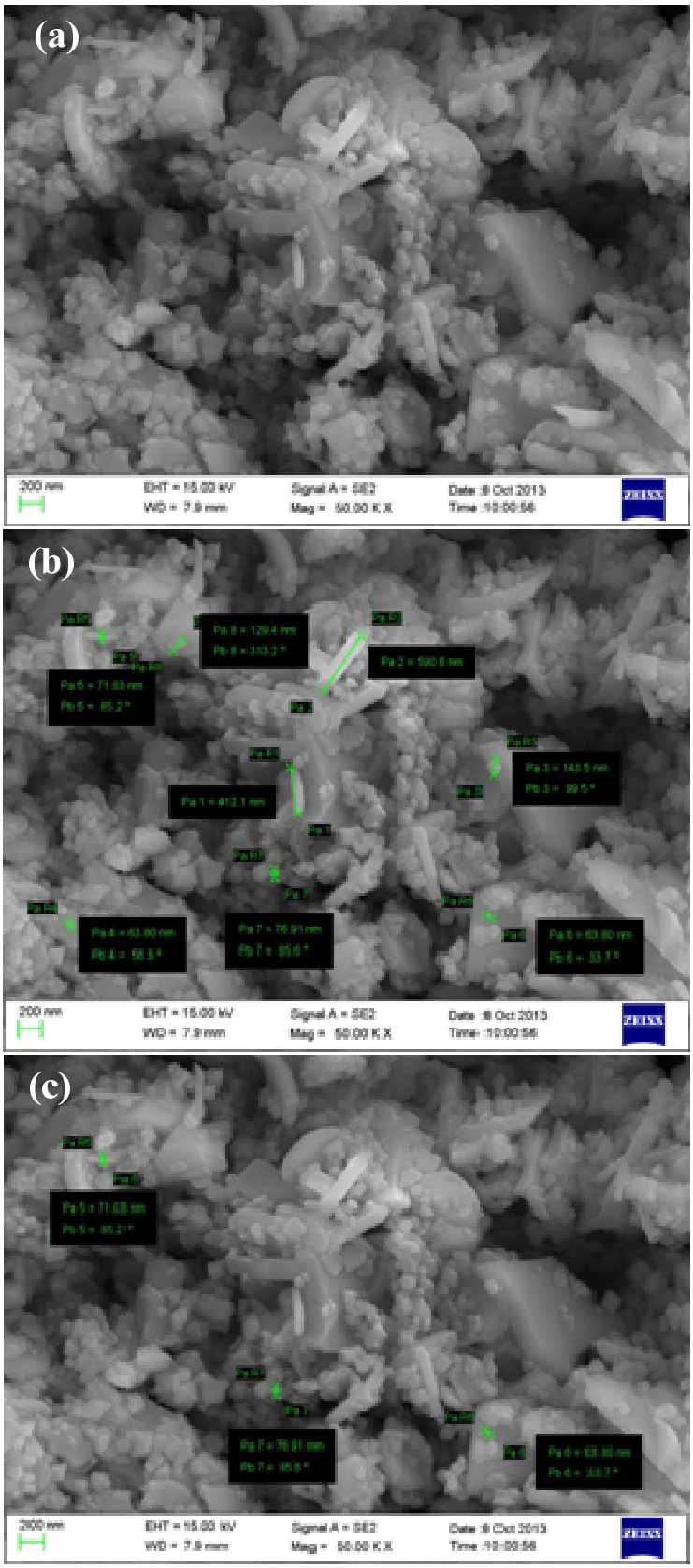

Figure 4.4.6. FE-SEM image of S(Fe-8) along with measurement of different size of particles.

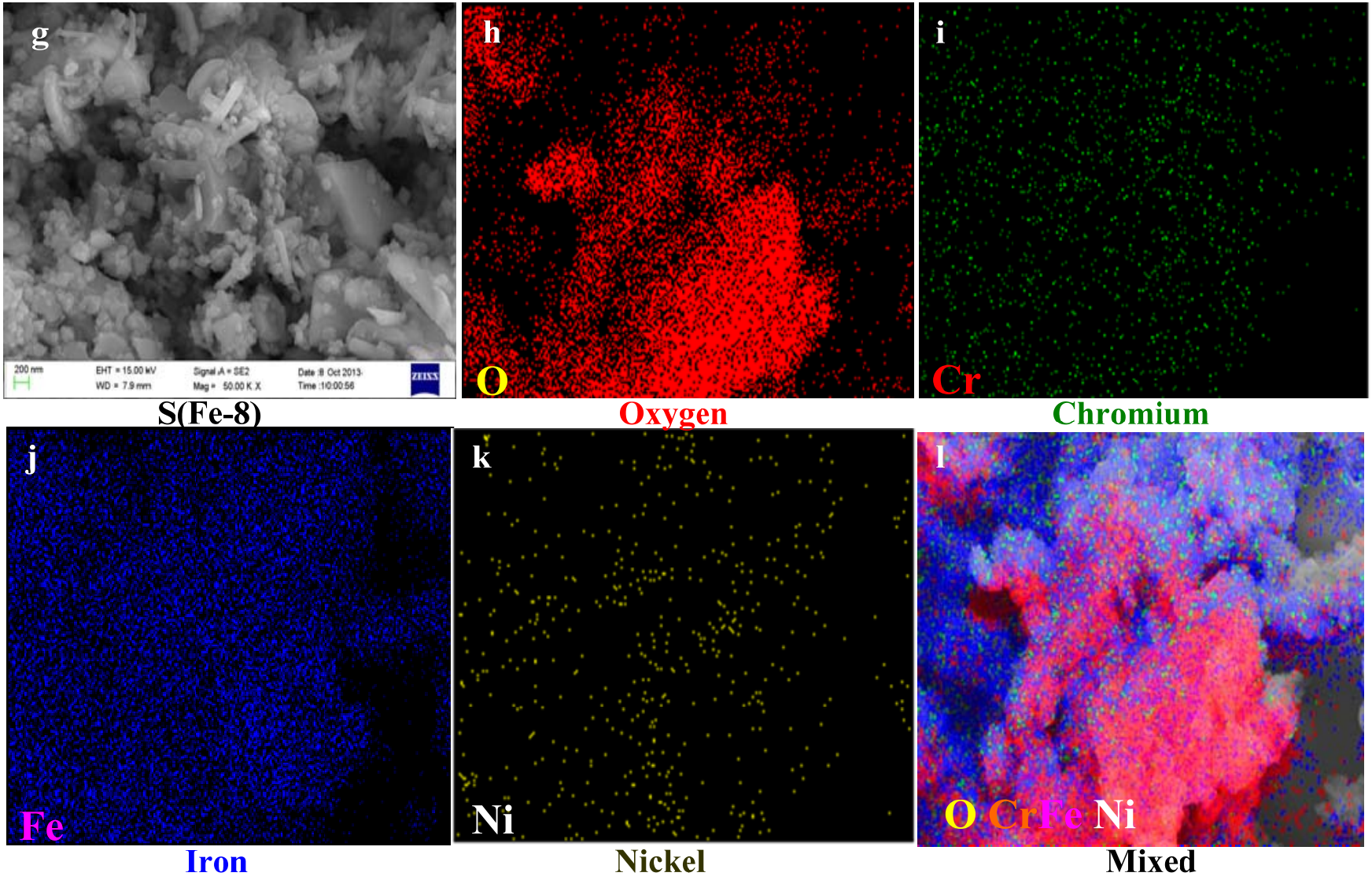

Figure 4.4.7. EDX mapping showing dispersion of elements in S(Fe-8) at 5,000,000× magnification

4.4.1.3. FE-SEM and TEM analysis

FE-SEM combined with TEM was used to identify the morphology of iron oxide NCMs. The SEM images of original sludge [S(Fe-0)] shows agglomerated particles of 50–200 μm size (Figure 4.4.8a). After heating, the crystallinity of sludge increases as shown by XRD and the average particle size decreases to 30-35 nm as evidenced by SEM and TEM images (Figure 4.4.8b-f). SEM image analysis of iron oxide NCMs [S(Fe-8)] show presence of nano-particles with different shape and sizes in the composite material (Figure 4.4.7g). Figure 4.4.8b-f at higher resolution showed the composite nature of S(Fe-8). Moreover, the same is also evidenced from the selected area electron diffraction (SAED) pattern (Figures 4.4.9a and 4.4.9b) depicting the diffused rings with distinct boundaries. The indexing of the ED pattern shown in Figure 4.4.9a and 4.4.9b agrees well with the PXD data of the constituent oxides present in the NCM (Figure 4.4.9a).

4.4.1.4. Atomic Force Microscopy (AFM) analysis

Figure 4.4.10a-d shows the 2D and 3D atomic force microscopy (AFM) images of S(Fe-0) and S(Fe-8). 2D image of S(Fe-0) (Figure 4.4.10a) shows non-uniform distribution of bright spots whereas that of S(Fe-8) (Figure 4.4.10c) shows smoother surface over long length scales with less heterogeneous distribution of bright spots. For S(Fe-0), the average maximum surface roughness (roughness distribution) was 2.5 nm (0.5−12.5 nm) (Figure 4.4.10b) which decreased to 0.5 nm (0.5−9.5 nm) for S(Fe-8) (Figure 4.4.10d) [Kumar et al., 2013]. Thus, sintering at higher temperature decreased the maximum surface roughness.

4.4.1.5. X-ray photoelectron microscopy (XPS) analysis

Figure 4.1.11 shows XPS analysis of S(Fe-0) and S(Fe-8) samples. It shows the change in oxidation state during the thermal treatment. Cr2p, Fe2p and Ni2p core level spectra of ScFe samples are shown in Figure 4.1.11. In both samples, $Cr2p_{3/2,1/2}$ peaks observed at 576.6 and 586.4 eV with 9.8 eV spin-orbit separation correspond to Cr^{3+} species [R1]. Observed $Fe2p_{3/2,1/2}$ core level peaks at 710.8 and 724.2eV with 13.4 eV spin-orbit separation and corresponding satellites are attributed to Fe^{3+} species [R1]. $Ni2p_{3/2}$ peak at 854.7 with satellite peak at 861.8 eV indicates the presence of Ni^{2+} in both the samples. Thus, XPS studies confirm that the NCM contains Cr^{3+}, Fe^{3+} and Ni^{2+} species.

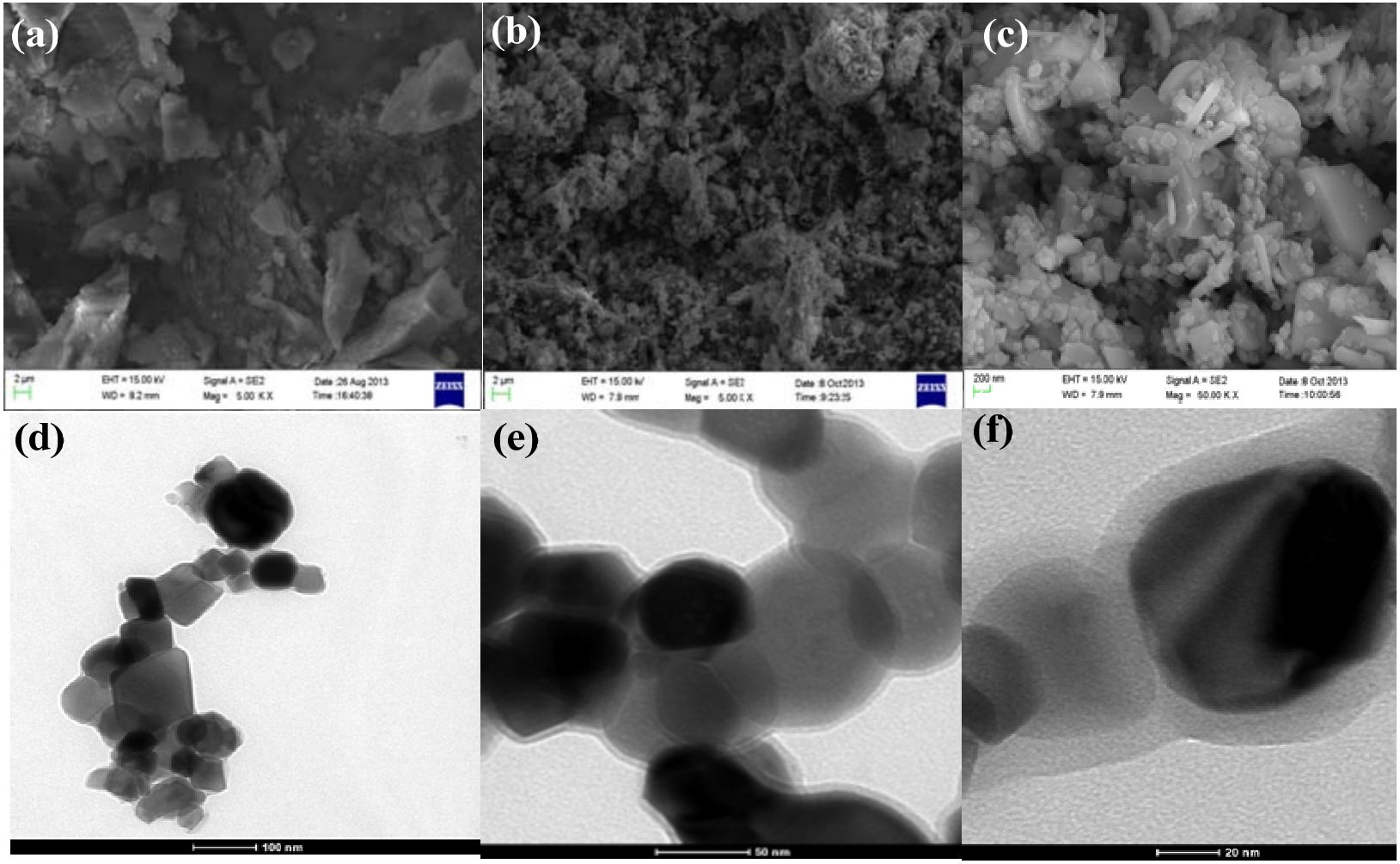

Figure 4.4.8. (a) FE-SEM image of S(Fe-0), (b) and (c) FE-SEM images of S(Fe-8) at 800°C for 3 h.(d) to (f) TEM images of S(Fe-8) at 800°C for 3 h at lower and higher magnification.

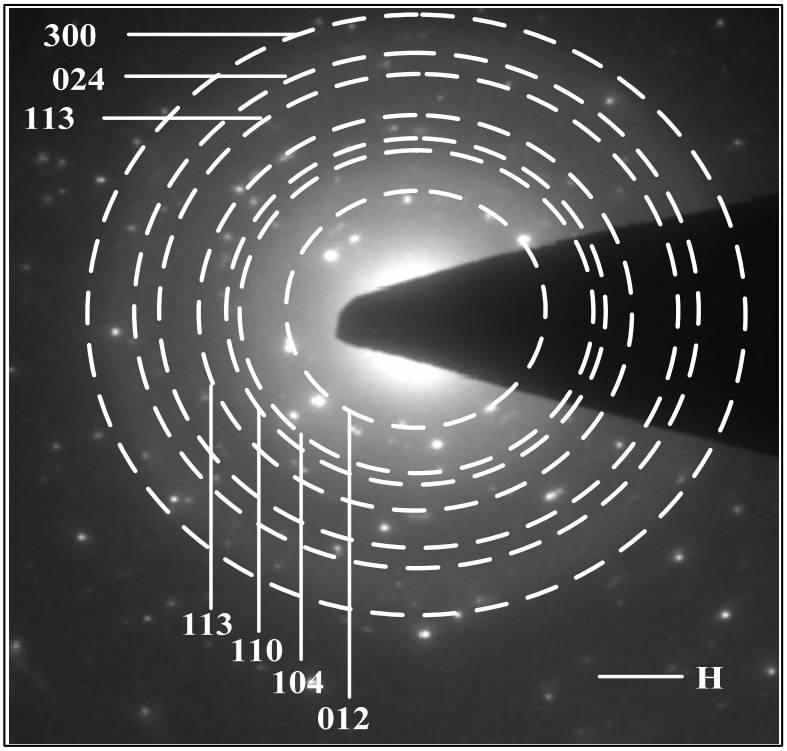

(a)

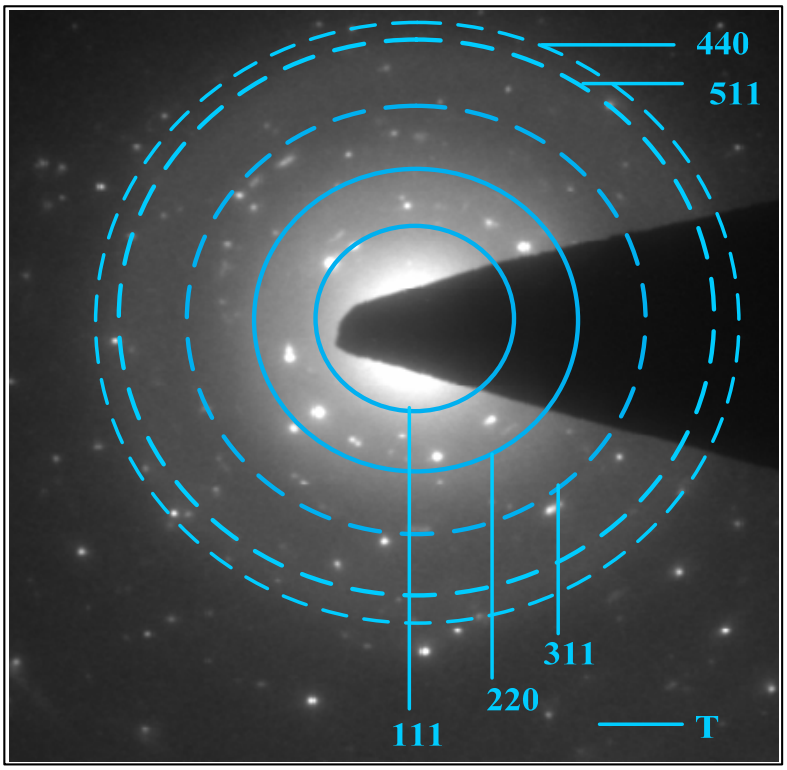

(b)

Figure 4.4.9. SAED Indexed pattern of (a) hexagonal (H) α-Fe_2O_3-type (b) cubic trevorite (T) $NiFe_2O_4$- type phase

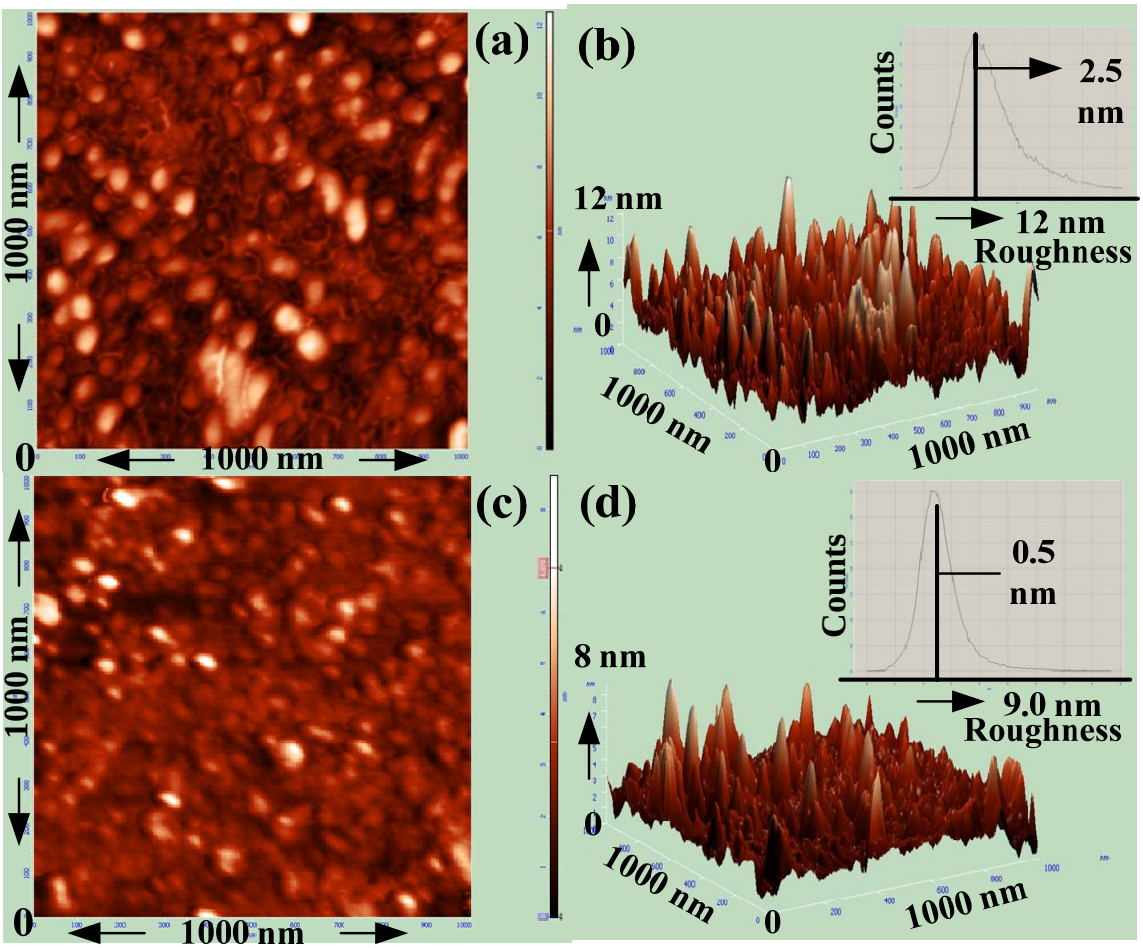

Figure 4.4.10. AFM analysis of S(Fe-0) and S(Fe-8), (a) 2-D image of S(Fe-0), (c) 2-D image of S(Fe-8), (b) 3-D image of S(Fe-0), and (d) 3-D image of S(Fe-8).

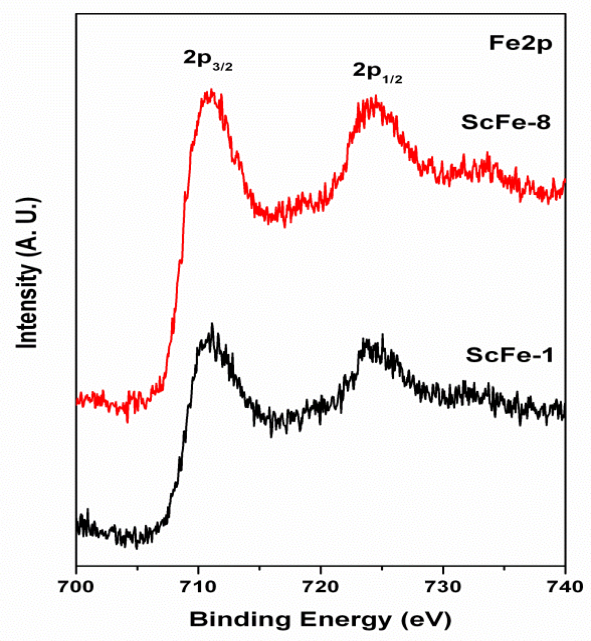

(a)

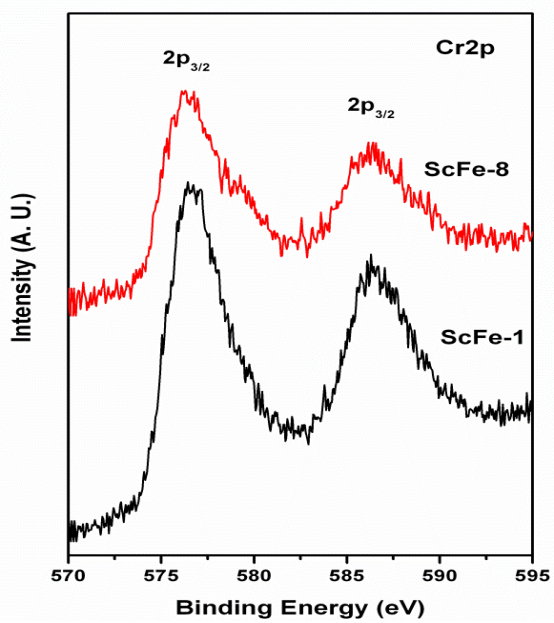

(b)

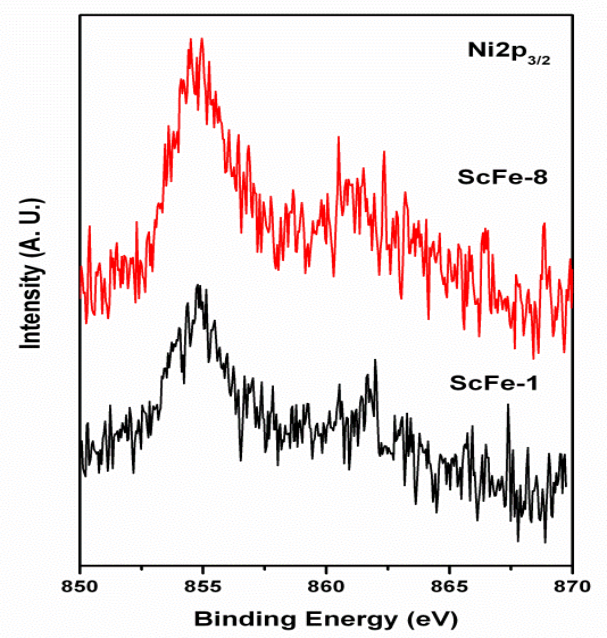

(c)

Figure 4.1.11. XPS analysis of S(Fe-0) and S(Fe-8) samples.

4.4.1.5. Brunauer, Emmet and Teller (BET) analysis

The textural analysis of iron oxide NCMs in terms of pore size distribution (PSD) was done by nitrogen adsorption–desorption isotherms. Figures 4.4.12a and b show the adsorption–desorption isotherms and BJH pore size distribution of S(Fe-0) and S(Fe-8), respectively. Adsorption–desorption isotherms of S(Fe-0) (Figure 4.4.12a inset) exhibit H1-type hysteresis loop with isotherm IV type curve as per IUPAC classification representing typical microprous structure [Groen et al., 2003; Iglesias et al., 2011]. However, S(Fe-8) (Figure 4.4.12b inset) shows H2-type hysteresis loop corresponding to reduction of the pore volume due to percolation effect and presence of three-dimensional network of pores in S(Fe-8). Figure 4.4.13a and b shows multiple peaks in S(Fe-8) in the range of 20-70 Å, while in S(Fe-0) peaks are absent. Thus, S(Fe-8) PSD is multimodal in nature. However, PSD data confirmed presence of micropores in all samples. BJH analysis of S(Fe-8) shows that 10% area is microporous and rest 90% mesoprous in nature. The textural properties of S(Fe-0) and S(Fe-8) are summarized in Table 4.4.1. The pore volume (V_p) and surface area (S_{BET}) gradually decrease with rise the heating temperature but pores diameter (D_P) increases [Groen et al., 2003; Singh et al., 2013c]. BJH average pore diameter of S(Fe-0) and S(Fe-8) samples were found to be 4.3 nm and 5.4 nm, respectively. It seems that high temperature heating of the EC solid waste caused sintering of the material which changed the amorphous nature of waste into crystalline nature with increase in particle size and pore diameter (Figure 4.4.4) and decrease in surface area and pore volume (Figure 4.4.12).

4.4.1.6. Fourier Transformation Infra Red (FTIR) Analysis

FTIR analysis of thermally treated electrochemical sludge is shown in Figure 4.4.14. The broadness in adsorption band at 3600–3200 cm^{-1}, 1680, and 1481 cm^{-1} confirmed the hydrogen bonding of water molecules and carbon dioxides adsorbed on the mesoporous structure of iron oxide NCMs due to environmental effect in all samples. Similarly, vibrations at ≈460 and ≈560 cm^{-1} confirmed the presence Fe-O-Fe stretching in all iron oxide NCMs. Peaks intensity at 1070-1100 cm^{-1} may be due to NCM–O stretching [Mahmoud et al., 2013]. It may be pointed that the absorption peak intensity decreases with an increase in the crystalline nature of samples because of higher temperature calcination.

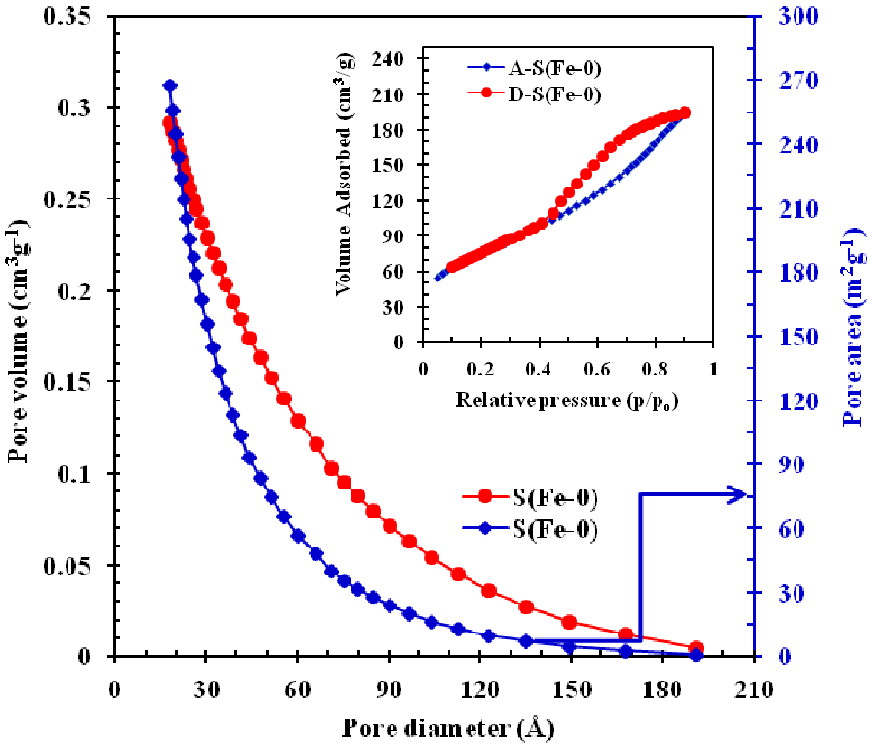

(a)

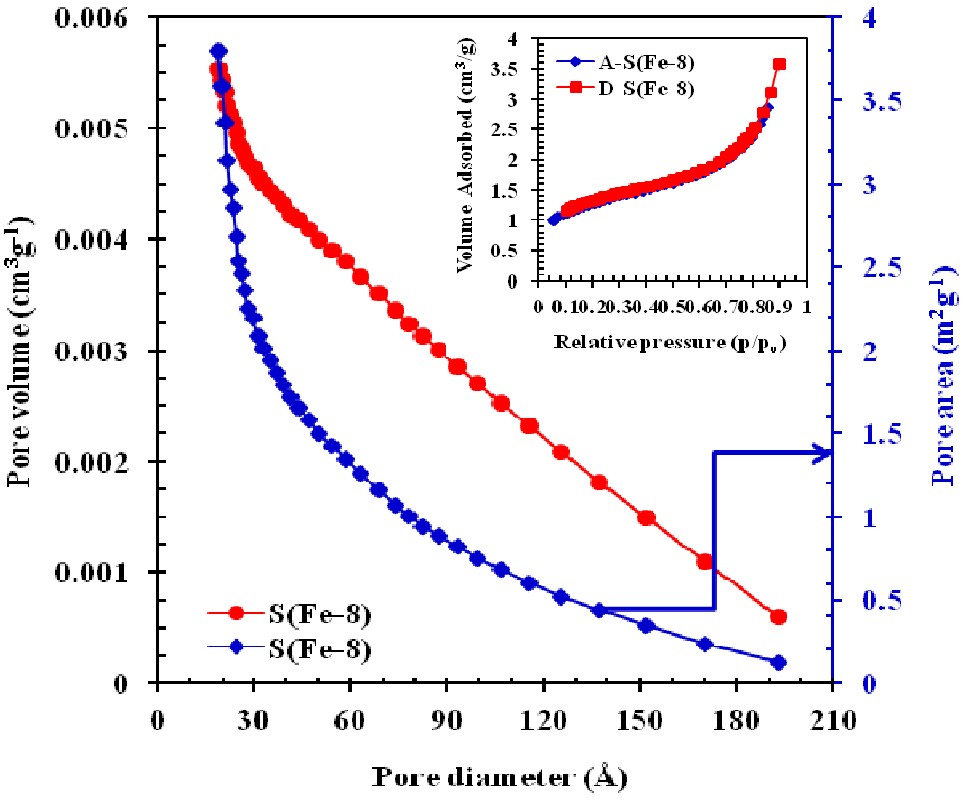

(b)

Figure 4.4.12. Pore size distributions and Nitrogen adsorption (A)–desorption (D) isotherms (inset) (a) S (Fe-0) and (b) S(Fe-8).

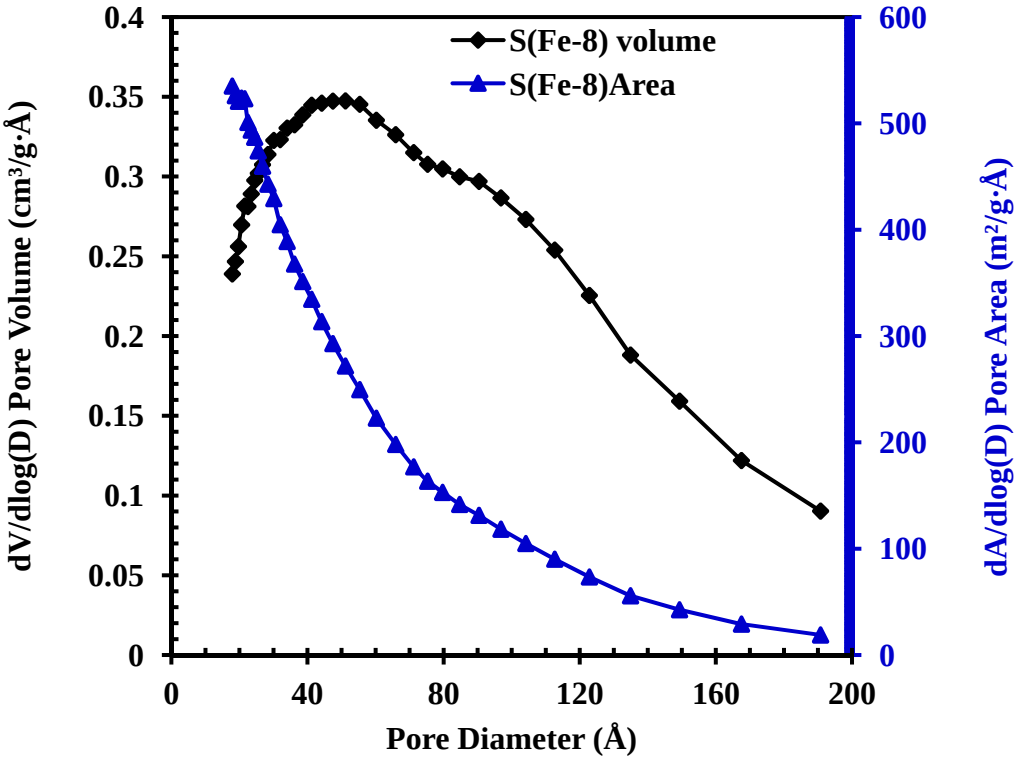

(a)

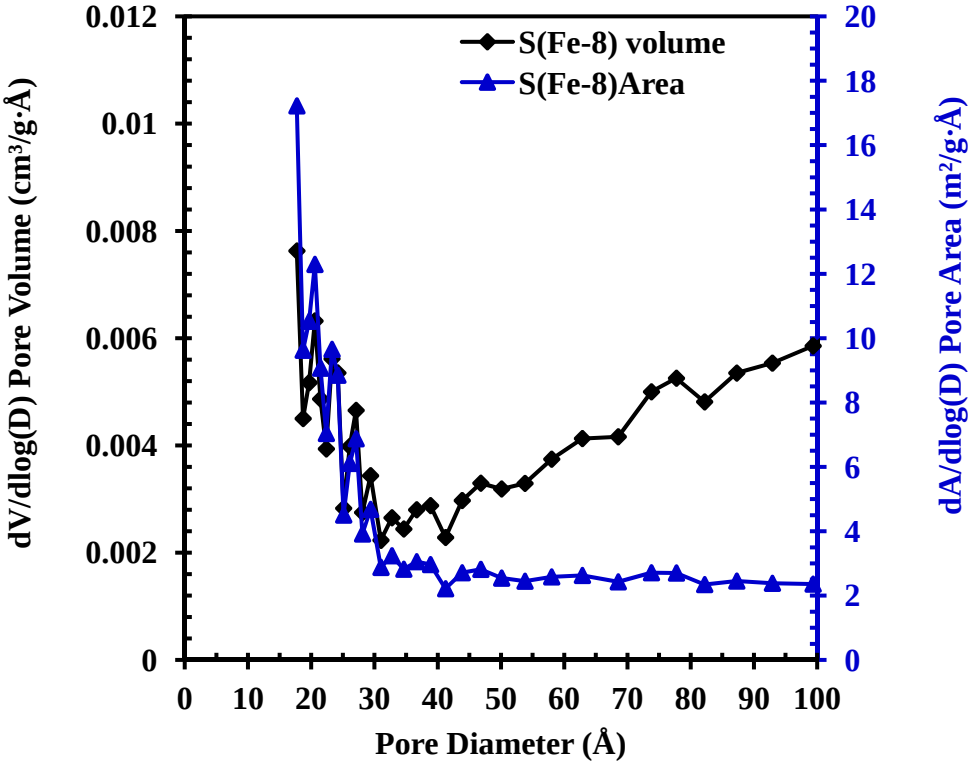

(b)

Figure 4.4.13. Nitrogen sorption isotherm of original sludge S (Fe-0) and iron oxide NCMs S(Fe-8).

4.4.1.7 Catalytic activity of NCMs

In recent years, wastewater treatment using catalytic methods has gained significant attention. Many researchers have already reported excellent performances of various iron oxide and their composite materials in removing organic pollutants and toxic ions from water [Chen et al., 2008]. However, to the best of our knowledge, it is first time the NCMs obtained from EC solid wastes are being used in water treatment. All the iron oxide NCMs were tested for their catalytic ability at 45^{o}C to decolourise and degrade methyl orange (MO) dye solution (100 mg/l) at natural pH 5.1 with catalyst dose of 1g/l in presence of H_2O_2 as an initiator. Results are shown in Figure 4.4.15a. It may be seen that the samples S(Fe-8) and S(Fe-10) have highest and similar treatment efficiencies as compared to other iron oxide NCMs.

Zeta potential of S(Fe-8) at varying pH (Figure 4.4.16) was used to determine its point of zero charge (pH_{PZC}). It may be seen in Figure 4.4.16 that the zeta potential varies from -15 mV to 16 mV with change the pH of distilled water from acidic to basic (3.5 to 9.5) [Zhang et al., 2010]. The value of pH_{PZC} for S(Fe-8) was found to be 8.0. At pH < pH_{PZC}, iron oxide NCMs are positively charged whereas at pH < pH_{PZC}, iron oxide NCMs are positively charged. At high acidic pH, amount of hydroxyl groups are very less in the solution, however, at higher pH (< pH_{PZC}) increased hydroxyl groups bind up strongly to the metals (in iron oxide NCMs) to form metal hydroxyl complex by the strong hard acid and hard base interaction.

The iron oxide NCMs having three different transition metal ions (iron, chromium and nickel) act as hard Lewis acid due to availability of vacant site in their valency shells and have the great ability to form the metal hydroxide complex with OH ions and free radicals generated in presence of H_2O_2. Dye degradation begins via H_2O_2 decomposition on the surface of iron oxide NCMs which generates $OH^{\bullet}$ radicals. Figure 4.4.15b represents the overall treatment mechanism by prepared iron oxide NCMs. In addition to the high catalytic activity of the prepared iron oxide NCMs, higher oxidation potential (2.8V) of hydrogen peroxide as strong oxidant, produces large active site and species during the degradation process and improves the overall treatment efficiency.

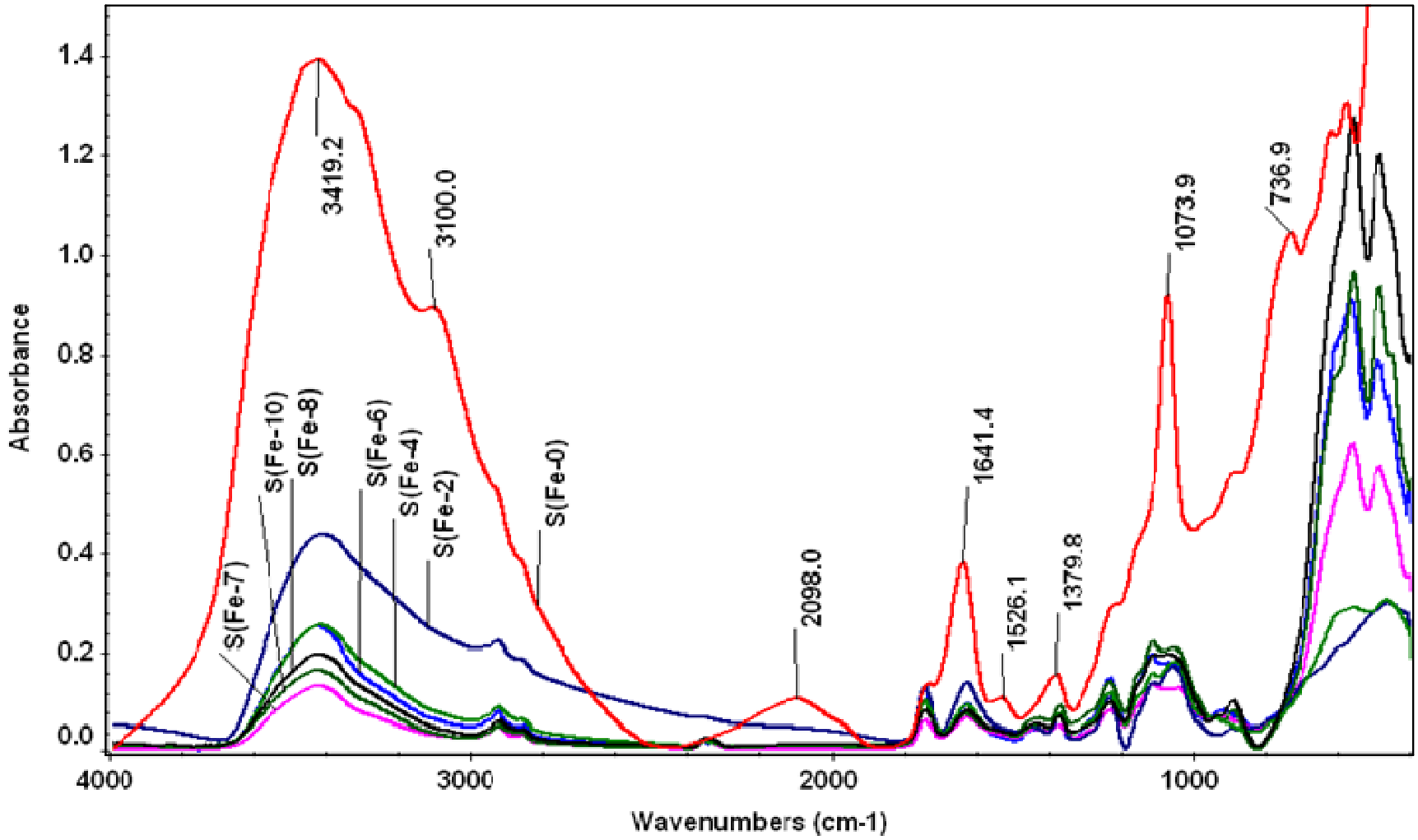

Figure 4.4.14. FTIR analysis of thermally treated electrochemical sludge: Original sludge [S(Fe-0), sludge calcined at 400^{o}C [S(Fe-4)], 600^{o}C [S(Fe-6)], 700^{o}C [S(Fe-7)], 800^{o}C [S(Fe-8)], and 1000^{o}C [S(Fe-10).

The performance of iron oxide NCMs for dye degradation depends upon its textural and other physico-chemical characteristics along with various types of vacancies (oxygen or cation or anion) created during the substitution of iron by another metal in iron oxide NCMs (Figure 4.4.15b) [Huang et al., 2001; Xue et al., 2009].

Transition metal ions generally substitute each other depending upon the principal of similar ionic radius, however, they may have same or one or two unit difference in the oxidation states e.g., octahedral Fe^{3+} replaced by Cr^{3+} in $Fe_{3-x}Cr_xO_4$ (64.5 pm vs. 61.5 pm) [Magalhaes et al., 2007], and tetrahedral Fe^{2+} replaced by Ni^{2+} (78 pm vs. 69 pm) [Costa et al., 2006] and Fe^{3+} by Ti^{4+} and V^{3+} in $Fe_{3-x-y}Ti_xV_yO_4$ (64.5 pm vs. 60.5 and 64 pm) [Liang et al., 2012]. For aliovalent substitutions, depending upon the amount of replacement, reduction of same amount of Fe^{3+} to Fe^{2+} may take place on the basis of electrovalence equilibrium [Pearce et al., 2010; Zhong et al., 2013]. However in the absence of reduction, the structural dislocations get adjusted by inducing oxygen vacancies. These oxygen vacancies also behave as the active sites for hydroxyl radical generation along with the metal ions [Moura et al., 2006]. Generally, the cations of octahedral sites are chiefly responsible for the catalytic activity and are about totally located on the surface of the crystal in the spinel structures [Jacobs et al., 1999]. First, they change the characteristics of the catalyst with respect to the active sites for enhanced pollutant degradation. Second, they are directly involved in co-oxidation processes via the conjugation of redox pairs and their efficient role in generation of active species (Figure 4.4.15b) [Jacobs et al., 1999; Oliveira et al., 2008]. Magalhaes et al. [2007] reported that the increase in the decolourisation and oxidation rate was because of the introduction of Cr in magnetite structure ($Fe_{2.93}Cr_{0.07}O_4$) and participation of Fe^{3+}/Fe^{2+} and Cr^{2+}/Cr^{3+} pairs in H_2O_2 oxidation. Various authors have also been reported the enhanced dye degradation/decolourisation with metal substituted iron oxides as compared to pure iron oxides [Costa et al., 2003].

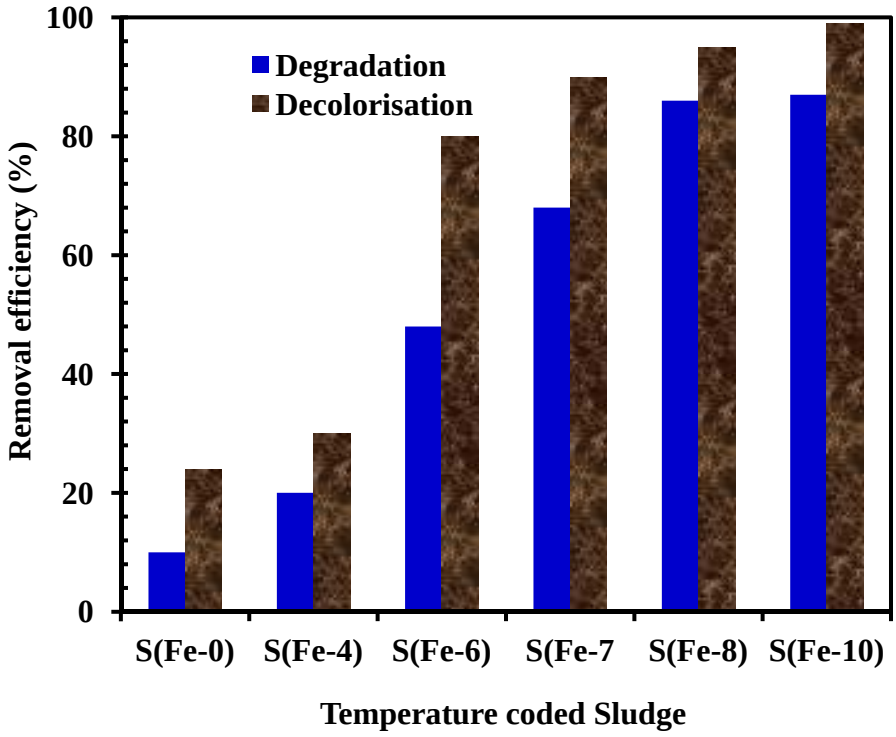

(a)

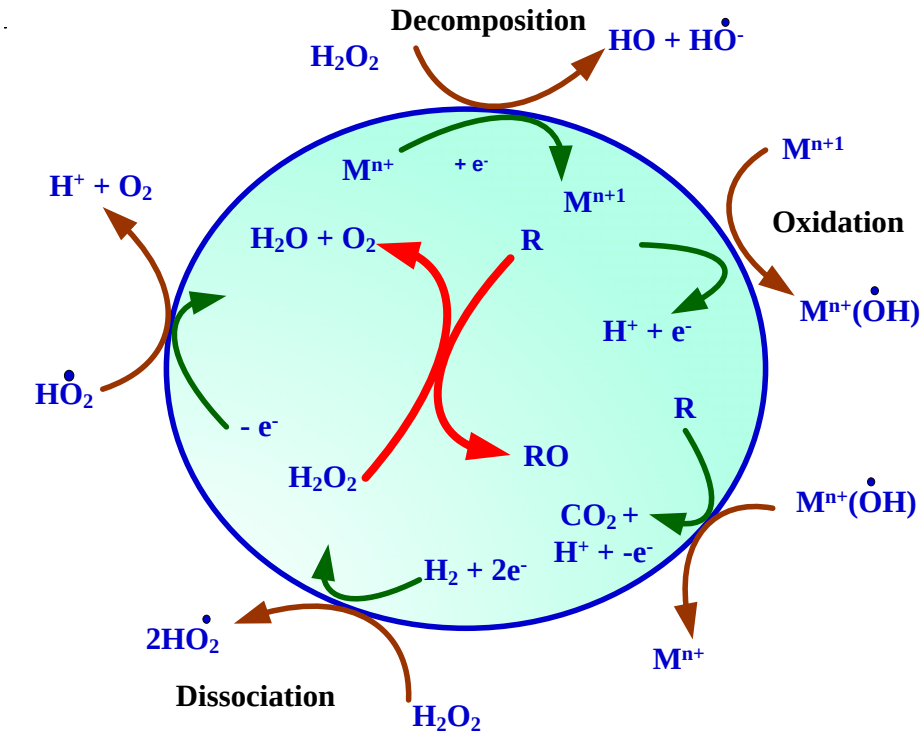

(b)

Figure 4.4.15. (a) Degradation and decolorisation efficiency with sludge sample at different temperature, (b) catalytic activity of iron nano-composite materials in dye degradation during wet per-oxidation.

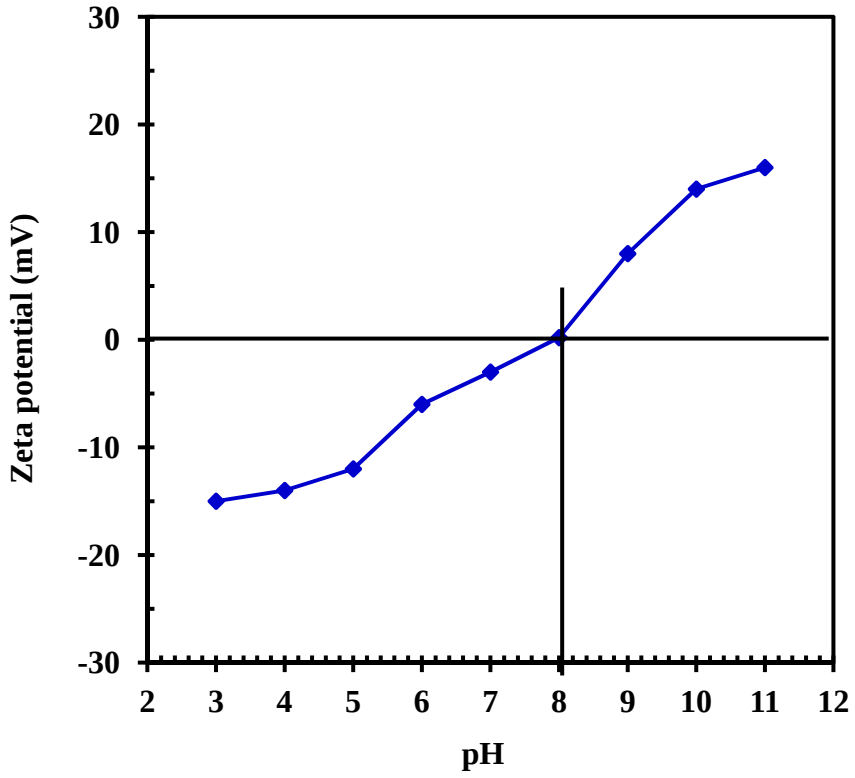

Figure 4.4.16. Zeta potential of iron oxide NCM, S(Fe-8), in distilled water at different pH.

4.4.2 Characterisation of nano materials (NMs) recycling by the conversion of aluminium electrode EC sludge

Alumina nano-materials of different morphology (α-Al_2O_3, β-Al_2O_3, γ-Al_2O_3 and both α,β-Al_2O_3) were prepared from aluminum electrode generated EC sludge by thermal heating method. EC sludge was calcined in muffle furnace at different temperatures and different time duration. Changes in characteristic properties and color of sludge were confirmed by thermal analysis (TG/DTA) and powder x-ray diffraction (PXD) analysis. After optimization of the thermal treatment conditions, the resulting materials were characterized by textural analysis such as scanning and transmission electron microscopy (SEM and TEM), selected area electron diffraction (SAED), atomic force microscopy (AFM), and Fourier-transform infrared (FTIR) analysis. The catalytic activity of NMs was checked by the basic green dye degradation during wet per-oxidation method.

4.4.2.1. Thermogravimetric analysis

The thermal analysis profile of aluminium sludge samples (calcined at 100 and 1000^{o}C coded as Al-100 and Al-1000, respectively) is shown in Figures 4.4.17a and 4.4.17b. For Al-100, dehydration and decarboylation of alumina sludge takes place from 200 to 450^{o}C in primary and secondary combustion zone. However, mass loss was continuous up to 1000^{o}C. Two clear endothermic peaks at 350 and 410^{o}C indicate the elimination of water and decomposition of carbonaceous substances of sludge (Figure 4.4.17b) [Cunha et al., 2014]. Mass loss of 65% was observed in the second degradation zone. Rest of mass loss from 400 to 1000^{o}C was very small.

The weight loss of Al-1000 sample is negligible as the sample exists in pure form. Well defined exothermic peak around 800^{o}C was also obtained in both samples and it can be associated with transformation of Al-sludge into nano alumina without any weight loss. The position of endothermic and exothermic peaks, intensity as well as width is the main difference between the Al-100 and Al-1000 sludge (Figure 4.4.17a and 4.4.17b). These differences are related to the change in morphology of initial compound Al-100 to Al-1000^{o}C heated compound. However, the diffuse broad exothermic peak position of Al-100 shift from 350 ^{o}C towards 210 ^{o}C and becomes single large broad in Al-1000 sample. TGA/DTA analysis results show that crystallization of different phases takes place when aluminum electrode generated EC sludge is heated at higher temperature [Alphonse et al., 2005; Nampi et al., 2011; Bleta et al., 2012].

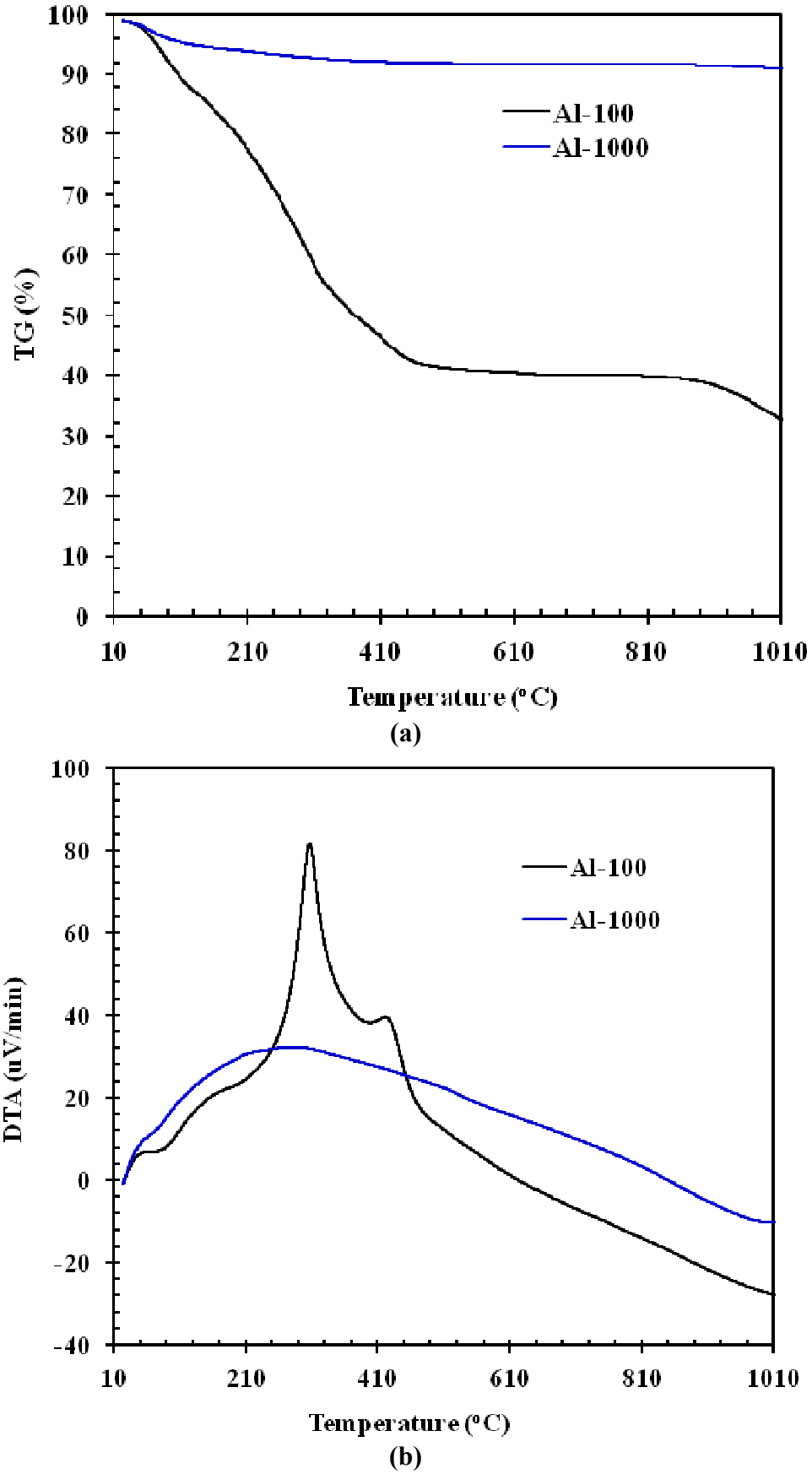

Figure 4.4.17.Thermogravimetric (a) TGA (b) DTA analysis of electrochemical alumina sludge Al-100 and Al-1000.

4.4.2.2. Powder X-ray diffraction (PXD) analysis

Analysis of the powder X-ray diffraction (PXD) patterns indicates the formation of crystalline phases only in those samples which were heated at 700°C and above (Figure 4.4.18 and Figure 4.4.19). EC sludge was incinerated at different temperature ranging from 100-1000°C initially and further at higher temperature upto 1200°C. Original sludge was dried at 100°C (Al-100) and was calcined at 200°C (Al-200), 400°C (Al-400), 500°C (Al-500), 600°C (Al-600), 700°C (Al-700) and 1000°C (Al-1000). Besides we have also heated samples at higher temperature and other duration. These are 1000°C/8 h, 1100°C/1 h, 1100°C/6 h, 1100°C/18 h, 1200°C/3 h and longer. On further heating up to 1200°C, no further change in the PXD patterns was observed suggesting that no additional phase evolution took place and not any change in the particle size and crystallinity of the sample was observed (Figure 4.4.18).

Analysis of PXD pattern indicates that the crystallinity in amorphous sludge sample increases around at 700°C. Phase analysis of the PXD pattern obtained at 1000°C shows presence of Al_2O_3 (γ-Al_2O_3, JCPDS-PDF #50-0741) type phase. The data of PXD pattern of γ-Al_2O_3 is given in Table 4.4.4. Heating the samples beyond 1000°C leads to interesting phase formation with variation of temperature and duration. By operating the temperature and duration we could stabilize a mixed corundum Al_2O_3 (α-Al_2O_3, JCPDS-PDF #46-1222) and hexagonal Al_2O_3 (β-Al_2O_3 a stoichiometric compound of sodium aluminates, JCPDS-PDF #46-1222) type phases. The data of PXD pattern of α-Al_2O_3 and β-Al_2O_3 is given in Tables 4.4.4 and 4.4.5, respectively. By carefully studying the phase evolution as a function of temperature and duration, we are able to stabilize β- Al_2O_3 as a major phase with minimum quantities of α-Al_2O_3. Similarly, stabilization of α-Al_2O_3 as a major phase with minor β-Al_2O_3 has been achieved. Further, we have also stabilized α and β-Al_2O_3 mixed phase where both α and β phases are present in nearly equal proportion. This was also confirmed from the X-ray intensity data.

The detailed of PXD pattern data analysis of different phases of Al_2O_3 is shown in Tables 4.4.4 and 4.4.5. The peaks observed at 1000°C in the PXD pattern arising due to the γ-Al_2O_3 type phase was indexable in the $fd\bar{3}m$ space group with least-square refinement of the lattice parameter gave the refined parameter a = 7.8943(3) Å. Similarly, maximum peaks observed in the PXD pattern of sample calcined at 1150°C at 6 h were due to the α-

Al_2O_3 (corondum) type phase. These peaks were indexable in the rhombohedral $R\bar{3}c$ space group with least-square refinement of the lattice parameter gaving the refined parameter *a* = 4.7528(3) Å, *c* = 12.992(8) Å. Maximum peaks observed in the PXD pattern of sample calcined at at 1150°C for 1 h were due to the due to the β-Al_2O_3 type phase which were indexable in the hexagonal $P6_3/mmC$ space group with a least-square refinement of the lattice parameter gaving the refined parameter as: *a* = 5.64(8) Å, *c* = 22.65(5) for β -Al_2O_3 type phase [Losocha annd Lewinski, 1994]. Least square parameters were similar to the observed parameters. However, the sample heated at 1150°C for18 h was found to give both α-Al_2O_3 and β-Al_2O_3 phases in nearly equally quantity (shown in Figure 4.4.18). After heating the same at same (1150°C) for longer duration and temperature above 1150°C upto 1200°C, no change in phase was observed (Figure 4.4.18). However, the possibility of a phase evolution and transition was takes place at different temperature and different time duration [Lan et al., 2013]. The phase identity and (*hkl)* indexing of α-Al_2O_3 and β -Al_2O_3 along with respective crystal structures are shown in Figure 4.4.19 and Figure 4.4.20.

Figure 4.4.18 indicates that the relatively crystallinity observed at lower temperature was lower while high temperature calcination increases the crystallinity and gives narrow and well-defined mixed pattern diffraction peaks. Figure 4.4.19 shows the diffraction pattern and hkl value of different γ-Al_2O_3, α-Al_2O_3 and β-Al_2O_3 and mixed α and β-Al_2O_3 phases (Table 4.4.4 and 4.4.5). PXD pattern of different calcined samples represent the narrow and well defined diffraction peaks with higher crystalline nature of materials at 1150°C for 1 h and 6 h samples. The difference between the PXD spectra of different samples was obtained by comparing the results of diffraction spectra.

PXD analysis (Figure 4.4.19 and 4.4.20) show that as the calcination temperature and time of calcination increases, the peak intensity increases along with decrease in the peaks width. A higher calcination temperature enhances atomic mobility, causes grain growth, and results in better crystallinity [Lopez-Delgado et al., 2012]. Figure 4.4.18 and Figure 4.4.19 indicates that each phase attained a maximum stable phase at fixed temperature and duration after which negligible changes in phase conversion was observed.

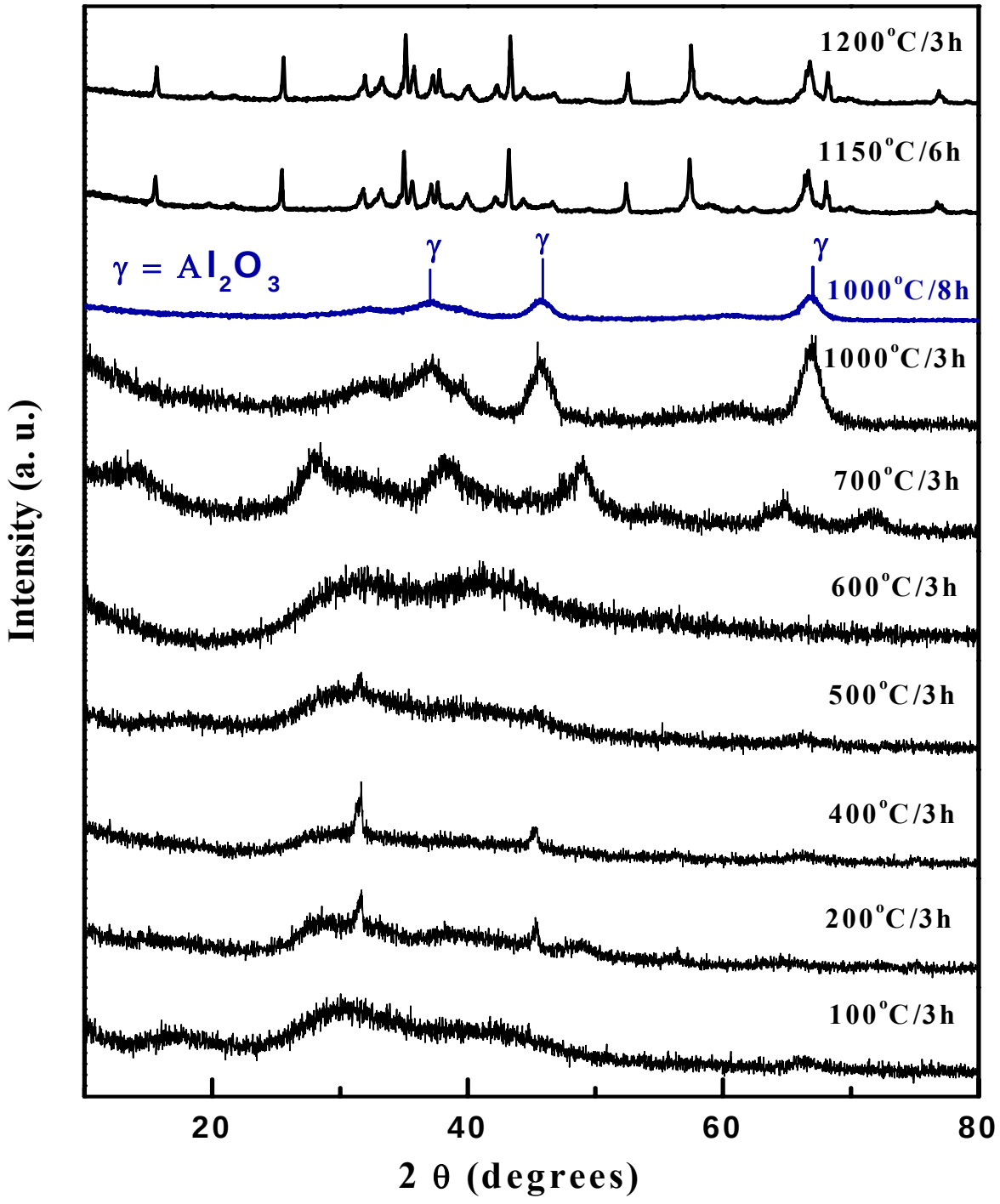

Figure 4.4.18. PXD patterns of thermally treated EC alumina sludge at different temperature and different duration.

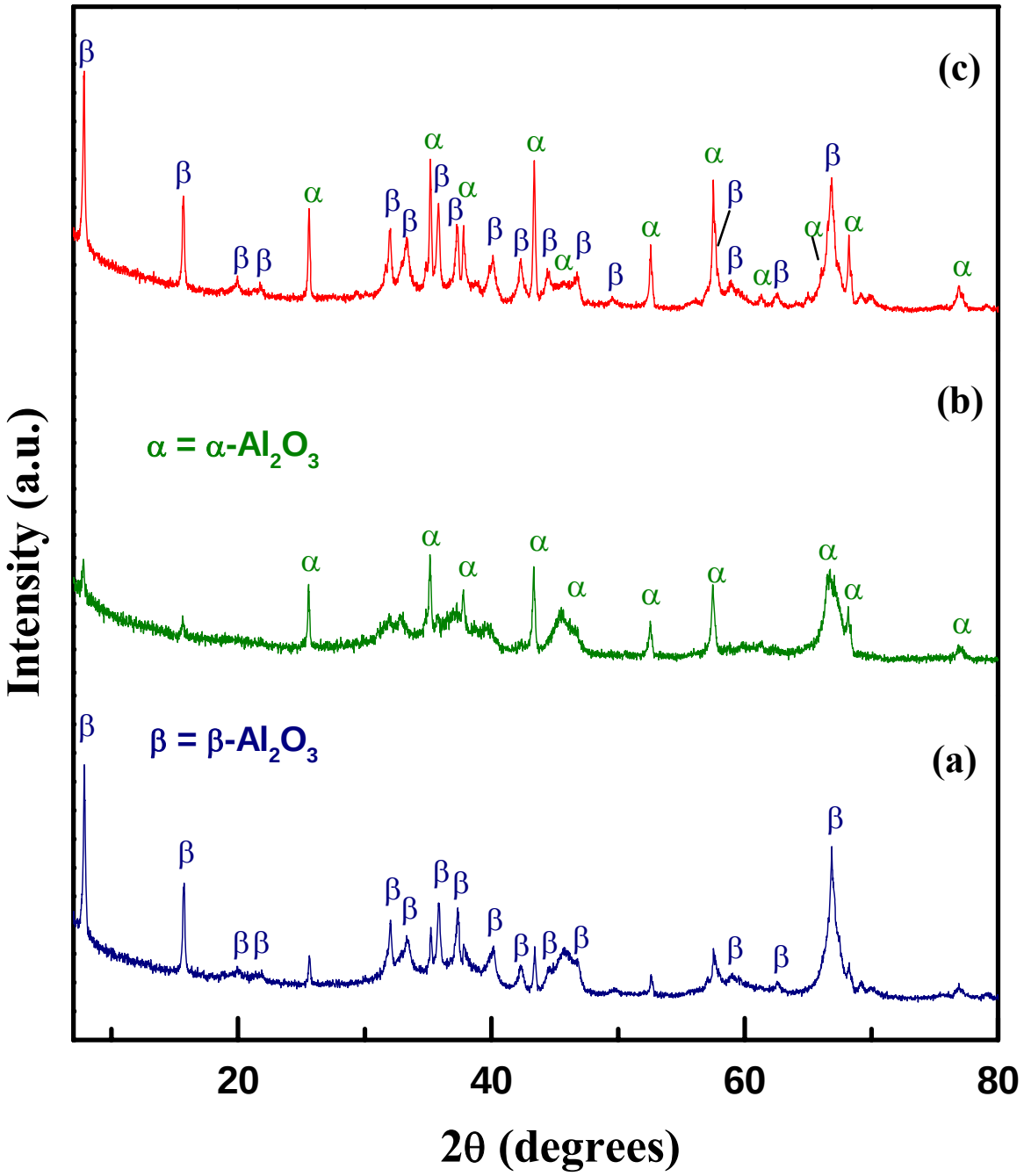

Figure 4.4.19. Indexed PXD pattern (a) gamma alumina (γ-Al_2O_3), (b) alpha alumina (α-Al_2O_3) and (c) beta alumina (β-Al_2O_3) and (d) alpha and beta (α-β-Al_2O_3) type phase.

Table 4.4.4. Powder XRD data for γ-Al_2O_3 and α-Al_2O_3

γ-Al_2O_3					
h	***k***	***l***	d_{obs}(Å)	d_{obs}(Å)	I_{obs}
2	2	0	2.7850	2.7910	32.13
3	1	1	2.3790	2.3802	37.81
4	0	0	1.9760	1.9760	45.92
5	1	1	1.5200	1.5192	60.95
4	4	0	1.3950	1.3955	67.09
α-Al_2O_3					
0	1	2	3.4810	3.481	25.58
1	0	4	2.5514	2.551	35.17
1	1	0	2.3808	2.380	37.78
0	0	6	2.1658	2.165	41.70
1	1	3	2.0861	2.086	43.37
2	0	2	1.9655	1.964	46.18
0	2	4	1.7406	1.740	52.57
1	1	6	1.6016	1.601	57.54
2	1	1	1.5475	1.547	59.75
0	1	8	1.5110	1.511	61.35
2	1	4	1.4048	1.405	66.56
3	0	0	1.3741	1.374	68.25
2	0	8	1.2756	1.275	74.36
1	0	10	1.2390	1.239	76.95
1	1	9	1.2345	1.234	77.28

Table 4.4.5. Powder XRD data for β-Al_2O_3

β-Al_2O_3					
h	***k***	***l***	d_{obs}(Å)	d_{obs}(Å)	I_{obs}
0	0	2	11.3247	11.314	7.80
0	0	4	5.6665	5.6574	15.63
1	0	2	4.4600	4.4548	19.90
1	0	3	4.0789	4.0772	21.78
1	0	6	2.9728	2.9764	30.05
0	0	8	2.8296	2.8287	31.61
1	1	0	2.7979	2.7979	31.98
1	0	7	2.6915	2.6893	33.28
1	1	4	2.5087	2.5080	35.79
2	0	1	2.4100	2.4093	37.31
0	0	10	2.2650	2.2629	39.79
1	1	6	2.2493	1.4050	66.56
2	0	4	2.2298	1.3740	68.25
2	0	5	2.1363	2.1362	42.30
2	0	6	2.0383	2.0386	44.44
2	0	7	1.9409	1.9389	46.80
3	0	2	1.5978	1.5991	57.69
3	0	4	1.5534	1.5533	59.50
3	0	6	1.4844	1.4849	62.57
1	1	14	1.3997	1.3996	66.83
2	2	4	1.3583	1.3580	69.15

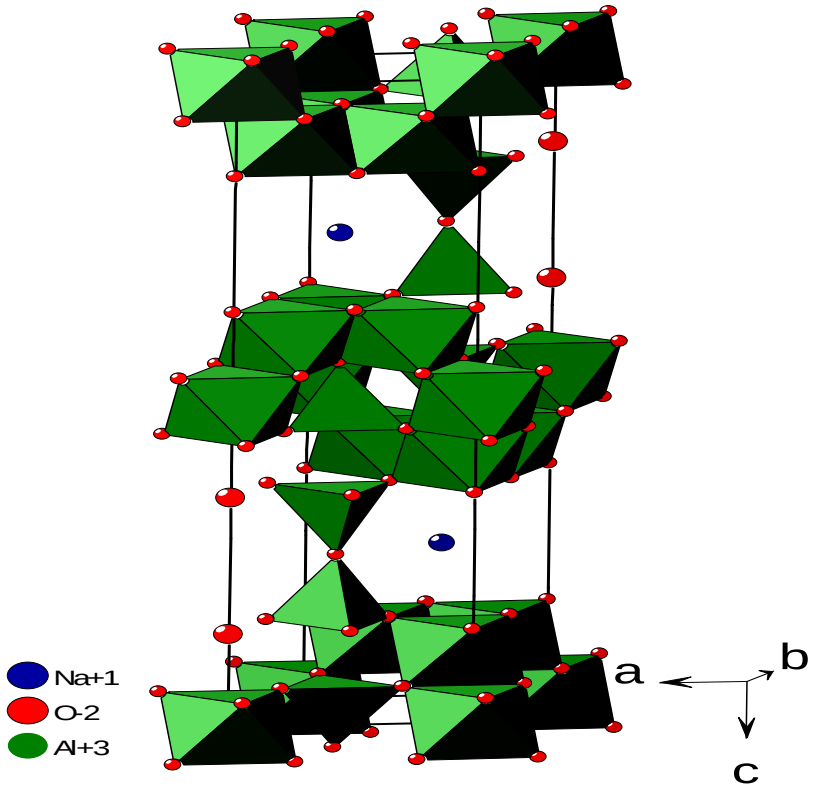

(a)

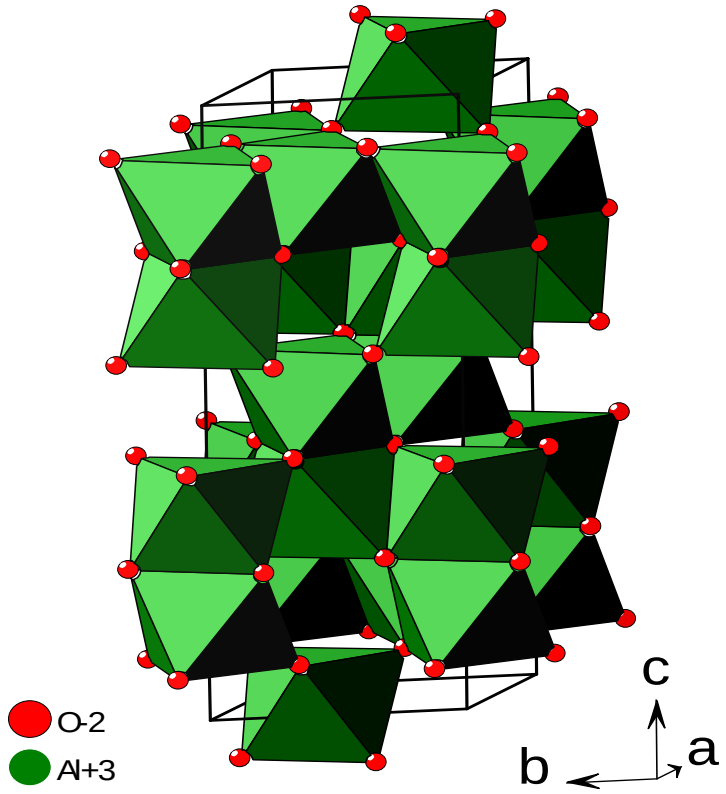

(b)

Figure 4.4.20. (a) Rhombohedral alpha alumina type phase and (b) Hexagonal beta alumina type phase.

4.4.2.3. Brunauer, Emmet and Teller (BET) analysis

Surface area and pore analysis of solid sample is an important characterization technique for understand the solid structure, and potential application of different phases of NMs of alumina. The BET textural analysis of various alumina NMs is shown in Figure 4.4.21. The variation of pore volume, pore area and pore diameter is reported in Table 4.4.6. The order of BET surface area of EC sludge and different phases of alumina NMs was found to be in the following order: Al sludge (390.92m^2/g) > γ-Al_2O_3 (126.76 m^2/g) > α-Al_2O_3 (52.1 m^2/g) > β -Al_2O_3 (41 m^2/g) > α-Al_2O_3 and β -Al_2O_3 (22.11 m^2/g).

Industrial application of the EC sludge generated alumina NMs is likely to be highly dependent upon its pore size distribution analysis. The internal structure and structure heterogeneity of EC sludge and alumina NMs can be determined in terms of pore size distribution with the help of Barret-Joyer-Halenda (BJH) analysis [Park et al., 2005; Afkhami et al., 2011]. BJH pore volume and pore area was found to be in the following order: EC sludge (0.323 cm^3/g) > γ-Al_2O_3 (0.269 cm^3/g) > α-Al_2O_3 (0.104 cm^3/g) > β-Al_2O_3 (0.072 cm^3/g) > α-Al_2O_3 and β-Al_2O_3 (0.042 cm^3/g). Similarly, BJH pore diameter was found to be in the following order: γ-Al_2O_3 (81.89 Å) > α-Al_2O_3 (79.44 Å) > β -Al_2O_3 (67.99 Å) > α-Al_2O_3 and β -Al_2O_3 (64.62 Å) > Al–Sludge (33.59 Å), respectively.

IUPAC classifies various types of pores based on pore diameter (d) as: super-micropores (d < 7Å) < ultra-micropores (7 Å < d < 20 Å) < micropores (d < 20 Å) < mesopores (20 Å < d < 500 Å) < macropores (d > 500 Å). Based on textural analysis, it can be said that all the alumina NPs and EC sludge are belong to meso-porous in nature.

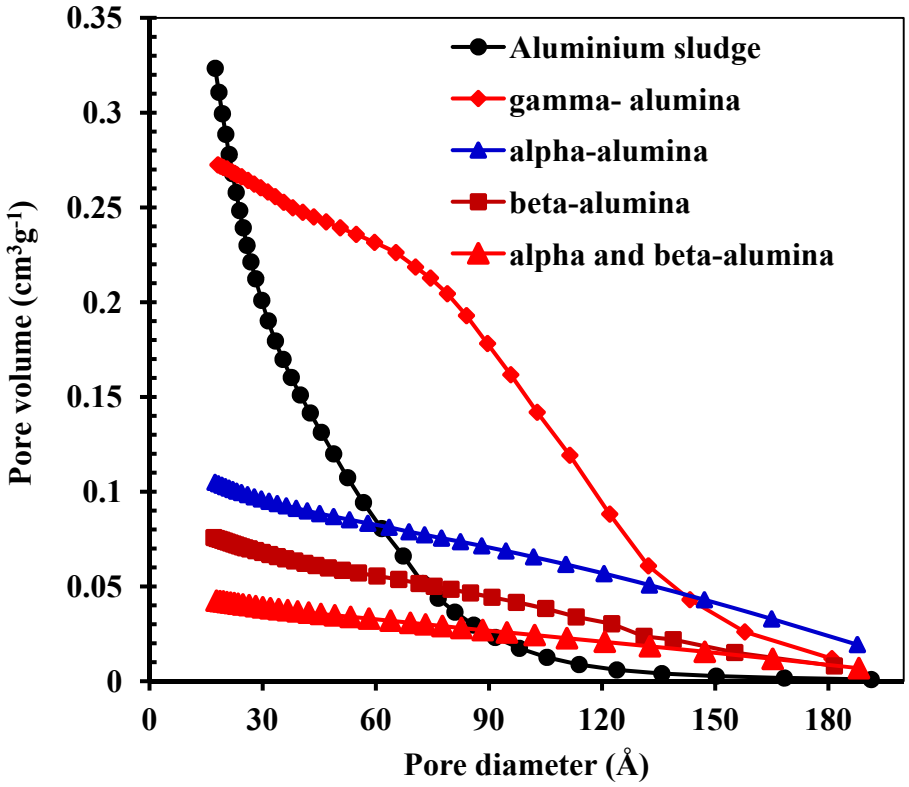

(a)

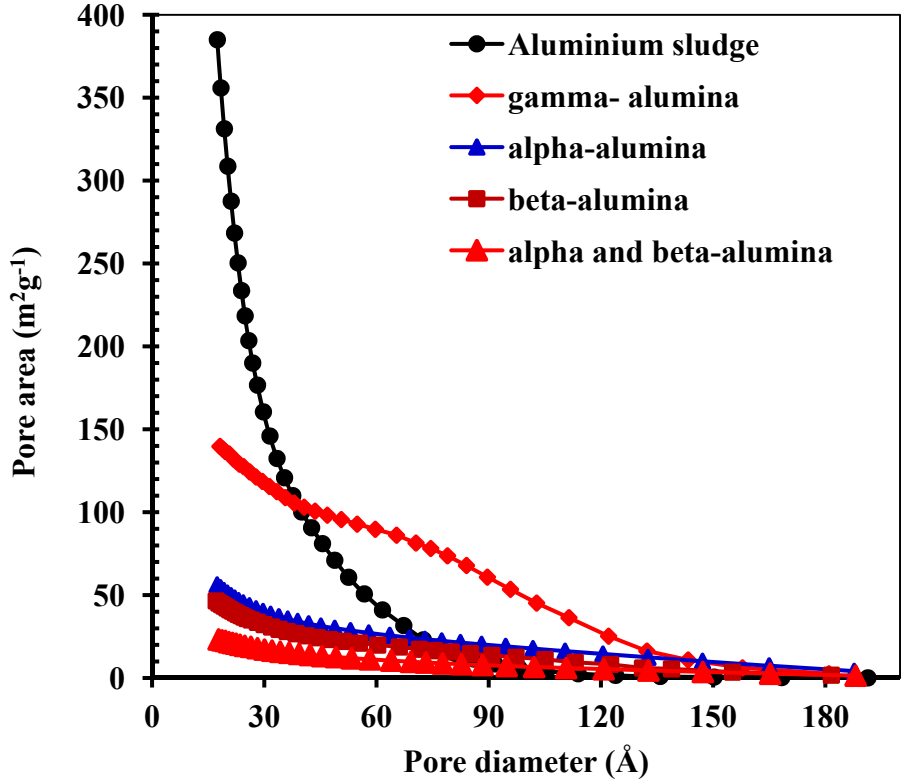

(b)

Figure 4.4.21. Pore size distributions (a) Pore volume and (b) Pore area of original aluminium sludge and different phases of alumina nano-materials.

Table 4.4.6. Textural analysis of the EC generated sludge of aluminium at different temperature and different phases.

Parameters	Original sludge	Gamma phase	Alpha phase	Beta phase	Alpha & beta phase
BET surface area (m^2/g)	390.92	126.7676	52.1076	41.7501	22.111
External surface area (m^2/g)	369.49	119.1992	62.3416	44.1513	23.8892
BJH cumulative surface area of pores (m^2/g)	385.03	131.758	56.232	42.908	23.330
BJH cumulative pores volume (cm^3/g)	0.3234	0.2697	0.1049	0.0729	0.0424
BJH pore diameter (Å)	33.59	81.893	74.623	68.995	64.4437

4.4.2.4. FE-SEM and TEM analysis

FE-SEM was used to identify the morphology of aluminium NMs. The SEM images of original sludge S(Al-100) shows agglomerated particles of 50–200 μm size (Figure 4.4.22). After heating, the crystallinity of sludge increases from 700°C as shown by PXD and the average particle size decreases to 30-35 nm as evidenced by SEM images (Figure 4.4.22). SEM image analysis of alumina NMs at different temperature i.e. 1000°C (Al-1000), 1100°C/1h, 1100°C/6h and 1100°C/18h shows different morphology due to presence of different nano-particles (γ-Al_2O_3, α-Al_2O_3 maximum, β-Al_2O_3 maximum) phases having different shape and sizes.

SEM images of the actual EC sludge and various NMs have different morphologies. Al_2O_3 shows that γ-Al_2O_3 does not possess any well defined porous structure and only few pores are present on its surface (Figure 4.4.22). However, α-Al_2O_3 NM has small round ball shape with quite uniform surface. Similarly, β-Al_2O_3 NM has rods like shape in SEM image with diameters 35−70 nm. NM having both α-Al_2O_3 and β-Al_2O_3 has non-uniform and a mixture of rod and small round ball shaped particles spread in its structure.

Element dispersion in different alumina NMs is shown in Figure 4.4.23 and Figure 4.4.24. The elemental dispersion of α-Al_2O_3 NM (Figure 4.4.23) indicates that Al (61.73%) and oxygen (38.27%) distributed on the surface non-uniformly, with lower and higher elements distribution. β-Al_2O_3, having 62.76% Al and 37.24% oxygen, both elements are cover most of the surface of NMs. However, small humps also observed. Figure 4.4.24 shows 68.08% Al and 31.92% oxygen in mixed α-Al_2O_3 and β-Al_2O_3 phase NM. Elements are uniformly and smoothly distributed on the surface.

Figure 4.4.25 and 4.4.26 shows the TEM images of different alumina NMs at different temperature. Figure 4.4.25 shows that the γ-Al_2O_3 NM forms aggregates of particles lower than 100 nm in size. Selected-area electron diffraction (SAED) inset pattern confirmed presence of small crystalline particles is present in γ-Al_2O_3. SAED indexing pattern of γ-Al_2O_3 shows that it is in amorphous form and not in completely crystalline form. The SAED indexing pattern confirmed the image with PXD *(hkl)* of γ-Al_2O_3 [Alphonse and Courty, 2005]. For α-Al_2O_3, spherical agglomerated particles with particle size around 60 nm can be observed in Figure 4.4.25. SAED pattern of α-Al_2O_3, inset in Figure 4.4.25, indicates that the phase is almost crystalline and aggregate are very small round plates, some of them are arranged in a plane [Jayaraman et al., 1998; Lopez-Delgado et al., 2012]. Similarly, β -Al_2O_3 indicates that most of the particles are tiny small square plate shapes having 30-40 nm particles size. SAED indexing pattern, inset in Figure 4.4.26, confirms the lattice pattern observed with PXD. It was found that most of β-Al_2O_3 have a tendency to present a hexagonal shape which was confirmed by the lattice plane. The SAED indexing pattern of different phases in TEM images was confirmed by comparing the PXD pattern of different phases of alumina (γ-Al_2O_3, α-Al_2O_3 and β -Al_2O_3) respectively (Figure 4.4.18 and 4.4.19) [Alphonse and Courty 2005; Lopez-Delgado et al., 2012]. Crystallinity is very flexible in alumina powder as compared to other ceramic compounds. It was found to vary with change in calcination temperature and duration of heating.

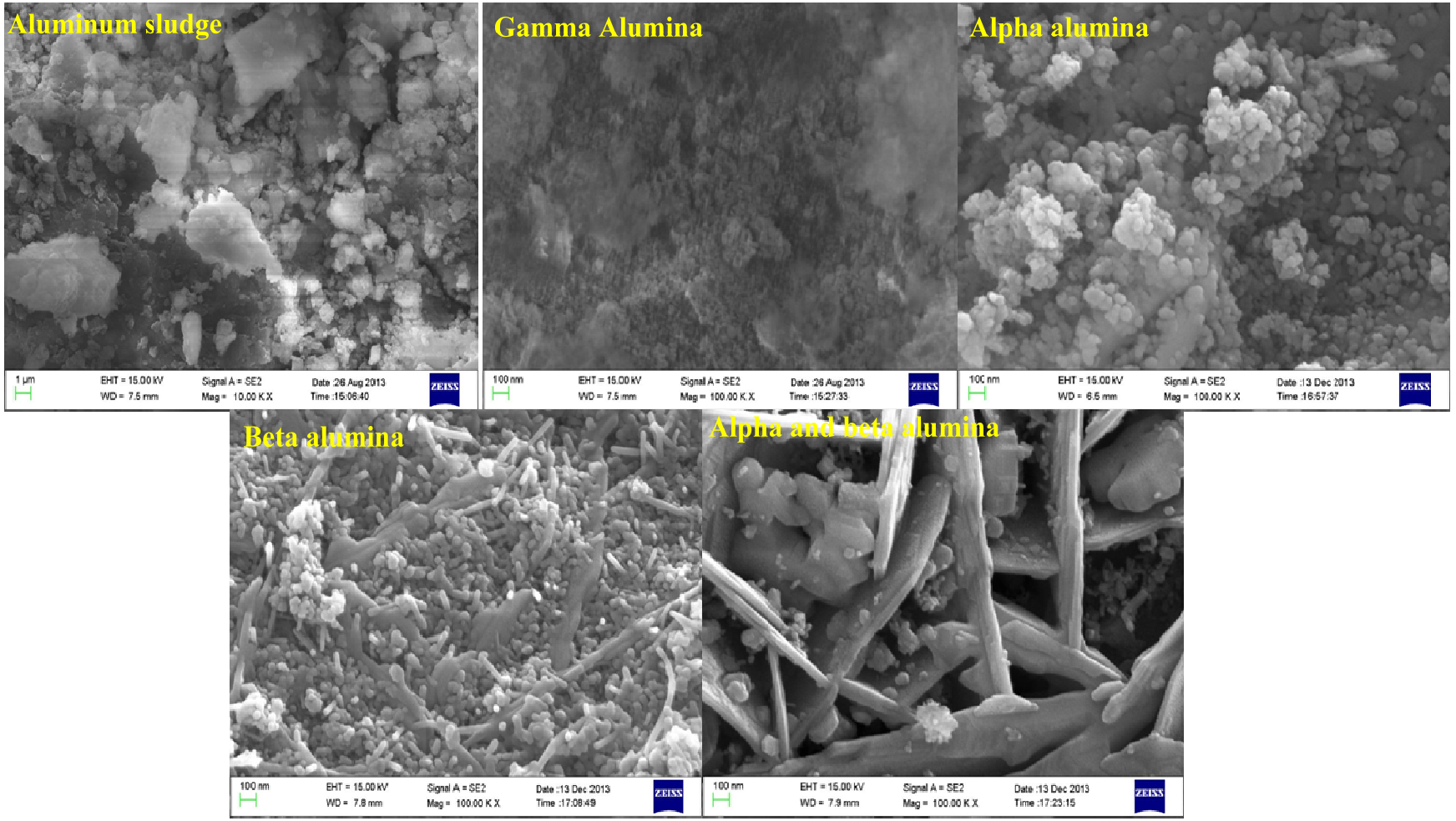

Figure 4.4.22. SEM image of aluminium sludge and different morphology of alumina NMs.

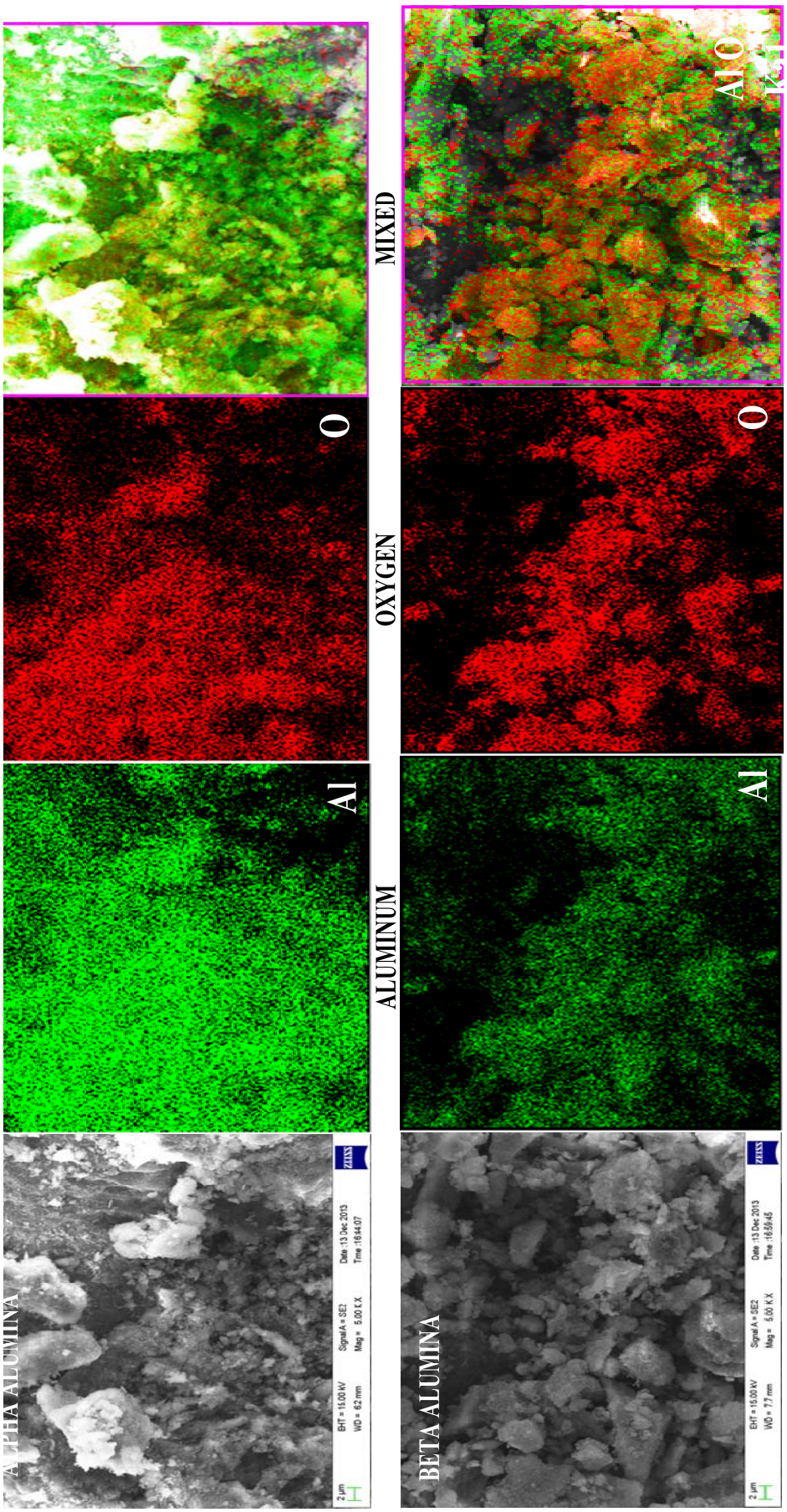

Figure 4.4.23. FE-SEM/EDX elemental dispersion analysis of alpha and beta maximum alumina NPs.

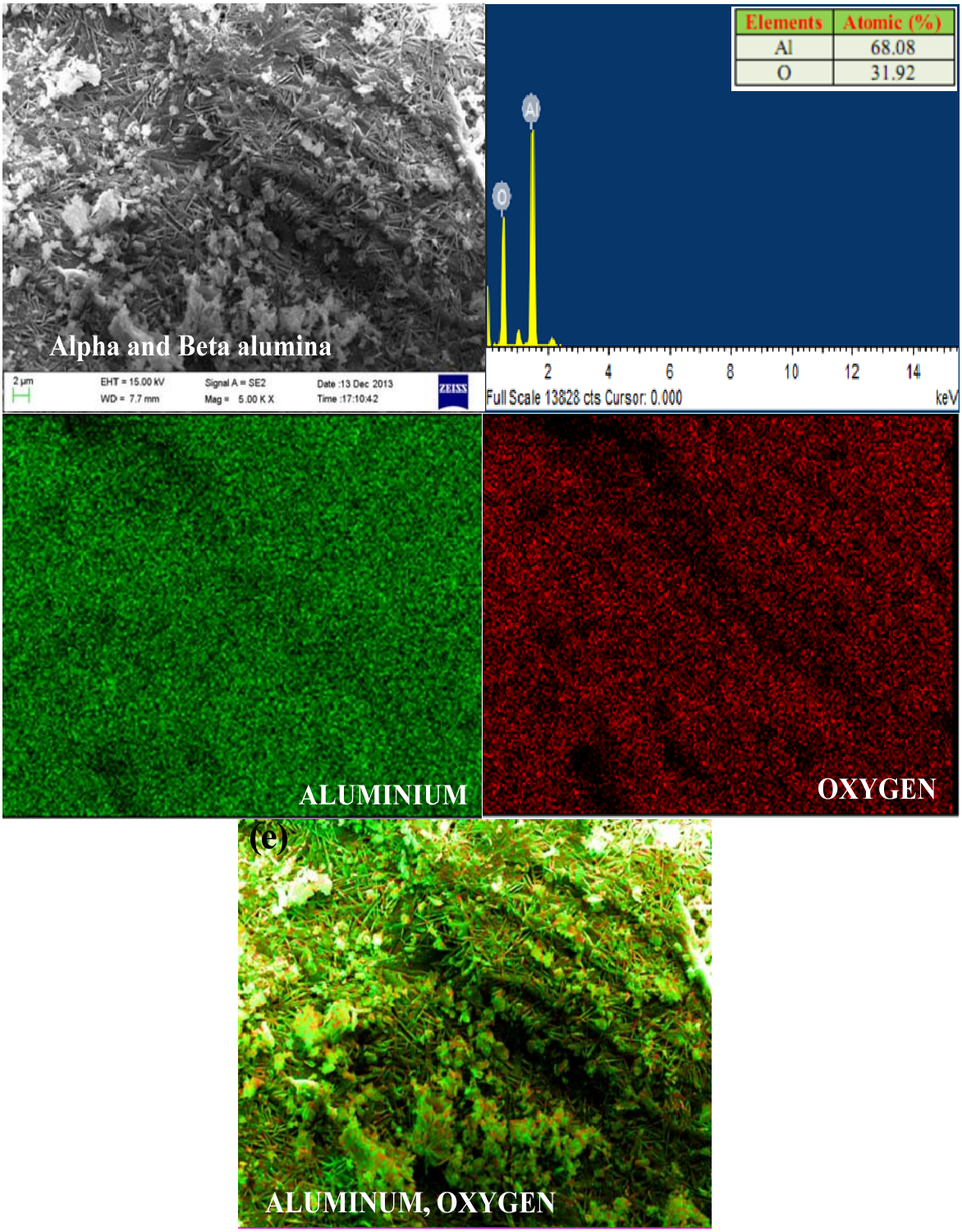

Figure 4.4.24. FE-SEM/EDX and elemental dispersion analysis of both alpha and beta mixed alumina NPs.

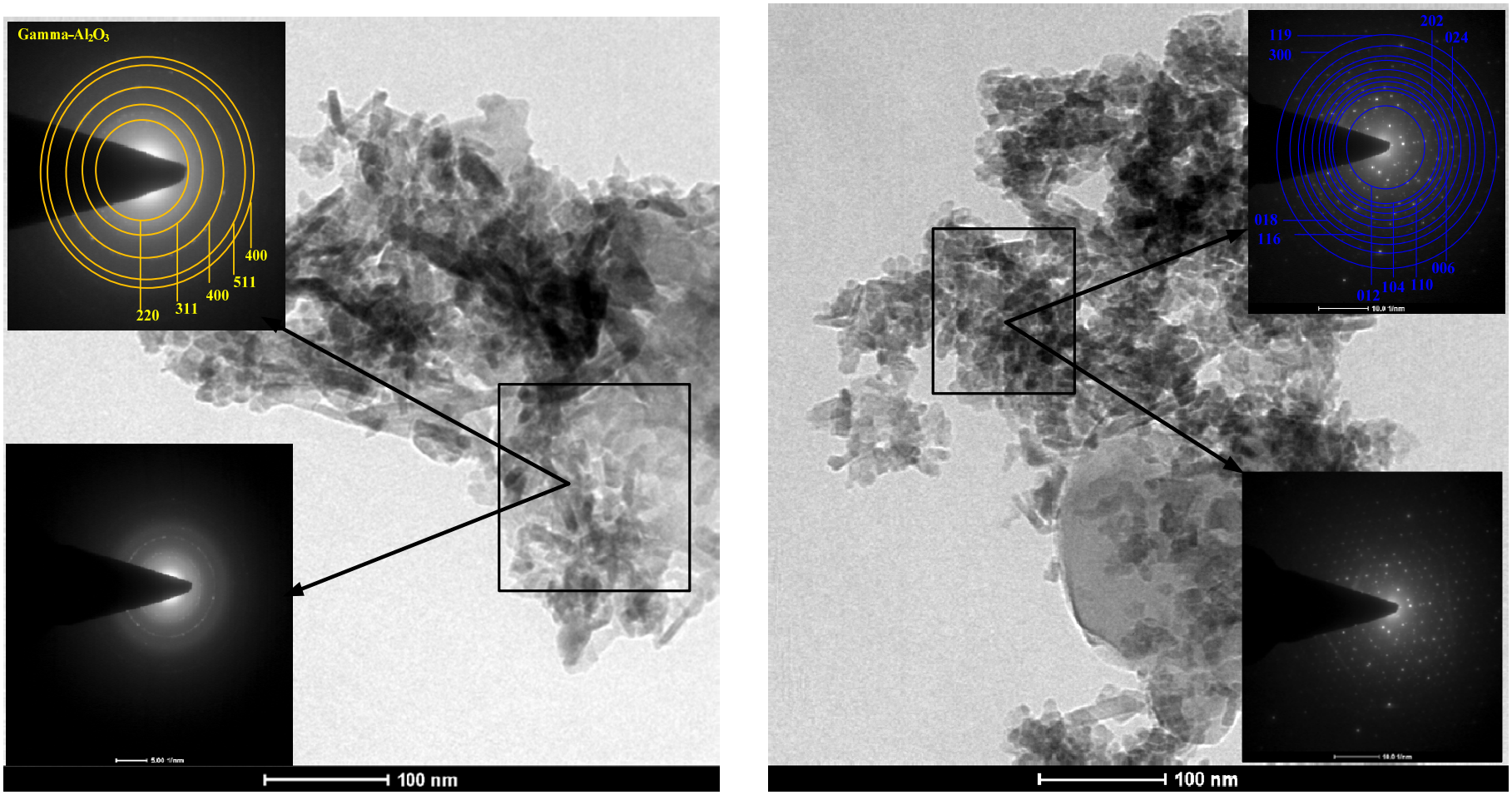

Gamma alumina

Alpha alumina

Figure 4.4.25. TEM image of gamma alumina and alpha alumina nanoparticles (NPs).

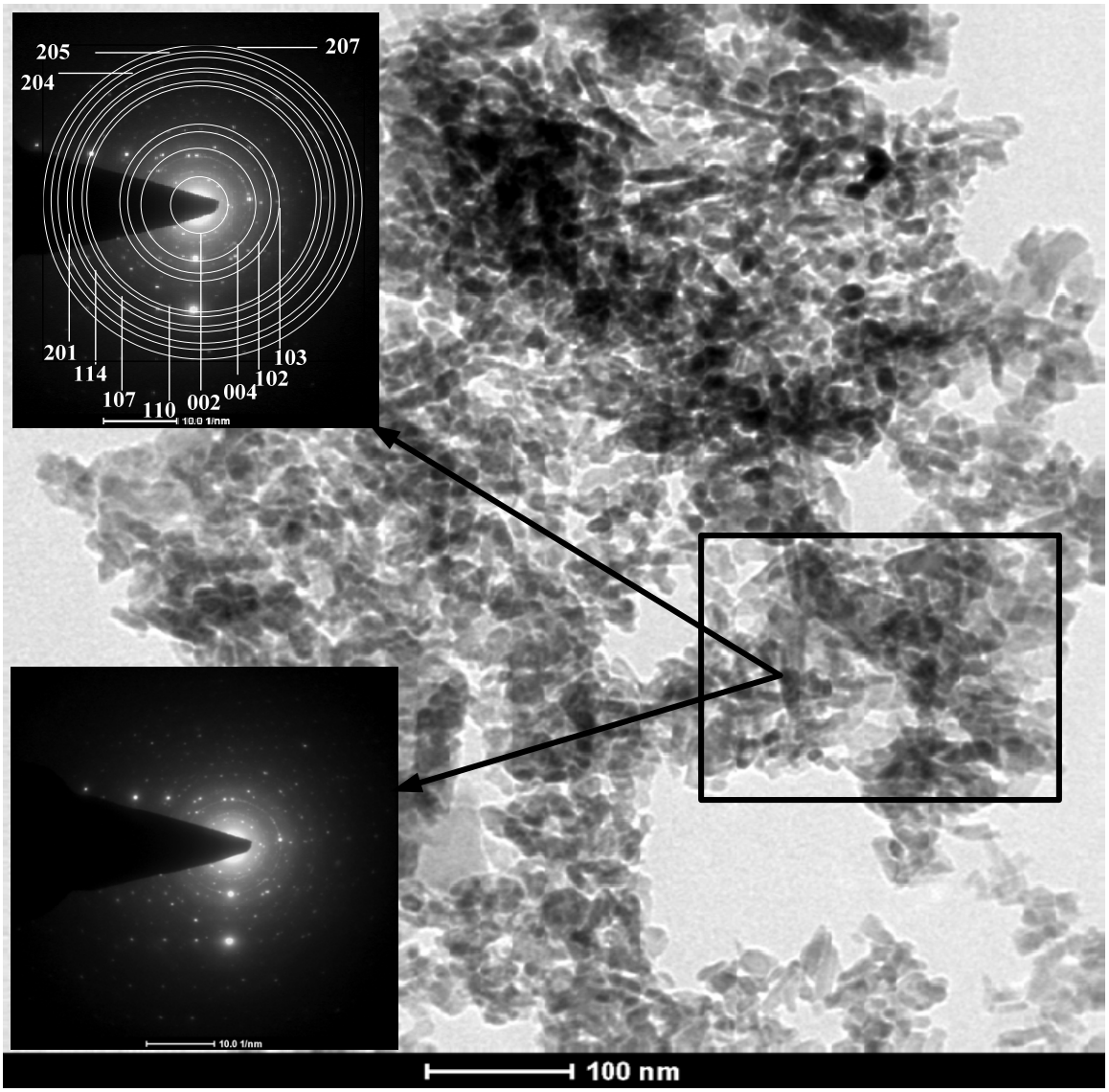

Figure 4.4.26. TEM image of β-Al_2O_3 nanoparticles (NPs).

4.4.2.5. Atomic Force Microscopy (AFM) analysis

SEM does not give an idea of quantitative information about height distributions, roughness and particles after drying in dispersion solution [Zeng et al., 1998]. AFM analysis provides better observation of the aggregation after drying the suspension in solid state. Three-dimensional information of atomic force microscopy (AFM) provides information about alumina nano clusters [Sukmanowski et al., 2005] and ceramic material surface [Vigui et al., 2007]. It is also helpful for the finding out the topography, shape, and size of the nano structure surface.

Figure 4.1.27a shows 2D AFM images of Al-100. It shows non-uniform distribution of bright spots with less heterogeneous distribution of bright spots. 3D AFM image shown in Figure 4.1.27a' shows that the average maximum surface roughness (roughness distribution) was 4.5 nm which decreased with an increase the temperature because of sintering. 2D image of Al-1000 (γ-Al_2O_3 as confirmed by PXD) shown in Figure 4.4.27b indicates that the particles are flat, compact and in regular arrangement. All the particles having almost 60 nm constant height and corresponding to the average diameter of the alumina NPs (Figure 4.4.27b') with 11.46 nm average roughness inset Figure 4.4.27b'. However, if the temperature increases change in phase and morphology of NPs takes place which was confirmed by SEM and TEM analysis. Figure 4.4.28 depict NPs aggregates has fibrillar structure. It may due to the anisotropic physical properties of alumina NPs. The solid state deposited on the surface indicates the quite compact arrangement of the spherical particles in the α-Al_2O_3. 3D image confirmed the 8.0 nm average roughness and 1.6 nm average height of the particles (Figure 4.4.28a and Figure 4.4.28a'). AFM analysis of β-Al_2O_3 was also confirmed in Figure 4.4.28b with small agglomeration between the particles. 3D AFM image confirmed the 4.5 nm average roughness and 0.34 nm average height of the particles (Figure 4.4.28b'). The topography of β-Al_2O_3 in 2D image indicates that the particles could not arrange on a flat layer. However, aggregates arrange in fibrillar structure in which pores inside the structure located at the junctions of spheres and their size is in the same order of size as one particle. Figure 4.4.28c and 4.4.28c' show that the rounded shape particles overlap to each others in mixed α-Al_2O_3 and β-Al_2O_3 phase NM. 3D image of Figure 4.4.28c' shows that maximum height of the particles is 0.74 nm with average surface roughness of 8.0 nm.

4.4.2.6. FTIR Analysis

FTIR spectra of EC treated aluminium sludge at different temperature Al-100, Al-1100 (α-Al_2O_3) and Al-1150 (β-Al_2O_3) is shown in Figure 4.4.29. Band in the range of 2923-2847 cm^{-1} arises due to the stretching vibration of $–CH_3$ group of dye molecules attached in side chain of benzene ring [Singh et al., 2013b,c]. Broad peak at ≈3450 cm^{-1} indicates the presence of -OH and $-NH_2$ group comes from the amine group of dye and water molecules as moisture present in the EC sludge samples. The presence of peaks within the range of 3000 to 3600 cm^{-1} alumina powder are related to the water molecule lattice of alumina powder due to the presence of moisture in KBr pellet. However, some of the new characteristic peaks generate after thermal treatment.

Most of the characteristic peaks of nano-alumina were obtained in finger-print region (1500-400 cm^{-1}) of FTIR spectrum [Afkhami et al., 2011]. In alumina, most of the characteristic peaks of alumina were observed around 802, 760 and 580 cm^{-1} due to OH, Al-OH, and Al-O bonds [Vazquez et al., 1997; Sharma et al., 2010; Lan et al., 2013]. FTIR stretching and bending vibration bands at 610, 650 and 460 cm^{-1} indicate the presence of Al-O presence in each spectra of alumina sample [Zaki et al., 2012]. The peaks in the fingerprint region present a number of peaks (Figure 4.4.29) due to the fundamental modes of vibration of amorphous or nanocrystalline nature of alumina powder [Lopez-Delgado et al., 2012]. These peaks are complex and are very sensitive to the crystallinity of samples.

PXD pattern (Figure 4.4.18 and Figure 4.4.19) confirmed the existence of different crystallography form in alumina powder. Some of the weak band around 1100-1200 cm^{-1} are due to the Al-O bonds [Ram, 2001].

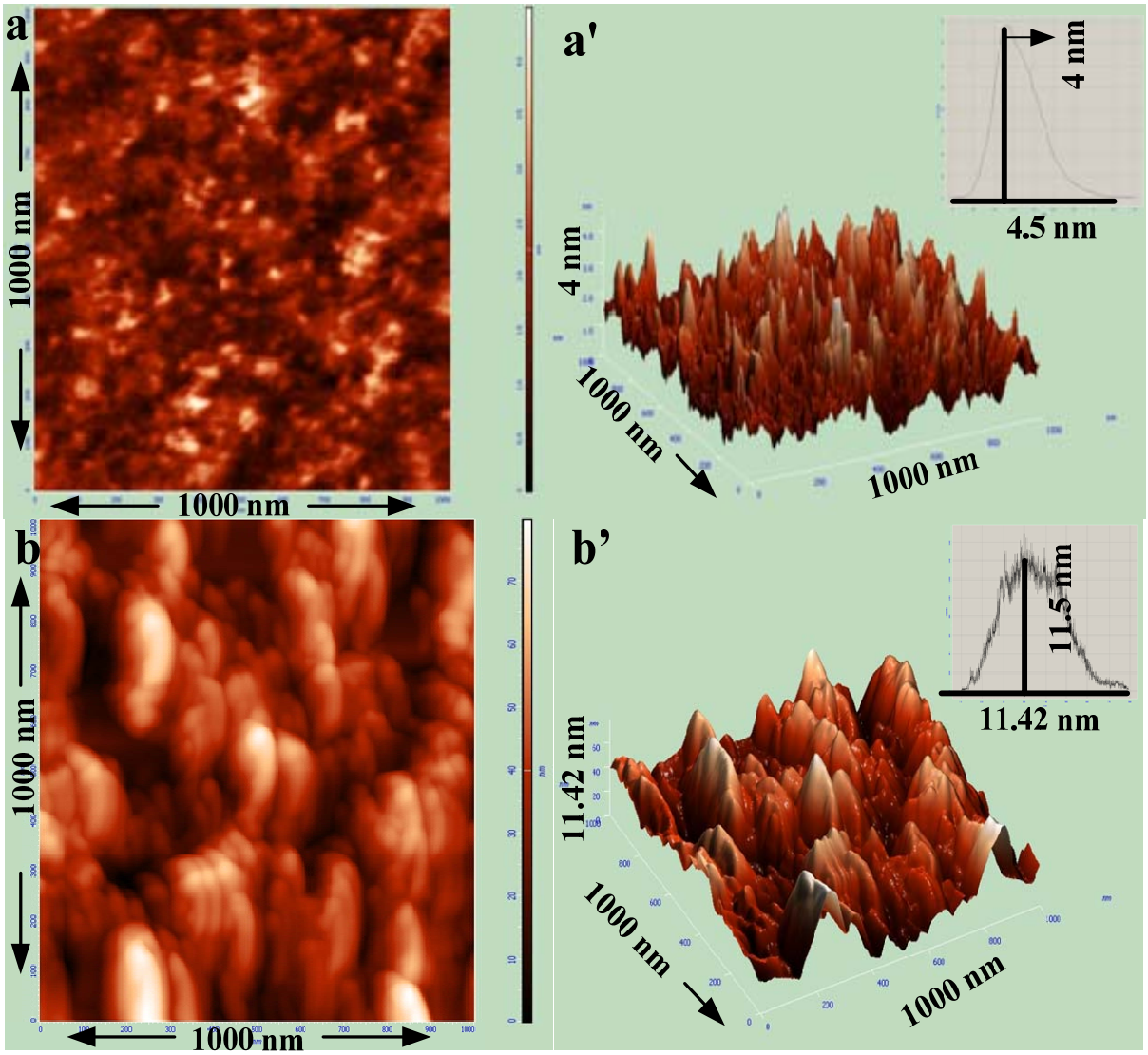

Figure 4.4.27. AFM analysis of alumina sludge (a) 2-D image of aluminium sludge, (a') 3-D image of aluminium sludge, (b) 2-D image of gamma alumina (b') 3-D image of gamma alumina.

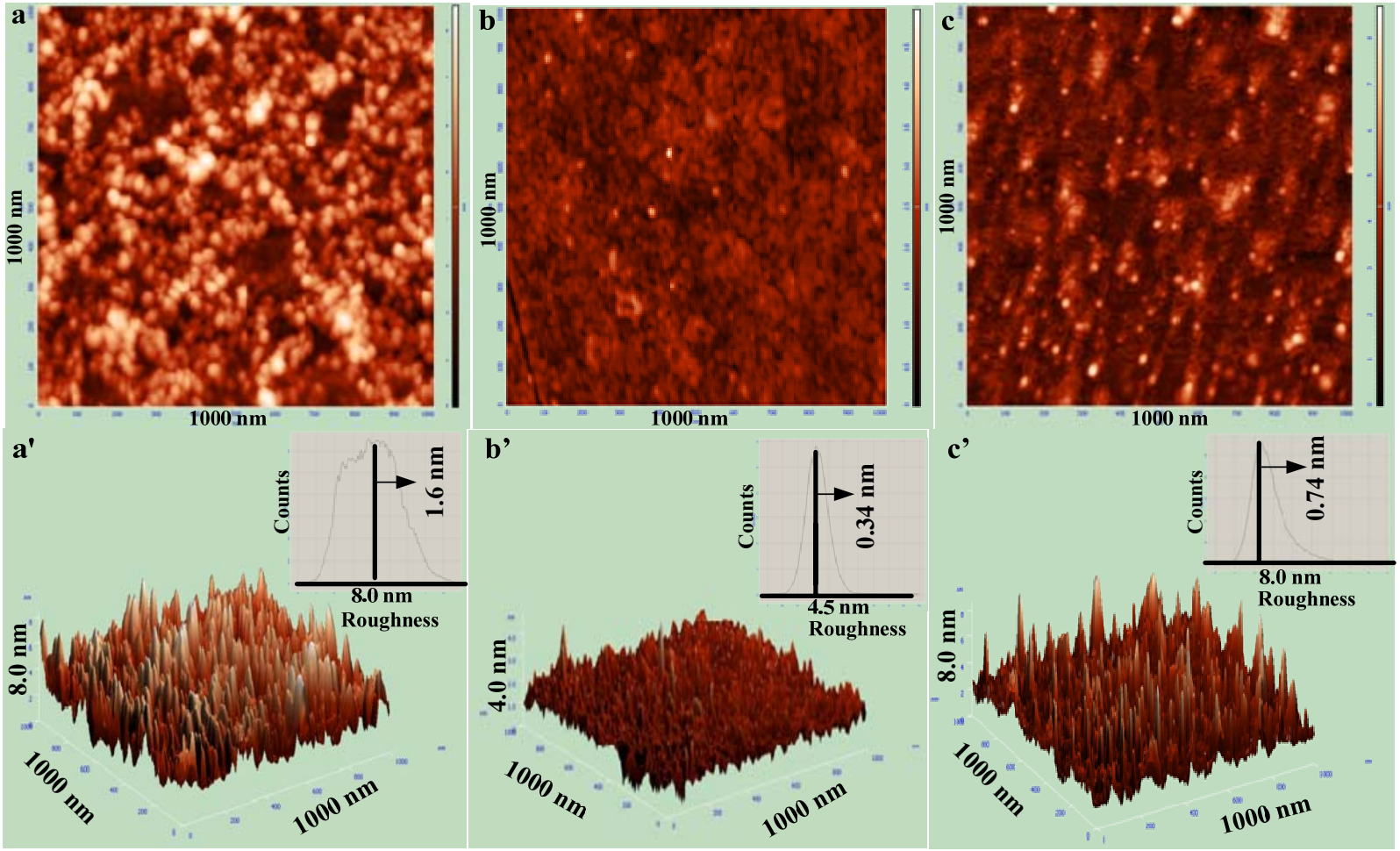

Figure 4.4.28. AFM analysis of alumina nanoparticles at different morphology (a) 2-D image of alpha alumina, (b) 2-D image beta alumina, (c) 2-D image of alpha and beta alumina (a') 3-D image of alpha alumina, (b') 3-D image of beta alumina and (c') 3-D image of alpha and beta alumina.

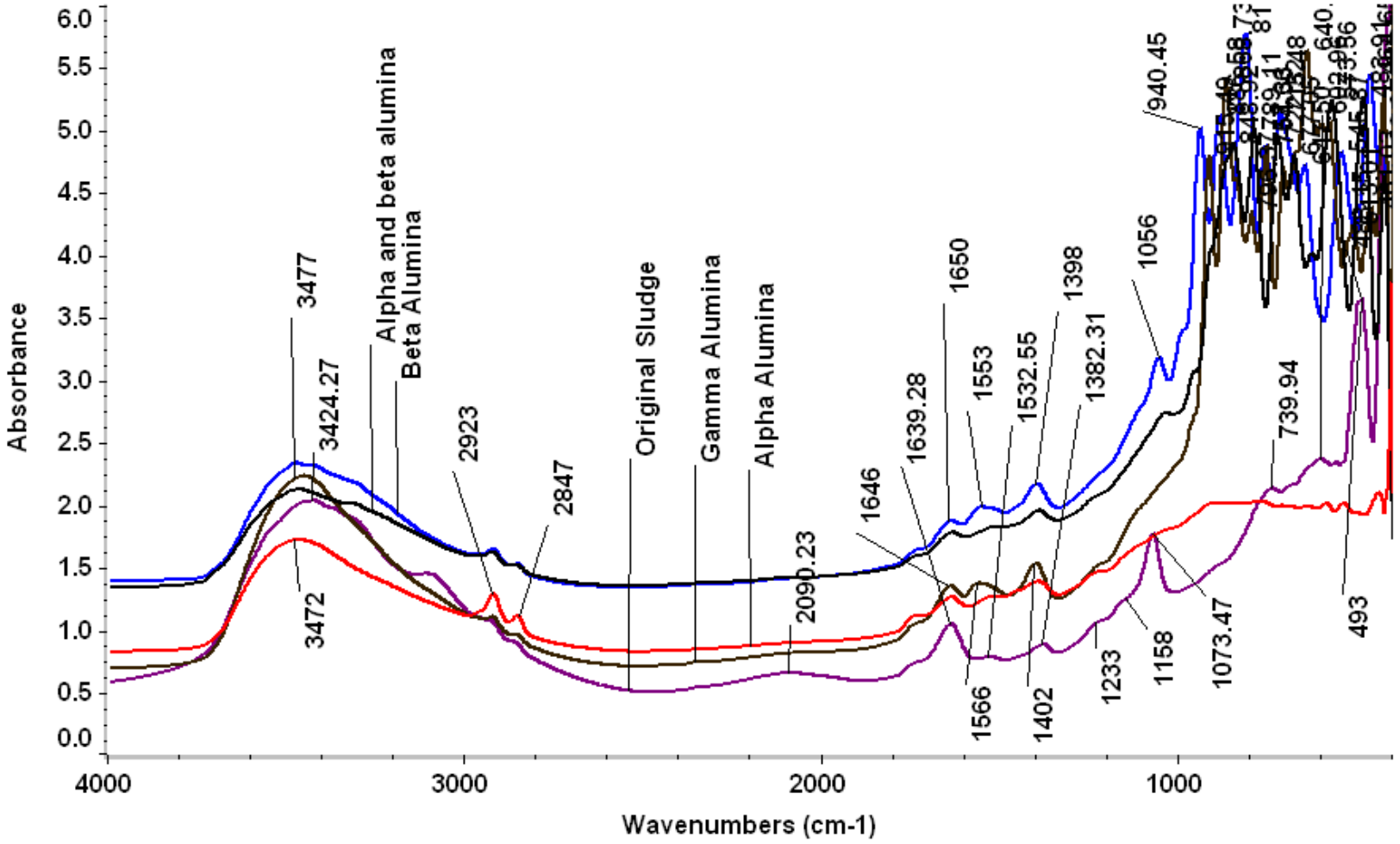

Figure 4.4.29. FTIR analysis of thermally treated electrochemical sludge: sludge at 100°C (Al-100), sludge calcined at 400°C [S(Al-400)], 600°C (Al-600) , 800°C (Al-800), 1000°C (γ-alumina), 1150/6h°C(alpha alumina), 1150/1h°C(beta alumina) and 1150/18h°C(alpha and beta alumina.

4.4.2.7 Catalytic activity of NCMs

Wastewater treatment using catalytic methods has gained significant attention in recent years [Wang et al., 2010]. However, very few studies are available in the literature where alumina NMs derived from solid waste has been used as nano catalyst for dye wastewater treatment. All phases of alumina NMs were tested for their catalytic ability at 45^{o}C for decolorization and degradation of basic green 4 (BG4) dye solution (100 mg/L) at natural pH 5.4 with catalyst dose of 1.0 g/L in presence of H_2O_2 as an initiator. Results are shown in Figure 4.4.30. It may be seen that the β-Al_2O_3 is more reactive as compared to α-Al_2O_3 and α-β Al_2O_3. The order of reactivity of alumina NPs follows as: β-Al_2O_3 > α -Al_2O_3> α-β Al_2O_3. γ-Al_2O_3 was found to posses very less reactivity and therefore, results are not reported here. β-Al_2O_3 has smaller surface area and pore volume than α-Al_2O_3 and γ-Al_2O_3, however, the catalytic activity of β-Al_2O_3 is higher for treatment of BG-4 as compared to other alumina NMs. During catalytic oxidation, alumina NPs provide the catalyst surface (having various functional groups) for initiating the H_2O_2 decomposition into free radicals which subsequently help in dye decomposition via free radical pathways [Legube and Leitner, 1999]. Alumina NPs have good ability to form the hydroxide complex with OH ions and free radicals generated in presence of H_2O_2. Dye degradation begins via H_2O_2 decomposition on the surface of alumina NMs which generates $OH^{\bullet}$ radicals. Higher catalytic activity of β-Al_2O_3 may be due to its different structure and crystallinity as compared to other alumina NMs. This may also be due to acidic nature of β-Al_2O_3.

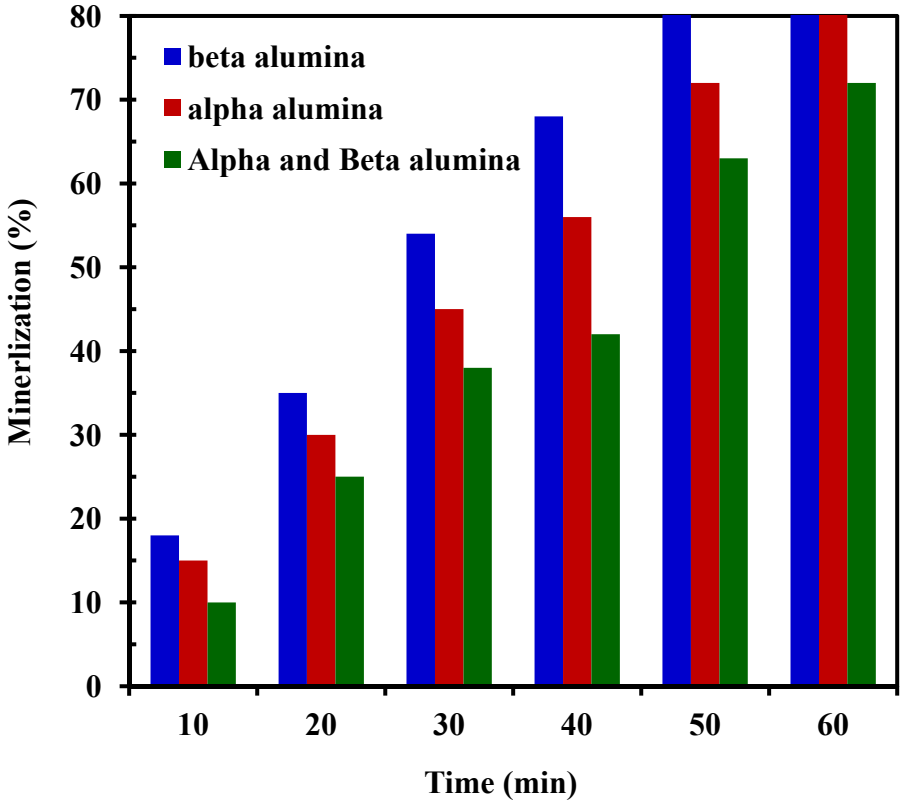

Figure 4.4.30. Removal- efficiency of different alumina NPs at different time intervals.

Chapter –5

CONCLUSIONS & RECOMMENDATIONS

5.1 CONCLUSIONS

On the basis of the results and discussion presented heretofore for the treatment of synthetic and actual dye bearing wastewater (DBW) by using electrochemical (EC) treatment methodology, following major conclusion can be drawn for various sections of studies performed in the present work:

EC treatment of synthetic textile wastewater (STW) containing basic dyes with aluminum electrode:

- In this section, multi-step optimization of EC treatment of synthetic textile wastewater was performed by aluminum electrode. Chemical oxygen demand (COD) and color removal efficiencies were maximized using Plackett-Burman design, steepest accent/descent method and Box-Behnken design.
- Plackett-Burman model has been used as a first step to determine the most important operating parameters. Box–Behnken design was further used to optimize the selected factors so as to achieve maximum COD and color removal efficiencies.
- Analysis of variance was used for developing a polynomial model and graphical response surfaces and contour plots. These were used to locate the optimum point. Maximum COD and color removal efficiency of 70.50% and 98.2%, respectively, was observed at optimum conditions of current density (j)=185.30 A/m^2, time (t)=190 min and initial pH (pH_o)≈5.
- Electro-coagulation and electro-flotation were found to be the main reasons for COD and color removal in STW.
- This study showed that multi-step optimization as adopted in the present study can be used not only for screening and optimizing large number of factors but also these help in studying possible interactions among various parameters.

Dye degradation mechanism of basic dye during EC treatment with aluminum electrode

(a) Mechanistic study using zeta-potential measurement

- In this study, changes in zeta potential were measured during the EC treatment of basic green 4 (BG) dye, a basic acrylic dye with triphenylmethane group, in aqueous solution.

The study was conducted in a batch electro-chemical reactor using the sacrificial aluminum anode.

- The use of aluminum as sacrificial electrode during the EC treatment of BG dye solution was found to be pH dependent processes. Higher value of j and lower value of initial concentration (C_o) were found to be better for higher treatment efficiency. At pH≈6.2 and C_o=100 mg/l, maximum COD, total organic carbon (TOC) and color removal efficiencies were found to be 82.4%, 63.5% and 99.4%, respectively, at j=117.64 A/m^2.
- It was found that the zeta potential of the dye solution was always negative during the treatment. More over, since BG dye itself is positively charged, maximum removal of dye was found to occur at the lowest value of negative zeta potential (-15.2 mV at pH≈6.2), that is, when the concentration of positively charged colloids in the solution were least.

(b) Step-by-step EC mineralization of dye

- In this section, step-by-step EC mineralization of BG was studied during EC treatment with aluminum electrode for understanding the EC degradation mechanism. Each step of degradation was determined by various spectroscopic and chromatographic methods. The intermediates were identified by mass spectroscopic techniques.
- UV–visible and Fourier transform infrared (FTIR) spectroscopy, high performance liquid chromatography (HPLC), gas chromatography–mass spectroscopy (GCMS) and high resolution mass spectroscopy (HRMS) analysis showed that the degradation occurred via the cleavage of conjugated structure and N–de–methylation in presence of •OH radicals.
- During the BG dye degradation, various short–life unstable intermediates were generated which were, on complete mineralization, converted into carbon dioxide, nitrates and easily decomposable small aliphatic compound as shown in last scheme of the present study. The intermediates products identified included hydroxymethylated intermediates during the N–de–methylation of the dye; and N, N, N', N'–tetramethyl–4,4'–diaminobenzophenone; 4, 4'–bis–aminobenzophenone and N–methyl–para–aminophenol after cleavage of conjugated triphenylmethane ring.
- The decolorization rate increased with an increase the pH from acidic to alkaline pH due to conversion of dye to leuco form. Zeta potential study helped to identify the conditions of maximum interaction between the hard acid (Al ions and hydroxides) and basic dye.
- The degradation mechanism of BG dye through EC, as reported in the present study, would be helpful in future application of EC technology for degradation of dyes. EC degradation of other triphenylmethane dyes is likely to be similar to that reported in the

present study, though, type of electrode and operating conditions may affect the degradation mechanism

Electrochemical treatment of real dye bearing effluent

- In this section, EC treatment of actual dye bearing effluent (DBE) was studied with aluminum (Al) and stainless steel (SS) electrodes in different anode-cathode combinations (Al–Al, Al–SS, SS–SS and SS–Al).
- Color, COD, TOC and turbidity removal efficiencies, residual zeta potential, average colloid particle diameter and specific energy consumption values after treatment were in the following order: SS–SS > SS–Al > Al–Al > Al–SS.
- It was found that higher value of j produced higher amount of metallic cationic species which in turn increased the color and COD removal efficiencies because of which zeta potential of the treated DBE moved toward positive value. Charge neutralization and sweep coagulation by respective hydroxides allowed the different particles at come together by van der Waals interaction and adsorption mechanism, respectively. These mechanisms increased the particle size at optimum pH which later on settle to the bottom and cause highest color and COD removal efficiencies.
- At high pH (>9), ClO^- formed via secondary reactions of chlorine direct oxidized the colloidal matter present in DBE.
- BET surface area of sludge was found to be in the following order: Al–Al > Al–SS > SS–SS >SS–Al. However, the trend was opposite for BJH pore volume and pore diameter. All the anode-cathode combinations sludge were meso-porous in nature.
- Thermo-gravimetric analysis showed that the heating value of sludge was about one-tenth of the Indian coal. Because of the good surface area, sludge can be directly used as an adsorbent or can be used for making nano-materials out of them by thermal treatment.

Recycling and disposal studied of EC sludge generated by stainless steel and aluminium electrodes

- In this study, solid waste (sludge) generated during EC treatment of textile industry wastewater with SS and Al electrode was recycled by heating the solid waste at different temperatures under controlled condition to produce nano composite materials (NCMs).
- For NCM prepared from SS sludge, powder X-ray diffraction (PXD), FE-SEM and EDX analyses showed that it contains iron, chromium, nickel and oxygen in the form of α-Fe_2O_3 (metal: oxygen= 40:60), $(Fe,Cr,Ni)_2O_3$ and trevorite $NiFe_2O_4$, $(Ni,Fe,Cr)(Fe,Cr,Ni)_2O_4$ (metal: oxygen = 43:57). TEM and AFM analysis demonstrated different

shape and size distribution of grains in the resulting NCM, which is primarily due to structure and compositional differences of the constituent oxides.

- Similarly, EC generated aluminium sludge can be converted into various types of alumina nanoparticles (α-Al_2O_3, β-Al_2O_3 and γ-Al_2O_3) of different structure, catalytic properties and morphology. Conversion of sludge to various form of alumina was found to be dependent upon calcination temperature and calcination time.
- Degradation studies using the recycled NCMs on dye wastewater showed high removal efficiency and good adaptability.
- A novel approach of recycling and reuse of the sludge generated during EC treatment of a wastewater in the form of NCMs was proposed. The prepared iron oxide NCMs showed excellent performance as a catalyst for further dye degradation during the wet per-oxidation of a dye due to its nanocrystalline nature and highly efficient catalytic properties. The proposed methodology of nanoparticle and NCM preparation not only solves the environmental issue of sludge disposal but also provides a research path for reuse of solid waste as NCMs for wastewater treatment.

5.2 RECOMMENDATIONS

This study has brought forth a number of considerations which may be of interest to pursue further research in the area of EC treatment of dye bearing effluents as also for various other industrial wastewaters. Based on the experiences gained during the present work, following recommendations are being made for future research:

- Other oxidation electrodes like $RuO_2/TiO_2/PbO_2$, etc. may be studied in combinations (anode and cathode) in series and bipolar arrangement for both batch and continuous EC processes.
- Conversion of EC sludge generated after treatment of various other types of wastewaters should be converted to NCMs and NPs for their possible use as potential catalyst.
- For successful industrial application of EC process, quantitative scale-up from batch laboratory scale is required. The key independent scale-up parameters must be identified to ensure dimensional consistency between small and large scale processes.

REFERENCES

Adhoum, N.; Monser, L.; Bellakhal, N.; Belgaied, J.-E. Treatment of electroplating wastewater containing Cu^{2+}, Zn^{2+} and Cr(VI) by electrocoagulation. J. Hazard. Mater. 2004, 112, 207–213.

Afkham, A. A.; Bagheri, H.; Afkhami, T. M. A. Alumina nanoparticles grafted with functional groups as a new adsorbent in efficient removal of formaldehyde from water samples. Desalination 2011, 281, 151–158

Aghaie-Khouzani, M.; Forootanfara, H.; Moshfegha, M.; Khoshayand, M. R.; Faramarzi, M. A. Decolorization of some syhthetic dyes using optimized culture broth of laccase producing ascomycete Paraconiothyrium Variabile. Biochem. Eng. J. 2012, 60, 9–15.

Ahlawat, R.; Srivastava, V. C.; Mall, I. D.; Sinha, S. Investigation of the electrocoagulation treatment of cotton blue dye solution using aluminum electrodes. Clean–Soil Air Water 2008, 36, 863–869.

Akbal, F.; Camcl, S. Treatment of metal plating wastewater by electroco-agulation. Environ. Progress Sustainable Energy 2012, 31 (3), 340-350.

Akbal, F; Kuleyin, A. Decolorization of levafix brilliant blue E-B by electrocoagulation method. Environ. Prog. Sustainable Energy. 2011, 30, (1), 29–36.

Akbari, A.; Desclaux, S.; Rouch, J. C. Aptel, P.; Remigy, J. C. New UV-photografted nanofiltration membranes for the treatment of colored textile dye effluents. J. Membrane Sci. 2006, 286, 342–350.

Al-Aseeri, M.; Bu-Ali, Q.; Haji, S.; Al-Bastaki, N. Removal of acid red and sodium chloride mixture from aqueous solutions using nano-filtration. Desalination 2007, 206, 407–413.

Albuquerque, L. F.; Salgueiro, A. A.; Melo, J. L. Chiavone-Filho, O. Coagulation of indigo blue present in dyeing wastewater using a residual bittern. Sep. Purif. Technol. 2012, 104, 246–249.

Aleboyeh, A.; Daneshvar, N.; Kasiri, M. B. Optimization of C.I. acid red 14 azo dye removal by electrocoagulation batch process with response surface methodology. Chem. Eng. Process. 2008, 47, 827–832.

Ali, I. New Generation Adsorbents for Water Treatment. Chem. Review. 2012, 112, 5073−5091.

Ali, N.; Hameed, A.; Ahmed, S.; Khan, A. G. Decolorization of structurally different textile dyes by Aspergillus niger SA1. World J. Microbiol. Biotechnol. 2008, 24, 1067–1072.

Alinsafi, A.; Khemis, M.; Pons, M. N.; Leclerc, J. P.; Yaacoub, A.; Benhammou, A.; Nejmeddine, A. Electro-coagulation of reactive textile dyes and textile wastewater. Chem. Eng. Process. 2005, 44, 461–470.

Alphonse, P.; Courty, M. Structure and thermal behavior of nanocrystalline bohemite. Thermochim. Acta 2005, 425 (2), 75–89.

Amani-Ghadima, A. R.; Oladc, A. A.; Ashassi-Sorkhabi, H. Optimization of electrocoagulation process for removal of an azo dye using response surface methodology and investigation on the occurrence of destructive side reactions. Chem. Eng. Process. 2013, 64, 68–78.

Amini, M.; Younesi, H.; Bahramifar, N.; Zinatizadeh Lorestani, A. A.; Ghorbani, F.; Daneshi, A.; Sharifzadeh, M. Application of response surface methodology for optimization of lead biosorption in an aqueous solution by Aspergillus niger. J. Hazard. Mater. 2008, 154, 694-702.

Andersena, W. C.; Turnipseeda, S. B.; Karbiwnyka, C. M.; Leeb, R. H.; Clark, B. S.; Rowe, W. D.; Madson, M. R.; Miller, K. E. Multiresidue method for the triphenylmethane dyes in fish: Malachite green, crystal (gentian) violet, and brilliant green. Analytica Chim. Acta 2009, 637, 279–289.

Aoudj, S.; Khelifab, A.; Drouichea, N.; Hecini, M.; Hamitouche, H. Electrocoagulation process applied to wastewater containing dyes from textile industry. Chem. Eng. Process. 2010, 49, 1176–1182.

Aouni, A.; Fersi, C.; Cuartas-Uribe, B.; Bes-Pia, A.; Alcaina-Miranda, M. I.; Dhahbi, M. Reactive dyes rejection and textile effluent treatment study using ultrafiltration and nanofiltration processes. Desalination 2012, 297, 87–96.

Arslan, I.; Balcioglu, I. A.; Bahnemann, D. W. Advanced chemical oxidation of reactive dyes in simulated dye house effluents by Ferrioxalate-Fenton/UV-A and TiO_2-UV-A processes. Dyes and Pigments 2000, 47, 207–218.

Arslan-Alaton, I.; Kabdas, I.; Vardar, I.; Tunay, B. O. Electro-coagulation of simulated reactive dye bath effluent with aluminum and stainless steel electrodes. J. Hazard. Mater. 2009, 164, 1586–1594.

Ayed, L.; Mahdhi, A.; Chere, A.; Bakhrou, A. Decolorization and degradation of azo dye Methyl Red by an isolated Sphingomonas paucimobilis: Biotoxicity and metabolites characterization. Desalination 2011, 274, 272–277.

Azadi, P.; Carrasquillo-Flores, R.; Pagan-Torres, Y. J.; Gurbuz, E. I.; Farnood, R.; Dumesic, J. A. Catalytic conversion of biomass using solvents derived from lignin. Green Chem. 2012, 14(6), 1573-1576.

Azadi, P.; Inderwildi, O.; Farnood, R.; Kinh, D. Liquid fuels, hydrogen and chemicals from lignin: A critical review. Renewable Sustainable Energy Reviews 2013, 21, 506-523.

Balasubramanian, N.; Kojima, T.; Srinivasakannan, C. Arsenic removal through electrocoagulation: kinetic and statistical modeling. Chem. Eng. J., 2009, 155, 76-82.

Banerjee, K.; Helwick, R. P.; Gupta, S. A treatment process for removal of mixed inorganic and organic arsenic species from groundwater. Environ. Progress. 1999, 18, 280–284.

Banerjee, P.; Das Gupta, S.; De, S. Removal of dye from aqueous solution using a combination of advanced oxidation process and nanofiltration. J. Hazard. Mater. 2007, 140, 95-103.

Barret, E. P.; Joyer, L. G.; Halenda, P. P. The determination of pore volume and area distributions in porous substances: Computations from nitrogen isotherms. J. Am. Chem. Soc. 1951, 73, 373-380.

Basha, C. A.; Sendhil, J.; Selvakuma, K. V.; Muniswaran, P. K. A.; Lee, C. W. Electrochemical degradation of textile dyeing industry effluent in batch and flow reactor systems. Desalination 2012, 285, 188–197.

Bassandeh, M.; Antony, A.; Le-Clech, P.; Richardson, D.; Leslie. G. Evaluation of ion exchange resins for the removal of dissolved organic matter from biologically treated paper mill effluent. Chemosphere 2013, 90(4), 1461-1469.

Bayramoglu, G.; Arica, M. Y. Biosorption of benzidine based textile dyes Direct Blue 1 and Direct Red 128 using native and heat-treated biomass of Trametes versicolor. J. Hazard. Mater. 2007, 143 (1-2), 135-143.

Bayramoglu, M.; Kobya M.; Can, O. T.; Sozbir, M. Operating cost analysis of electrocoagulation of textile dye wastewater. Sep. Purif. Technol. 2004, 37, 117–125.

Beckett, R.; Le, N. P. The role of organic matter and ionic composition in determining the surface charge of suspended particles in natural waters. Colloids and Surfaces 1990, 44, 35-49.

Behnajady, M. A.; Modirshahla, N.; Shokri, M.; Vahid, B. Effect of operational parameters on degradation of Malachite Green by ultrasonic irradiation. Ultrasonics Sonochem. 2008, 15, 1009–1014.

Bhatnagar, R.; Joshi, H.; Mall, I. D.; Srivastava, V. C. Electrochemical treatment of acrylic dye-bearing textile wastewater: Optimization of operating parameters. Desalination and Water Treatment 2013, 52(1-3), 111–122.

Bleta, R.; Alphonse, P.; Pin, L.; Gressier, M.; Menu, M. An efficient route to aqueous phase synthesis of nanocrystalline y-Al2O3 with high porosity: from stable bohemite colloids to large pore mesoporous alumina. J. Colloid Interface Sci. 2012, 367 (1), 120–128.

Boumaza, A.; Favaro, L.; Ledion, J.; Sattonnay, G.; Brubach, J. B.; Berthet, P.; Huntz, A. M.; Roy, P.; Tetot, R. Transition alumina phases induced by heat treatment of boehmite: An X-ray diffraction and infrared spectroscopy study. J. Solid State Chem. 2009, 182, 1171–1176.

Boyd, J. M.; Hrudey, S. E.; Richardson, S. D.; Li, X. F. solid-phase extraction and high-performance liquid chromatography mass spectrometry analysis of nitrosamines in treated drinking water and wastewater. Trends in analytical chemistry. Elsevier Science Ltd, New York, NY, 2011, 30 (9), 1410-1421.

Cameselle, Ch.; Pazos, M.; Sanroman. M. A. Selection of an electrolyte to enhance the electrochemical decolourisation of indigo: optimisation and scale-up. Chemosphere 2005, 60, 1080–1086.

Can, O. T.; Bayramoglu, M.; Kobya, M. Decolorization of reactive dye solutions by electrocoagulation using aluminum electrodes. Ind. Eng. Chem. Res. 2003, 42, 3391-3396.

Can, O. T.; Kobya, M.; Demirbas, E.; Bayramoglu, M. Treatment of the textile wastewater by combined electrocoagulation. Chemosphere 2006, 62, 181–187.

Canizares, P.; Carmona, M.; Lobato, J.; Martınez, F.; Rodrigo, M. A. Electrodissolution of aluminum electrodes in electrocoagulation processes. Ind. Eng. Chem. Res. 2005, 44, 4178–4185.

Canizares, P.; Jimenez, C.; Martınez, F.; Saez, C.; Rodrigo, M. A. Study of the Electrocoagulation Process Using Aluminum and Iron Electrodes. Ind. Eng. Chem. Res. 2007, 46, 6189-6195.

Canizares, P.; Martinez, F.; Carlos, J.; Lobato, J.; Rodrigo, M. A. Coagulation and electrocoagulation of wastes polluted with dyes. Environ. Sci. Technol. 2006a, 40, 6418–6424.

Canizares, P.; Martinez, F.; Jimenez, C.; Lobato, J.; Rodrigo, M. A. Comparison of the aluminum speciation in chemical and electrochemical dosing processes. Ind. Eng. Chem. Res. 2006b, 45, 8749–8756.

Charoenlarp, K.; Choyphan, W. Reuse of dye wastewater through color removal with electrocoagulation process. Asian J. Energy and Environ. 2009, 10 (4), 250-260.

Chen, C. C.; Lu, C. S.; Chung, Y. C.; Jan, J. L. UV light induced photodegradation of malachite green on TiO_2 nanoparticles. J. Hazard. Mater. 2007a, 141, 520–528.

Chen, C.; Lu, C. S. Photocatalytic Degradation of Basic Violet 4: Degradation Efficiency, Product Distribution, and Mechanisms. J. Phys. Chem. C 2007b, 111, 13922–13932.

Chen, C.–H.; Chang, C.–F.; Liu, S.–M. Partial degradation mechanisms of malachite green and methyl violet B by Shewanella decolorationis NTOU1 under anaerobic conditions J. Hazard. Mater. 2010, 177, 281–289.

Chen, C.–Y.; Kuo, J.–T.; Chen, C.–Y.; Huang, Y.–T.; Hob, I.–H.; Chung, Y.–C. Biological decolorization of dye solution containing malachite green by Pandoraea pulmonicola YC32 using a batch and continuous system. J. Hazard. Mater. 2009, 172, 1439–1445.

Chen, H.; He, J. Facile synthesis of monodisperse manganese oxide nanostructures and their application in water treatment. J. Phys. Chem. C 2008, 112, 17540–17545.

Chen, K. C.; Wu, J. Y.; Huang, C. C.; Liang, Y. M.; Hwang, S. C. J. Decolorization of azo dye using PVA-immobilized microorganisms. J. Biotechnol. 2003, 101, 241–252.

Chen, W. F.; Iyer, S.; Sasaki, K.; Wang, C. H.; Zhu, Y.; Muckerman, J. T.; Fujita, E. Biomass-derived electrocatalytic composites for hydrogen evolution. Energy Environ. Sci. 2013, 6, 1818–1826.

Chen, X.; Chen, G.; Yue, P. L. Separation of pollutants from restaurant wastewater by electrocoagulation. Sep. Purif. Technol. 2006, 19, 65–76.

Chen, Y.; Su, Y.; Zheng, X.; Chen, H.; Yang, H.; Alumina nanoparticles-induced effects on wastewater nitrogen and phosphorus removal after short-term and long-term exposure. Water Res. 2012, 46 , 4379 -4386.

Cherepy, N.; Liston, J. D. B.; Lovejoy, J. A.; Deng H.; Zhang, J. Z. Ultrafast studies of photoexcited electron dynamics in γ- and α-Fe_2O_3semiconductor nanoparticles, J. Phys. Chem. B 1998, 102, 770 776.

Cherney, D. P.; Duirk, S. E.; Tarr, J. C.; Colette, T. W. Monitoring the speciation of aqueous free chlorine from pH 1 to 12 with Raman spectroscopy to determine the identity of potent low pH oxidant. Appl. Spectroscopy, 2006, 60, 764–772.

Cho, B. P.; Yang, T.; Blankenship, L. K.; Moody, J. D.; Churuchwell, M.; Bebland, F. A.; Culp, S. C. Synthesis and characterisation of N-demethylated metabolites of malachite green and leucomalachite green. Chem. Res. Toxicol. 2003, 16, 285–294.

Christie, R. Colour Chemistry. The Royal Society of Chemistry, Cambridge, 2001. United Kingdom.

Chung, W. H.; Lu, C. S.; Lin, W.; Wang, Y. J. X.; Wu, C. W.; Chen, C. C. Determining the degradation efficiency and mechanisms of ethyl violet using HPLC-PDA-ESIMS and GC-MS. Chem. Central J. 2011, 6, 63–85.

Coskun, T.; Ilhan, F.; Manav, N. M.; Debik, E.; Kurt, U. Optimization of energy costs in the pre-treatment of olive mill wastewaters by electroco-agulation. Environ. Technol. 2012, 33, 801–807.

Costa, R. C. C.; Lelis, M. F. F.; Oliveira, L. C. A.; Fabris, J. D.; Ardisson, J. D.; Rios, R. R. V. A.; Silva, C. N.; Lago, R. M. Novel active heterogeneous Fenton system based on $Fe_{3-x}M_xO_4$ (Fe, Co, Mn, Ni): the role of M^{2+} species on the reactivity towards H_2O_2 reactions. J. Hazard. Mater. 2006, 129, 171-178.

Costa, R. C. C.; Lelis, M. F. F.; Oliveira, L. C. A.; Fabris, J. D.; Ardisson, J. D.; Rios, R. R. V. A.; Silva, C. N.; Lago, R. M. Remarkable effect of Co and Mn on the activity of $Fe_{3-x}M_xO_4$ promoted oxidation of organic contaminants in aqueous medium with H_2O_2. Catal. Commun. 2003, 4, 525-529.

Cotillas, S.; Llanos, J.; Canizares, P.; Mateo, S.; Rodrigo, M. A. Optimization of an integrated electrodisinfection/electrocoagulation process with Al bipolar electrodes for urban wastewater reclamation. Water Res. 2013, 47, 1741-1750.

Crini, G.; Peindy, H. N.; Gimbert, F.; Robert, C. Removal of C. I. Basic Green 4 (Malachite Green) from aqueous solutions by adsorption using cyclodextrin-based adsorbent: Kinetic and equilibrium studies. Sep. Purif. Technol. 2007, 53, 97–110.

Cunha, G. d. C.; Pimenta, L.; Romao, C.; Macedo S. Z. Production of alpha-alumina nanoparticles using aquatic humic substances. Powder Technol. 2014, 254,344–351.

Dalvand, A.; Gholami, M.; Joneidi, A.; Mahmoodi, N. M. Dye removal, energy consumption and operating cost of electrocoagulation of textile wastewater as a clean process. CLEAN – Soil Air Water, 2011, 39 (7), 665–672.

Daneshvar, N.; Aleboyeh, A.; Khataee, A. R. The evaluation of electrical energy per order (E_{Eo}) for photooxidative decolorization of four textile dye solutions by the kinetic model. Chemosphere 2004a, 59 (6), 761–767.

Daneshvar, N.; Ashassi-Sorkhabi, H.; Tizpar, A. Decolorization of orange II by electrocoagulation method. Sep. Purif. Technol. 2003, 31, 153-162.

Daneshvar, N.; Oladegaragoze, A.; Djafarzadeh, N. Decolorization of basic dye solutions by electrocoagulation: An investigation of the effect of operational parameters. J. Hazard. Mater. 2006, 129, 116–122.

Daneshvar, N.; Sorkhabi, H. A.; Kasiri, M. B. Decolorization of dye solution containing acid red 14 by electrocoagulation with a comparative investigation of different electrode connections. J. Hazard. Mater. 2004b, 112, 55–62.

Deborde, M.; Gunten, U. Reactions of chlorine with inorganic and organic compounds during water treatment—Kinetics and mechanisms: A Critical Review. Water Res., 2008, 42, 13– 51.

Deng, S.; Zhou, Q.; Yu, G.; Huang, J.; Fan, Q. Removal of perfluorooctanoate from surface water by polyaluminium chloride coagulation. Water Res. 2011, 45, 1774–1780.

Dos Santos, A. B.; Cervantes, F. J.; van Lier, J. B. Review paper on current technologies for decolourisation of textile wastewaters: Perspectives for anaerobic biotechnology. Biores. Technol. 2007, 98, 2369–2385.

Dowling, G.; Mulder, P. P. J.; Duffy, C.; Regan, L.; Smyth, M. R. Confirmatory analysis of malachite green, leucomalachite green, crystal violet and leucocrystal violet in salmon by liquid chromatography–tandem mass spectrometry. Analytica Chim. Acta 2007, 586, 411–419.

Drouiche, N.; Aoudj, S.; Hecini, M.; Ghaffourb, N.; Lounici, H.; Mameri, N. Study on the treatment of photovoltaic wastewater using electrocoagulation: Fluoride removal with aluminum electrodes—Characteristics of products. J. Hazard. Mater. 2009, 169, 65–69.

Drouiche, N.; Ghaffour, N.; Lounici, H.; Mameri, M. Electrocoagulation of chemical mechanical polishing wastewater. Desalination 2007, 214, 31–37.

Du, L.–N.; Wang, S.; Li, G.; Bing, B.; Jia, X.–M.; Zhao, Y.–H.; Chen, Y.–L. Biodegradation of malachite green by Pseudomonas sp. strain DY1 under aerobic condition: characteristics, degradation products, enzyme analysis and phytotoxicity. Ecotoxicology 2011b, 20,438–446.

Duan, J.; Gregory, J. Coagulation by hydrolysing metal salts. Adv. Colloid Interface Sci. 2003, 100, 475–502.

Durango-Usuga, P.; Guzman-Duque, F.; Mosteo, R.; Vazquez, M. V.; Penuela, G.; Torres-Palma, R. A. Experimental design approach applied to the elimination of crystal violet in water by electro-coagulation with Fe or Al electrodes. J. Hazard. Mater. 2010, 179,120–126.

E. Ellouze, N. Tahri, R. B. Amar, Enhancement of textile wastewater treatment process using nano-filtration, Desalination 2012, 286, 16–23.

Ekici, P.; Leupold, G.; Parlar, H. Degradability of selected azo dye metabolites in activated sludge systems. Chemosphere 2003, 44, 721–728.

El-Bindary, A. A.; Diab, M. A.; Hussien, M. A.; El-Sonbati, A. Z.; Eessa, A. M. Adsorption of Acid Red 57 from aqueous solutions onto polyacrylonitrile/activated carbon composite. Spectrochim. Acta Mol. Biomol. Spectroscopy. 2014, 124, 70–77.

Elmorsi, T. M.; Riyad, Y. M.; Mohamed, Z. H.; Abd El Bary, H. M. H. Decolorization of Mordant red 73 azo dye in water using H_2O_2/UV and photo-Fenton treatment. J. Hazard. Mater. 2010, 174, 352–358.

Espinosa-Jimenez, M.; Padilla-Weigand, R.; Ortega, A. O.; Perea-Carpio, R.; Ramos-tejada, M.; Chibowski, E. Investigation of the Polyamide 6,6 dyeing process with Acid Blue 45 dye. Part II. Surface free energy, zeta potential and dye/polyamide interactions. J. Adhesion Sci. Technol. 2002, 16, 303–316.

Fan, Y.; Zhang F. S.; Feng, Y. An effective adsorbent developed from municipal solid waste and coal co-combustion ash for As(V) removal from aqueous solution. J. Hazard. Mater. 2008, 159, 313–318.

Farabegoli, G.; Chiavola, A.; Rolle, E.; Naso, M. Decolorization of Reactive Red 195 by a mixed culture in an alternating anaerobic–aerobic sequencing batch reactor. Biochem. Eng. J. 2010, 52, 220–226.

Feng, J.; Sun, Y.; Zheng, Z.; Zhang, J.; Li, S.; Tian, Y. Treatment of tannery wastewater by electro-coagulation. J. Environ. Sci. 2007, 19, 1409–1415.

Fersi, C.; Dhahbi, M. Treatment of textile plant effluent by ultrafiltration and/ or nanofiltration for water reuse. Desalination 2008, 222, 263-271.

Forgacs, E.; Cserhati, T.; Oros, G. Removal of synthetic dyes from wastewaters: a review. Environ. Int. 2004, 30, 953–971.

Furlan, F. R.; de Melo da Silva, L. G.; Morgado, A. F.; de Souza, A. A.; de Souza, U. S. M. A. G. U. Removal of reactive dyes from aqueous solutions using combined coagulation/flocculation and adsorption on activated carbon. Resour. Conserv. Recycl. 2010, 54, 283–290.

Gao, B.; Yue, Q.; Wang, B. Kinetics of phenol and chlorophenol utilization by Acinetobacter species. Chemosphere 2002, 46, 809–813.

Ghosh, D.; Medhi, C. R.; Purkait, M. K. Treatment of fluoride containing drinking water by electrocoagulation using monopolar and bipolar electrode connections. Chemosphere 2008, 73, 1393–1400.

Gibson, J.; Droppo, I. G.; Farnood, R.; Mahendran, B.; Seto, P.; Liss, S. N. Hydrodynamic treatment of wastewater effluent flocs for improved disinfection. Water Environ. Res. 2012, 84 (5), 387-395.

Golob, V.; Vinder, A.; Simonic, M.; Efficiency of coagulation/flocculation method for treatment of dye bath effluents. Dyes and Pigments 2005, 67, 93-97.

Gregory, J. Particles in water: properties and processes. London: CRC Press, Taylor & Francis Group. 2006.

Groen, J. C.; Peffer, L. A. A.; Perez-Ramırez, J. Pore size determination in modified micro- and mesoporous materials. Pitfalls and limitations in gas adsorption data analysis. Microporous Mesoporous Mater. 2003, 60, 1−17.

Gupta, V. K.; Suhas. Application of low-cost adsorbents for dye removal- a review. J. Environ. Manage. 2009, 90, 2313-2342.

Hachem, C.; Bocquillon, F.; Zahraa, O.; Bouchy, M. Decolorization of textile industry wastewater by the photocatalytic degradation process. Dyes and Pigments 2001, 49, 117–125.

Hai, F. I.; Yamamoto, K.; Nakajima, F.; Fukushi, K. Application of a GAC-coated hollow fiber module to couple enzymatic degradation of dye on membrane to whole cell biodegradation within a membrane bioreactor. J. Membr. Sci. 2012, 389, 67–75.

Hayati, B.; Mahmoodi, N. M.; Arami, M.; Mazaheri, F. Dye removal from colored textile wastewater by poly (propylene imines) dendrimer: operational parameters and isotherm studies. Clean – Soil Air Water 2011, 39 (7), 673–679.

He, C.; Xiong, Y.; Chen, J.; Zha, C.; Zhu, X. Photoelectrochemical performance of Ag–TiO_2/ITO film and photoelectrocatalytic activity towards the oxidation of organic pollutants. J. Photochem. Photobiol. A: Chem. 2003, 157, 71–79.

Holt, P. K.; Barton, G. W.; Mitchell, C. A. The future for electro-coagulation as a localised water treatment technology. Chemosphere 2005, 59, 355–367.

Holt, P. K.; Barton, G. W.; Wark, M.; Mitchell, C. A. A quantitative comparison between chemical dosing and electrocoagulation. Colloids Surf. A Physicochem. Eng. Asp. 2002, 211, 233–248.

http://www.cpcb.nic.in/dye.pdf

http://www.cpcb.nic.in/Industry-Specific-Standards/Effluent/500.pdf

http://www.cpcb.nic.in/Industry-Specific-Standards/Effluent/412.pdf

http://www.cpcb.nic.in/Industry-Specific-Standards/Effluent/402.pdf

Hu, Z.; Antony, A.; Leslie, G.; Le-Clech, P. Real-time monitoring of scale formation in reverse osmosis using electrical impedance spectroscopy. J. Membr. Sci. 2014, 453, 320-327.

Huan, M.; Lian–Tai, L.; Cai–Fang, Y.; Jin-Jin, S.; Yuan, G.; Hong, Q.; Shun–Peng, L. Biodegradation of malachite green by strain Pseudomonas sp. K9 and cloning of the tmr2 gene associated with an ISPpu12. World J. Microbiol. Biotechnol. 2011, 27, 1323–1329.

Huang, H.–H.; Lu, M.–C.; Chen, J.–N. Catalytic decomposition of hydrogen peroxide and 2-chlorophenol with iron oxides Water Res. 2001, 35, 2291-2299.

Huo, S.–H.; Yan, X –P. Metal–organic frame work MIL-100 (Fe) for the adsorption of malachite green from aqueous solution. J. Mater. Chem. 2012, 2, 7449–7455.

Iglesias, J. A.; Melero, L. F.; Bautista, G.; Morales, R.; Sanchez-Vazquez, M. T.; Andreola, A. Zr-SBA-15 as an efficient acid catalyst for FAME production from crude palm oil. Catal. Today 2011, 167, 46–55.

Ip, A. W. M.; Barford, J. P, McKay, G. A comparative study on the kinetics and mechanisms of removal of Reactive Black 5 by adsorption onto activated carbons and bone char. Chem. Eng. J. 2010a, 157(2-3), 434-442.

Ip, A.; W, M.; Barford, J. P; McKay, G. A comparative study on the kinetics and mechanisms of removal of Reactive Black 5 by adsorption onto activated carbons and bone char. Chem. Eng. J. 2010b, 157(2-3), 434-442.

ISPCH, 1995. Industrial Safety and Pollution Control Handbook. 2nd reprint, second.

Jacobs, J. P.; Maltha, A.; Reintjes, J. G. H.; Drimal, J.; Ponec, V.; Brongersma, H. H. The surface of catalytically active spinels. J. Catal. 1999, 147, 294-300.

Jadhav, J. P.; Kalyani, D. C.; Telke, A. A.; Phugare, S. S.; Govindwar, S. P. Evaluation of the efficacy of a bacterial consortium for the removal of color, reduction of heavy metals, and toxicity from textile dye effluent. Biores. Technol. 2010, 101, 165–173.

Janos, P.; Buchtova, H.; Ryznarova, M. Adsorption of dyes from aqueous solution onto fly ash. Water Res. 2003, 37, 4938–4944.

Jayaraman, V.; Periaswami, G.; Kutty, T. R. N. Influence of the preparative conditions on the precursor phases formed during the synthesis of beta-alumina by the wet chemical gel to crystallite conversions. Mater Chem Phys. 1998, 52(1), 46–53.

Kabdasli, I.; Vardar, B.; Arslan-Alaton, I.; Tunay, O. Effect of dye auxiliaries on color and COD removal from simulated reactive dye bath effluent by electro-coagulation. Chem. Eng. J. 2009, 148, 89–96.

Kadam, A. A.; Telke, A. A.; Jagtap, S. S.; Govindwar, S. P. Decolorization of adsorbed textile dyes by developed consortium of Pseudomonas sp. SUK1 and Aspergillus ochraceus NCIM-1146 under solid state fermentation. J. Hazard. Mater. 2011, 189, 486–494.

Karcher, S.; Kornmuller, A.; Jekel, M. Anion exchange resins for removal of reactive dyes from textile wastewaters. Water Res. 2002, 36, 4717-4724.

Kargbo, D. M. Biodiesel Production from Municipal Sewage Sludges. Energy Fuels 2010, 24, 2791–2794.

Kariminiaae-Hamedaani, H.; Sakurai, R. A.; Sakakibara, M. Decolorization of synthetic dyes by a new manganese peroxidase producing white rot fungus. Dyes and Pigments 2007, 72, 157–162.

Keith, J. A.; Carter, E. A. Electrochemical reactivities of pyridinium in solution: consequences for CO_2 reduction mechanisms. Chem. Sci. 2013, 4, 1490-1496.

Khaled, A.; El-Nemr, A.; El-Sikaily, A.; Abdelwaha , O. Treatment of artificial textile dye effluent containing direct yellow 12 by orange peel carbon. Desalination 2009, 238, 210-232.

Khan, T. A.; Ali, I.; Singh, V. V.; Sharma, S. Utilization of fly ash as low-cost adsorbent for the removal of methylene blue, malachite green and rhodamine b dyes from textile wastewater. J. Environ. Protection sci. 2009, 3, 11–22.

Khandegar, V.; Saroha, A. K. Electrochemical treatment of distillery spent wash using aluminum and iron electrodes. Chin. J. Chem. Eng. 2012, 20(3), 439-443.

Khandegar, V.; Saroha, A. K. Electrocoagulation for the treatment of textile industry effluent-A review. J. Environ. Manage. 2013, 128, 949-96.

Khattri, S. D.; Singh, M. K. Use of Sagaun Sawdust as an adsorbent for the removal of crystal violet dye from simulated wastewater. Environ. Prog. Sustainable Energy 2012, 31(3), 435- 442.

Kılıc, M. G.; Hostena, C.; Demirci, S. A. A parametric comparative study of electrocoagulation and coagulation using ultrafine quartz suspensions. J. Hazard. Mater. 2009, 171, 247–252.

Kim, H. K.; Kim, J. G.; Cho, J. D.; Hong, J. W. Optimization and characterization of UV-curable adhesives for optical communication by response surface methodology. Polymer Test 2003, 22, 899-906.

Kim, T. H.; Park, C.; Yang, J.; Kim, S. Comparison of disperse and reactive dye removals by chemical coagulation and Fenton oxidation. J. Hazard. Mater. 2004, 112, 95–103.

Ko, D. C. K.; Lee, V. K. C.; Porter, J. F.; McKay, G. Improved design and optimisation models for the fixed bed adsorption of acid dye and zinc ions from effluents. J. Chem. Technol. Biotechnol. 2002, 77, 1289-1295.

Kobya, M.; Akyol, A.; Demirbas, E.; Oncel, M. S. Removal of arsenic from drinking water by batch and continuous electrocoagulation processes using hybrid Al-Fe plate electrodes. Environ.Prog. Sustainable Energy 2014, 33, 131-140.

Kobya, M.; Can, O. T.; Bayramoglu, M. Treatment of textile wastewaters byelectrocoagulation using iron and aluminum electrodes. J. Hazard. Mater. 2003, B100, 163–178.

Kobya, M.; Demirbas, E.; Akyol, A. Electrochemical treatment and operating cost analysis of textile wastewater using sacrificial iron electrodes. Water Sci. Technol. 2009, 60. 2261-2270.

Kobya, M.; Demirbas, E.; Can, O.T.; Bayramoglu, M. Treatment of levafix orange textile dye solution by electrocoagulation. J. Hazard. Mater. 2006b, 132, 183–188.

Kobya, M.; Gengec, E. Decolourization of melanoidins by a electrocoagulation process using aluminium electrodes. Environ. Technol. 2012, 1, 1-10.

Kobya, M.; Senturk, E.; Bayramoglu, M. Treatment of poultry slaughterhouse wastewaters by electrocoagulation. J. Hazard. Mater. 2006a, 133, 172–176.

Konsowa, A. H.; Ossman, M. E.; Chen, Y.; Crittenden, J. C. Decolorization of industrial wastewater by ozonation followed by adsorption on activated carbon. J. Hazard. Mater. 2010, 176, 181–185.

Korbahti, B. K. Response surface optimization of electrochemical treatment of textile dye wastewater. J. Hazard. Mater. 2007, 145, 277–286.

Körbahti, B. K.; Tanyolac, A. Electrochemical treatment of simulated textile wastewater with industrial components and levafix blue CA reactive dye: optimization through response surface methodology. J. Hazard. Mater. 2008, 151, 422–431.

Koupaiea, E. H.; Alavi Moghaddama, M. R.; Hashemi, S. H. Post-treatment of anaerobic degraded azo Acid Red 18 using aerobic moving bed biofilm process: Enhanced removal of aromatic amines. J. Hazard. Mater. 2011, 195,147–154.

Kucheryavy, P.; He, J.; John, V. T.; Maharjan, P.; Spinu, L.; Goloverda G. Z.; Kolesnichenko, V. L. Superparamagnetic iron oxide nanoparticles with variable size and an iron oxidation state as prospective imaging agents. Langmuir 2013, 29, 710−716.

Kumar, A.; Prasad, B.; Mishra, I. M. Optimization of process parameters for acrylonitrile removal by a low-cost adsorbent using Box–Behnken design. J. Hazard. Mater. 2008a, 150, 174–182.

Kumar, A.; Singh, B. Zn^{2+}-induced folding of RNA to produce honeycomb-like RNA-mediated fluorescing Zn^{2+}/PbSe nanostructures. J. Phys. Chem. C 2013, 117, 5386−5396.

Kumar, P.; Prasad, B.; Mishra, I. M.; Chand, S. Treatment of composite wastewater of a cotton textile mill by thermolysis and coagulation. J. Hazard. Mater. 2008b, 151, 770–779.

Kumar, S.; Srivastava, V. C.; Badoni, R. P. Studies on adsorptive desulfurization by zirconia based adsorbents. Fuel 2011, 90, 3209-3216.

Kurbus, T.; Slokar, Y. M.; Marechal, A. M. The study of the effects of the variables on H_2O_2/UV decolouration of vinylsulphone dye: Part II. Dyes and Pigments 2002, 54, 67-78.

Kurt , E.; Koseoglu-Imer, Y. D.; Dizge, N.; Chellam, S.; Koyunc, I. Pilot-scale evaluation of nanofiltration and reverse osmosis for process reuse of segregated textile dyewash wastewater. Desalination 2012,302, 24–32.

Kushwaha, J. P.; Srivastava, V. C.; Mall, I. D. Organics removal from dairy wastewater by electrochemical treatment and residue disposal. Sep. Purif. Technol. 2010, 76, 198–205.

Kushwaha, J. P.; Srivastava, V. C.; Mall, I. D. Studies on electrochemical treatment of dairy wastewater using aluminum electrode. AIChE J. 2011, 57, 2589– 2598.

Kusmierek, E.; Chrzescijanska, E.; Szadkowska-Nicze, M.; Kaluzna-Czaplinska, J. Electrochemical discolouration and degradation of reactive dichlorotriazine dyes: reaction pathways. J. Appl. Electrochem. 2011, 41, 51–62.

Lakshmanan, D.; Clifford, D. A.; Samanta, G. Ferrous and ferric ion generation during iron electrocoagulation. Environ. Sci. Technol. 2009, 43, 3853–3859.

Lakshmi, U. R.; Srivastava, V. C.; Mall, I. D.; Lataye, D. H. Rice husk ash as an effective adsorbent: evaluation of adsorptive characteristics for Indigo Carmine dye. J. Environ. Manage. 2009, 90, 710-720.

Lan, Shi.; Guo, N.; Liu, L.; Wu, Xi.; Li, L.; Gan, S. Facile preparation of of hierarchical hollow structure gamma alumina and a study of its adsorption capacity. Applied Surface Science 2013, 283, 1032– 1040.

Lau, W. J.; Ismail, A. F. Polymeric nanofiltration membranes for textile dye wastewater treatment: Preparations, performance evaluation, transport modelling, and fouling control- a review. Desalination 2009, 245, 321-348.

Lee, W.; Westerhoff, P. Dissolved organic nitrogen removal during water treatment by aluminum sulfate and cationic polymer coagulation. Water Res. 2006, 40, 3767-3774.

Legube, B.; Leitner, N. K. V. Catalytic ozonation: a promising advanced oxidation technology for water treatment, Catal. Today 1999, 53, 61–72.

Leiknes, T.O. The effect of coupling coagulation and flocculation with membrane filtration in water treatment: a review. J. Environ. Sci. 2009, 21, 8-12.

Liang, X.; Zhong, Y.; Zhu, S.; Ma, L.; Yuan, P.; Zhu, J.; He, H.; Jiang, Z. The contribution of vanadium and titanium on improving methylene blue decolorization through heterogeneous UV-Fenton reaction catalyzed by their co-doped magnetite. J. Hazard. Mater. 2012, 199-200, 247-254.

Lima, S. L.; Chu, W. L.; Phang, S. M. Use of Chlorella vulgaris for bioremediation of textile wastewater. Biores. Technol. 2010, 101, 7314–7322.

Liu, G.; Li, X.; Zhao, J.; Hidaka, H.; Serpone, N. Photooxidation pathway of sulforhodamine-B. Dependence on the adsorption mode on TiO_2 exposed to visible light radiation, Environ. Sci. Technol. 2000, 34, 3982–3990.

Liu, M.; Lu, Z.; Chen, Z.; Yu, S.; Gao C. Comparison of reverse osmosis and nano-filtration membranes in the treatment of biologically treated textile effluent for water reuse. Desalination. 2011,281, 372–378

Liu, S.; Fang, Y.; Wang, M. L. S.; Chen, L. Optimization of the production of organic solvent-stable protease by bacillus sphaericus DS11 with response surface methodology. Biores. Technol. 2010, 101, 7924–7929.

Liu, X.; Liu, J.; Chang, Z.; Sun X.; Li, Y. Crystal plane effect of Fe_2O_3 with various morphologies on CO catalytic oxidation. Catal. Commun. 2011, 12, 530–534.

Lopez-Delgado, A.; Fillali, L.; JimenezJ, A.; Lopez-Andres, S. Synthesis of a-alumina from a less common raw material. J Sol-Gel Sci Technol . 2012, 64, 162–169.

Losocha, W.; Lewinski, K. PROSZKI - a system of programs for powder diffraction data analysis. J. Appl. Crystallogr. 1994, 27, 437-438.

Loukas, L. A placket-burman screening design directs the efficient formulation of multicomponent DRV liposomes. J. Pharm. Biomed. Anal. 2001, 26, 255–262.

Luna, A. S.; Costa, A. L. H.; Da Costa, A. C. A.; Henriques, C. A. Competitive biosorption of cadmium(II) and zinc (II) ions from binary system by Sargassum filipendula. Biores. Technol. 2010, 101, 5104-5111.

Magalhaes, F.; Pereira, M. C.; Botrel, S. E. C.; Fabris, J. D.; Macedo, W. A.; Mendonca, R.; Lago, R. M.; Oliveira, L. C. A. Cr-containing magnetites $Fe_{3-x}Cr_xO_4$: the role of Cr^{3+} and Fe^{2+} on the stability and reactivity towards H_2O_2 reactions. Appl. Catal. A: Gen. 2007, 332, 115-123.

Mahesh, S.; Prasad, B.; Mall, I. D.; Mishra, I. M. Electrochemical Degradation of Pulp and Paper Mill Wastewater. Part 1. COD and Color Removal. Ind. Eng. Chem. Res. 2006, 45, 2830-2839.

Mahmoud, H. R.; El-Molla, S. A.; Saif, M. Improvement of physicochemical properties of Fe_2O_3/MgO nanomaterials by hydrothermal treatment for dye removal from industrial wastewater. Powder Technol. 2013, 249, 225–233.

Maiti, A.; Basu, J. K.; De, S. Experimental and kinetic modelling of As (V) and As(III) adsorption on treated laterite using synthetic and contaminated groundwater: Effect of phosphate , silicates and carbonate ions. Chem. Eng. J. 2012, 191, 1-12.

Maiti, A.; Das Gupta, S.; Basu, J. K.; De, S. Adsorption of arsenite using natural laterite as adsorbent. Sep. Purif. Technol. 2007, 55, 350-359.

Mall, I. D.; Srivastava, V. C.; Agarwal, N. K. Adsorptive removal of Auramine-O: Kinetic and equilibrium study. J. Hazard. Mater. 2007, 143, 386–395.

Mall, I. D.; Srivastava, V. C.; Agarwal, N. K. Removal of Orange-G and Methyl Violet dyes by adsorption onto bagasse fly ash kinetic study and equilibrium isotherm analyses. Dyes and Pigments 2006a, 69, 210-223.

Mall, I. D.; Srivastava, V. C.; Agarwal, N. K.; Mishra, I. M. Adsorptive removal of malachite green dye from aqueous solution by bagasse fly ash and activated carbon-kinetic study and equilibrium isotherm analyses. Colloids and Surfaces A: Physicochem. Eng. Aspects 2005, 264, 17–28.

Mall, I. D.; Srivastava, V. C.; Kumar, G. V. A.; Mishra, I. M. Characterization and utilization of mesoporous fertilizer plant waste carbon for adsorptive removal of dyes from aqueous solution. Colloids Surfaces A Physicochem. Eng. Aspects 2006b, 278(1-3), 175-187.

Mane, V. S.; Mall, I. D.; Srivastava, V. C. Kinetic and equilibrium isotherm studies for the adsorptive removal of Brilliant Green dye from aqueous solution by rice husk ash. J. Environ. Manage. 2007a, 84, 390–400.

Mane, V. S.; Mall, I. D.; Srivastava, V. C. Use of bagasse fly ash as an adsorbent for the removal of brilliant green dye from aqueous solution. Dyes and Pigments 2007b, 73, 269-278.

Marin, M. L.; Santos-Juanes, L.; Arques, A.; Amat, A. M.; Miranda, M. A. Organic Photocatalysts for the Oxidation of Pollutants and Model Compounds. Chem. Rev. 2012, 112, 1710–1750.

Martin, R. C.; Rossi, A. F.; Castro-Silva, S.; Quinta-Ferreira, R. M. Fenton's Process for Post-Biologically Treated Cheese Production Wastewaters Final Remediation: Toxicity Assessment. Int. J. Chem. React. Eng. 2010, 8, 235-246.

Martınez–Huitle, C. A.; Brillas, E. Decontamination of wastewaters containing synthetic organic dyes by electrochemical methods: A general review. Appl. Catal. B: Environ. 2009, 87, 105–145.

Martinez–Huitle, C. A.; Ferro, S. Electrochemical oxidation of organic pollutants for the wastewater treatment: direct and indirect processes. Chem. Soc. Review. 2006, 35, 1324–1340.

Masion, A.; Vilge –Ritter, A.; Rose, J.; Stone, W. E. E.; Teppen, B. J.; Rybacki, D.; Bottero, J.-Y. Coagulation-flocculation of natural organic matter with al salts: speciation and structure of the aggregates. Environ. Sci. Technol. 2000, 34, 3242–3246.

Matos, J.; Rosales, M.; Garcia, A.; Nieto-Delgado, C.; Rangel-Mendez, J. R. Hybrid photoactive materials from municipal sewage sludge for the photocatalytic degradation of methylene blue. Green Chem. 2011, 13, 3431–3439.

Merzouk, B.; Madani, K.; Sekki, A. Using electrocoagulation electroflotation technology to treat synthetic solution and textile wastewater, two case studies. Desalination 2010, 250, 573-577.

Metcalf, Eddy, Wastewater Engineering Treatment and Reuse, fourth ed. McGraw-Hill, New York, 2005.

Mezohegyi, G.; van der Zee, F. P.; Font, J.; Fortuny, A.; Fabregat, A. Towards advanced aqueous dye removal processes: A short review on the versatile role of activated carbon. J. Environ. Manage. 2012, 102, 148-164.

Minhalma, M.; De Pinho, M. N. Flocculation/flotation/ultrafiltration integrated process for the treatment of cork processing wastewaters. Environ. Sci. Technol. 2001, 35, 4916– 4921.

Mohan, J. Organic Spectroscopy. Principles and applications, 2nd Edition, Narosa Publishing House, Delhi 2004.

Mohan, N.; Balasubramanian, N.; Subramanian, V. electrochemical treatment of simulated textile effluent. Chem. Eng. Technol. 2001, 24, 749–753.

Mohan, S. V.; Ramanaiah, S. V.; Sarma, P. N. Biosorption of direct azo dye from aqueous phase onto Spirogyra sp. I02: Evaluation of kinetics and mechanistic aspects. Biochem. Eng. J. 2008, 38, 61–69.

Mohan, S. V.; Rao, N. C.; Karthikeyan, J. Adsorptive removal of direct azo dye from aqueous phase onto coal based sorbents: a kinetic and mechanistic study. J. Hazard. Mater. 2002, B90, 189-204.

Mohan, S.; Srivastava, S.; Divecha, J.; Madamwar, D. Response surface methodology for optimization of medium for decolorization of textile dye Direct Black 22 by a novel bacterial consortium. Biores. Technol. 2008, 99, 562-569.

Mollah, M. Y. A.; Gomes, J. A. G.; Das, K. K.; Cock, D. L. Electrochemical treatment of Orange II dye solution—Use of aluminum sacrificial electrodes and floc characterization. J. Hazard. Mater. 2010, 174, 851–858.

Mondal, B.; Srivastava, V. C.; Kushwaha, J. P.; Bhatnagar R.; Singh, S.; Mall, I. D. Parametric and multiple response optimizations for the electrochemical treatment of textile printing dye-bath effluent. Sep. Purif. Technol. 2013, 109, 135–143.

Mondal, B.; Srivastava, V. C.; Mall, I. D. Electrochemical treatment of textile printing wastewater by stainless steel electrodes: multiple response optimization and residue analysis. J. Environ. Sci. Health Part A 2012, 47, 2040–2051.

Montanaro, D.; Petrucci, E. Electrochemical treatment of remazol brilliant blue on a boron-doped diamond electrode. Chem. Eng. J. 2009, 153, 138–144.

MoT-GoI, (Ministry of Textiles, Government of India) Annual Report 2012-13, www.ministryoftextiles.gov.in.

Moura, F. C. C.; Oliveira, G. C.; Araujo, M. H.; Ardisson, J. D.; Macedo, W. A. A.; Lago, R. M. A comparative study about the effects of isomorphous substitution of transition metals (Ti, Cr, Mn, Co and Ni) on the UV/Fenton catalytic activity of magnetite. Appl. Catal. A: Gen. 2006, 307, 195-204.

Mui, E. L. K.; Cheung, W. H.; Valix, M.; McKay, G. Mesoporous activate carbon from waste tyre rubber for dye removal from effluents. Microporous and Mesoporous Mater. 2010, 130(1-3), 287-294.

Murthy, Z. V. P.; Nancy, C.; Kant, A. Separation of pollutants from restaurant wastewater by electocoagulation. Sep. Sci. Technol. 2007, 42(4), 819-833.

Murthy, Z. V. P.; Parmar, S. Removal of strontium by electro-coagulation using stainless steel and aluminum electrodes. Desalination 2011, 282(1), 63–67.

Murugananthan, M.; Raju, G. B. Removal of organic dyes and tannins by electrochemical techniques. Photo-Electrochemistry & Photo-Biology for the Sustainability. Photochem. Photobiol. Sci. 2010, 1, 189-215.

Muthukumar, M.; Karuppiah, M. T.; Raju, G. B. Electrochemical removal of CI Acid orange 10 from aqueous solution. Sep. Purif. Technol. 2006, 55, 198–205.

Myers, R. H.; Montgomery, D. C. Response Surface Methodology: Process and Product Optimization Using Designed Experiments.2nd edition, John Wiley & Sons, New York, 2002.

Namasivayam, C.; Radhika, R.; Suba, S. Uptake of dyes by a promising locally available agricultural solid waste: coir pith. Waste Manage. 2001, 21, 381–387.

Nampi, P. P.; Ghosh, S.; Krishna, W. G. Calcination and associated structural modifications in bohemite and their influence on high temperature densification of alumina. Ceram. Int. 2011, 37 (8), 3329–3334.

Oguz, E.; Keskinler, B. Removal of colour and COD from synthetic textile wastewaters using O_3, PAC, H_2O_2 and HCO_3. J. Hazard. Mater. 2008, 151, 753–760.

Oliveira, L. C. A.; Ramalho, T. C.; Souza, E. F.; Goncalves, M.; Oliveira, D. Q. L.; Pereira, M. C.; Fabris, J. D. Catalytic properties of goethite prepared in the presence of Nb on oxidation reactions in water: computational and experimental studies. Appl. Catal. B: Environ. 2008, 83, 169-176.

Ong, Y. K.; Li, F. Y.; Sun, S.-P.; Zhao, B.-W.; Liang, C.-Z.; Chung, T.-S. Nano-filtration hollow fiber membranes for textile wastewater treatment: Lab-scale and pilot-scale studies. Chem. Eng. Sci. 2014,114, 51–57.

Ordonez, R.; Hermosilla, D.; Merayo, N.; Gasco, A.; Negro, C.; Blanco, A. Application of Multi-Barrier Membrane Filtration Technologies to Reclaim Municipal Wastewater for Industrial Use. Sep. Purific. Rev., 2014, 43, 263–310,.

Oturan, M. A.; Guivarch, E.; Oturan N.; Sires, I. Oxidation pathways of malachite green by Fe^{3+}– catalyzed electro–Fenton process. Appl. Catal. B: Environ. 2008, 82, 244–254.

Ozkan-Yucel, U. G.; Gokcay, C. F. Effect of initial azo dye concentration and biomass acclimation on sludge digestion and dye co-treatment. Clean–Soil Air Water 2010, 38 (4), 387–393.

Padoley, K. V.; Mudliar, S. N.; Banerjee, S. K.; Deshmukh, S. C.; Pandey, R. A. Fenton oxidation: A pre-treatment option for improved biological treatment of pyridine and 3-cyanopyridine plant wastewater. Chem. Eng. J. 2011,166, 1-9.

Pagga, U.; Brown, D. The degradation of dyestuffs. Part II. Behaviour of dyestuffs in aerobic biodegradation tests. Chemosphere 1987, 15, 479–491.

Pakshirajan, K.; Kheria, S. Continuous treatment of coloured industry wastewater using immobilized Phanerochaete chrysosporium in a rotating biological contactor reactor. J. Environ. Manage. 2012, 101, 118-123.

Pakshirajan, K.; Kheria, S. Continuous treatment of coloured industry wastewater using immobilized Phanerochaete chrysosporium in a rotating biological contactor reactor. J. Environ. Manage. 2012, 101, 118-123.

Pandey, A.; Singh, P.; Iyengar, L. Bacterial decolorization and degradation of azo dyes (a review). Int. Biodeter. Biodeg. 2007, 59, 73–84.

Pandit, P.; Basu, S. Removal of ionic dyes from water by solvent extraction using reverse micelles. Environ. Sci. technol. 2004, 38 (8), 2435-2442.

Pandit, P.; Basu, S. Removal of organic dyes from water by liquid-liquid extraction using reverse micelles. J. colloid interface sci. 2002, 245 (1), 208-214.

Panizza M.; Cerisola G. Application of diamond electrodes to electrochemical processes. Electrochim. Acta 2005, 51, 191–199.

Panizza, M.; Cerisola, G. Electrocatalytic materials for the electrochemical oxidation of synthetic dyes. Appl. Catal. B: Environ. 2007, 75, 95–101.

Panizza, M.; Cerisola, G. Electrochemical degradation of methyl red using BDD and PbO_2 Anodes. Ind. Eng. Chem. Res. 2008, 47, 6816–6820.

Panizza, M.; Cerisola, G. Olive mill wastewater treatment by anodic oxidation with parallel plate electrodes. Water Res. 2006, 40, 1179– 1184

Park, O. K.; Erica, H.; Tadd, M. Z.; Tannenbaum, R. Size-controlled synthesis of alumina nanoparticles from aluminum alkoxides. Materials Research Bulletin 2005, 40, 1506–1512.

Parsa, J. B.; Vahidian, H. R.; Soleymani, A. R.; Abbasi, M. Removal of Acid Brown 14 in aqueous media by electrocoagulation: Optimization parameters and minimizing of energy consumption. Desalination 2011, 278, 295–302.

Parshetti, G.; Kalme, S.; Saratale, G.; Govindwar, S. Biodegradation of Malachite Green by Kocuria rosea MTCC 1532. Acta Chimcal Socity. 2006, 53, 492–498.

Paschoal, F. M. M.; Anderson, M. A.; Zanoni, M. V. B. The photoelectrocatalytic oxidative treatment of textile wastewater containing disperse dyes. Desalination 2009, 249, 1350-1355.

Patel, H.; Vashi, R. T. Treatment of textile wastewater by adsorption and coagulation. Environ. J. Chem. 2010, 7 (4), 1468-1476.

Patel, U. D.; Ruparelia, J. P.; Patel, M. U. Electro-coagulation treatment of simulated floor-wash containing Reactive Black 5 using iron sacrificial anode. J. Hazard. Mater. 2011, 197, 128–136.

Pearce, C. I.; Henderson, C. M. B.; Telling, N. D.; Pattrick, R. A. D.; Charnock, J. M.; Coker, V. S.; Arenholz, E.; Tuna, F.; van der Laan, G. Fe site occupancy in magnetite-ulvöspinel solid solutions: a new approach using X-ray magnetic circular dichroism. Am. Mineral 2010, 95, 425-439.

Pearce, C. I.; Lloyd, J. R.; Guthrie, J. T. The removal of color from textile wastewater using whole bacterial cells. Dyes and Pigments 2003, 58, 179–196.

Perret, D.; Newman, M. E.; Negre, J. C.; Chen, Y.; Buffle, J. Submicron particles in the Rhine River–I: Physico-chemical characterization. Water Res.1994, 28(1), 91-106.

Phalakornkule, C.; Polgumhang, S.; Tongdaung, W.; Karakat, B.; Nuyut, T. Electrocoagulation of blue reactive, red disperses and mixed dyes, and application in treating textile effluent. J. Environ. Manage. 2010, 91, 918–926.

Pietrzak-Bandosz, T. J. Interactions of NO_2 with sewage sludge based composite adsorbents. J. Hazard. Mater. 2008, 154, 946–953.

Ponselvan, F. I. A.; Kumar, M.; Malviya, J. R.; Srivastava, V. C.; Mall, I. D. Electrocoagulation studies on treatment of biodigester effluent using aluminum electrodes. Water Air Soil Poll. 2009, 199 (1-4), 371-379.

Pouran, S. R.; Raman, A. A. A.; Daud, W. M. A. W. Review on the application modified iron oxides as heterogeneous catalysts in Fenton reactions. J. Cleaner Production 2014, 64, 24-35.

Prevot, A. B.; Baiocchi, C.; Brussino, M. C.; Pramauro, E.; Savarino, P.; Augugliaro, V.; Marci, G.; Palmisano, L. Photocatalytic degradation of acid blue 80 in aqueous solutions containing TiO_2 suspensions. Environ. Sci. Technol. 2001, 35, 971–976.

Priya, B.; Uma, L.; Ahamed, A. K.; Subramanian, G.; Prabaharan, D. Ability to use the diazo dye, C.I. Acid Black 1 as a nitrogen source by the marine cyanobacterium Oscillatoria curviceps BDU92191. Biores. Technol. 2011, 102, 7218–7223.

Qin, J.-J; Oo, M. H.; Kekre, K. Nano-filtration for recovering wastewater from a specific dyeing facility. Sep. Purif. Technol. 2007, 56, 199–203.

Qin, L.; Zhang, G.; Meng, Q.; Xu, L.; LvEnhanced, B. MBR by internal micro-electrolysis for degradation of anthraquinone dye wastewater. Chem. Eng. J. 2012, 210, 575–584

Qu, Y.; Shi, S.; Ma, F.; Yan, B. Decolorization of Reactive Dark Blue K-R by the synergism of fungus and bacterium using response surface methodology. Biores. Technol. 2010, 101, 8016–8023.

Quezado, M.; Linares, I.; Buitron, G. Use of a sequencing batch biofilter for degradation of azo dyes (acids and bases). Water Sci. Technol. 2000, 42, 329–336.

Raghu, S.; Basha, C. A. Electrochemical treatment of procion black 5B using cylindrical flow reactor—a pilot plant studies. J. Hazard. Mater. 2007, B139, 381–390.

RajKumar, D.; Kim, J. G. Oxidation of various reactive dyes with in situ electro-generated active chlorine for textile dyeing industry wastewater treatment. J. Hazard. Mater. 2006, 136, 203–212.

Rajkumar, D.; Palanivelu, K. Electrochemical degradation of cresols for wastewater treatment. Ind. Eng. Chem. Res. 2003, 42, 1833-1839.

Ram, S. Infrared spectral study of molecular vibrations in amorphous, nanocrystalline and AlO(OH).alpha H_2O bulk crystals. Infrared Phys Technol. 2001, 42(6), 547–560.

Rameshraja, D.; Srivastava V. C.; Kushwaha, J. P.; Mall, I. D. Quinoline adsorption onto granular activated carbon and bagasse fly ash. Chem. Eng. J. 2012, 181–182, 343–351.

Rangel, M.; Nava1, J. L.; Peralta-Hernandez, J. M.; Carreno, G.; Guerra-Sanchez, R. J. Electrochemical oxidation of reactive blue 222 on Boron-Doped Diamond electrodes. Int. J. Electrochem. Sci. 2013, 8, 3310 – 3320.

Reife, A.; Freeman, H. S. Environmental chemistry of dyes pigments. Wiley, New York. 1996.

Richardson, S. D. Environmental Mass Spectrometry. Anal. Chem. 2000, 72, 4477–4496.

Richardson, S. D. environmental mass spectrometry: emerging contaminants and current issues. Environmental Mass Spectrometry: Emerging Contaminants and Current Issues. Anal. Chem. 2008, 80, 4373–4402.

Robinson, T.; McMullan, G.; Marchant, R.; Nigam, P. Remediation of dyes in textile effluent: a critical review on current treatment technologies with a proposed alternative. Biores. Technol. 2001, 77, 247–255.

Robinson, T.; McMullan, G.; Marchant, R.; Nigam, P. Remediation of dyes in textile effluent: a critical review on current treatment technologies with a proposed alternative. Biores. Technol. 2000, 77, 247–255.

Rodgers, J. D.; Jedral, W.; Bunce, N. J. Electrochemical oxidation of chlorinated phenols. Environ. Sci. Technol. 1999, 33, 1453−1457.

Rodriduez, J. D.; Jedral, W.; Bunce, N. J. Electrochemical oxidation of chlorinated phenols. Environ. Sci. Technol. 2008, 33, 1453−1457.

Rong, H.; Gao, B.; Li, R.; Wang, Y.; Yue, Q.; Li, Q. Effect of dose methods of a synthetic organic polymer and PFC on floc properties in dyeing wastewater coagulation process. Chem. Eng. J. 2014, 243, 169–175.

Sahan, T.; Ceylan, H.; Sahiner, N.; Aktas, N. Optimization of removal conditions of copper ions from aqueous solutions by Trametes versicolor. Biores. Technol. 2010, 101, 4520–4526.

Saroha, A. K.; Khera, R. Hydrodynamic Study of Fixed Beds with Co current Up-flow and Down-flow. Chem. Eng. Proc. 2006, 45(6), 455-460.

Sengil, I. A.; Ozacar, M. The decolorization of C.I. Reactive Black 5 in aqueous solution by electrocoagulation using sacrificial iron electrodes. J. Hazard. Mater. 2009, 161, 1369–1376.

Shannon, R. D. Revised effective ionic radii and systematic studies of interatomic distances in halides and chalcogenides. Acta Cryst. 1976, A32, 751.

Sharma Y. C.; Upadhyay, S. N. Removal of a cationic dye from wastewater by adsorption on activated carbon developed from coconut coir. Energy & Fuel 2009, 23 (6), 2983-2988.

Sharma, S.; Mukhopadhyay, M.; Murthy, Z. V. P. Degradation of 4- chlorophenol in waste water by organic oxidants. Ind. Eng. Chem. Res. 2010, 49 (7), 3094-3098.

Sharma, Y. C.; Srivastava, V.; Mukherjee, A. K. Synthesis and Application of Nano-Al2O3 Powder for the Reclamation of Hexavalent Chromium from Aqueous Solutions. J. Chem. Eng. Data 2010, 55, 2390–2398.

Sharma, Y. C.; Srivastava, V.; Singh, V. K.; Kaul, S. N.; Weng, C. H. Nano-adsorbents for the removal of metallic pollutants from water and wastewater. Environ. Technol. 2009, 30, 583-609.

Sharma, Y. C.; Srivastava, V.; Upadhyay, S. N.; Weng, C. H. Aluminium nanoparticles for the removal of Ni (II) from aqueous solutions. Ind. Eng. Chem. Res. 2008, 47, 8095-8100.

Shon, H. K.; Phuntsho, S.; Vigneswaran, S.; Kandasamy, J.; Nghiem, L. D.; Kim, G. J.; Kim, G. B.; Kim, J.-H. Preparation of titanium dioxide nanoparticles from electrocoagulated sludge using sacrificial titanium electrodes. Environ. Sci. Technol. 2010, 44, 5553–5557.

Shon, H. K.; Vigneswaran, S. I.; Kim, N. S.; Chog, J.; Kim, J.; Kim J. B.; Kim, J.-H. Preparation of titanium dioxide (TiO_2) from sludge produced by titanium tetrachloride ($TiCl_4$) flocculation of wastewater. Environ. Sci. Technol. 2007, 41, 1372-1377.

Shon, H. K.; Vigneswaran, S.; Kandasamy, J.; Kim, J.-B.; Park, H. J.; Choi, S. W.; Kim, J.-H. Preparation of titanium oxide, iron oxide, and aluminium oxide from sludge generated from Ti-salt, Fe-salt and Al-salt flocculation of wastewater. J. Ind. Eng. Chem. 2009, 15, 719–723.

Singh, K.; Arora, S. Removal of synthetic textile dyes from wastewaters: A critical review on present treatment technologies. Critical reviews. Environ. Sci. Technol. 2011, 41, 807–878.

Singh, S.; Srivastava, V. C.; Mall, I. D. Mechanistic study of electrochemical treatment of basic green 4 dye with aluminum electrodes through zeta potential, TOC, COD and color measurements, and characterization of residues. RSC Adv. 2013b, 3, 16426–16439.

Singh, S.; Srivastiva, V. C.; Mall, I. D. Electrochemical treatment of dye bearing effluent with different anode-cathode combinations: mechanistic study and sludge analysis. Ind. Eng. Chem. Res. 2014, (DOI: 10.1021/ie4042005).

Singh, S.; Srivastiva, V. C.; Mall, I. D. Mechanism of dye degradation during electrochemical treatment. J. Phys. Chem. C 2013c, 117, 15229−15240.

Singh, S.; Srivastiva, V. C.; Mall, I. D. Mechanistic study of electrochemical treatment of basic green 4 with aluminum electrodes through zeta potential measurement and characterization of residues. RSC Advance 2013b, 1–14.

Singh, S.; Srivastiva, V. C.; Mall, I. D. Multi-step Optimization and Residue Disposal Study for Electrochemical Treatment of Textile Wastewater Using Aluminum Electrode. Inter. J. Chem. Reactor Eng. 2013a, 11(1), 1–16.

Singh, S.; Srivastiva, V. C.; Mall. I. D. Electrochemical treatment of malachite green dye solution using iron electrode. Inter. J. Chem. Tech. Research. 2013d, 5(2), 592-596.

Solisa, M.; Solisa, A.; Perez, H. I.; Norberto, M.; Maribel, F. Microbial decolouration of azo dyes: A review. Process. Biochem. 2012, 47, 1723–1748.

Soloman, A.; Basha, M.; Velan, M.; Balasubramanian, N. Electro oxidation of malachite green and modeling using ANN. Chem. Biochem. Eng. Q. 2010, 24, 445–452.

Souza-Santos, P.; Souza-Santos, H.; Toledo, S. P. Standard transition aluminas. Electron microscopy studies. Mater Res. 2000, 3(4), 11.

Srivastav, A.; Srivastava, V. C. Adsorptive desulfurization by activated alumina. J. Hazard. Mater. 2009a, 170, 1133-1140.

Srivastava, S.; Sinha, R.; Roy, D. Toxicological effects of malachite green: Review. Aquatic Toxicol. 2004, 66, 319–329.

Srivastava, V. C.; Mall, I. D.; Mishra, I. M. Adsorption of toxic metal ions onto activated carbon study of sorption behaviour through characterization and kinetics. Chem. Eng. Process. 2008, 47, 1269–1280.

Srivastava, V. C.; Mall, I. D.; Mishra, I. M. Characterization of mesoporous rice husk ash (RHA) and adsorption kinetics of metal ions from aqueous solution onto RHA. J. Hazard. Mater. 2006c, 134, 257–267.

Srivastava, V. C.; Mall, I. D.; Mishra, I. M. Equilibrium modelling of single and binary adsorption of cadmiumand nickel onto bagasse fly ash. J. Chem. Eng. 2006a, 117(1), 79–91.

Srivastava, V. C.; Mall, I. D.; Mishra, I. M. Equilibrium modelling of ternary adsorption of metal ions onto rice husk ash. J. Chem. Eng. Data 2009b, 54, 700–711.

Srivastava, V. C.; Swamy, M. M.; Mall, I. D.; Prasad, B.; Mishra, I. M. Adsorptive removal of phenol by bagasse fly ash and activated carbon: equilibrium, kinetics and thermodynamics. Colloid Surface A: Physchem. Eng. Aspects 2006b, 272, 89–104.

Sudova1, E.; Machova1, J.; Svobodova, Z.; Vesely, T. Negative effects of malachite green and possibilities of its replacement in the treatment of fish eggs and fish: a review. Vet. Medicina 2007, 52, 527–539.

Sukmanowski, J.; Viguie, J.-R.; olting, B. N.; Royer, F. X. Light absorption enhancement by nanoparticles, J. Appl. Phys. 2005, 97,104332–104338.

Sun, H.; Qi, H. Capillary electrophoresis combined with accelerated solvent extraction as an improved methodology for effective separation and simultaneous determination of malachite green, crystal violet and their leuco-metabolites in aquatic products. Anal. Methods 2013, 5, 267–272.

Suwandi, A. C.; Indraswati, N.; Ismadji, S. Adsorption of N-methylated diaminotriphenilmethane dye (malachite green) on natural rarasaponin modified kaolin. Desalination Water Treatment 2012, 41, 342–355.

Szpyrkowicz, L. Hydrodynamic effects on the performance of electro-coagulation/electro-flotation for the removal of dyes from textile wastewater. Ind. Eng. Chem. Res.2005a, 44, 7844-7853.

Szpyrkowicz, L.; Juzzolino, C.; Kaul, S. N. A comparative study on oxidation of disperses dyes by electrochemical process, ozone, hypochlorite and Fenton Reagent. Water Res. 2001, 35, 2129–2136.

Szpyrkowicz, L.; Kaul, S. N.; Neti, R. N.; Satyanarayan, S. Influence of anode material on electrochemical oxidation for the treatment of tannery wastewater. Water Res. 2005b, 39, 1601–1613.

Tavares, M. G.; da Silva. L. V. A.; Solano. A. M. S.; Tonholo, J.; Martinez-Huitle, C. A.; Zanta, C. L .P. S. Electrochemical oxidation of Methyl Red using $Ti/Ru_{0.3}Ti_{0.7}O_2$ and Ti/Pt anodes. Chem. Eng. J. 2012, 204–212,141–150.

Terrazasa, E.; Vazqueza, A.; Brionesa, R.; Lazaroa; I.; Rodriguez, I. EC treatment for reuse of tissue paper wastewater: Aspects that affect energy consumption. J. Hazard. Mater. 2010, 181, 809–816.

Thomas, S.; Sreekanth, R.; Sijumon, V. A.; Aravind, U. K.; Aravindakumar, C. T. Oxidative degradation of Acid Red 1 in aqueous medium. Chem. Eng. J. 2014, 244, 473–482.

Tian, Y.; Ji, C.; Wang, K.; Le-Clech, P. Leslie. G. Assessment of an anaerobic membrane bio-electrochemical reactor (AnMBER) for wastewater treatment and energy recovery. J. Membr. Sci. 2014, 450, 242-248.

UNICEF, 2008. At a glance: Czech Republic Statistics, basic indicators. http://www.unicef.org/infobycountry/crepublic_statistics.html.

USEPA, 1997. EPA Office of Compliance Sector Notebook Project. Profile of the Textile Industry, Washington.

Vaghela, S. S.; Jethva, A. D.; Mehta, B. B.; Dave, S. P.; Adimurthy, S.; Ramachandraiah, G. Laboratory Studies of Electrochemical Treatment of Industrial Azo Dye Effluent. Environ. Sci. Technol. 2005, 39, 2848–2855.

Vazquez, A.; Lopez, T.; Gomez, R.; Bokhimi, M.; Novarot, O. J. X-Ray Diffraction, FTIR, and NMR characterization of Sol-Gel Alumina Doped with Lanthanum and Cerium. Solid State Chem. 1997, 128, 161–168.

Verma, A. K.; Dash, R. R.; Bhunia, P. A review on chemical coagulation/flocculation technologies for removal of color from textile wastewaters. J. Environ. Manage. 2012, 93, 154-168.

Verma, A.; Sharma, A.; Basu, S. Electro-oxidation study of methanol and ethanol in alkaline medium in a fuel cell. Ind. Chem. Eng. 2007, 49(4), 330-340.

Verma, S.; Prasad, B.; Mishra, I. M. Thermochemical treatment (thermolysis) of petrochemical wastewater: COD removal mechanism and floc formation. Ind. Eng. Chem. Res. 2011, 50, 5352–5359.

Vigui, J.-R.; Sukmanowski, J.; Bengt, N.; Royer, F.-X. Study of agglomeration of alumina nanoparticles by atomic force microscopy (AFM) and photon correlation spectroscopy (PCS). Colloids and Surfaces A: Physicochem. Eng. Aspects 2007, 302, 269–275.

Vinodgopal, K.; Wynkop, D. E.; Kamat, P. V. Environmental photochemistry on semiconductor surfaces. A photosensitization approach for the degradation of a textile Azo Dye, Acid Orange 7. Environ. Sci. Technol. 1996, 30, 1660–1666.

Wang X. H.; Lu, G. Z.; Guo, Y.; Wang, Y. S.; Guo, Y. L. () Preparation of high thermal-stabile alumina by reverse microemulsion method. Mater Chem Phys . 2005, 90(2–3), 225–229.

Wang, B.; Chang, X.; Hongzhu M. Electrochemical oxidation of refractory organics in the coking wastewater and chemical oxygen demand (COD) removal under extremely mild conditions. Ind. Eng. Chem. Res. 2008, 47, 8478–8483.

Wang, H.; Su, J. Q.; Zheng, X. W.; Tian, Y.; Xiong, X. J.; Zheng, T. L. Bacterial decolorization and degradation of the reactive dye Reactive Red 180 by Citrobacter sp. CK3. Int. Biodeterior. Biodegrad. 2009, 63, 395–399.

Wang, H.-L.; Dong, J.; Jiang, W.-F. Study on the treatment of 2-sec-butyl-4,6-dinitrophenol (DNBP) wastewater by ClO_2 in the presence of aluminum oxide as catalyst. J. Hazard. Mater. 2010, 183, 347–352.

Wei, M. C.; Wang, K. S.; Huang, C. L.; Chiang, C. W.; Chang, T. J.; Lee, S. S.; Chang, S. H. Improvement of textile dye removal by electrocoagulation with low-cost steel wool cathode reactor. Chem. Eng. J. 2012, 192, 37–44.

Wei, S. C.; Zhang, H.; Huang, Y. Q.; Wang, W. K.; Xia, Y. Z.; Yu, Z. B. Pig bone derived hierarchical porous carbon and its enhanced cycling performance of lithium–sulfur batteries. Energy Environ. Sci. 2011, 4, 736–740.

Wesolowski, D. J.; Palmer, D. A. Aluminum speciation and equilibria in aqueous solutions: V. Gibbsitesolubility at 50^0C and pH 3–9 in 1 molal NaCl solutions (a general model for aluminum speciation; analytical methods). Geochim. Cosmochim. Acta 1994, 58, 2947-2969.

World Bank, 2005. World Development Indicators Table 3.6: Water pollution, Table 3.11: Urban Environment.

Wu, C.; Wang, Y.; Gao, B.; Zhao, Y.; Yue, Q. Coagulation performance and floc characteristics of aluminum sulfate using sodium alginate as coagulant aid for synthetic dying wastewater treatment. Sep. Purif. Technol. 2012, 95, 180–187.

Wu, J.; Li, L.; Du, H.; Jiang, L.; Zhang, Q.; Wei, Z.; Wang, X.; Xiao L.; Yang, L. Biodegradation of leuco derivatives of triphenylmethane dyes by sphingomonas sp. CM9. Biodegradation 2011, 22, 897–904.

www.fibre2fashion.com., 2010

www.ipomonitor.net

Xin, B.; Xia, Y.; Zhang, Y.; Aslam, H.; Liu, C.; Chen, S. A feasible method for growing fungal pellets in a column reactor inoculated with mycelium fragments and their application for dye bioaccumulation from aqueous solution. Biores. Technol. 2012, 105, 100–105.

Xue, X.; Hanna, K.; Deng, N. Fenton-like oxidation of Rhodamine B in the presence of two types of iron (II, III) oxide. J. Hazard. Mater. 2009, 166, 407–414.

Yang, C-L.; McGarrahan, J. Electrochemical coagulation for textile effluent decolorization. J. Hazard. Mater. 2005, 127, 40–47.

Yeap, K. L.; Teng, T. T.; Poh, B. T.; Morad, N.; Lee, K. E. Preparation and characterization of coagulation/flocculation behavior of a novel inorganic–organic hybrid polymer for reactive and disperse dyes removal. Chem. Eng. J. 2014, 243, 305–314.

Yildiz, Y. S. Optimization of bomaplex red CR-L dye removal from aqueous solution by electrocoagulation using aluminum electrodes. J. Hazard. Mater. 2008, 153,194–200.

Yılmaz, A. E.; Boncukcuoglu, R.; Kocakerim, M. M.; Kocadagistan, E. An empirical model for kinetics of boron removal from boron containing wastewaters by the electrocoagulation method in a batch reactor. Desalination 2008, 230, 288–297.

Yu, S. J.; Teng, J. Y. Anaerobic decolorization bacteria for the treatment of azo dye in a sequential anaerobic and aerobic membrane bioreactor. J. Taiwan Inst. Chem. Eng. 2009, 40, 500–504.

Yuksel, E.; Eyvaz, M.; Gurbulak, E. Electrochemical treatment of colour index reactive orange 84 and textile wastewater by using stainless steel and iron electrodes. Environ. Prog. Sustainable Energy 2013, 32(1), 60-68.

Yuksel, E.; Gurbulak, E.; Eyvaz, M. Decolorization of a reactive dye solution and treatment of a textile wastewater by electro-coagulation and chemical coagulation: Techno—economic comparison. Environ. Prog. Sustainable Energy 2013, 31 (4), 524-535.

Zahrim, A.Y.; Tizaoui, C.; Hilal, N. Evaluation of several commercial synthetic polymers as flocculant aids for removal of highly concentrated C.I. Acid Black 210 dye. J. Hazard. Mater. 2010,182, 624-630.

Zaki, T.; Kabel, K. I.; Hassan, H. Using modified Pechini method to synthesize a-Al2O3 nanoparticles of high surface area. Ceramics International 2012, 38, 4861–4866.

Zaroual, Z.; Azzi, M.; Saib, N.; Chainet, E. Contribution to the study of electrocoagulation mechanism in basic textile effluent. J. Hazard. Mater. 2006, 131, 73–78.

Zeng, W. M.; Gao, L.; Guo, J. K. A new sol-gel route using inorganic salt forsynthesizing ai,o, nanopowders. Nanostnrctured Materials. 1998, 10(4), 543-550.

Zhang, S.; Niu, H.; Cai Y.; Zhao, X.; Shi, Y. Arsenite and arsenate adsorption on co-precipitated bimetal oxide magnetic nano-materials: $MnFe_2O_4$ and $CoFe_2O_4$. Chem. Eng. J. 2010, 158, 599–607.

Zhang, X. D.; Hao, J. D.; Li, W. S.; Jin, H. J.; Yang, J.; Huang, Q. M.; Lu, D. S.; Xu, H. K. Synergistic effect in treatment of C.I. acid red 2 by electrocoagulation and electrooxidation. J. Hazard. Mater. 2009, 170, 883–887.

Zheng, Y. M.; Yunus, R. F.; Nanayakkara, K. G. N.; Chen, J. P. Electrochemical decoloration of synthetic wastewater containing rhodamine 6G: behaviours and mechanism. Ind. Eng. Chem. Res. 2012, 51, 5953–5960.

Zheng, Y.; Yu, S.; Shuai, S.; Zhou, Q.; Cheng, Q.; Liu, M.; Gao, C. Color removal and COD reduction of biologically treated textile effluent through submerged filtration using hollow fiber nanofiltration membrane. Desalination 2013, 314, 89–95.

Zhong, Y.; Liang, X.; Tan, W.; Zhong, Y.; He, H.; Zhu, J.; Yuan, P.; Jiang, Z. A comparative study about the effects of isomorphous substitution of transition metals (Ti, Cr, Mn, Co and Ni) on the UV/Fenton catalytic activity of magnetite. J. Mol. Catal. A: Chem. 2013, 372, 29-34.

Zhou, X. J.; Guo, W. Q.; Yang, S. S.; Ren, N. Q. A rapid and low energy consumption method to decolorize the high concentration triphenylmethane dye wastewater:

Operational parameters optimization for the ultrasonic-assisted ozone oxidation process. Biores. Technol. 2012, 105, 40–47.

Zhou, X.-J.; Guo, W.-Q.; Yang, S.-S.; Zheng, H.-S.; Ren, N.-Q. Ultrasonic assisted ozone oxidation process of triphenylmethane dye degradation: evidence for the promotion effects of ultrasonic on malachite green decolorization and degradation mechanism. Biores. Technol. 2013, 128, 827-830.

Zhuo, Q.; Deng, S.; Yang, B.; Huang, J.; Yu, G. Efficient Electrochemical Oxidation of Perfluorooctanoate Using a Ti/SnO_2-Sb-Bi Anode. Environ. Sci. Technol. 2011, 45, 2973–2979.

PUBLICATION FROM THESIS

Papers Published in SCI (International) Journals

1. Seema Singh, Vimal Chandra Srivastiva, Indra Deo Mall. Multi-step optimization and residue disposal study for electrochemical treatment of textile wastewater using aluminum electrode. ***International Journal of Chemical Reactor Engineering,*** 2013, 11(1), 1–16.

2. Seema Singh, Vimal Chandra Srivastiva, Indra Deo Mall. Mechanistic study of electrochemical treatment of basic green 4 with aluminum electrodes through zeta potential measurement and characterization of residues. ***RSC Advances,*** 2013, 3, 16426-16439.

3. Seema Singh, Vimal Chandra Srivastiva, Indra Deo Mall. Mechanism of dye degradation during electrochemical treatment. ***Journal of Physical Chemistry C,*** 2013, 117, 15229−15240.

4. Seema Singh, Vimal Chandra Srivastiva, Indra Deo Mall. Electrochemical treatment of dye bearing effluent with different anode-cathode combinations: mechanistic study and sludge analysis. ***Industrial & Engineering Chemistry Research,*** *2014, (In Press)* DOI: 10.1021/ie4042005.

Paper Communicated in SCI (International) Journals

1. Seema Singh, Vimal Chandra Srivastiva, Tapas Kumar Mondal, Indra Deo Mall. Eco-friendly recycle by conversion of electrochemical sludge into mixed-metal oxide nanocomposites with high adaptability and sustainability in wastewater treatment. ***Environmental Science & Technology*** *(Communicated, 2014).*

Papers in Conferences

1. Seema Singh, Vimal Chandra Srivastiva, Indra Deo Mall. The effect of zeta potential on removal of malachite green dye using electrochemical treatment method. *International Conference on Interface between Chemistry and Environment (ICICE), Ramjas College, University of Delhi, India*. December 13–14, 2012 *(Poster presentation).*

2. Seema Singh, Vimal Chandra Srivastiva, Indra Deo Mall. Electrochemical treatment of malachite green dye solution using iron electrode. *International Journal of ChemTech Research,* 2013, 5(2), 592-596. *ISSN: 0974-4290. (Paper presentation in International Conference on* "Global Scenario in Environment and Energy", Organized by the Department of Chemical Engineering, Maulana Azad National Institute of Technology (MANIT), Bhopal, India. March 14-16, 2013).